

Aliphatic hydrogen bonded oligomers and polymers from natural resources

Citation for published version (APA):

Villani, M. (2012). *Aliphatic hydrogen bonded oligomers and polymers from natural resources*. [Phd Thesis 1 (Research TU/e / Graduation TU/e), Chemical Engineering and Chemistry]. Technische Universiteit Eindhoven. <https://doi.org/10.6100/IR734093>

DOI:

[10.6100/IR734093](https://doi.org/10.6100/IR734093)

Document status and date:

Published: 01/01/2012

Document Version:

Publisher's PDF, also known as Version of Record (includes final page, issue and volume numbers)

Please check the document version of this publication:

- A submitted manuscript is the version of the article upon submission and before peer-review. There can be important differences between the submitted version and the official published version of record. People interested in the research are advised to contact the author for the final version of the publication, or visit the DOI to the publisher's website.
- The final author version and the galley proof are versions of the publication after peer review.
- The final published version features the final layout of the paper including the volume, issue and page numbers.

[Link to publication](#)

General rights

Copyright and moral rights for the publications made accessible in the public portal are retained by the authors and/or other copyright owners and it is a condition of accessing publications that users recognise and abide by the legal requirements associated with these rights.

- Users may download and print one copy of any publication from the public portal for the purpose of private study or research.
- You may not further distribute the material or use it for any profit-making activity or commercial gain
- You may freely distribute the URL identifying the publication in the public portal.

If the publication is distributed under the terms of Article 25fa of the Dutch Copyright Act, indicated by the "Taverne" license above, please follow below link for the End User Agreement:

www.tue.nl/taverne

Take down policy

If you believe that this document breaches copyright please contact us at:

openaccess@tue.nl

providing details and we will investigate your claim.

This research forms part of the research program of Dutch Polymer Institute (DPI), Technology Area Bio-inspired Polymers (project #587).

The support from DPI is gratefully acknowledged.



Aliphatic Hydrogen Bonded Oligomers and Polymers from Natural Resources

PROEFSCHRIFT

ter verkrijging van de graad van doctor aan de
Technische Universiteit Eindhoven, op gezag van de
rector magnificus, prof.dr.ir. C.J. van Duijn, voor een
commissie aangewezen door het College voor
Promoties in het openbaar te verdedigen
op maandag 2 juli 2012 om 16.00 uur

door

Maurizio Villani

geboren te Napels, Italië

Dit proefschrift is goedgekeurd door de promotoren:

prof.dr. S. Rastogi
en
prof.dr. P.J. Lemstra

Maurizio Villani

Aliphatic Hydrogen Bonded Oligomers and Polymers from Natural Resources

A catalogue record is available from the Eindhoven University of Technology
Library

ISBN: 978-90-386-3182-0

Copyright © 2012 by Maurizio Villani

Cover design: Maurizio Villani

Printed by Ridderprint

“The world is full of obvious things which nobody by any chance ever observes.”

“It has long been an axiom of mine that the little things are infinitely the most important.”

Sir Arthur Conan Doyle

“I’ m picking up good vibrations”

The Beach Boys



Alla mia famiglia



Table of contents

| | |
|----------------------|----------|
| Summary | V |
|----------------------|----------|

Chapter 1

| | |
|-------------------|---|
| Introduction..... | 1 |
| References..... | 9 |

Chapter 2-Morphogenesis in the Self-Assembling Process of Oligopeptides Obtained from Keratins

| | |
|--|----|
| 2.1 Introduction..... | 12 |
| 2.1.1 Feather keratin..... | 13 |
| 2.1.2 Keratin in hair..... | 21 |
| 2.1.3 Influence of water on hydrolysis of Keratin..... | 22 |
| 2.2 Experimental section..... | 26 |
| 2.2.1 Materials..... | 26 |
| 2.2.2 Sample preparation..... | 26 |
| 2.2.3 Crystallization..... | 27 |
| 2.2.4 Solid State Peptide Synthesis (SSPS)..... | 27 |
| 2.2.5 Synthesis of 1 KDa oligopeptide Val-Val-Val-Thr-Leu-Pro-Gly-Pro-Ile- Leu..... | 28 |
| 2.2.6 Synthesis of 1 KDa alkylated tail-oligopeptide C16H310-Val-Val-Val- Thr-Leu-Pro-Gly-Pro-Ile-Leu..... | 28 |
| 2.2.7 Synthesis of 1 KDa aliphatic-amide tail-oligopeptide N9H102C58O12- Val-Val-Val-Thr-Leu-Pro-Gly-Pro-Ile-Leu..... | 29 |
| 2.2.8 Characterization techniques..... | 29 |
| 2.2.8.1 Optical Microscopy (OM)..... | 29 |
| 2.2.8.2 Thermogravimetric Analysis (TGA)..... | 29 |
| 2.2.8.3 Differential scanning calorimetry (DSC)..... | 29 |

| | |
|---|----|
| 2.2.8.4 Fourier Transform Infrared Spectroscopy (FTIR)..... | 29 |
| 2.2.8.5 Liquid chromatography and Mass spectrometry (LC-MS-HPLC-MS2). | 30 |
| 2.2.8.6 Wide Angle X-Ray Diffraction (WAXD)..... | 30 |
| 2.2.8.7 Atomic Force Microscopy (AFM)..... | 31 |
| 2.3 Results and Discussion..... | 31 |
| 2.3.1 Crystallization and self assembling process of oligopeptides..... | 31 |
| 2.3.2 Morphogenesis; self assembling process of hair keratin..... | 37 |
| 2.3.3 Thermal stability of oligopeptides..... | 38 |
| 2.3.4. Sequencing and Fractionation of oligopeptides obtained from feather keratin..... | 39 |
| 2.3.5 Synthesis of the oligopeptide in solid state..... | 48 |
| 2.3.6 Conformational and structural analysis of the oligopeptides obtained from the natural (feather keratin) and the synthesized sources..... | 54 |
| 2.4 Conclusions..... | 60 |
| References..... | 62 |
| Appendix A..... | 66 |

Chapter 3- Novel, Fully Biobased Semi-Crystalline Polyamides

| | |
|---|----|
| 3.1 Introduction..... | 74 |
| 3.2 Experimental Section..... | 76 |
| 3.2.1 Materials..... | 76 |
| 3.2.2 Polymerization of Salt Monomers..... | 77 |
| 3.2.3 Interfacial Polycondensation..... | 78 |
| 3.2.4 Measurements..... | 78 |
| 3.3 Results and Discussion..... | 79 |
| 3.3.1 Synthesis and Molecular Characterization of Polyamides..... | 79 |
| 3.3.2 Thermal Properties of Polyamides..... | 88 |
| 3.3.3 Wide-Angle X-ray Diffraction..... | 90 |
| 3.4 Conclusions..... | 92 |

| | |
|-----------------|----|
| References..... | 94 |
|-----------------|----|

Chapter 4- Local Conformation and Cocrystallization Phenomena in Renewable Diaminoisoidide-Based Polyamides Studied by FT-IR, Solid State NMR and WAXD

| | |
|--|-----|
| 4.1 | |
| Introduction..... | 100 |
| 4.2 Experimental Section..... | 103 |
| 4.2.1 Materials..... | 103 |
| 4.2.2 FT-IR..... | 104 |
| 4.2.3 DSC..... | 104 |
| 4.2.4 Solid State NMR..... | 104 |
| 4.2.5 Geometry Optimization and NMR Chemical Shift Calculations..... | 105 |
| 4.2.6 WAXD..... | 105 |
| 4.3 Results and Discussion..... | 106 |
| 4.3.1 Infrared Analysis of the Polyamides..... | 106 |
| 4.3.2 Variable-Temperature Solid State NMR Study..... | 111 |
| 4.3.3 DAII Conformers from <i>ab initio</i> Calculations..... | 121 |
| 4.3.4 WAXD..... | 124 |
| 4.4 Conclusions..... | 132 |
| References..... | 135 |
| Appendix B..... | 139 |

Chapter 5- Structure-Property Relationships of Diaminoisoidide-based Copolyamides

| | |
|---|-----|
| 5.1 Introduction..... | 168 |
| 5.2 Experimental Section..... | 169 |
| 5.2.1 Synthesis and characterization..... | 169 |
| 5.2.2 Structural characterization..... | 170 |
| 5.2.3 Mechanical properties..... | 170 |

| | |
|--|------------|
| 5.3 Results and Discussion..... | 171 |
| 5.3.1 Mechanical properties..... | 188 |
| 5.4 Conclusions..... | 191 |
| References..... | 192 |
| Chapter 6- Technological Assessment and outlook | 195 |
| Acknowledgements..... | 199 |
| Curriculum Vitae..... | 203 |
| List of publications..... | 205 |

Summary

Aliphatic Hydrogen Bonded Oligomers and Polymers from Natural Resources

Chemistry is by definition the science of matter, the science of the transformation of the substances and for this reason and also for practical issues derived from its technological applications, has interested the different populations since ancient times. The strong connection of this branch of science with the industrial world has promoted its interest in the development of new materials that could substitute or improve traditional and natural materials. Although this development has not always been a direct consequence of a well specified research or demand, (in fact many important discoveries are result of serendipity) periods can be distinguished during the history of the chemistry in which the different industrial processes or researches were born considering demands and requests of the moment. For example the Alkali industry, probably the first important chemical industrial process, can be considered as born to serve the textile industry, leading sector of the second industrial revolutions. This continuous adaptation also led to development of materials such as plastics and synthetic polymers directly correlated to petroleum industry.

Synthetic polymers, initially introduced in order to substitute more expensive materials like natural fibers or traditional materials like wood, glass, and ceramics, were improved with different and better properties with respect to the natural materials. In particular, exploitation of chemistry to meet challenges in material science, a detailed understanding of structure-property relationship is essential to meet the ultimate properties. These materials are characterized by their simple chemical structure and therefore good thermal stability that makes

them processable in the molten state and outperform the thermal degradation of many natural materials is essential.

Nowadays the scarcity of oil resources and the environmental and political issues are encouraging the production of environmental friendly materials. A new request is once again influencing the chemistry world and new answers from polymer science are expected. Many different projects on bio-polymers have been carried out in the last decades in several different laboratories. A lot of interest is paid by petrochemical industry to bio-based materials with the intent of replacing existing plastics. The industrial interest is from one side promoted by the possibility of achieving green image and from the other side is due to the possibility of minimizing the exploitation of oil resources. However, many bio-based plastics represent durable materials that cannot prevent one of the most important issues, the biocompostability.

In this thesis we have explored the possibility of using alternative feedstock in order to produce plastics. We have focused our attention on bio based monomers and the application of such monomers as a powerful method of tailoring thermal and mechanical properties of interesting known materials. In particular the role of secondary interactions such as hydrogen bonds on the crystallization of new bio-based polyamides and the role of bio-based monomers in influencing the secondary interactions has been investigated. Among many materials that can be considered as a source of bio-based polymers or monomers we have also explored a new approach using water under specific pressure-temperature conditions to hydrolyze keratins that is a part of Chapter 2 in this thesis.

Our observations are that under controlled hydrolysis conditions it is feasible to extract oligopeptides with well defined sequences of amino acids (LC-MS and HPLC) and re-synthesize them via Solid State Peptide Synthesis by attaching

aliphatic and hydrogen bonding motifs to the synthesized oligopeptides in order to promote self assembling phenomena.

New semi-crystalline polyamides and co-polyamides from bio-based sebacic acid (SA), 2,5-diamino-2,5-dideoxy-1,4;3,6-dianhydroiditol (diaminoisoidide, DAII) as well as from 1,4-diaminobutane (DAB), have been synthesized. These monomers can be derived from castor oil (SA), starch (DAII) and putrescine (DAB). Synthetic routes, involving interfacial polycondensation, solvent-free bulk polycondensation accomplished by Solid State Polymerization (SSP) after a prepolymerization in the melt are reported in Chapter 3 where the chemical structure of the synthesized bio based polyamides and copolyamides was proven using 2D NMR and FT-IR spectroscopy. Moreover the influence of DAII/DAB content on the crystal structure and melting points of the polyamides were investigated using wide-angle X-ray diffraction and DSC techniques.

In chapter 4, FT-IR, CP/MAS NMR and WAXD are successfully employed for the analysis of the structural behavior and mobility of the polyamides and copolyamides with a different DAII/DAB content as function of temperature. The contribution of DAII causes a conformational disorder of the polyamides and thus influences the crystal structure and the properties of these materials. Transmission electron micrographs of crystals of bio-based polyamides and the respective electron diffraction patterns, coupled with XRD data and modeling experiments confirm the influence of DAII content on the crystal structure of these materials and also on the mechanical properties. The latter is confirmed by DMTA (chapter 5).

Last chapter in the thesis highlights possible technological aspects in these bio-polymers.

Chapter 1

Introduction

Polymers are composed of repeating structural units typically connected by covalent chemical bonds. They represent a large class of compounds, natural and synthetic materials with a wide variety of properties. Their extraordinary wide range of properties plays an essential role in everyday life, going from familiar synthetic plastics and elastomers to natural biopolymers such as nucleic acids and proteins that are essential for life. Many polymer products used in everyday life, from fibers to many goods available in the supermarket, are semi-crystalline.

Their semi-crystalline nature derives from crystallization of these long molecules governed by the balance between kinetics and thermodynamics.¹ In a quiescent molten state or solution, individual polymer chains exist in a random coil conformation characterized by no apparent order.² At high solute concentration, as well as in the melt, polymer chains are entangled resulting in physical constraints. In the case of defined regular architecture, polymers tend to crystallize on cooling from the melt or when the solvent characteristics are changed either by temperature or concentration.

Polymer crystallization can be imaged as a self-assembling process where a three dimensional order evolves with the alignment of chains within a certain degree of regularity, parallel to each other and packing them along the lateral directions. Prerequisites that ensure the crystallization are constitutional, configurational and conformational regularities of the repeating structural units.^{3, 4, 5} This implies that if long monomer sequences with the same chemical

structure can assume different spatial configurations, the succession of the configurations has to be regular. Polymers like for example polypropylene can present a succession of a single configuration of the chiral monomer, i.e. isotactic polypropylene, or an alternate succession of the two opposite enantiomers, i.e. syndiotactic polypropylene, and both can crystallize. On the contrary, when the two configurations of the stereo-centers in the repeating units are randomly encountered along the chain as in atactic polypropylenes, fully amorphous materials are obtained. Moreover, the chains must adopt a regular conformation, which typically corresponds to the minimum intramolecular conformational energy and enables an efficient packing in the unit cell.^{1,4,7-9} It should be taken into account that the chain configuration and its influence on chain packing, in the three dimension crystalline lattice, arises with the formation of a nuclei.¹ Its implications in the formation of higher order structures arises with the formation of dislocations that travel beyond the nm length scale, resulting into spherulitic structures when crystallized from melt. In the case of crystallization from solution they lead to dendritic structures strongly influenced by the diffusion controlled process depending on the supercooling and the cooling rate. Both, spherulitic and dendritic, morphologies are observed in polymers as well as inorganic materials independent of the molecular length.^{2, 10-12} However, polymer crystallization adds further complexity of chain folding that normally arises at the length of 10nm, thus length of the Burgers vector for dislocation arises from the crystal surface having chain folds.¹⁰ This often leads to spiral terrace formation and is considered to be the origin of spherulitic structures having a Maltese-cross. It is to be realized that the crystal surface having chain folding contributes to the amorphous component in the semi-crystalline material. The very nature of the amorphous region, i.e. the entanglement density, has implications for the mechanical deformation of the polymer.¹³ A well-known example where the entanglement density residing in the amorphous region has implications in the mechanical deformation is solution or solid state processing of Ultra High

Molecular Weight Polyethylene, having molar mass greater than a million g/mol.^{14, 15-17}

In broad generality, polymer chemistry is purely related to covalent bonding where several physical and mechanical properties can be influenced by changing the molecular length. The covalent description is almost always fully adequate, going from an isolated molecule in free space to more complex molecular structures on changing the molecular configuration. The importance of non-covalent, secondary interactions becomes evident when chains tend to pack in a three dimensional order. The neighboring secondary interactions can vary from weak van der Waals to strong hydrogen bonding. The very nature of hydrogen bonding builds a bridge between the synthetic polymers and the biopolymers. The simplest example is the class of the polyamides where hydrogen bonding and its strength is influenced by the number of amide motifs.

Secondary interactions are a type of bond that does not involve the sharing of pairs of electrons, but rather involves more dispersed variations of electromagnetic interactions. There are four commonly mentioned types of secondary interactions: ionic interactions, hydrogen bonds, van der Waals forces, and hydrophobic interactions.¹⁸ They range from coordinative bonds with a strength of several hundreds of kJ mol^{-1} to weak van der Waals interactions of a few kJ mol^{-1} . They can also be classified as attractive or repulsive interactions, depending on if the interaction is between (partial) charges with opposite polarity (attraction) or the same polarity (repulsion). The brief overview on the secondary interactions presented here has been recalled considering some interesting information reported in the cited reference.¹⁸

Ionic interactions are the strongest interactions having bond energies in the range of ca. 100 to 350 kJ mol^{-1} . In an ionic bond, the atoms are bound by attraction of opposite ions, without sharing electrons to attain stable electron

configurations like in a covalent bond. Purely ionic bonds cannot exist, and a certain degree of sharing electron density is allowed between entities involved in the bond. Therefore, all ionic bonds have some covalent character. For example, Na–Cl bonds have a few percent of covalency.¹⁸

Weaker interactions occur between ions and dipoles (ca. 50–200 kJ mol⁻¹). For example, coordination complexes with transition metal ions as the cores are often used in supramolecular assembly. Here, the dative bond has a greater covalent contribution, which makes it difficult to characterize because these bonds are much more sensitive to the environment than covalent bonds. Even weaker than ion–dipole forces (5–50 kJ mol⁻¹) are the interactions between two dipoles where the relative orientation of the two interacting dipoles plays an important role.

Hydrogen bonding is crucial in biochemistry (e.g. in the formation of double stranded DNA and protein folding) and for this reason greatly employed in supramolecular chemistry.^{18, 19} An important reason is the directionality of the hydrogen bond which allows the control of the geometry of the complexes and specific design for supramolecular architectures. A first distinction can be made between strong hydrogen bonds with binding energies in the range of 60–120 kJ mol⁻¹ and heteroatom–heteroatom distances between 2.2 and 2.5 Å, moderate hydrogen bonds (15–60 kJ mol⁻¹; 2.5–3.2 Å), and weak hydrogen bonds with binding energies below ca. 15 kJ mol⁻¹ and long donor–acceptor distances of up to 4 Å. This classification also expresses different covalent contributions in the hydrogen bonded polymers. One distinguishes strong hydrogen bonding with a major covalent contribution, and moderate or weak hydrogen bonding arising due to electrostatic nature of the atoms.¹⁸ Moreover, the range of possible hydrogen bond angles is narrow in strong H bonds (175⁰–180⁰), while moderate (130⁰–180⁰) and weak (90⁰–150⁰) hydrogen bonds are more flexible. Furthermore, the difference between hydrogen bonding between neutral

molecules and charged hydrogen bonds should always be considered. For example, the F-H----- F⁻ hydrogen bond is the strongest hydrogen bond known (160 kJ mol⁻¹).¹⁸

Non-covalent forces also involve π -systems-cations or π -systems- π -systems interactions. π -systems such as aromatic rings have a quadrupole moment with a partially positive σ -scaffold and a partially negative π -cloud above and below the ring plane. Alkali metal and other cations can form an attractive interaction if located above the center of the aromatic ring. The cation- π interaction²⁰ plays an important role in biomolecules having binding energies in the range of ca. 5–80 kJ mol⁻¹. Another important point is the solvation of the corresponding anion. Water is able to solvate anions by forming hydrogen bonds.²¹ The very existence of a liquid phase, and also all related effects like solvation phenomena, can be attributed to non-covalent interactions. The existence of a condensed phase probably represents the most important example of non-covalent interactions and it must be stated that theory still has serious problems in describing adequately the role of solvents in general and, more specifically, the role of liquid water. Whereas covalent systems can now be investigated with chemical accuracy (~1 kcal/mol), the error in evaluation of hydration energies is much larger and, even worse, results from various theoretical methods differ significantly.

An important class of secondary interactions is the hydrophobic interactions. They are usually described referring to the phenomenon of apparent repulsion between water and hydrocarbons, therefore to the tendency of hydrocarbons (or of lipophilic hydrocarbon-like groups in solutes) to form intermolecular aggregates in an aqueous medium, and analogous intramolecular interactions.²² However, the hydrophobic effect relies on the minimization of the energetically unfavorable surface between polar/protic and unpolar/aprotic molecules.

The weakest non covalent interactions are van der Waals forces ($<5 \text{ kJ mol}^{-1}$) which arise from the interaction of an electron cloud polarized by adjacent nuclei. Van der Waals forces are the sum of the attractive or repulsive interactions, which decrease with the distance r in a r^{-6} dependence.¹⁸ There are more non covalent interactions which cannot all be introduced here. Forces between multipoles have been reviewed recently.²³

If the role of secondary interactions has been defined in terms of influence on material properties,²⁴ it has yet to be defined in terms of influence on crystallization behavior. Polyamides can be considered as a good example of polymers exhibiting a complex crystallization where the interplay between hydrogen bonding interactions, van der Waals interactions and conformational flexibility has to be taken into consideration.²⁵

In this dissertation we have explored the role of secondary interactions such as hydrogen bonds on the crystallization of new bio-based polyamides and the role of bio-based monomers in influencing the secondary interactions. We have also explored a new approach to extract oligopeptides, building blocks for several hydrogen bonded polymers, having well-defined sequences of amino acids from insoluble proteins such as keratin obtained from sustainable sources such as feather and hair. The extraction process has been carried out using water under well specified pressure-temperature conditions.

In the past several attempts have been made to dissolve keratin from natural sources as feathers or hair. The interest in such studies was driven from the interesting properties of this natural fiber and abundance of feathers. In spite of traditional chemical ways adopted to dissolve or hydrolyze this protein, in this thesis a new approach has been used for extraction of the oligopeptides. Hydrolysis of keratin in the “superheated state” (or subcritical state) of water represents a new eco-friendly approach to generate a fundamental

understanding of the keratin structure, and also an unexplored possibility to extract oligopeptides with well defined sequences of amino acids. This has been the subject of our study described in chapter 2. In this chapter it is shown that under controlled hydrolysis conditions, it is feasible to extract oligopeptides with well-defined sequences of amino acids (characterized by LC-MS and HPLC), and using Solid State Peptide Synthesis to resynthesize the identified oligopeptides by attaching aliphatic and hydrogen bonding motifs to the oligopeptides. This route is adopted to follow self-assembling phenomena.

To investigate the influence of hydrogen bonding in aliphatic polyamides monomers obtained from renewable sources such as diaminoisoidide (DAII), 1,4-diaminobutane (DAB) and sebacic acid (SA) have been used. The work has been done in collaboration with the group of Prof. Cor Koning where the synthesis was performed under another DPI program. In this thesis the physical properties of these bio-based hydrogen bonded polymers and the resultant crystal structures have been investigated.

In chapter 3, new semi-crystalline polyamides and copolyamides from bio-based sebacic acid (SA), 2,5-diamino-2,5-dideoxy-1,4;3,6-dianhydroiditol (diaminoisoidide, DAII) as well as from 1,4-diaminobutane (DAB), have been synthesized. These monomers can be derived from castor oil (SA), starch (DAII) and putrescine (DAB). Synthetic routes, involving interfacial polycondensation or solvent-free bulk polycondensation, accomplished by Solid State Polymerization (SSP) after a pre-polymerization in the melt, are reported. The chemical structure of the synthesized biobased polyamides and copolyamides was determined using 2D NMR and FT-IR spectroscopy. Moreover, the influence of the DAII/DAB content on the crystal structure and melting points of the polyamides was investigated using wide-angle X-ray diffraction and DSC techniques.

In chapter 4, FT-IR, CP/MAS NMR and WAXD were successfully employed for the analysis of the structural behavior and mobility of the polyamides and copolyamides with a different DAII/DAB content as function of temperature. The contribution of DAII introduces conformational disorder into the polyamides and thus influences the crystal structure and the properties of these materials.

The chapter 5 shows Transmission Electron Micrographs of crystals from bio-based polyamides and the respective electron diffraction patterns are coupled with XRD data. Modeling is performed to show the influence of the DAII content on the crystal structure of these materials. Mechanical properties of the co-polyamides have been investigated using DMTA.

Chapter 6 highlights some technological relevance of the studies performed.

References

1. Mandelkern, L. *Crystallization of Polymers*; Mc-Graw-Hill Book Company: New York, **1964**
2. Flory, P.J. *Principles of Polymer Chemistry*, Cornell University Press, Ithaca, New York, **1953**.
3. R. Napolitano, B. Pirozzi, *Gazz. Chim. Ital.* **1986**, *116*, 323. (Reg. costituzionale)
4. P. Corradini, In *The Stereochemistry of Macromolecules*, Vol. 3. Ketley, A. D. (Ed.) Marcel Dekker, New York, **1968**, p. 1.
5. R. Napolitano, B. Pirozzi, *Macromol. Theory Simul.* **1999**, *8*, 15.
6. R. Napolitano, B. Pirozzi, *Makromol. Chem.* **1986**, *187*, 1993.
7. G. Natta, P. Corradini, *Angew. Chem.* **1956**, *68*, 615; G. Natta, P. Corradini, *Nuovo Cimento, Suppl.* **1960**, *15*, 111.
8. G. Natta, P. Corradini, L. Porri, *Rend. Fis. Acc. Lincei* **1956**, *20*, 728.
9. P. A. Kollman, *Acc. Chem. Res.* **1977**, *10*, 365
10. Bassett, D.C., Frank, F.C., Keller, A. *Nature* **1959**, *184*, 810-811.
11. Keller, A. *In Growth and Perfection of Crystals*, John Wiley and sons Inc., New York, **1948**, 499-528.
12. Abo el Maaty, M.I., Hosier, I. L., Bassett, D.C., *Macromolecules*, **1988**, *31*, 153-157.
13. Smith, P., Lemstra, P.J., Booij, H.C. *J. Polym. Sci., Polym. Phys. Edn.*, **1981**, *19*, 877-888.
14. Smith, P., Lemstra, P.J., *J. Mater. Sci.*, **1980**, *15*, 505-514.
15. Smith, P., Lemstra, P.J., Kalb, B., Pennings, A.J., *Polym. Bull.*, **1979**, *1*, 733-736.
16. Smith, P., Matheson, Jr., R.R. and Irvine, P.A., *Polym. Commun.*, **1984**, *25*, 294.

17. Smook, J., Pennings, A.J., *Polym. Bull.*, **1983**, 10, 291-297.
18. TEXT BOOK: *Analytical Methods in Supramolecular Chemistry*. Edited by Christoph Schalley Copyright © 2007 WILEY-VCH Verlag GmbH & Co. KGaA, Weinheim ISBN: 978-3-527-31505-5
19. G. A. Jeffrey, *An Introduction to Hydrogen Bonding*, Oxford University Press, Oxford **1997**.
20. J. C. Ma, D. A. Dougherty, *Chem.Rev.* **1997**, 97, 1303.
21. Dill, K.A., Truskett, T.M., Vlachy, V., and Hribar-Lee, B., *Modeling water, the hydrophobis effect and ion solvation*. *Annu. Rev. Biomol. Struct.* **2005**. 34: p. 173-199.
22. IUPAC. Compendium of Chemical Terminology, 2nd ed. (the "Gold Book"). Compiled by A. D. McNaught and A. Wilkinson. Blackwell Scientific Publications, Oxford (1997). XML on-line corrected version: <http://goldbook.iupac.org> (2006-) created by M. Nic, J. Jirat, B. Kosata; updates compiled by A. Jenkins. ISBN 0-9678550-9-8)
23. R. Paulini, K. Muller, F. Diederich, *Angew. Chem.* **2005**, 117, 1820; *Angew. Chem. Int. Ed.* 2005, 44, 1788.
24. Meijer H.E.H, Govaert L.E, *Prog. Polym. Sci.* 30, **2005**, 915.
25. Heintz, A.M., McKiernan, R.L., Gido, S.P., Penelle, J., Hsu, S.L. *Macromolecules* **2002**, 35, 3117.

Chapter 2

Morphogenesis in the Self-Assembling Process of Oligopeptides Obtained from Keratins*

Considering that feathers are the main waste product of the poultry industry, with an amount of about 4 million tons per annum, and that more than 90% of their structure consists of keratins, feathers can be a valuable source of some amino acids and oligopeptides. The difficulty, which has limited the use of this material, is connected with the environmentally unfriendly process involved in the extraction process of the oligopeptides. We have explored a different approach using water hydrolysis to break down the keratins. Here we report the hydrolysis of keratin under specific pressure-temperature conditions. Above 100 °C, and with a pressure sufficiently high to maintain the liquid state, water is in the “superheated state”. In these conditions water has an expanded structure in which intermolecular interactions like hydrogen bonding weaken. The weakening of the hydrogen bonding between the water molecules enhances the molecular mobility making water a good solvent for several hydrogen bonded synthetic and biological polyamides. For example, the “superheated state” of water is highly effective in the hydrolysis of keratins.³² In this chapter, we have made use of this eco-friendly dissolution route to obtain the oligopeptides and have followed the self-assembling phenomenon during evaporation of the solvent i.e. water. Methods have been also developed for sequencing and extraction of the oligopeptides obtained during the dissolution process. Synthesis of the identified oligopeptides with other hydrogen bonding motifs has been performed to investigate their influence on the aggregation process.

* Partially reproduced from Maurizio Villani, Dennis W. P. M. Löwik, Jan C. M. van Hest, and Sanjay Rastogi, *ACS 241st National meeting and exposition – PMSE* and Maurizio Villani, Dennis W. P. M. Löwik, Jan C. M. van Hest, and Sanjay Rastogi, *Biomacromolecules*, to be submitted.

2.1 Introduction.

Keratin is a fibrous structural protein well known in nature for its important role in providing protective outer covering for human skin and for being a structural component of hair and nails. Like every protein, keratin is characterized by one or more polypeptides typically folded into a globular or fibrous form, facilitating a biological function. A polypeptide is a single linear polymer chain composed of amino acid sequences bonded together by peptide bonds generated from the carboxyl and amino groups of adjacent amino acid residues. The sequence of amino acids in a protein is defined by the sequence of a gene, which is encoded in the genetic code. In general, the genetic code specifies 20 standard amino acids. The amino acids are molecules containing an amine group, a carboxylic acid group, and a side-chain that is specific for each amino acid. They serve as building blocks in proteins and can be linked together in varying sequences leading to numerous conformations and structural variations resulting into different proteins with different functions. The specific side chain of each amino acid in a polypeptide sequence defines structural and biological properties of the peptide and therefore also of the protein. Polypeptides based on natural amino acids may locally fold into an α -helix or can locally form a β -sheet depending on the side groups of the amino acid sequences. If a large number of hydrogen bonds can be formed and if there is the condition in order that the NH group of one amino acid can form a hydrogen bond with the carbonyl group of 3.6 residues earlier, the peptide may locally fold into an α -helix structure. In this case the side groups of the amino acids will point on the outer side of the helix. On the contrary, if the side groups of the amino acids constituting the peptide sequence are characterized by small lateral groups, like glycine and alanine, they can closely pack promoting the formation of β -sheets. It is clear that the prerequisites for the crystallization are different from synthetic polymers and both secondary structures, α -helix and β -sheet, can be found in the same protein or even single peptide according to its primary

structure, the sequence of amino acids. The tertiary structure of a protein is in fact the placement of all the secondary structures in a protein and the quaternary structure is the placement of proteins with respect to each other.

Keratin like others fibrous proteins adopts an extended, fiber-like structure while globular proteins are compact, vaguely spherically-shaped proteins. Keratin is mainly composed of extensive regions of regular secondary structures where hydrogen bonding constitutes one of the main sources of attraction between backbone peptide links. It can be of two different types; traditionally called “soft” and “hard”¹ depending on the amount of cysteine residues, mainly present as disulphide bonds formed between the thiol groups of cysteine residues. A low content of cysteine disulphide bonds is referred to as soft keratins, while hard keratins are so called for their high content of disulphide bonds. Another basic classification depends on the secondary structure of the polypeptide chain. The keratin chain could be in α -helix or β -sheet structure. Several different studies show specific X-ray diffraction patterns, in which it is possible to distinguish between these different structures.²⁻⁴

Soft keratins and mammalian hard keratins are called α -keratins, while avian and reptilian hard keratins are called β -keratins. The interest for these proteins derives from their structural properties and the abundant availability in nature. Considering that feathers are an important waste product of the poultry industry with more than 4-5 million tons of available waste products per year and that they consist for 90% of keratin, they are of considerable commercial and academic interest. The development of products for environmentally sustainable applications from protein waste streams is growing and feather keratins have received great attention for eventual applications as compostable packaging or agricultural films.^{1-3, 5-8}

2.1.1 Feather keratin

Feathers keratins, the object of our study, belong to the hard keratins and have a molecular weight of approximately 10KDa. They consist of a central part with

β -sheet crystalline structure and two randomly ordered chain ends.⁹ The dimers, made of two β -sheets, form a chain called microfibril with a diameter of 3 nm. The microfibril is embedded in an amorphous matrix made of inter- and intrachain crosslinks in the form of disulphide bonds. The disulphide bonds together with the molecular structure are responsible for the insolubility of keratin.¹⁰ Since the feathers are rich in keratins it should be possible to extract the protein from different parts constituting the feather structure.

The feather structure is characterized by a main shaft, called the rachis. A series of branches, known as barbs, are attached to the rachis; the barbs are also branched and form the barbules through minute hooks called barbicels for cross-attachment.¹¹

The basal part of feathers is a hollow tube called calamus inserted into the follicle in the skin (Figure 1).

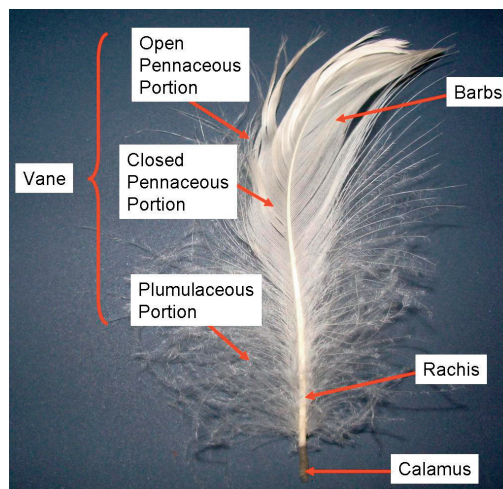


Figure 1. The Branched Structure of a Pennaceous Feather.

The notable influence of the amino acid sequencing on the secondary structure of this protein has rendered the crystal structure solving a quite complex and long process. Several detailed studies have been performed in order to achieve this result and they mostly concentrated on specific keratins contemplating this

diversification in the primary structure. Therefore a brief overview of the feather keratin structure and a comparison with some mammalian soft keratins like hair will be presented here. One of the first problems encountered in the structure determination of feather keratin is related to the relative abundance of the α -helix or β -sheet domains. For example, X-ray diffraction (XRD) studies on seagull feathers suggested a helical structure whereas infrared spectroscopy studies indicated that on average one third of the keratin chains are in anti-parallel β -sheet conformation forming the central crystalline core. A first attempt to explain these double conformational ordering was the simplified model proposed by Bear and Rugo in which, according to XRD data, the feather keratin is characterized by microfibrils containing a double helical array of β -crystallites with two sheets related by a diad perpendicular to the fiber axis (Figure 2). Independent studies of electron microscopy investigations on ultrathin stained feathers¹² confirmed the presence of microfibrillar domains with dimensions consistent to the model proposed by Bear and Rugo. However, XRD observations demonstrated that this trial structure was not sufficient and several possible variations were considered.

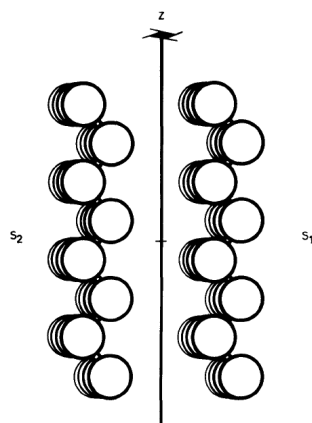


Figure 2. Trial structure for the pleated sheet framework of feather keratin. The sheets are related by horizontal diad and each of them contains four chains. The eight residues per chain are represented by Gaussian spheres of electron density. (Reproduced from ref.)¹⁴

To accommodate distortion, without destroying the hydrogen bonding, Fraser et al. proposed a helical twist in which interchain distance and corresponding point on neighboring chains is suggested to stay in the exact lateral register. This structural transformation, combined with the β -sheet framework of feather keratin is depicted in Figure 3.

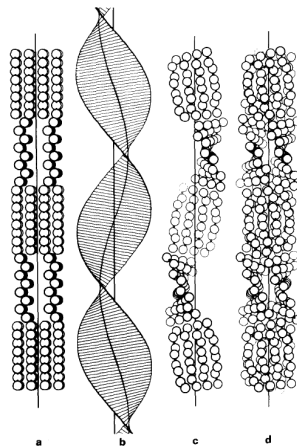


Figure 3. Stages in the development of a model for the structure of the pleated sheet framework of feather keratin. (a) Trial structure with pairs of pleated sheets; (b) left-hand ruled surface; (c) a strand of β -sheets distorted so as to conform to the ruled surface in; (d) complete model for the core of the feather keratin microfibril consisting of two strands of β -sheets (Reproduced from ref.).¹³

In particular Fraser and Parry¹³ related the structure model of a β -sheet framework of feather keratin with the amino acid sequence of avian keratins, taken from different publications.¹⁴⁻¹⁶ These authors suggested that the original model shown in Figure 2 could be refined considering a repeating hairpin motif and the sequence mapped on this framework (Figure 4).

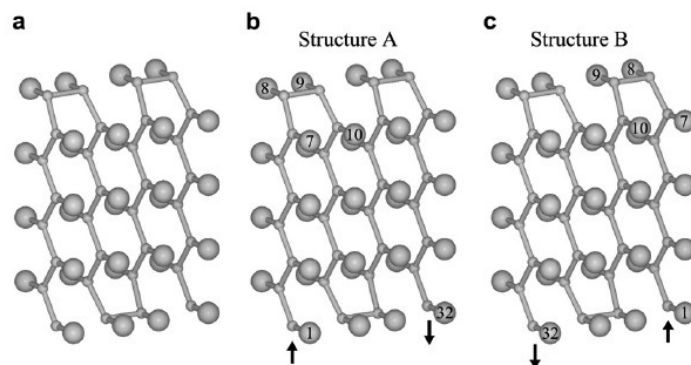


Figure 4. (a) A model for the 32-residue asymmetric unit of the framework of the filament in feather keratin-like materials. It contains a repeating hairpin motif and the sequence can be mapped on to this framework in two different ways, leading to the two distinct structures, A and B, shown in (b) and (c) (Reproduced from ref.).¹³

However, according to the original X-ray study of Fraser et al., the β -sheet was distorted to have a right-handed twist. This transformation, shown in Figure 5, used earlier by Fraser et al. to explain the crystallographic data, takes into consideration the amino acid sequence and the interactions between the dimer components.

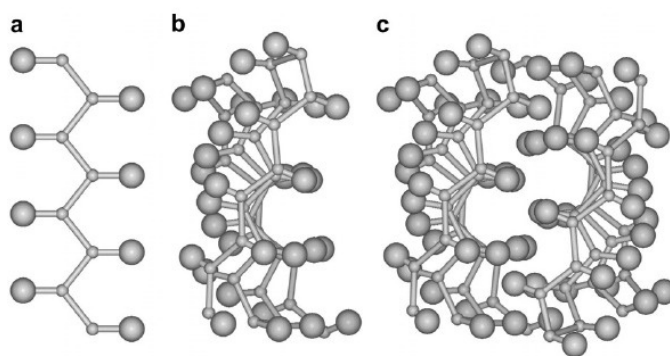


Figure 5. (a) An undistorted sheet viewed down the x (hydrogen bond) axis. (b) the same sheet distorted to give a right-handed twist using the ruled surface transformation developed by Fraser et al. (1971). (c) A pairs of twisted sheets related by a diad along the x-axis, note how the rows of side chains in the interior interleave along the vertical (filament) axis (Reproduced from ref.).¹³

In both structures, the charged residues are on the surface and contribute to the formation of hydrogen bonds, while the hydrophobic residues are on the interface between the two twisted sheets being an important stabilizing factor. The cysteine units in either structure are not close enough to one another to form an S-S bond, another stabilizing factor, but are involved in the remaining two third of the molecule that constitutes the matrix.

The two structures suggested by Fraser et al.¹³ seem reasonable, considering also the electron microscopy studies of Filshie and Rogers¹².

The earlier studies on the amino acids composition of feathers keratin were obtained considering soluble derivatives prepared in different chemical ways.¹⁷⁻

²¹ In Table 1 it is possible to observe that the content of glycine, serine, proline and aliphatic amino acids is quite high compared to histidine, lysine and methionine.²²

| Amino acid | Residues per 100 residues | | |
|---------------|---------------------------|-------------------|---------------|
| | Whole feather | Insoluble residue | Whole extract |
| Lysine | 1.2 | 5.3 | 0.4 |
| Histidine | 0.3 | 1.4 | trace |
| Arginine | 4.7 | 4.2 | 4.8 |
| SCM-Cysteine | 0 | 8.7 | 8.3 |
| Aspartic acid | 6.3 | 8.5 | 5.0 |
| Threonine | 5.3 | 6.2 | 4.5 |
| Serine | 15.7 | 8.1 | 14.6 |
| Glutamic acid | 8.6 | 11.3 | 7.7 |
| Proline | 11.7 | 7.5 | 11.8 |
| Glycine | 11.5 | 8.5 | 11.9 |
| Alanine | 5.6 | 5.8 | 5.3 |
| Cystine | 4.2 | 0 | 0 |
| Valine | 7.7 | 7.3 | 9.1 |
| Methionine | 0.3 | 1.2 | trace |
| Isoleucine | 4.3 | 4.0 | 4.9 |
| Leucine | 7.4 | 6.8 | 7.0 |
| Tyrosine | 1.6 | 2.8 | 1.2 |
| Phenylalanine | 3.6 | 2.4 | 3.5 |

Table 1. Amino acid analyses of fowl body feather keratins and their fractions. Results unconnected for destruction during hydrolysis; tryptophan not determined. Figure taken from Akahane et al paper.²²

Moreover it was observed that the amino acid composition of these derivatives varied marginally considering different morphological parts of the feathers,^{6, 18} or various bird species.²⁰ Often protein sequencing of feathers from different bird species suggests the same positioning of some amino acids having implications on the structure. This positioning of the amino acids can be as high as 82 amino acids, where most of these positioned amino acids are located in the central portion of the keratin.^{15, 16}

Since keratin is a molecule made of 95 to 102 amino acid residues precise sequencing of the amino acids is required for the structural organization of these molecules. Often cysteine residues maintain the same position in feathers independent of its origin. These important observations are addressed in the work of Fraser et al.¹³ To recall, Figure 4 shows the arrangement of 32 amino acid residues. The decoding of these residues is illustrated in Figure 6. Fraser et al observed that invariant residues of the filament framework, in avian and reptilian keratins, are concentrated in the vicinity of the reversal in chain direction – at the U-turn of the hairpin model.

In fact, comparing the amino acid sequences (Figure 6)²³ of the 32 residues that are believed to constitute the framework, it has been observed that in particular the proline residues were found in the positions in which there are U-turns in the chain direction of the hairpin motif in view of their influence on protein conformation.²⁴

The proline, characterized from its five-membered rings impedes any rotation around the N- α C bond and its presence in positions $i+1$ and $i+3$ of the 32 residues framework represent the nucleating site for the formation of the hairpin structure of the sheet.¹³

The amino compositions of the filament framework segments in avian and reptilian keratins

| n | Avian | | | | | | Reptilian | | | | | | | |
|----|-------|----|----|----|----|----|-----------|----|----|----|----|----|----|----|
| | SA | EF | SF | CF | TV | CS | VC | G1 | G3 | G4 | G5 | Sa | Sb | La |
| 1 | T3 | P | P | P | P | P | P | P | P | P | P | P | P | P |
| 2 | T4 | C | C | C | C | C | V | S | S | S | S | S | S | K |
| 3 | B | L | - | - | - | - | L | C | C | C | C | C | C | G |
| 4 | B | F | V | V | V | V | V | I | I | I | I | I | I | I |
| 5 | B | R | R | R | R | R | D | N | N | N | N | N | N | N |
| 6 | B | Q | Q | Q | Q | Q | T | Q | Q | Q | Q | Q | Q | Q |
| 7 | T1 | C | C | C | C | C | G | I | I | I | I | I | I | V |
| 8 | T2 | Q | Q | Q | Q | P | S | P | P | P | P | P | P | P |
| 9 | T3 | D | A | D | D | D | T | P | P | P | P | P | A | A |
| 10 | T4 | D | D | D | S | D | T | A | A | A | A | S | S | A |
| 11 | B | T | R | R | R | T | D | E | E | E | E | E | E | E |
| 12 | B | V | V | V | V | T | V | V | V | V | V | V | V | V |
| 13 | B | V | V | V | I | V | H | V | V | V | V | T | T | V |
| 14 | B | I | I | I | I | I | V | I | L | I | I | I | I | V |
| 15 | T1 | E | Q | Q | E | Q | Q | Q | Q | Q | Q | Q | Q | Q |
| 16 | T2 | P | P | P | P | P | P | P | P | P | P | P | P | P |
| 17 | T3 | S | S | S | S | P | G | P | P | P | P | P | P | P |
| 18 | T4 | P | T | P | P | P | G | P | P | P | P | A | A | A |
| 19 | B | V | V | V | V | V | C | V | V | V | V | V | V | C |
| 20 | B | V | V | V | V | V | S | V | V | V | V | V | V | I |
| 21 | B | V | V | V | V | V | L | M | V | M | L | V | V | L |
| 22 | B | T | T | T | T | T | T | T | T | T | T | T | T | T |
| 23 | T1 | L | L | L | L | F | I | L | L | L | L | I | I | I |
| 24 | T2 | P | P | P | P | P | P | P | P | P | P | P | P | P |
| 25 | T3 | G | G | G | G | G | G | G | G | G | G | G | G | G |
| 26 | T4 | P | P | P | P | P | P | P | P | P | P | P | P | P |
| 27 | B | I | I | I | I | I | R | I | I | I | I | I | I | I |
| 28 | B | L | L | L | L | L | L | L | L | L | L | L | L | L |
| 29 | B | S | S | S | S | S | I | S | S | S | S | A | S | S |
| 30 | B | S | S | S | S | S | S | A | A | A | A | A | A | A |
| 31 | T1 | F | F | F | F | F | Y | T | T | T | T | S | S | S |
| 32 | T2 | P | P | P | P | P | S | G | G | G | G | C | C | C |

Figure 6. Amino acid compositions of the filament framework segments in avian and reptilian keratins. Figure taken from Fraser et al. paper.²²

Position in the 32-residue framework segment of the sequence.

SA: structural assignment T1–T4 turn residues, B b-sheet residue.

EF: emu (*Dromaius novaehollandiae*) feather, residues 24–55 (O'Donnell, 1973).

SF: seagull (*Larus novaehollandiae*) feather, residues 21–51 (O'Donnell and Inglis, 1974).

CF: chicken (*Gallus domesticus*) feather, residues 21–51 (Walker and Rogers, 1976) The same 32-residue sequence occurs in Duck (*Anas platyrhynchos*)

and Pigeon (*Columba livia*) feather, (Arai et al., 1986).

TV: turkey vulture (*Cathartes aura*) keratin, residues 22–52 (Sawyer et al., 2003). The same 32-residue sequence occurs in Wood Stork (*Mycteria americana*)

(Sawyer et al., 2003).

CS: chicken (*Gallus domesticus*) scale, residues 25–55 (Walker and Bridgen, 1976).

VC: lizard (*Varanus varius*) claw, residues 36–67 (Inglis et al., 1987).

G1: gecko (*Tarentola mauritanica*) skin protein component GE-GPRP 1–2, residues 93–124 (Toni et al., 2007a,b).

G3: gecko (*Tarentola mauritanica*) skin protein component GE-GPRP 3, residues 91–122 (Toni et al., 2007a,b).

G4: gecko (*Hemidactylus turcicus*) skin protein component GE-GPRP 4, residues 89–120 (Toni et al., 2007a,b).

G5: gecko (*Hemidactylus turcicus*) skin protein component GE-GPRP 5, residues 82–113 (Toni et al., 2007a,b).

Sa: snake (*Elaphe guttata*) keratin protein (Sn-gprp-5), residues 56–87 (Valle et al., 2007).

Sb: snake (*Elaphe guttata*) keratin protein (Sn-gprp-2-3 and Sn-gprp-4), residues 5 6–87 (Valle et al., 2007) (Reproduced from ref.),¹³

2.1.2 Keratin in Hair.

Determination of the keratin structure contained in hair imposes the same difficulties as the keratin contained in feather. This is related to the coexistence of helical and sheet structures.

On the basis of the principles proposed by Huggins et al.²⁵ it is possible to unravel the development of the alpha helix structure in general, which is linked with the maximization of hydrogen bonding between the amide motifs. Thus each polypeptide chain in α -keratin has an internally hydrogen-bonded helical structure. For the resolution of the α -keratin structure Huggins et al. made use of some of the structural principles (close packing, maximum hydrogen bonding, the tendency of such groups to be surrounded in like manner, and the approximate constancy of inter-atomic distances and bond angles) that Pauling and Corey^{26, 27} used to determine the 13-atom-ring helix structure of synthetic polypeptides. The sharpness of some meridional and equatorial x-ray reflections point out that molecular helices are stacked, with parallel axes, in a close-packed manner.

The helices are grouped into “3-stacks”, in which each chain is rotated and shifted vertically over a distance equal to the helix pitch ($\sim 5.15 \text{ \AA}$), relative to the other two. This shift can be also justified by meridional x-ray reflection at this spacing. The 3-stack structure repeats after three turns, and each of these units are grouped into 9-stacks and these into 27-stacks (all twisting), giving a crystallographic unit containing 81 chains, as shown in Figure 7.

The dimensions of the 27-stacks agree well with estimates of the “effective radius” of microfibrils. The changes in Bragg spacing during fiber extension are explained due to the alternation of zones having high and low cross-linking, for example between disulphide bonds. However, the proposed model by Huggins et al. does not consider the local irregularities in α -keratin such as for example the irregularities related to the sequencing of residues.

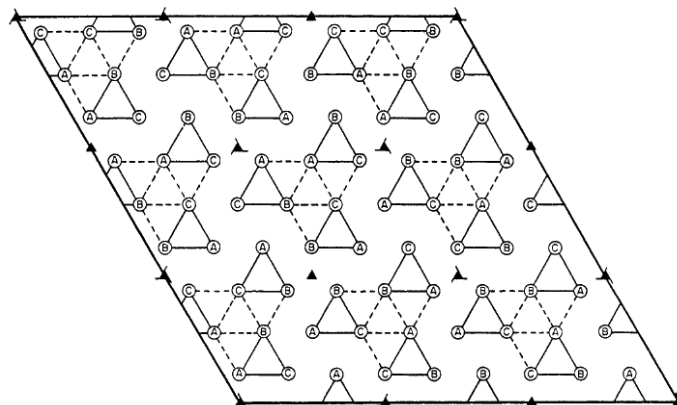


Figure 7. A model for the α -keratin structure contained in hair. It is reported a crystallographic unit containing 81 chains packed in 9-stacks arrangement.²⁵

2.1.3 Influence of water on hydrolysis of Keratin

Keratin present in natural materials is insoluble in most common solvents and is resistant to proteolytic enzymes. This unique behavior is attributed to a large number of disulphide bonds that contribute to the formation of a rigid molecular conformation resistant to several chemicals. Thus dissolution of keratin requires oxidation, sulphitolysis or reduction of the disulphide bonds. It is also to be realized that the dissociation energy of S-S bond in alkyl disulphides is about 293 kJ/mol.⁵³ The oxidation of cystine disulphide bond is possible when treating it with organic peracids like performic acid. The oxidation mechanism is complex and it involves a number of unstable oxidation products as intermediates.^{17, 18}

Sulphitolysis and oxidative sulphitolysis have been used to prepare the S-sulpho derivatives of feather keratin.^{17, 18} The reaction proceeds optimally at alkaline pH (above pH 9) and oxidizing agents (like cupric ions or tetra thionate) are usually included to convert all cysteine residues to the corresponding S-sulphonate derivatives.²⁸

Reduction by thiols represents the most used method for cleaving of the disulphide bonds. It is a reaction with two successive nucleophilic substitutions, with the formation of a mixed-disulphide intermediate which reacts subsequently with another thiolate to assure the cleavage of the S-S bond of cystine.²⁹ However, the dissolution by 2-mercaptoethanol in the presence of a denaturant, such as urea and subsequent alkylation with iodoacetic acid, has become a standard procedure for various types of keratin.

We have adopted a different approach using water as solvent for hydrolysis of the keratins, unlike dissolution. Here we report the hydrolysis of keratin from sustainable sources in water under specific pressure-temperature conditions. Water is the most important fluid on our planet and the simplest hydrogen-bonded material. Although water is similar to simpler fluids in its van der Waals attractions and repulsion, it is interesting due to its ability to form hydrogen bonds and to vary their efficiency with temperature, pressure, ionic concentration and their sizes.³⁰ To recall, a water molecule in its utmost simplicity is formed by two hydrogen atoms and an oxygen atom. The hydrogen bond can form between molecules of water because the oxygen of one water molecule has two lone pairs of electrons, each of which can form a hydrogen bond with hydrogens on two other water molecules. When more molecules are present, more bonds are possible, so that every water molecule is H-bonded with up to four other molecules.

The presence of hydrogen bonding in abundance in the low molecular mass of water provides some unique features that are significantly different from liquids where the hydrogen bonding is absent. For example the bulk water shows a boiling point and a freezing temperature, a surface tension and a vaporization enthalpies all strongly influenced by the hydrogen bonding efficiency at different temperatures. Moreover, it has a high dielectric constant and exists in numerous crystalline polymorphs. In its most known crystalline form the ice has a lower density than liquid water whereas most solids are denser than their corresponding liquids.³¹ Ultimately, it has a large heat capacity that well

explains why the oceans are considered the vastest thermostats governing the planet's temperature.

All these peculiarities lead to the study of water modeling. Thus, starting from these physical properties different models of water were studied and proposed, as for example the Mercedes-Benz logo model (Figure 8). A two dimensional model was derived from Ben-Naim's model³¹ in which each molecule of water is represented as a two dimensional disk with three radial arms (like Mercedes Benz logo).

The energy of interaction between two water molecules is the sum of Lennard-Jones attraction and repulsion and an orientation-dependent hydrogen bond interaction.

According to this model, hydrogen bonds are possible when an arm of one water molecule aligns with an arm of another water molecule. Although this model is two dimensional and for this reason presents some gaps, it properly explains some properties correlated to hydrogen bonding.

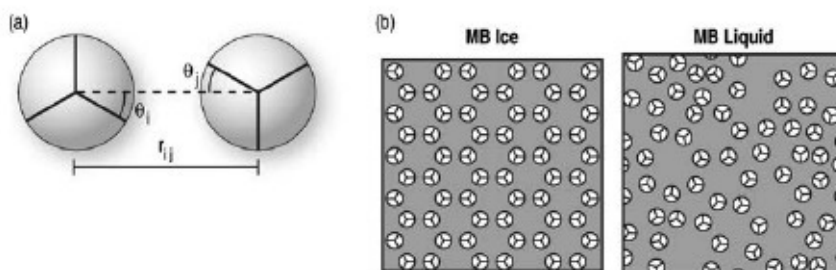


Figure 8. (a) MB logo water model. Each water is a LJ disk, with three hydrogen bonding arms. (b) (Left) MB ice, the stable state at low temperature. (Right) A typical liquid configuration at $T^* = 0.20$, density $\beta^* = 0.9$. Figure taken from Dill et al. paper.³¹

Water can assume different states of matter and the most common ones are solid (ice), liquid (water) and gas (steam). Variations of temperature or pressure, can promote the passage from one state to another. Above 100 °C and with a

pressure sufficiently high to maintain the liquid state, water is in the “superheated state”. In these conditions water has an expanded structure in which intermolecular interactions like hydrogen bonds become weak. Due to the high mobility caused by the high temperature and weak hydrogen bonds the “superheated water” becomes a very powerful solvent. This “superheated state” of water is highly effective in the hydrolysis of keratins to obtain oligopeptides.

32

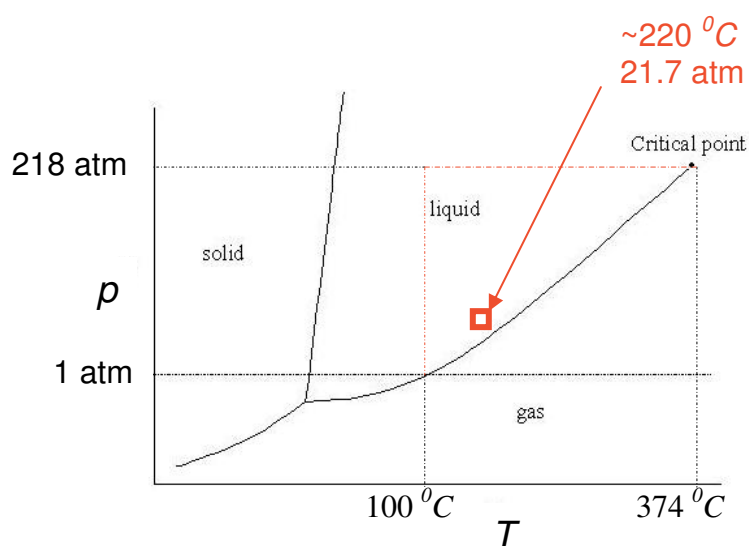


Figure 9. Phase Diagram of water.

Thus in a polymer where hydrogen bonding exists, as for example aliphatic polyamides³³ and keratin³², the superheated water with its enhanced diffusion permeability, can act as a solvent and lead to the complete dissolution and/or hydrolysis of such hydrogen bonded materials.

2.2 Experimental section

2.2.1 Materials

2.2.2 Sample preparation

Chicken feathers and hair used for the experiments were cleaned following a modified procedure based on a standard test method (ASTM D584).³⁴ For simplicity we refer to barbs feather in the procedure described below but the same procedure has been used for hair keratins. In this procedure feathers (0.5g) are immersed in a scouring solution which is composed of 2L of water at 50°C, containing 4g of sodium carbonate, 6g of Brij35 a non-ionic detergent, and 4g of polyphosphate which is added to complex divalent cations. The feathers are removed from the solution after 24 hours and were washed with hot water. The wet feathers are then left to dry in a fume hood. The barbs of dry feathers are cut into small pieces. To remove grease, dry cut feathers are immersed in petroleum ether at room temperature for 12 hours. The feathers are filtered from the ether solution and are left to dry in the fume hood. Barbs from the dry feathers or hair after the pre-treatment are sealed in a steel pressure cell with water at a concentration of 20 mg/mL and placed in a preheated oven. The initial conditions used have been chosen referring to Yin et al.³². Since the steel vessel is sealed, pressure in the cell increases with temperature, the increase occurs due to building up of the vapor pressure. At 220 °C, the pressure in the vessel reaches to ~22 bar. Hydrolysis occurs on leaving the sample for 2 hours at 220C. After cooling of the pressure vessel under flowing water to room temperature, a suspension with only a small amount of feather residue (0.4 mg) is obtained. The obtained solution is composed of oligopeptides as described in the next paragraph. Part of this solution is used for crystallization experiments, and a part for fractionation and sequencing of these oligopeptides. The latter is required for sequencing of the amino acids. The hydrolysis of the feather barbs or hair can be affected by varying physical parameters of the superheated water

treatment, like temperature or heating time of the process. For this reason, several solutions have been prepared using different conditions (Table 2).

| Solution N. | Concentration of feather barbs in water (mg/mL) | Temperature of superheated water process (°C) | Heating time (min) |
|-------------|---|---|--------------------|
| 1 | 20 | 220 | 60 |
| 2 | 20 | 220 | 120 |
| 3 | 20 | 260 | 60 |
| 4 | 20 | 180 | 120 |
| 5 | 20 | 260 | 120 |
| 6 | 30 | 180 | 60 |
| 7 | 30 | 180 | 120 |
| 8 | 30 | 220 | 60 |
| 9 | 30 | 220 | 120 |
| 10 | 30 | 260 | 120 |
| 11 | 10 | 180 | 60 |
| 12 | 10 | 180 | 120 |
| 13 | 10 | 220 | 60 |
| 14 | 10 | 220 | 120 |
| 15 | 10 | 260 | 120 |

Table 2. List of solutions prepared for the experiments.

2.2.3 Crystallization. Crystals from the prepared hydrolyzed solutions have been obtained by leaving drops of these solutions to dry on clean glass substrates. Birefringent entities are observed to grow by optical microscopy between crossed polars (Figure 10).

2.2.4 Solid State Peptide Synthesis (SSPS). Solid State Peptide Synthesis can be defined as the process in which a peptide is constructed by the successive addition of protected amino acids constituting its sequence, anchored via its C-terminus to an insoluble polymer. To confirm the determined sequence of the amino acids of some oligopeptides, obtained after the hydrolysis in “superheated water”, the peptides were synthesized on a Labortec SP4000 or a Labortec SP6450 semi-automatic peptide synthesizer. Peptide couplings were

followed to completion using the Kaiser test.³⁵ Films of the synthesized peptides were prepared by dissolving powders of the synthesized peptides in DCM (dichloromethane) or DMF (dimethylformamide). These experiments were performed in Nijmegen at Radboud University in collaboration with Prof. van Hest's group.

2.2.5 Synthesis of 1 KDa oligopeptide Val-Val-Val-Thr-Leu-Pro-Gly-Pro-Ile-Leu.

The peptide was synthesized using standard Fmoc peptide synthesis on a breiphol resin. (REF 27.28 tesi maier) Peptide coupling was achieved using 3 equivalents of Fmoc amino acid and diisopropylcarbodiimide (DIPDCI, 3.3 eq.) with N-hydroxy benzotriazole (HOBt, 3.6 eq.) in DMF. The resin was swollen in DMF for 20 minutes prior to use. The Fmoc-group was removed using piperidine in DMF. After coupling of the final amino acid the Fmoc – protected peptide on the resin was washed thoroughly with DMF, dichlorometane, methanol and diethyl ether. The resin was dried in vacuum and divided in batches. The peptides were cleaved from the resin by treatment with trifluoroacetic acid /water (95/5 v/v) for 4 hours, and after precipitation in diethyl ether the peptide was lyophilized from acetic acid. The peptides were characterized as reported in the next paragraphs.

2.2.6 Synthesis of 1 KDa alkylated tail-oligopeptide C₁₆H₃₁O-Val-Val-Val-Thr-Leu-Pro-Gly-Pro-Ile-Leu.

The procedure similar to that described earlier was used for the synthesis of the peptide. After coupling of the final amino acid, and removal of the Fmoc protecting group by using piperidine in DMF (20% v/v), 3 equivalents of the aliphatic carboxylic acid were dissolved in dichloromethane, and 3.6 equivalents of HOBt (1M in DMF) were added. After mixing, 3.3 equivalents of neat of DIPDCI were added. The solution was added to the resin, and the resin with the solution was agitated for 18 hrs.

2.2.7 Synthesis of 1 KDa aliphatic-amide tail-oligopeptide $N_9H_{102}C_{58}O_{12}$ -Val-Val-Val-Thr-Leu-Pro-Gly-Pro-Ile-Leu.

The same procedures for the peptide synthesis, and coupling of the aliphatic amide tails, described above for the synthesis of the alkylated peptide were used.

2.2.8 Characterization techniques.

2.2.8.1 Optical Microscopy (OM). The self-assembling process of oligopeptides in the hydrolyzed solution was observed using optical microscopy. For this purpose crossed polarizers on a Zeiss Axioplan 2 microscope equipped with a Zeiss AxioCam camera were used. The images were analyzed with the AxioVision v3.0.6 software. Thermal behavior of the self-assembled oligopeptides in the form of crystals was investigated by OM equipped with a Linkam TMS94 hotstage. Heating/cooling cycle of the sample was performed in the temperature range of 30-180 °C.

2.2.8.2 Thermogravimetric Analysis (TGA). Crystals from the hydrolyzed solution and finely cut barb chicken feathers were analyzed in order to determine their thermal stability. TGA experiments were performed on a TA Q500 instruments (TA Instruments). Samples with a typical weight of 5 mg were heated with 10 °C/min to 600 °C under N_2 atmosphere. Synthesized oligopeptides were subjected to the same procedure.

2.2.8.3 Differential scanning calorimetry (DSC). The thermal behavior of the crystals from the hydrolyzed solution, and the synthesized oligopeptides was investigated using a TA Instrument Q1000 calorimeter. Hermetically sealed aluminum pans were used with a typical sample weight of 5 mg. The samples were subjected to heating/cooling cycles with a rate of 10 °C/min. No crystallization or melting phenomena were observed during the heating/cooling cycles in the temperature range of 30-220 °C.

2.2.8.4 Fourier Transform Infrared Spectroscopy (FTIR). Fourier Transform Infrared spectra (FT-IR) were obtained using a Varian 610-IR

spectrometer equipped with a FT-IR microscope. The spectra were recorded in a transmission mode with a resolution of 2 cm^{-1} . Chicken feather powder obtained as described and crystals obtained from the super heated water treatment were analyzed on a zinc selenium disk. Powders of the synthesized peptides were also analyzed on a zinc selenium disk. Varian Resolution Pro software version 4.0.5.009 was used for the analysis of the spectra.

2.2.8.5 Liquid chromatography and Mass spectrometry (LC-MS-HPLC-MS²). To determine the molar mass range of the oligopeptides in the water solution and to fractionate the oligopeptides with discrete molar masses, liquid chromatography (LC) experiments with the Finnigan LTQ a 2-dimensional linear quadrupole ion trap coupled to a Mass spectrometer (MS) and with a Gilson Reverse phase Chromatographer (HPLC) with a Reprisil analytical column 100 C18 3μ (150X3 mm) and a preparative column Reprisil 100 C18 5μ (250X10 mm) were performed. Water and formic acid, and water and acetonitrile were used as solvents for these experiments. The volume of sample solutions was chosen such that the concentration of the feather solution was about $100\text{ pmol}/\mu\text{L}$. Solutions of the matrix and the sample were mixed in a ratio of 1:1 vol %.

To determine the amino acid sequencing of oligopeptides, having molar mass of 1KDa, MSⁿ scan experiments were performed with Mass Spectrometer. In the simplest case of a full scan, the Finnigan Ion Trap follows two steps only, collection and ejection of the ions preformed in ionisation source, during a MS² a single ion with a chosen m/z is isolated from the group. In peptide, fragmentation of the selected ion having specific molar mass, gives information on the amino acid sequences that constitutes the peptide

2.2.8.6 Wide Angle X-Ray Diffraction (WAXD). X-ray characterization was performed at the European Synchrotron Radiation Facility (ESRF) in Grenoble (France). Wide Angle X-ray scattering (WAXD) experiments were performed at the beamline BM26/DUBBLE. The size of the X-ray beam was approximately $200\text{ X }200\text{ }\mu\text{m}^2$ with a wavelength of 0.755 \AA . For the

measurements a Frelon detector having 2048 X 2048 pixels and a pixel size of 48.82 X 48.82 μm^2 at a sample detector distance of 237.49 mm was used.

2.2.8.7 Atomic Force Microscopy (AFM). The AFM investigations were performed on the synthesized peptides by using MFP-3D (Asylum Research) and PPP-NCHR probes (Nanosensors) tips. The AFM was operated in tapping mode in air. The resonance frequencies applied were 115-190 kHz.

2.3 Results and Discussions.

2.3.1 Crystallization and self assembling process of oligopeptides.

Influence of dissolution temperature

When a drop of a solution of a hydrolyzed protein is left to dry on a clean glass substrate, growth of needle-like birefringent entities between cross polars is observed. Crystal growth is observed with time (days) at room temperature.

Typical optical micrographs taken for crystals obtained from solution 2 (see Table 2) are shown in Figure 10. Nucleation of the crystals occurs from any heterogeneity present on the substrate. Crystallization leads to the formation of dendritic-like crystals, an example of diffusion-controlled pattern generation in a non-equilibrium system.³⁶ Here, we may assume that the growth rate is controlled by the evaporation rate of water. In fact, the diffusion rate of the keratin molecules to the growing crystal interface has an important consequence on the crystal growth.³⁷ The crystals are embedded in a non birefringent matrix which is waxy in appearance. The waxy matrix could be attributed to some lipids and fatty acid residues that were not completely removed during the pre-cleaning treatment of the feathers. These residues play an important role in the self assembling of oligopeptides.³⁸ It is known that lipids or fatty acids are determinant in dendritic-like crystallization of peptides, similar to crystallization of bacterial protein streptavidin on layers of biotinylated lipids.³⁹⁻⁴¹ The presence of such impurities has the ability to manipulate crystal morphology and influence the ramification of the dendrites.⁴² Different

morphological structures are enhanced by varying the peptide/lipids-fatty acid concentration. This illustrates the effect of crystal growth instabilities arising due to the diffusion controlled crystallization.⁴³

To prove the influence of lipid/peptide concentration on the self-assembling process of the peptides, different dissolution conditions listed in Table 2 have been applied. For example, milder hydrolysis conditions such as a lower dissolution temperature have been considered to ensure the presence of larger molecules of oligopeptide. The larger peptides represent a non-crystallizing impurity and in a transport-limited system, such impurities diffuse slowly, preventing their accumulation and the consequent crystallization.

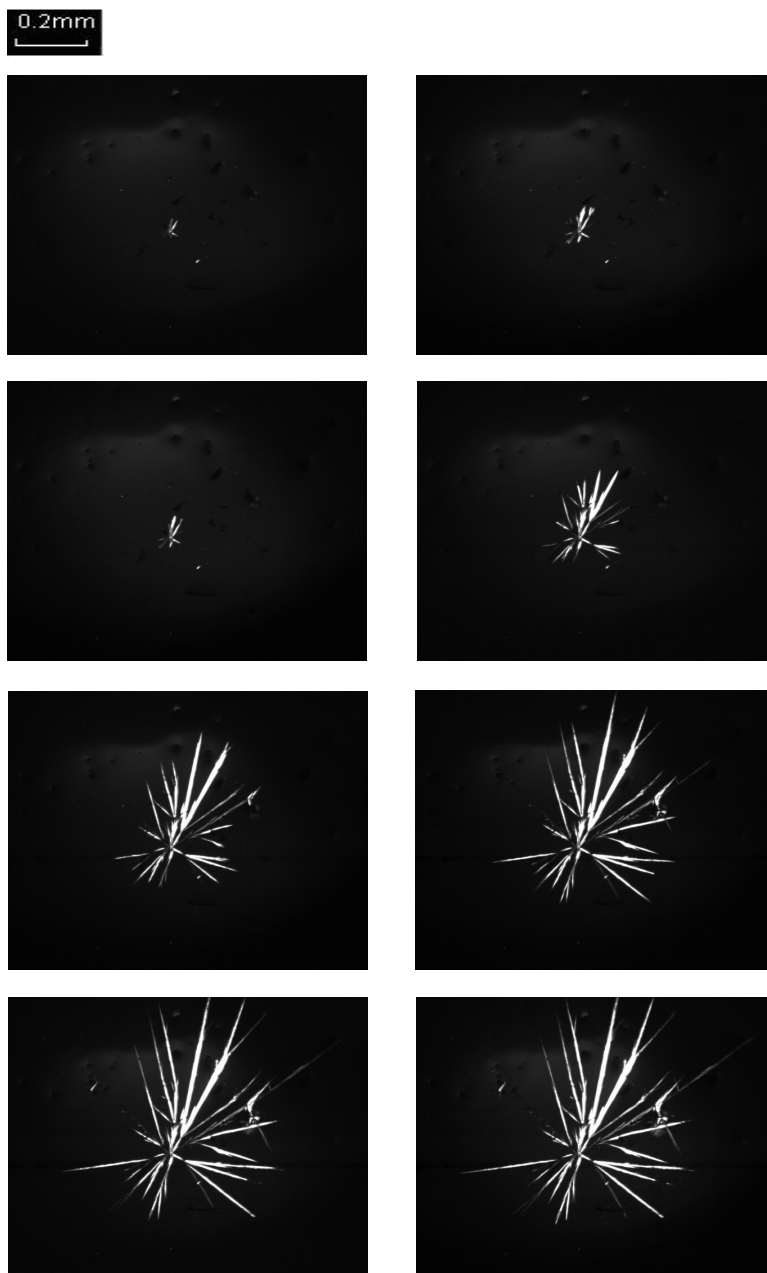


Figure 10. Crystal growth of oligopeptides obtained on dissolution of chicken feathers in super heated water. The solution was prepared from feather concentration of 20mg/ml treated at 220°C for 120min. The crystals grow with time (days) when left at room temperature.

In Figure 11, it is shown that no crystals were formed for the samples prepared from Solution 7 and Solution 12 (see Table 2). Both samples were heated below 180°C for 120 min. The different concentration of the two solutions (10 mg/ml-30mg/ml) results to be marginal compared to the effect of the lowered temperature. A similar result is presented in Figure 12, where the samples from solution 6 (30mg/ml) were prepared by heating the suspension to 180°C and leaving isothermally for 60 min.

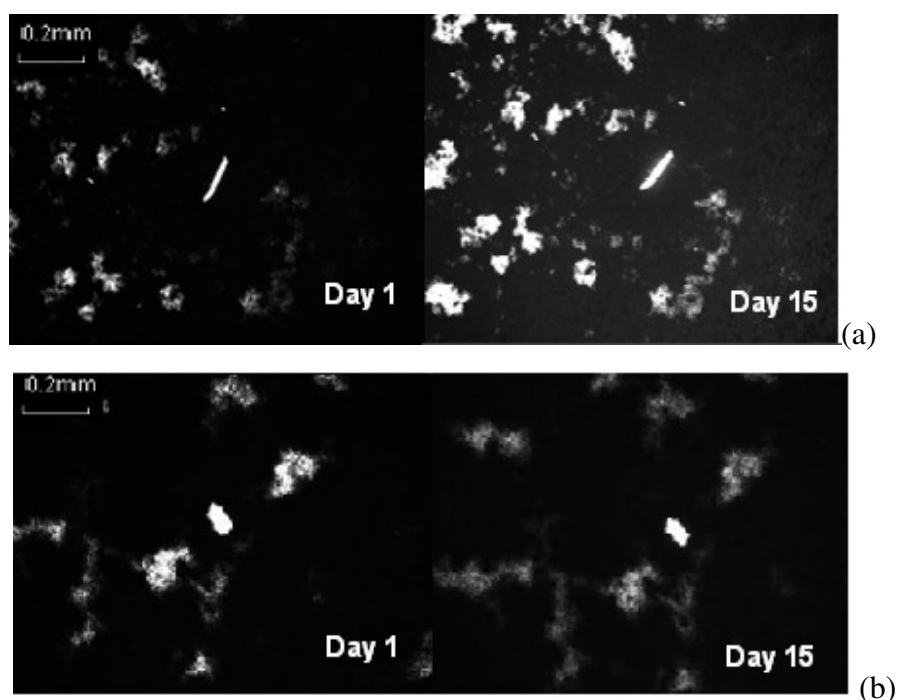


Figure 11. Optical micrographs obtained during evaporation process of solution 7 (a), and Solution 12 (b). Both solutions were prepared at 180°C. The samples were left for 120min under isothermal condition. The concentration of solutions 7 and 12 was 30mg/ml and 10mg/ml, respectively.

The comparison of optical micrographs in Figures 10 and 11 clearly demonstrate the influence of lowering the temperature on the dissolution process and the resultant self-assembling process. The lowering of the temperature of the process is likely to influence the length of oligopeptides and

the associated self-assembling process. In contrast, on increasing the temperature of the process or time it is possible to hydrolyze oligopeptides to the extent that single platelets of amino acids can be obtained, changing the morphology from dendritic to plate-like (see Figure 14). The complete hydrolysis occurs, ultimately resulting in a solution containing amino acids, by preparing a solution of dried chicken feathers in a 6 mol/L HCl solvent, and by heating the suspension to 110°C and leaving isothermally for 22 hrs. Crystals prepared from solution 3 (Figure 13), appear smaller than the ones obtained at lower temperatures.

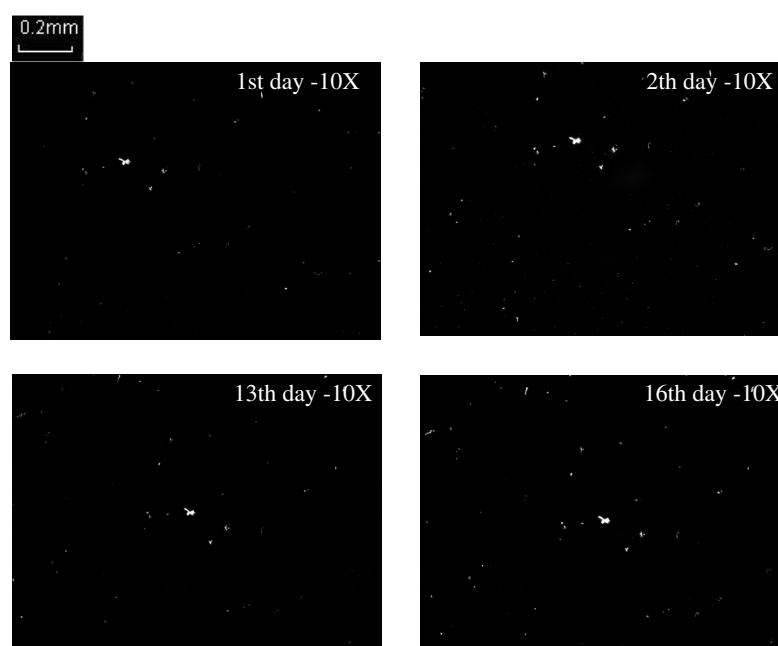


Figure 12. The optical micrographs of the sample of solution 6, obtained from 180°C superheated water for 60min. The concentrations of Solutions 6 was 30mg/ml. The light particles were dusts that clearly showed the same position on the samples. Comparison with Figure 11 shows influence of dissolution time, under isothermal condition, on the self-assembling process at room temperature.

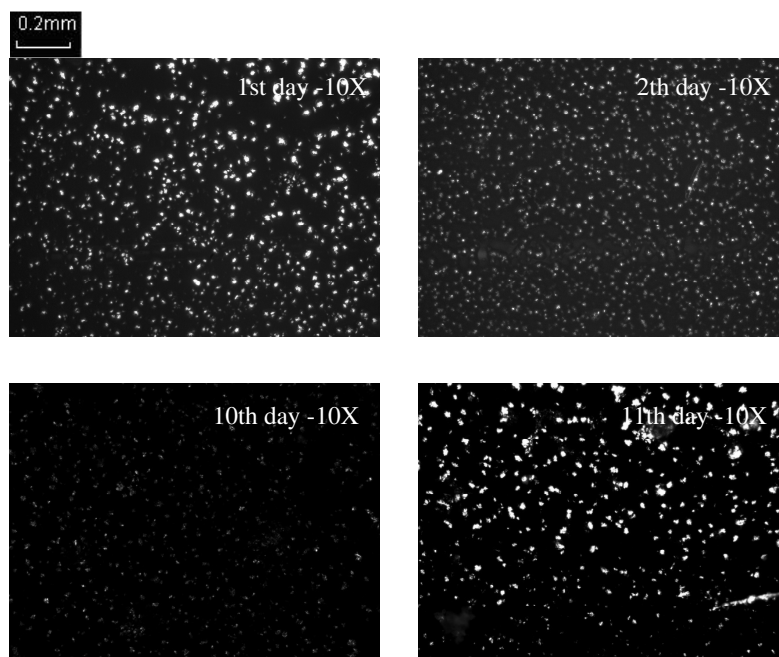


Figure 13. The optical micrographs of the sample of solution 3, obtained from 260°C superheated water for 60min. The concentration of Solution 3 was 20mg/ml. Crystals prepared from solution 3, appear smaller than the ones obtained at lower temperatures.

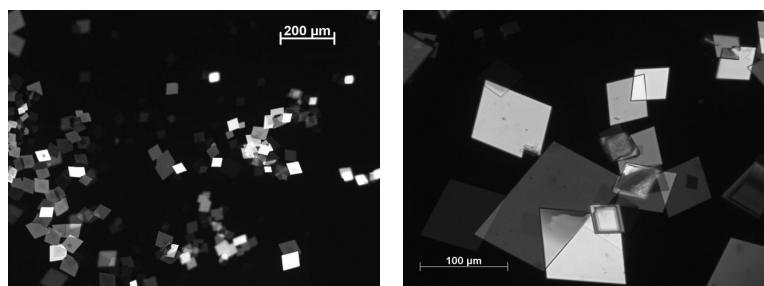


Figure 14. The optical micrographs of single crystals of an amino acid viewed in between cross-polars. The sample has been prepared from a solution of dried chicken feathers in a 6mol/L HCl solvent, obtained by heating the suspension to 110°C and leaving isothermally for 22 hrs.

Influence of feather concentration in water:

Crystal growth is also strongly influenced by the feather concentration in the water solution. Figure 15 shows the self-assembling process of oligopeptides during hydrolysis of different amounts of chicken feather barbs hydrolyzed in water (5 and 50 mg/mL) at 220 °C for 120 min. When left to crystallize in a fume hood at 25 °C for 2 weeks a drop of solution, crystal growth of self-assembled oligopeptides is observed. From the optical micrographs it is evident that the crystal density strongly depends on the oligopeptide concentration, influencing the overall crystal growth.

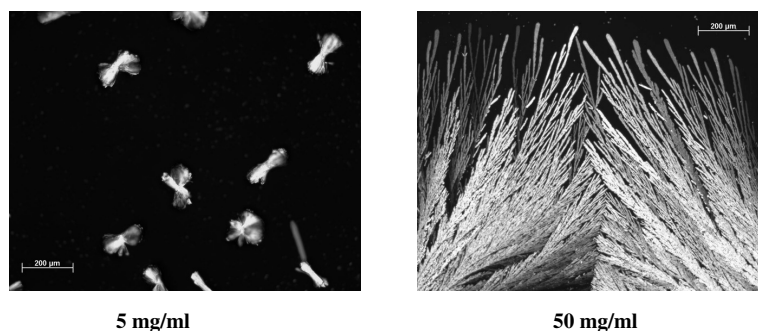


Figure 15. Chicken feather barbs of varying amounts in water (from 5 (left) to 50 (right) mg/mL) are hydrolyzed at 220 °C for 120 min. A drop of solution placed on a glass slide is left to crystallize in fume hood at 25 °C, for 2 weeks. Optical micrographs show self-assembly of the oligopeptides with increasing concentration of the oligopeptides in the water solution. Crystal density increases with the increasing concentration.

2.3.2 Morphogenesis; self assembling process of hair keratin

To elucidate the influence of the amino acids sequence of the keratin on the self-assembling process of peptides derived by its hydrolysis and to strengthen the concepts of morphogenesis, we made use of hair as an alternative keratin source and followed the self assembling process after hydrolysis along the route adopted for the feathers. Figure 16, depicts the self-assembling process of the oligopeptides obtained after hydrolysis of the hair keratin. To our surprise the oligopeptides tend to self assemble in the morphology expected for the growth

of hair, confirming the influence of the amino acids sequence of the peptide residues on the crystallization behavior.

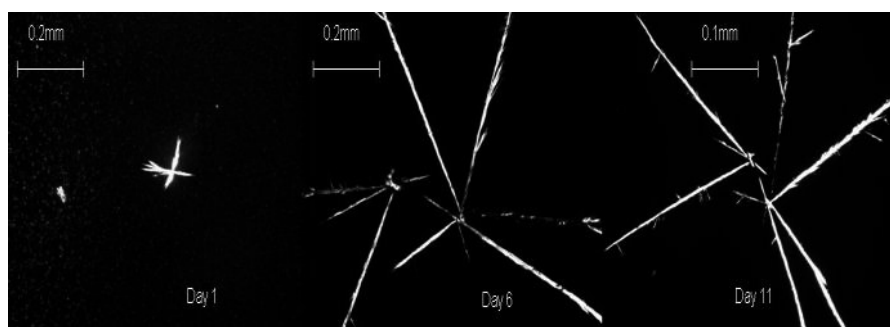


Figure 16. The optical micrographs of crystal growth of oligopeptides obtained on hydrolysis of hair in super heated water. The solution was prepared from hair concentration of 20 mg/ml in water at 220 °C for 120 min. The crystals grow with time (days) when left at room temperature.

2.3.3 Thermal stability of oligopeptides

The thermal behavior of the crystals obtained from hydrolyzed solutions was investigated by OM equipped by a Linkam TMS94 hotstage and by several techniques that will be described later. In Figure 17 the thermal behavior of crystals obtained from hydrolysis of the solution 2 is shown. Upon heating the crystals tend to loose birefringence and completely disappear around 165 °C. On cooling the samples, no birefringent entities reappeared confirming the degradation of the crystals in this range of temperature as was also observed by TGA experiments. The melting and re-crystallization of these crystals has not been observed in the entire temperature range considered. This data is consistent with DSC data from experiments on the same crystals.

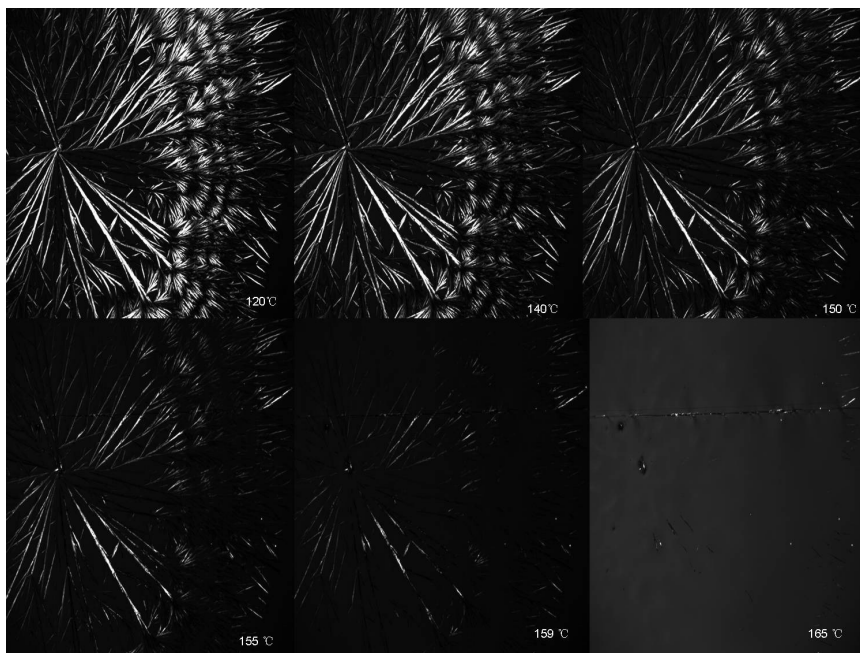


Figure 17. The optical microscopy micrographs on heating of crystals obtained from solution 2. On heating crystals tend to lose birefringence and completely disappear around 165 °C.

2.3.4. Sequencing and Fractionation of oligopeptides obtained from feather keratin.

LC-MS experiments were performed to determine the molar mass of the oligopeptides obtained on dissolution of feathers in water. Analysis of the solution indicates the presence of peptide sequences with different molar masses. In particular as shown in Figure 18, a water solution of feather keratin with a concentration of 20 mg/mL, obtained after hydrolysis in “superheated water” at 220 °C for 120 min, is rich in peptides with molar mass of around 1 kDa. Thus, assuming an average molecular weight of 100 for each amino acid, the obtained peptide has a sequence of 10 amino acids in length, suggesting that on hydrolysis a considerable proportion of the amino acid sequence is conserved. In all mass spectra for the different solutions, it is possible to observe the presence of this predominant signal corresponding to oligopeptides

with a molar mass of about 1 KDa. The mass spectra are reported in the Appendix A section (Figure S11-S14).

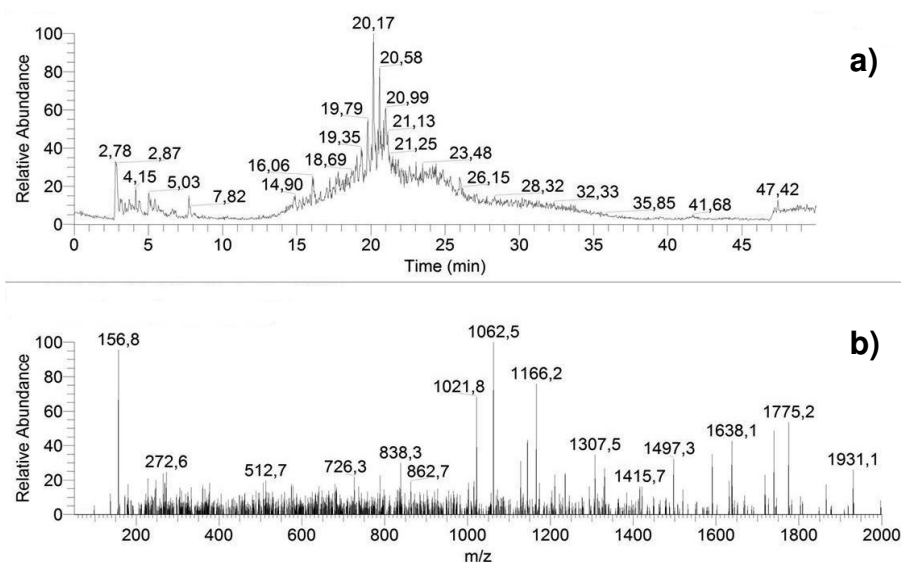


Figure 18. (a) LC chromatogram performed on solution 2 (b) and relative MS spectrum

Unlike the results of the optical microscopy in which the processing parameters applied in the preparation of the different solutions result are determinant in the morphology of the crystals, MS data seem to be not affected by the different processing parameters.

In particular, according to optical microscopy data shown in Figures 11, 12, the lower processing temperature does not permit the formation of crystals because in these conditions it was anticipated that keratin chains can only break into several larger oligopeptides that obstruct the crystallization. This observation is not justified by MS data. According to the MS analyses the masses of oligopeptides seem to have the same value and consequently the same length. Thus the self assembling behavior in the hydrolyzed keratins appears to be promoted by the presence of complex residues that may include fatty acids etc described previously.³⁸

It is quite clear analyzing MS data that the “superheated water” process, even though it promotes the formation of oligopeptides with a mass of 1 KDa, also enhances the formation of oligopeptides with a broad distribution of masses (Figure 18b). For example, as shown in Figure 20, values of the mass of around 200 Da were sometimes found to have a larger relative abundance. The results confirm the complexity of this process.

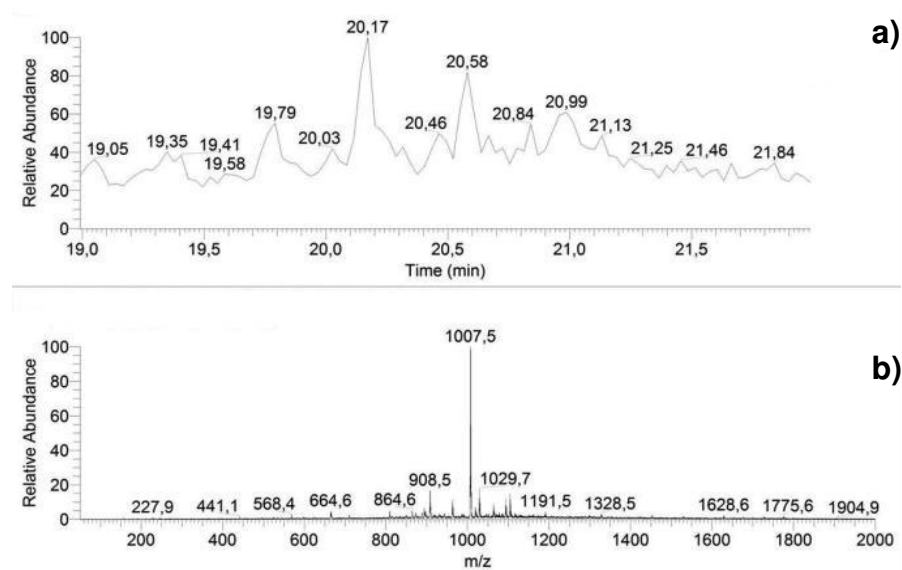


Figure 19. (a) A selected retention time zone of LC chromatogram performed on 20 mg/ml water solution of chicken feathers (b) and relative MS spectrum.

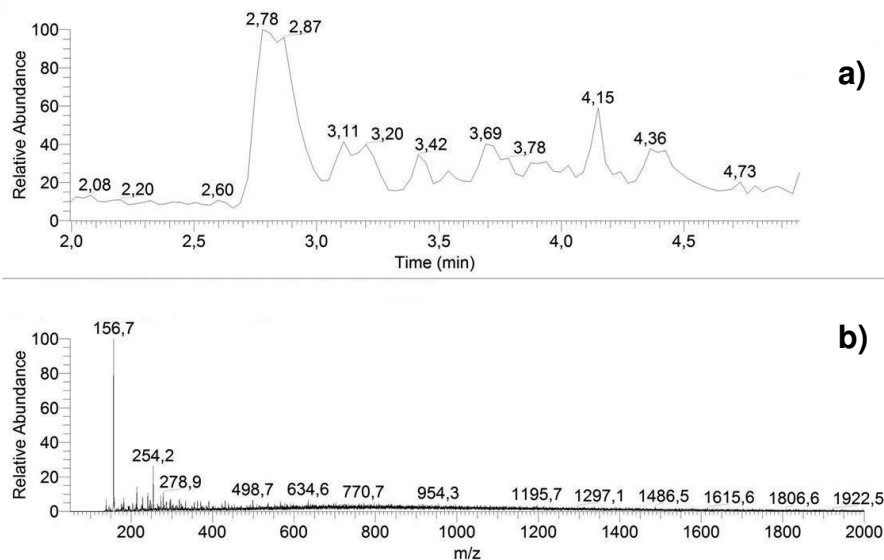


Figure 20. (a) A selected retention time zone of LC chromatogram performed on solution 2 (b) and relative MS spectrum.

The formation of oligopeptides could in fact be attributed to either the simple breaking of the keratin backbone under these conditions or it could be triggered by a more complicated mechanism in which the breaking comes with a rearrangement of the oligopeptide residues obtained from keratin. For this reason LC-MC, HPLC and MS-MS data will be reported and commented below.

Similar to optical microscopy data, the situation appears different for hair solutions. In fact the main signals present in mass spectra of Figure S15-S17 in the Appendix A have a different value between 960 and 990 Da, and in particular the mass distribution for the different hair solutions appear to be reduced compared to the feather keratin solutions previously considered.

Clearly, this could be attributed to the different structure and amino acid sequencing of hair keratin. The predominant and repeated presence of oligopeptides with a molar mass of about 1KDa in all the different prepared and

analyzed solutions focused our attention on the possibility of investigating the eventual mechanism that occurs during hydrolysis in “superheated water”. To investigate and better understand this process, we decided to fractionate this 1 KDa oligopeptide and determine the sequence of amino acids that constitute it. For this reason experiments with HPLC and LC-MS were performed. In particular, LC-MS experiments were useful to understand the retention times of the solutions richer in oligopeptides of 1KDa. Reversed Phase-LC and or RP-HPLC operate on the principle of hydrophobic interactions, which originates from interactions between the stationary phase contained in the column, and the mobile phase and sample components that moves through the column. Therefore the retention time is longer for molecules which are less polar, while polar molecules elute more readily (early in the analysis).

Initially a first HPLC experiment was performed on a solution of 20 mg/ml prepared with the usual process at 220 °C for 2 hours. The sample was diluted according to the procedure reported in the experimental section.

In Figure 21 the result of this experiment is reported. It is possible to observe a quite complex chromatogram, characterized by the presence of many peaks attributable to different eluates. The composition of the different eluates is responsible of their different retention times.

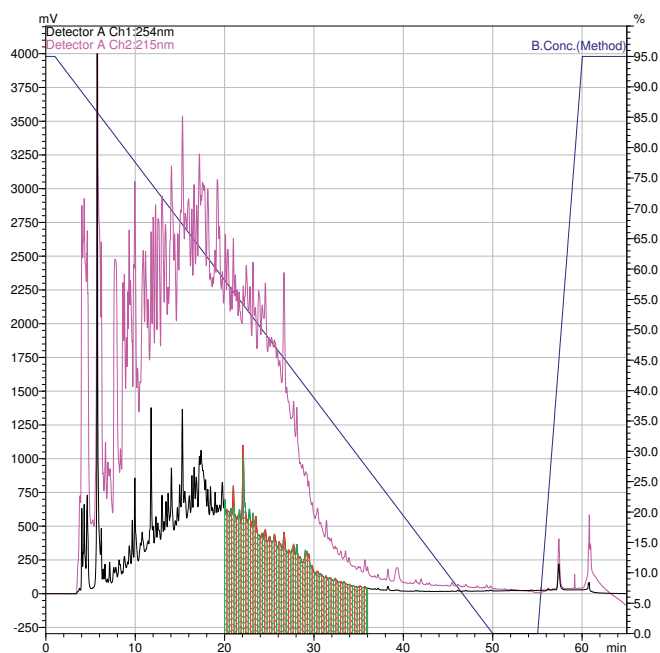


Figure 20. HPLC chromatogram performed on solution 2.

To find out which of these eluates contains the larger amount of 1KDa oligopeptides, several solutions with the same features were prepared and analyzed with LC-MS. A singularity of LC-MS analysis is the possibility of collecting all possible MS spectra for all the different eluates. Thus using this technique it becomes very easy to identify the composition of each eluates.

In Figure 19(a), the chromatogram obtained by LC-MS experiments performed for solution 2 is shown and in particular refers to eluates having a particular retention time of about 20 min. The correlated MS spectrum of Figure 19(b) confirms that the composition of the solution with a retention time of about 20 min is rich in oligopeptides with a molar mass of 1 KDa. Varying the retention time, the eluates clearly present a different composition, Figure 20.

This information, as written before, was used to collect the desired oligopeptide via fractionation with HPLC. In fact, once the retention time of the solution was known, it was possible to get all the different solutions with different composition of peptide residues, using a fraction collector.

The collected fraction rich in 1KDa oligopeptide is the object of the characterization reported in the following paragraph. To better understand the mechanism that leads to the dissolution of keratin, some experiments were performed with mass spectrometer in order to determine the sequence of amino acids of oligopeptides as the one with a Molar Mass of 1KDa. In the simplest case of a full scan the Finnigan Ion Trap only follows two steps, collection and ejection. The trap opens and all of the ions that are focused through the ion optics, regardless of mass, are collected. Then all of the ions are scanned out of the trap at a specified rate and detected, resulting in a full scan. In the case of a MSⁿ scan, only one of these ions is of interest. The instrument applies another step to the process, the isolation. Using the mass spectrometer for a MSⁿ all of the ions are collected, as in the case of a full scan, but then a single m/z is isolated from the group. In the end, the ions are scanned out as before.

This operation gives the possibility to get the sequencing of a particular chosen ion mass because the purpose of this step is to fragment ions for MSⁿ experiments. The starting point for an MSⁿ scan would be that the isolated ion is fragmented into product ions during the excitation step. Finally, the remaining fragments can then be ejected from the trap and detected.

In Figure 22, a MS² spectrum is presented in which it is possible to observe the fragmentation of the oligopeptide with a mass of 1007.6 Da. As shown in Figure 22, the fragmentation generates a large amount of residues with different molar masses and for this reason it is easy to recognize the sequencing.

Taking the entire sequence of amino acids of feather keratins into account (Figure 6), the hypothesis that the oligopeptides is a result of the simple breaking of the keratin peptide backbone without any rearrangement of the same has been considered. On the basis of this idea two hypothesis were made:

The breaking occurs:

- Close to cystein units which disappear after the superheated water process.

- Close to prolyne units which by their presence guarantee the folding of the mother chain.

For these reasons, looking at all the proline and all the cysteine residues present in the entire sequence it was found that there is only one possibility to get a sequence of ten amino acids that fits well with the data obtained by MS² analysis. In fact considering the proline in position 18 according to the sequence reported in Figure 6, and taking into account the amino acid peptide length of ten units, is possible to define a sequence that fits well with the data.

The contemplated sequence is the following:

Val Val Val Thr Leu Pro Gly Pro Ile Leu

In Table 3, all the possible fragments that are obtainable via the fractionation of this oligopeptide calculated with opportune software are reported. It must be taken into account that the fragmentation of the chain could occur in different parts of the backbone. In Table 3 all the possibilities as shown in Figure 23 were considered.

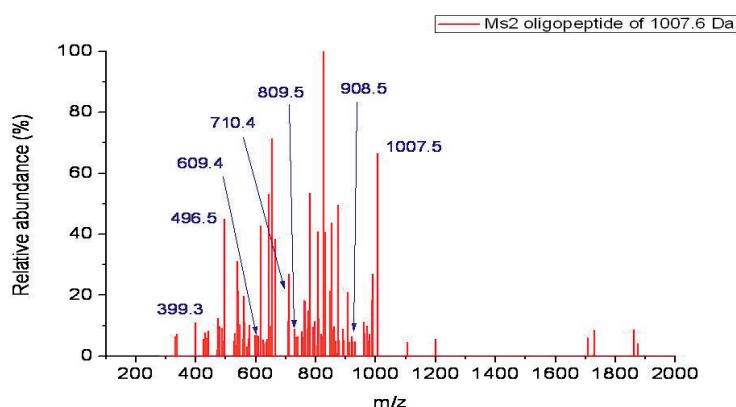


Figure 22. MS² performed on oligopeptide of 1007.6 Da obtained from dissolution of solution 2.

| Seq | # | A | B | C | X | Y |
|-----|----|-----------|-----------|-----------|-----------|------------|
| V | 1 | 72.08137 | 100.07628 | 117.10283 | - | 1007.65054 |
| V | 2 | 171.14978 | 199.14470 | 216.17125 | 934.56139 | 908.58212 |
| V | 3 | 270.21820 | 298.21311 | 315.23966 | 835.49297 | 809.51371 |
| T | 4 | 371.26587 | 399.26079 | 416.28734 | 736.42456 | 710.44529 |
| L | 5 | 484.34994 | 512.34485 | 529.37140 | 635.37688 | 609.39762 |
| P | 6 | 581.40270 | 609.39762 | 626.42417 | 522.29282 | 496.31355 |
| G | 7 | 638.42417 | 666.41908 | 683.44563 | 425.24005 | 399.26079 |
| P | 8 | 735.47693 | 763.47184 | 780.49839 | 368.21859 | 342.23933 |
| I | 9 | 848.56099 | 876.55591 | 893.58246 | 271.16583 | 245.18656 |
| L | 10 | 961.64506 | 989.63997 | - | 158.08176 | 132.10250 |

| | Mass | |
|----------------------|------------|------------|
| | Mono | Avg |
| (M) | 1006.64271 | 1007.28168 |
| (M+H) ⁺ | 1007.65054 | 1008.28962 |
| (M+2H) ²⁺ | 504.32920 | 504.64880 |
| (M+3H) ³⁺ | 336.55543 | 336.76853 |
| (M+4H) ⁴⁺ | 252.66854 | 252.82839 |

Table 3. Mass fragments calculation considering the fractionation of 1007.6 Da oligopeptide, calculated using an opportune Ion fragmentation software. A, B, C, X, Y represent the possible fragments obtainable performing MS² experiments as shown in Figure 22.

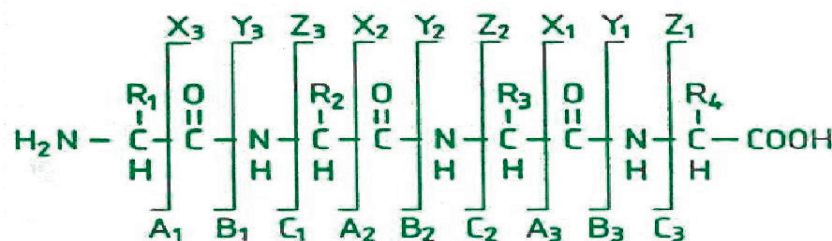


Figure 23. General scheme of all possible fragments obtainable for peptides in MS² experiments

The information obtained through these experiments seems to suggest the sequence of this 1 KDa oligopeptide and this data seems to be confirmed considering the work of Fraser et al, described above in the introduction.

As written before these authors suggested that the proline well represents the nucleating site for the formation of the hairpin structure of the sheet and for this reason they are concentrated in the vicinity of the reversal in chain direction. In

addition, there is a high concentration of hydrophobic residues in the interface between the two components related by the diad, at the core of the structure proposed by them.

This seems to justify that the 1 KDa oligopeptide, made of a sequence of non-polar amino acids, could lie in the inner core of the structure and for this reason it could become difficult to be hydrolyzed from the water in superheated conditions.

Clearly this hypothesis could justify the mechanism of dissolution, supporting the hypothesis of the simple breaking of the keratin backbone in “superheated water” under hydrolysis conditions and confirm the model described by Fraser et al.¹³

To strengthen our hypothesis we have synthesized peptide sequences as reported in the next paragraph and have followed the self assembling process by attaching aliphatic and hydrogen bonding motifs to the synthesized oligopeptides.

2.3.5 Synthesis of the oligopeptide in solid state

Solid Phase Peptide Synthesis can be defined as the process in which a peptide is synthesized by the successive addition of the protected amino acids constituting its sequence, anchored via its C-terminus to an insoluble polymer.

Each amino acid addition step is referred to as a cycle consisting of:

- Cleavage of an α amino protecting group
- Coupling of a protected amino acid
- Intermediate washing steps

The fact that the growing chain binds to an insoluble support makes it possible to eliminate the excess of reagents and by-products by simple filtration. Washing steps with appropriate solvents results into the complete elimination of reagents. In our experiments the solid support used is Breipohl polystyrene resin. Protecting groups must be easy to introduce and to remove; their role is to

mask particular functionality/reactivity and preventing these functionalities from interfering with the rest of the synthesis. After the desired sequence of amino acids has been obtained, the peptide can be removed from the polymeric support. The general scheme for solid phase peptide synthesis is outlined in Figure 24. The solid support is a synthetic polymer having reactive groups such as -OH. These groups are added so that they can react easily with the carboxyl group of N- α -protected amino acid, thereby covalently binding it to the polymer. The amino protecting group (X) can then be removed and a second N- α -protected amino acid can be coupled to the attached amino acid. These steps are repeated until the desired sequence is obtained.⁴⁴ At the end of the synthesis, a different reagent is applied to cleave the bond between the C-terminal amino acid and the polymer support. The cleaved peptide from the substrate is collected from the solution.

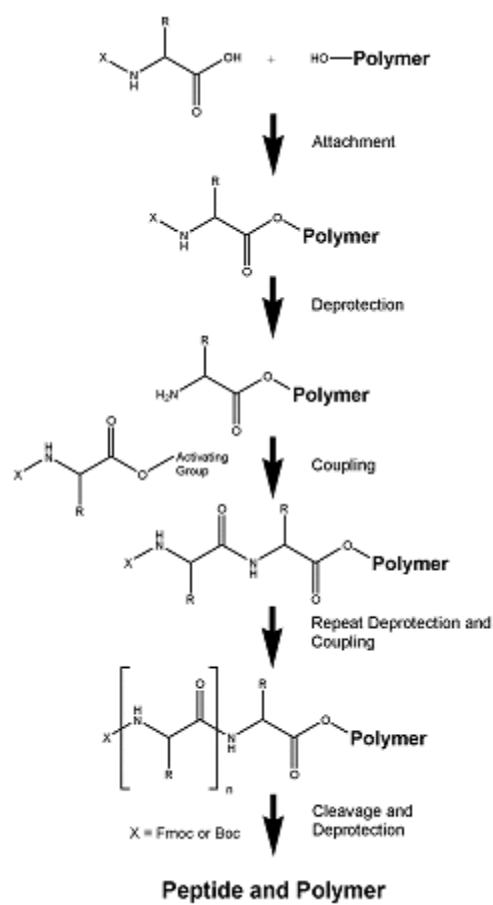


Figure 24. General scheme for Solid Phase Peptide Synthesis.

In Table 4, the scheme of the oligopeptide synthesis is presented. The Table depicts the quantity of the amino acids added for the coupling, and the results of the test made after each step of the synthesis are reported.

| | | | | | |
|---|------------------------|----------------------|--------------------------|------------------------------|--------------|
| Operator: Dennis Lowik, Maurizio Villani | | Datum: 27/10/2008 | | Protocol: DIPCDI | |
| Nodig: 4.25 mL 1M HOBt | | Hoeveelheid 2 gr | | Belading: 0.59 mmol/gr | |
| 3.89 mL 1M DIPCDI | Type Hars: Breipohl | | | | |
| | Fmoc-AA-OH | mg | Kaiser test Acylering | | Ontscherming |
| | 0 | | XXX | XXX | + |
| 1 | FmocLeu | 1251 | - | | + |
| 2 | FmocIle | 1251 | - | | + |
| 3 | FmocPro | 1194 | - | | + |
| 4 | FmocGly | 1052 | - | | + |
| 5 | FmocPro | 1194 | - | | + |
| 6 | FmocLeu | 1251 | - | | + |
| 7 | FmocThr(tBu) | 1407 | - | | + |
| 8 | FmocVal | 1201 | - | | + |
| 9 | FmocVal | 1201 | - | | + |
| 10 | FmocVal | 1201 | - | | + |
| 11 | 0 | 0 | | | |

Table 4. Scheme of the utilized procedure to synthesize the oligopeptide of 1 KDa.

The Kaiser test was performed to monitor deprotection during the solid phase peptide synthesis. When the N-terminus of the growing peptide chain is deprotected, a deep blue color is evolved. When the next peptide residue is coupled to the growing chain the solution turns colorless or yellow.

The synthesized oligopeptide was washed with dichloromethane, methanol and ether several times before analyzing it with LC-MS.

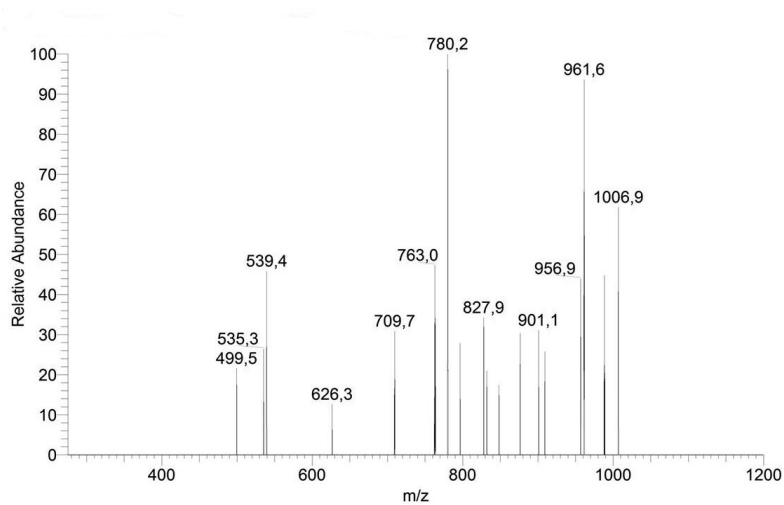


Figure 25. MS² on synthesized oligopeptide.

In Figure 25, MS² of the synthesized oligopeptides is reported. The figure shows that the main peaks present in the fragmentation of this oligopeptide are different from those presented in Figure 22. The intensity difference in the MS² spectra of the synthesized (Figure 25) and the extracted (Figure 22) oligopeptide from feather keratin suggests that there are some differences in chain conformation of the peptides in the two solutions. Since the position of the peaks is in good agreement, the intensity difference may arise due to the different fragmentation of amino acid sequences of the peptides having different chain conformation in the two obtained solutions. Subsequently alkylated tails and aliphatic amide tails were attached to the synthesized oligopeptide having a molar mass of 1kDa. The tails were attached to promote the self-assembling process similar to the oligopeptides obtained from the natural resources. The structures of these modified synthetic oligopeptides are shown in Figure 26.

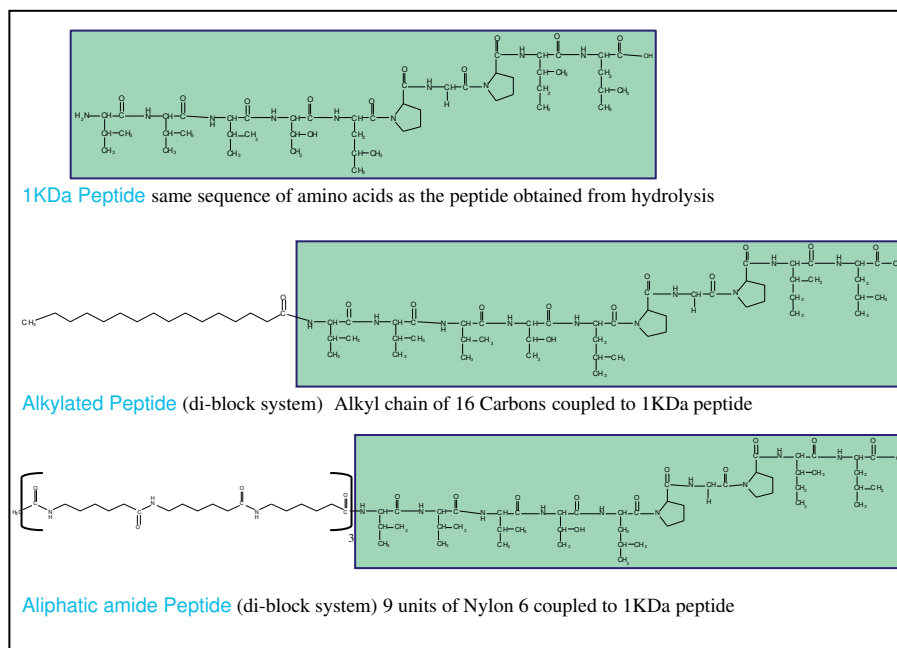


Figure 26. Structures of the synthesized 1KDa oligo peptide. The amino acid sequences used for the synthesis are similar to the peptide fractionated from feather keratins.

To promote the self-assembling process, a hydrophobic alkylated tail is added to the synthesized 1KDa peptide. It is anticipated that by increasing the length of the hydrophobic group the self-assembling process could be realized at lower concentrations. The addition of the alkylated tail is also likely to enhance the thermal stability. Similar to the hydrophobic alkylated modified oligopeptide, the synthesis of the oligopeptide is also performed with the aliphatic-amide tail. It is anticipated that in the modified synthetic oligopeptide the self-assembling process will be driven by the hydrogen bonding motifs linked to the tail.

2.3.6 Conformational and structural analysis of the oligopeptides obtained from the natural (feather keratin) and the synthesized sources

To investigate the conformation and the thermal stability of the crystals grown from solution and compare them with native chicken feathers, FTIR spectroscopy and TGA have been used. Figure 27 shows FTIR spectra at room temperature (RT) of the feather before dissolution and of crystals grown from the feather-water solution. The signals at 3288 cm^{-1} are assigned to the NH stretch. It is interesting, however, that for the crystals grown from solutions, this band appears broader and weaker compared to the relative band of native chicken feathers powder, which suggests a decrease and a rearrangement of the hydrogen bonds as direct consequence of the hydrolysis and consequent self-assembling. The signals at 2960 and 2850 cm^{-1} correspond to the asymmetric and symmetric methylene bands. They remain invariant comparing the two spectra. The infrared spectra in the region $1800\text{-}800\text{ cm}^{-1}$ show signals related to carbonyl stretching (CO stretch, 1636 and 1670 cm^{-1}), amide II (in-plane NH deformation with CO and CN stretches, 1540 cm^{-1}), CH_2 scissoring close to NH groups (1450 cm^{-1}), amide III coupled with hydrocarbon skeleton (1230 cm^{-1}). Interesting information is provided by the carbonyl stretching that is observed at higher wavenumber for the crystal grown from solution, which can also be related to a decrease and/or rearrangement of the hydrogen bonds as a consequence of the self-assembling. This hypothesis is strengthened considering that the typical signal for non hydrogen bonded carbonyl is usually observed at 1700 cm^{-1} . Other important confirmations are the disappearance of amide II (1540 cm^{-1}) and amide III (1230 cm^{-1}) signals observed for the crystals grown from solution. The disappearance of these bands confirms the hydrolysis of the keratin suggesting that a different conformation and local molecular environment is observed for crystals grown from solution.

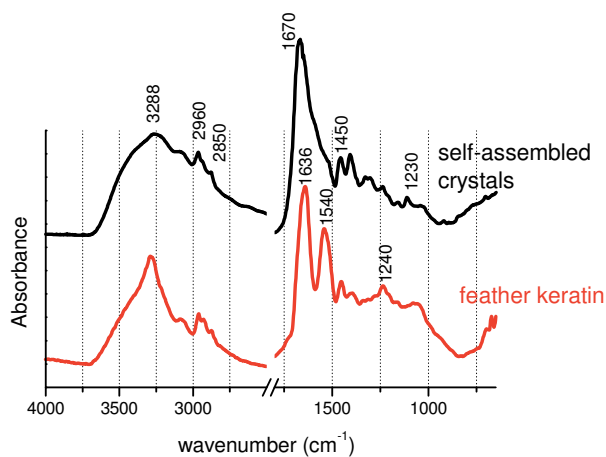


Figure 27. FT-IR spectra of native chicken feathers powder and crystal grown from solution 2 recorded at 30 °C. The spectra show frequency ranges 4000-600 cm^{-1} .

In Figure 28, TGA experiments recorded for chicken feathers and crystals grown from solutions are reported. The thermal stability of the two samples is significantly different and the temperature at which a weight loss of 5% ($T_{5\%} \sim 180 \text{ }^\circ\text{C}$) is reached for the crystals prepared from solution is quite consistent with our observation of the thermal behavior of the crystals investigated by OM equipped by a Linkam TMS94 hotstage, as previously reported.

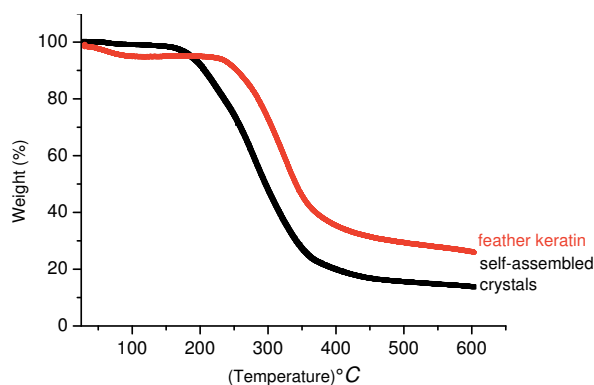


Figure 28. TGA curves of native chicken feathers powder and crystal grown from solution 2.

Conformational and structural analyses were also performed on the synthesized peptides.

Figure 29 shows FTIR spectra of the 3 different synthesized peptides powders compared with native chicken feather powders. All the spectra of the synthesized peptides show the presence of NH (3288 cm^{-1}) and CO (1638 cm^{-1}) groups in the crystals, suggesting a similar conformation for the 3 synthesized peptides. The thermal behavior of the synthesized oligopeptides was also investigated by TGA experiments. Figure 30 shows the increased thermal stability obtained attaching alkylated and aliphatic amide motifs to the synthesized 1KDa peptide, confirming the initial purpose of making use of these tails in order to promote stability and self assembling. By DSC, no crystallization and melting phenomena were observed for the synthesized peptides in the region of $30\text{-}220\text{ }^{\circ}\text{C}$ and it can be associated with the denaturation process that occurs before. XRD analysis on the contrary, suggests the presence of some structural ordering for the synthesized oligopeptides. In Figure 31 it is possible to observe the presence of a diffraction peak at $2\theta = 9.47^{\circ}$ common to all synthesized peptides. The peak appears to be stronger in intensity for the alkylated-peptide and aliphatic-amide-peptide compared to the normal synthesized peptide and corresponds to a diffraction spacing of 0.934 nm .

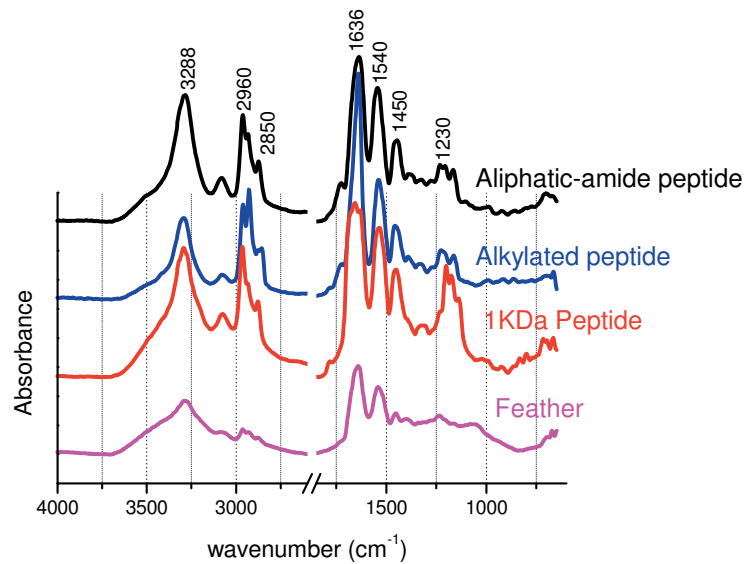


Figure 29. FT-IR spectra of native chicken feathers powder and all peptides synthesized by SPPS recorded at 30 °C. The spectra show frequency ranges 4000-600 cm^{-1} .

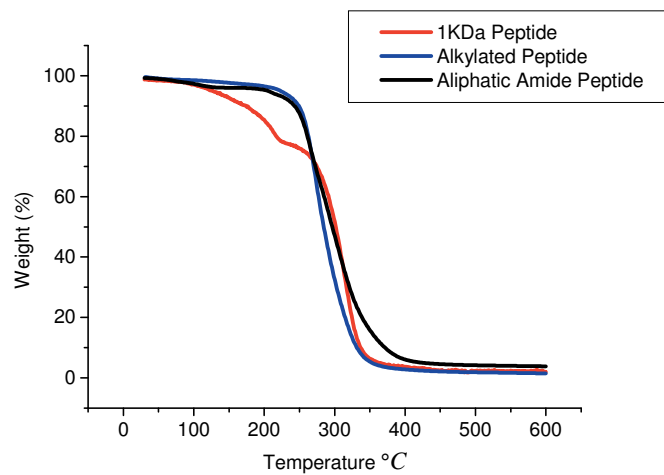


Figure 30. TGA curves of peptide powders synthesized by SPPS.

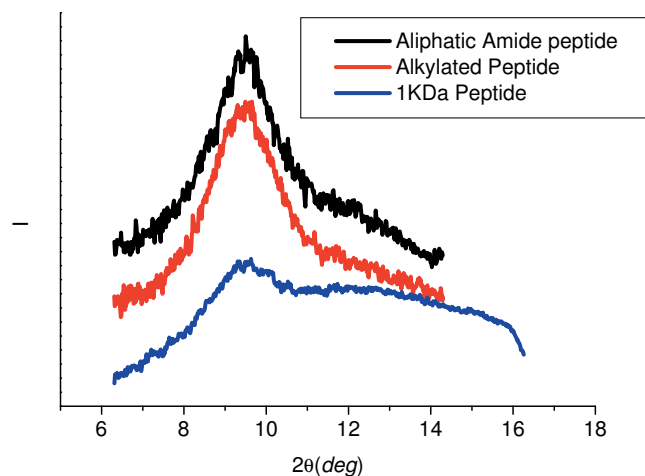


Figure 31. X-ray powder diffraction patterns of peptide powders synthesized by SPPS.

The observed d-spacing seems to be consistent with what has been observed in some AFM experiments performed on drop casted films of the synthesized peptides. In fact considering the low observed d-spacing value and that no self assembling phenomena were observed for the films prepared from solutions of the synthesized peptides by OM, AFM was chosen to study possible self assembling phenomena. In Figure 32, AFM height and phase angle images of the alkylated peptide film prepared after dissolving it in DCM (5mg/ml) are shown. The pictures show the presence of fibrils probably originated by the aggregation of the peptides. The dimensions of the fibrils seem to be variable in length and difficult to measure considering their high entanglement degree. Assuming that the fibrils have a cylindrical shape, the measured diameter of the fibril has a value of around 1 nm. This result confirms our XRD observations and relates the d-spacing measured to the diameter of the fibril. A similar result has been observed for films prepared from an aliphatic-amide peptide /DMF solution (5mg/ml) reported in Figure 33.

The obtained fibrils present the same dimensions, but they appear to be more oriented even though the procedure used for the film preparation was the same as used for the alkylated peptide films.

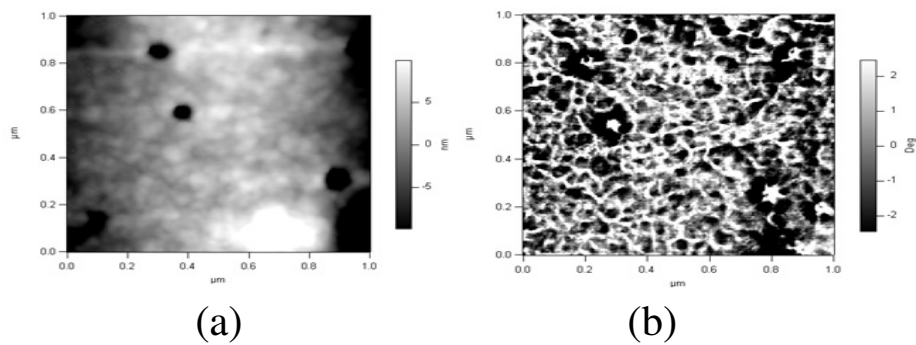


Figure 32. AFM height (a) and phase angle (b) images of the alkylated peptide film prepared dissolving the synthesized peptide in DCM (5mg/ml).

Probably the increased amount of hydrogen bonding interactions, related to the aliphatic- amide tail introduced, affects the orientation of the fibrils promoting a more ordered self-assembling, influencing the directionality of the fibrils.

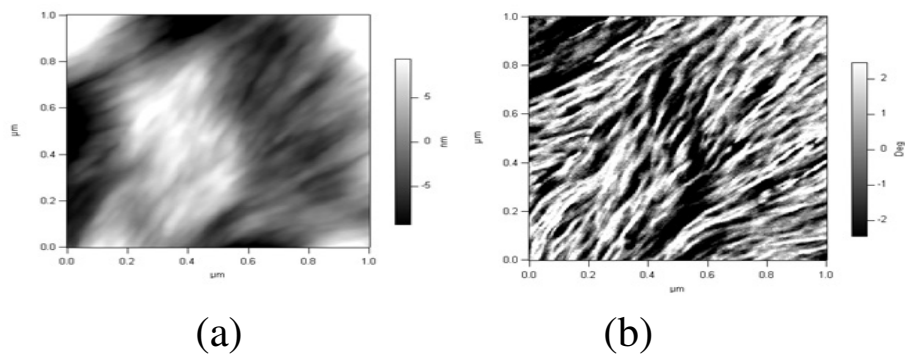


Figure 33. AFM height (a) and phase angle (b) images of the aliphatic-amide peptide film prepared dissolving the synthesized peptide in DMF (5mg/ml).

Therefore the peptides can be considered as sticky groups that promote the self assembling in the presence of the two different tails that control the morphology of the aggregates and result in a higher stability of the fibrils.

2.4 Conclusions

In the “superheated state”, water molecules could easily permeate into the polymer chains and weaken the hydrogen bonds and disulphide bonds so that feather keratins could be hydrolyzed into oligopeptides which contain a few to several tens of amino acid residues in the chains. Observations on the crystal growth of the oligopeptides obtained from the solutions of feather keratins showed self-assembling phenomena. These oligopeptides are able to self-assemble into crystalline structures as shown in the optical micrographs of this chapter, obtained upon drying a solution of the hydrolyzed feather keratin.

By changing parameters such as heating time, temperature and concentration of the solutions it is possible to influence the shape and size of the crystals.

MS data confirm the hydrolysis in “superheated water” and the consequent formation of oligopeptides. To accurately analyze the lengths of oligopeptides, different MS experiments have been performed. The results show the presence of these oligopeptide with discrete molar masses around 1 KDa. The amino acids sequence of the 1 KDa oligopeptide, made of non-polar amino acids, is in agreement with the proposed mechanism of dissolution and the hypothesis of the simple breaking of the keratin backbone in “superheated water” under hydrolysis conditions and confirms the structural model proposed by Fraser et al.²² The presence of fatty acid-lipid impurities affect the morphology of such crystals and influence the ramification of the dendrites. To strengthen our hypothesis, we have synthesized peptides with the same sequences as the peptide obtained by hydrolysis and have followed the self assembling process by attaching aliphatic and hydrogen bonding motifs to the synthesized

oligopeptides. The alkylated and aliphatic-amide were coupled to the peptide in order to promote the thermal stability and self-assembling phenomena, also considering the important role played by lipids and fatty acid residues in self assembling of peptides obtained from the hydrolysis of chicken feathers in “superheated water”.

The results confirm that the proteins can be extracted or purified from waste products of feathers or other natural resources in a similar way. Therefore, this work is valuable for eco-friendly recycling of protein wastes, and reuse of these proteins.

References

1. Fraser., R.D.B. and MacRae, T.P., *Current views on keratin complex, in The skin of vertebrates*, Spearman and P.A. Riley, Editors. 1980, Academic Press, London, New York. p. 67-86.
2. Astbury, W.T. and Street, A., *X-ray studies of the structure of wool and related fibers I. General*. Philosophical Transactions of the Royal Society (A), 1931. **230**: p. 75-101.
3. Astbury, W.T. and Marwick, T.C., *X-ray interpretation of the molecular structure of feather keratin*. Nature, 1932. **130**(3278): p. 309-310.
4. Rudall, K.M., *X-ray studies of the distribution of protein chain types in the vertebrate epidermis*. Biochimica biophysica Acta, 1947. **1**: p. 549-562.
5. Van Ingen, G.A., Faber, T.A., Obdam, J., and Kolster, P., *Method for manufacturing a biodegradable thermoplastic material*. 1998, WO 98/03591.
6. Schroeder, W.A., Kay, L.M., Leewis, B., and Munger, N., *The amino acid composition of certain morphologically distinct parts of white turkey feathers, and goose feather barbs and goose down*. Journal of the American Chemical Society, 1955. **77**: p. 3901-3908.
7. Fraser, R.D.B. and MacRae, T.P., *Molecular organisation in feather keratin*. Journal of Molecular Biology, 1959. **1**:p. 387-397.
8. Schor, R., and Krimm, S., *Studies on the structure of feather keratin I. X-ray diffraction studies and other experimental data*. Biophysics Journal, 1961. **1**: p. 467-488.
9. Fraser, R.D.B., MacRae, T.P. and Rogers, G.E., *Keratins. Their composition, structure and biosynthesis*. 1972, Springfield, Ill., Charles C. Thomas.

10. Marwick, T.C., *The X-ray classification of epidermal proteins*. Journal of Textile Science, 1931. **4**: p. 31.
11. Lucas, A.M., Stettenheim, P.R., *Avian anatomy-Intergument*. Agricultural Handbook **362**. Washington (DC): Government Printing Office, 1972.
12. Filshie, B.K. and Rogers, G.E., *An electron microscope study of the fine structure of feather keratin*. The Journal of Cell Biology, 1962. **13**.
13. Fraser, R.D.B. and Parry, D.A.D., *Molecular packing in the feather keratin filament*. Journal of Structural Biology. 2008. **162**: p. 1-13.
14. Fraser., R.D.B. and MacRae, T.P., Parry, D.A.D., and Suzuki, E., *The structure of feather keratin*. Polymer, 1971. **12**: p. 35-56.
15. O`Donnell, I.J. *The complete amino acid sequence of a feather keratin from emu (Dromaius novae-hollandiae)*. 1973. Aust. J. Biol. Sci. **26**: p. 415-437.
16. O`Donnell, I.J., Inglis, A.S., *Amino acid sequence of a feather keratin from silver gull (Larus novae-hollandiae) and comparison with one from emu (Dromaius novae-hollandiae)*.1974. Aust. J. Biol. Sci. **27**: p. 369-382.
17. Woodin, A.M., *Molecular size, shape and aggregation of soluble fether keratin*. Biochemical Journal, 1954. **57**: p. 99-109.
18. Harrap, B.S. and Wood, E.F. *Soluble derivatives of feather keratin 1. Isolation, fractionation and amino acid composition*. Biochem. J. 1964. **92**: p. 8-18.
19. Harrap, B.S. and Wood, E.F. *Soluble derivatives of feather keratin 2. Molecular weight and conformation*. Biochem. J. 1964. **92**: p. 19-26.
20. Harrap, B.S. and Wood, E.F. *Species differences in the proteins of feathers*. Comp. Biochem. Physiol. 1967. **20**: p. 449-460.
21. Kemp, D.J. and Rogers, G.E. *Differentiation of avian keratinocytes. Characterization and relationships of the keratin proteins of adult and embryonic feathers and scales*. Biochemistry. 1972. **11**: p. 969-975.

22. Akahane, K., Murozon, S., and Murayama, K. *Soluble proteins from fowl feather keratin I. Fractionation and properties*. Journal of Biochemistry. 1977. **81**: p. 11-18.
23. Presland, B.R., Whitbread, L.A. and Rogers, G.E. *Avian keratin genes II. Chromosomal Arrangement and Close linkage of three gene families*. J. Mol. Biol. 1989. **209**: p. 561-576.
24. MacArthur, M.W., Thornton, J.M. *Influence of proline residues on protein conformation*. J. Mol. Biol. 1991. **218**: p. 397-412.
25. Huggins, M. *The structure of α -Keratin*. Macromolecules. 1977. **10**(No.5): p. 893-898.
26. Bragg, W. L., Kendrew, J. C., and Perutz, M. F. *Proc. R. SOC. London, Ser. A*. 1950. **203**: p. 321.
27. M. L. Huggins, *J. Am. Chem. SOC.* 1952. **74**: p. 3963.
28. Swan, J.M. *Nature*, 1957. **180**: p. 643.
29. Cleland, W.W. *Dithiothreitol, a new protective reagent for SH groups*. Biochemistry. 1964. **3**: p. 193-202.
30. George A. Jeffrey, *An introduction to hydrogen bonding*, Oxford University Press, **1997**.
31. Dill, K.A., Truskett, T.M., Vlachy, V. and Hribar-Lee, B. *Modeling Water, the Hydrophobic effect, and ion solvation*. Annu. Rev. Biophys. Biomol. Struct. 2005. **34**: p. 173-199.
32. Yin, J., Rastogi, S., Ann E. Terry, and Popescu, C. *Biomacromolecules*, 2007.
33. Rastogi, S., Ann E. Terry, and Ester Vinken, *Macromolecules*, 2004, **37**: p. 8825-8828, **25**: 917-924.
34. Schrooyen, P. *Feather keratins: modification and film formation*, PhD thesis, 1999, University of Twente, Enschede, the Netherlands
35. Kaiser, E., Colescot, R.L., Bossinge, C.D. Cook, P.I., *Anal. Biochem.* 1970, **34**, 595.
36. Kessler, D.A., Koplik, J., Levine, H. *Phys. Rev. A* 1986, **33**, 3352.

37. Yang, C. H.; Brown, J. N.; Kopple, K. D. *Int. J. Peptide Protein Res.* **1979**, *14*, 12-20.
38. R. Rissmann, M.H. Oudshoorn, R. Zwier, M. Ponec, J.A. Bouwstra, W. E. Hennink, *Int. J. Pharm.* **2009**, *372*, 59.
39. Blankenburg, R., Meller, P., Ringsdorf, H., Salesse, C., *Biochemistry* 1989, *28*, 8214.
40. Darst, S. A., et al. *Biophys. J.* 1991, *59*, 387.
41. Kubalek, E. W., Kornberg, R.D., Darst, S.A. *Ultramicroscopy* 1991, *35*, 295.
42. Ku, A.C., Darst, S.A., Kornberg, R.D., Robertson, C.R., Gast, A.P. *Langmuir* 1992, *8*, 2357.
43. Langer, J.S. *Rev. Mod. Phys.* 1980, *52*, 1.
44. Information and Materials (slides) furnished by Dennis Lowik researcher in Van Hest group at Radboud University of Nijmegen.

Appendix A

“Superheated water” treatment

The material used for our studies is the barb of feathers or hair finely cut. Once the feathers are pretreated by cleaning, cutting, degreasing, and drying according with the procedure described in the chapter, the barbs from dry feathers or hair are sealed in a steel pressure cell (Figure S1) with water at several different concentrations and placed in a preheated oven. The hydrolysis can be affected changing the processing parameters.



Figure S1. Sequence of pictures in which are shown the three steps of the “superheated water” treatment.

Optical microscopy measurements

In this section some optical micrographs of the several different prepared solutions are reported. The micrographs show the role of processing parameters on the self-assembling and the crystallization of the peptides confirming our conclusions reported in chapter 2.

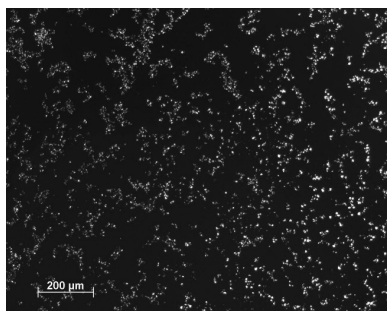


Figure S2. The optical micrographs of the sample of solution 10, obtained from 260°C superheated water for 120min. The concentration of Solution 10 was 30mg/ml. Crystals prepared from solution 10, appear smaller than the ones obtained at lower temperatures.

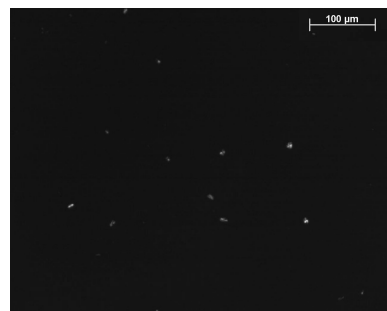


Figure S3. The optical micrographs of the sample of solution 15, obtained from 260°C superheated water for 120min. The concentration of Solution 15 was 10mg/ml. Crystals prepared from solution 15, appear smaller than the ones obtained at lower temperatures.

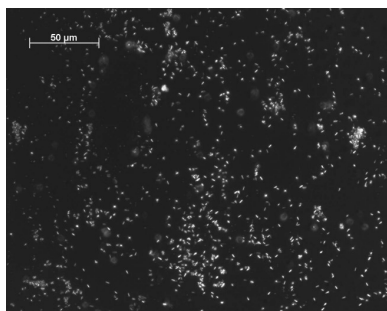


Figure S4. The optical micrographs of the sample of solution 5, obtained from 260°C superheated water for 120min. The concentration of Solution 5 was 20mg/ml. Crystals prepared from solution 5, appear smaller than the ones obtained at lower temperatures.

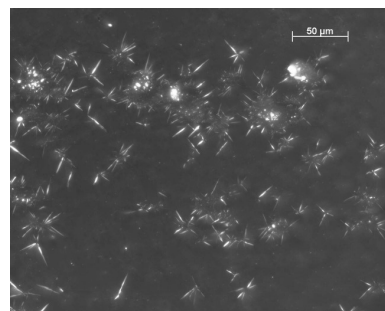


Figure S5. The optical micrographs of the sample of solution 1, obtained from 220°C superheated water for 120min. The concentration of Solution 1 was 20mg/ml. Crystals prepared from solution 1, appear smaller than the ones obtained using longer processing time.

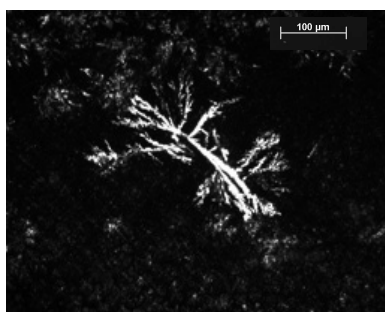


Figure S6. The optical micrographs of the sample of solution 9, obtained from 220°C superheated water for 120min. The concentration of Solution was 30mg/ml. Crystals prepared from solution 9, appear to be dendritic in nature.



Figure S7. The optical micrographs of the sample of solution 8, obtained from 220°C superheated water for 60min. The concentration of Solution 8 was 30mg/ml. Crystals prepared from solution 8, appear to be dendritic in nature.

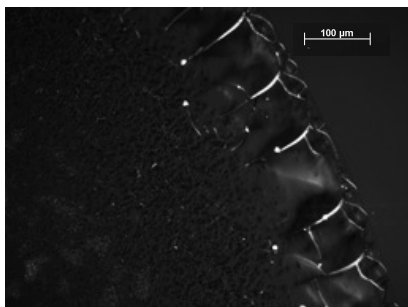


Figure S8. The optical micrographs of the sample of solution 11, obtained from 180°C superheated water for 60min. The concentration of Solution 11 was 10mg/ml. Crystals are not present.

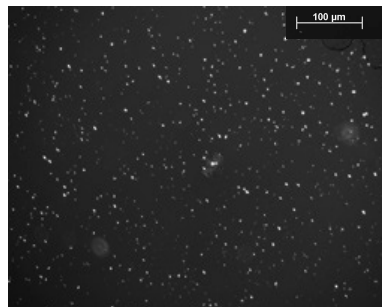


Figure S9. The optical micrographs of the sample of solution 13, obtained from 220°C superheated water for 60min. The concentration of solution 13 was 10mg/ml. Crystals prepared from solution 13, appear smaller than the ones obtained using longer processing time and higher concentration.

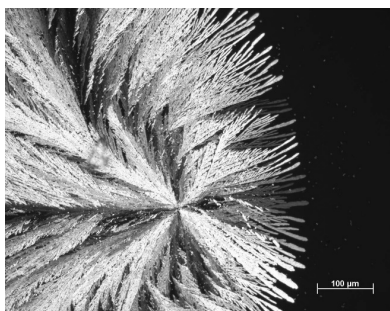


Figure S10. The optical micrographs of the sample of solution 2, obtained from 220°C superheated water for 120min. The concentration of solution 2 was 20mg/ml. Crystals prepared from solution 2, appear to be dendritic in nature.

Mass Spectra

In Figure S11-S14 several mass spectra for the different prepared solutions are reported. In all spectra it is possible to observe the presence of this predominant signal corresponding to oligopeptides with a molar mass of about 1 KDa. In Figure S15-S17 The Mass spectra of 3 different hair solutions with different concentrations are reported. The main signals present in these mass spectra have a different value between 960-990 Da and this could be attributed to the different structure and amino acid sequencing of hair Keratin.

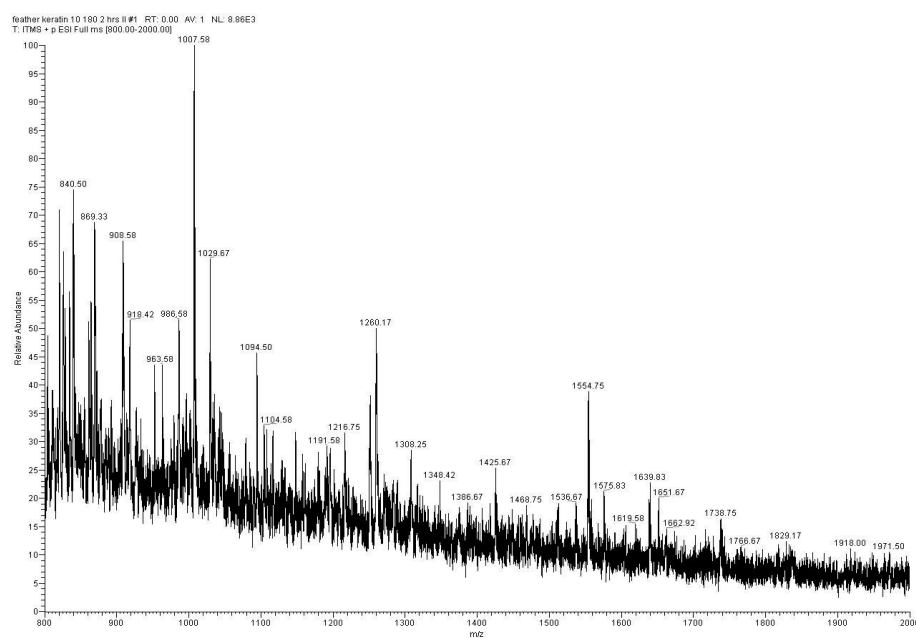


Figure S11. MS spectrum of the solution 12.

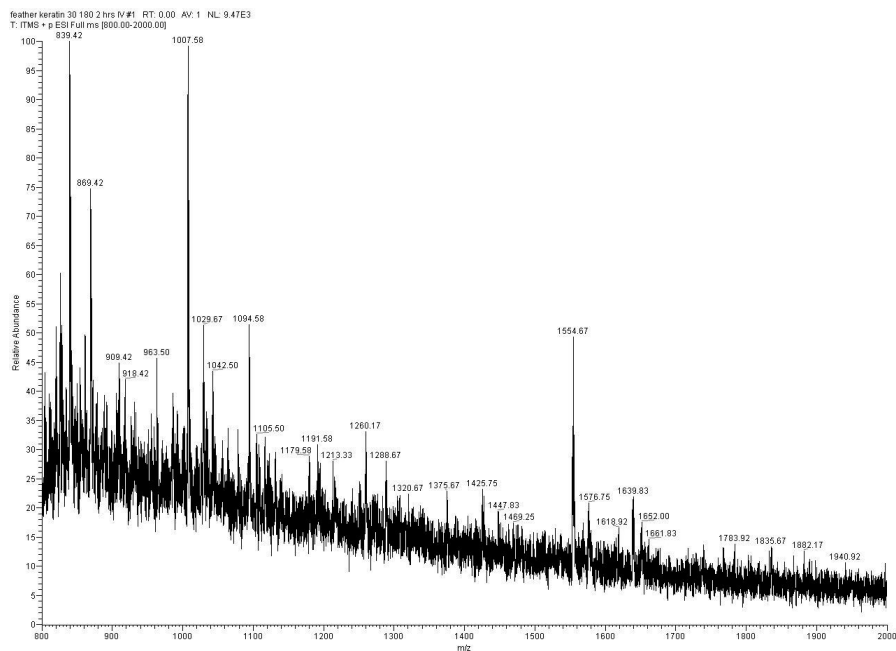


Figure S12. MS spectrum of the solution 7.

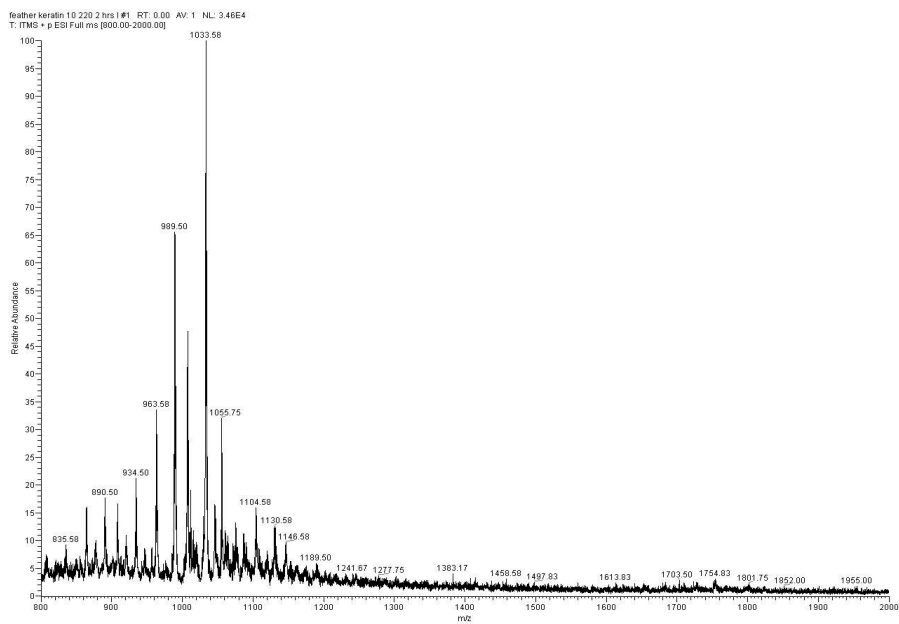


Figure S13. MS spectrum of the solution 14.

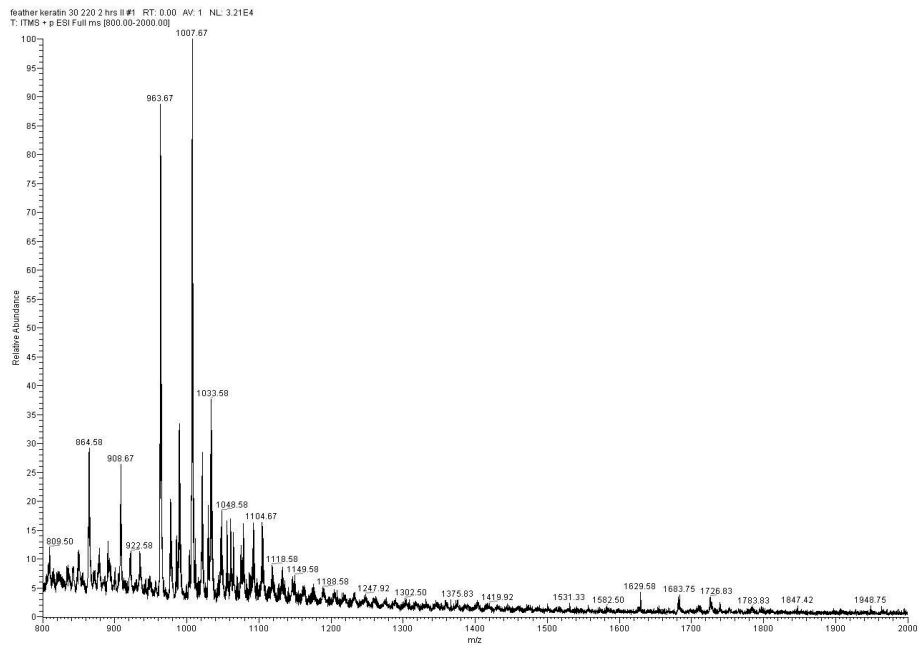


Figure S14. MS spectrum of the solution 9.

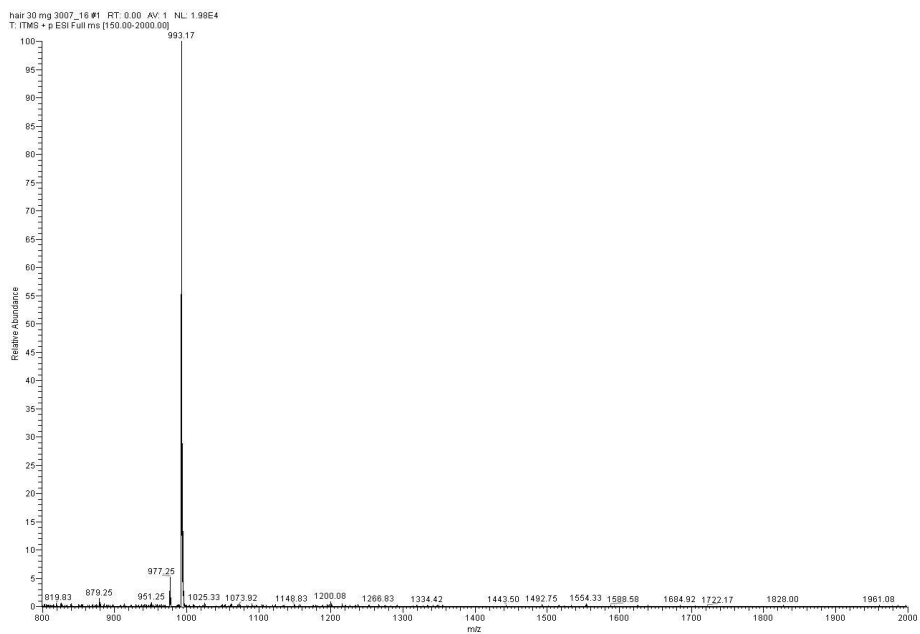


Figure S15. MS spectrum of hair keratin-water solution. The solution was prepared from hair concentration of 30mg/ml treated at 220°C for 120min.

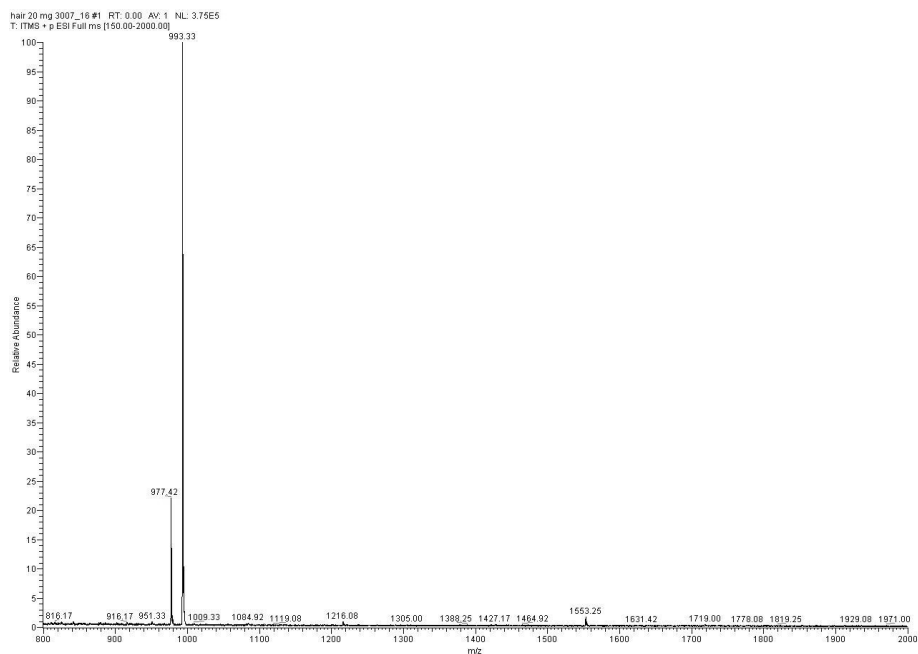


Figure S16. MS spectrum of hair keratin-water solution. The solution was prepared from hair concentration of 20mg/ml treated at 220°C for 120min.

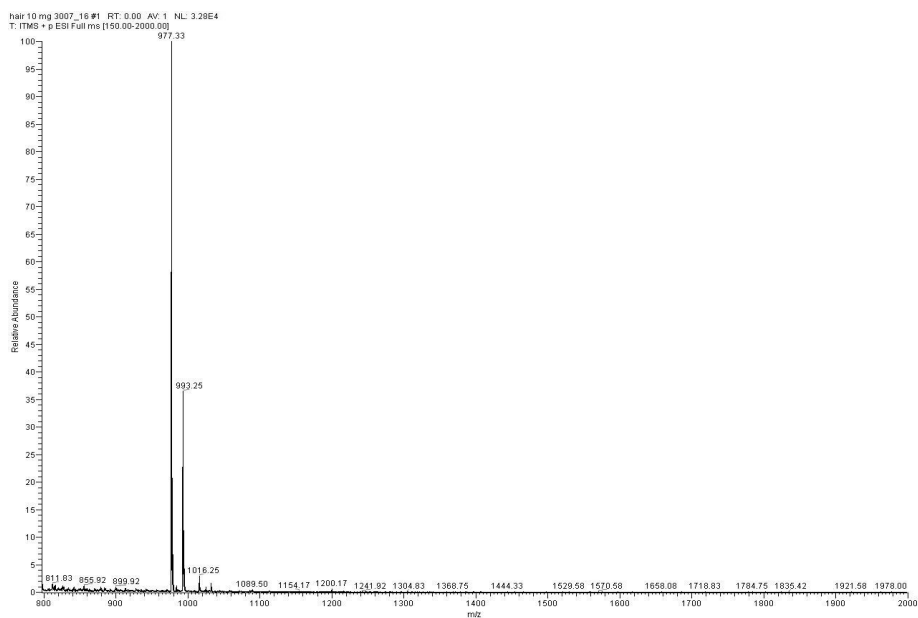


Figure S17. MS spectrum of hair keratin-water solution. The solution was prepared from hair concentration of 10mg/ml treated at 220°C for 120min.

Chapter 3

Novel, Fully Biobased Semi-Crystalline Polyamides*

New semi-crystalline polyamides and copolyamides from biobased sebacic acid (SA), 2,5-diamino-2,5-dideoxy-1,4;3,6-dianhydroiditol (diaminoisoidide, DAII) as well as from 1,4-diaminobutane (DAB), also known as putrescine in nature, have been synthesized. Low molecular weight polyamides were obtained by the melt polycondensation of the salts based on these monomers or by interfacial polycondensation. In order to increase the molecular weight of the polyamide prepolymers Solid State Polymerization (SSP) was used. The chemical structure of the polymers was proven by 2D NMR Correlation Spectra (COSY), Heteronuclear Multiple-Bond Correlation Spectra (HMBC) and by FT-IR spectroscopy. In the present work FT-IR and X-ray techniques were used as a tool for the investigation of the crystal structure of the polymers after Solid State Polymerization. The X-ray diffractograms of the polyamides point to crystals containing both 4.10- and DAII.10-based repeat units. Due to the presence of diaminoisoidide residues the synthesized fully renewable products exhibit tunable polarities and melting points. Since most commercial polyamides have a much higher melting point than their end application requires, especially for fiber applications, this simple adaption can result in a significant reduction of energy consumption during processing.

*reproduced from Lidia Jasinska, Maurizio Villani, Jing Wu, Daan van Es, Enno Klop, Sanjay Rastogi, and Cor E. Koning, *Macromolecules*, **2011**, *44* (9), pp 3458–3466.⁵⁰

3.1 Introduction

Remarkable features of polyamides (PA) are responsible for their multiple potential uses in several applications. Exhibiting good physicochemical and mechanical properties as well as low cost, this class of polymers is an interesting candidate for high performance engineering thermoplastics and for fibers. Numerous studies, reporting an advantage of polyamides over other thermoplastic polymers, have been published so far.¹⁻⁵ However, it is known that many of the commonly used polyamides like polyamide 6⁶⁻⁸ and polyamide 6.6⁹⁻¹¹ are based on petrochemical compounds. Therefore, following the increasing demand for the production of environmentally friendly materials the development of biomass-based polymers is entirely justified.

Of significant interest and, hence, widely reported are biobased polyamides from brassylic acid,¹²⁻¹⁶ sebacic acid¹⁷⁻²⁰ or 1,4-diaminobutane.^{4, 5, 19, 21-26} Along with different synthetic approaches their morphology and crystalline transitions have been intensively studied. The application of such monomers for the synthesis of polyamides with different spacial separation between the amide groups, and thus with different hydrogen bond densities, may be a powerful method of tailoring their thermal and mechanical properties.

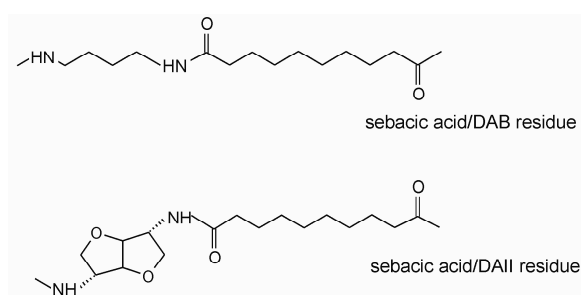
Currently, very promising and revealing opportunities are offered by biobased monomers like 1,4;3,6-dianhydrohexitols with *endo-exo*, *endo-endo* or *exo-exo* conformation. Examples are 1,4;3,6-dianhydro-D-glucitol (isosorbide), 1,4;3,6-dianhydro-D-mannitol (isomannide), 1,4;3,6-dianhydro-L-identol (isoidide)²⁷ and their diamino derivatives.^{28, 29} However, due to the formation of intramolecular hydrogen bonds and due to steric hindrance by one of the rings the *endo*-oriented hydroxyl or amino groups reveal relatively low reactivity. On the other hand, the use of monomer moieties with L-ido conformation or modified products with enhanced reactivity may provide fully biobased polymers including liquid-crystalline materials.³⁰ Thiem et al.²⁸ presented a series of

polyamides synthesized by interfacial polycondensation of aromatic or aliphatic diacylchlorides with isomannide- (DAIM), isosorbide- (DAIS), and isoidide-derived (DAII) diamines. They found that by using DAII or DAIS polyamides with high degrees of polymerization and T_g values in the range 50-70 °C can be obtained. Recent studies of Bartolussi^{31, 32} focused on interfacial polycondensation, microwave-assisted polymerization and Higashi's Method as synthetic routes for biobased polyamides. In these studies isosorbide was derivatized into diamine or diacylchloride and used for the preparation of optically active products. The comparative analysis performed by these authors proved that microwave-assisted polycondensation leads to the highest molecular weight of the studied polyamides (140,000 g/mol) with thermal stabilities ranging up to 400 °C.

In the light of reports concerning biodegradable polymers, poly(ester-amides) based on 1,4;3,6-dianhydrohexitols attracted special attention.³³⁻³⁵ These biobased products were successfully obtained by the reaction of *p*-toluenesulfonic acid salts of *O,O'*-bis(α -aminoacyl)-1,4;3,6-dianhydro-D-glucitol with bis(*p*-nitrophenyl) esters of dicarboxylic acids and tested for their thermal properties and enzymatic degradation. The analyses have shown a particular suitability of these polyamides as drug delivery systems. Another application for biobased poly(ester-amides) was proposed by Philip and Sreekumar.³⁶ These authors synthesized optically active materials, having biphenolic azo chromophores and isosorbide as T_g -increasing building blocks, with a potential application in electro-optic devices.

Herein, we present synthetic routes, structural characterization and thermal properties of semi-crystalline polyamides and copolyamides entirely based on renewable monomers, namely diaminoisoidide (DAII, prepared from isomannide), 1,4-diaminobutane (DAB, in nature known as putrescine) and sebacic acid (see Scheme 1). One of the synthetic methods is based on interfacial polycondensation of the diacyl chloride derivative of sebacic acid with DAII, while another method involves solvent-free bulk polycondensation

accomplished by Solid State Polymerization (SSP) after a prepolymerization in the melt. SSP provided the ability to achieve biobased polyamides with molecular weights above 18,000 g/mol. The chemical structure of the synthesized polymers was proven using 2D NMR and FT-IR spectroscopy. To investigate the influence of diaminoisoidide on the crystal structure and melting points of the polyamides, wide-angle X-ray diffraction and DSC techniques were applied. As far as we know these fully biomass-based copolyamides have not yet been described in the literature.



Scheme 1. Chemical structure of sebacic acid/1,4-diaminobutane and sebacic acid/diaminoisoidide repeat units in the synthesized co- and homopolyamides.

3.2 Experimental Section

3.2.1 Materials. 2,5-Diamino-2,5-dideoxy-1,4;3,6-dianhydroiditol (diaminoisoidide, DAII) was prepared by the published method from 1,4:3,6-dianhydro-D-mannitol.²⁹ Sebacic acid (99 %), sebacoyl chloride (99 %), 1,4-diaminobutane (99 %), 1,4:3,6-dianhydro-D-mannitol (isomannide, 95 %), p-toluenesulfonyl chloride (≥ 99 %), potassium phthalimide (≥ 99 %), dimethyl sulfoxide (≥ 99.9 %), hydrochloric acid (reagent grade 37 %), ethanolic HCl solution (1.25 N), Amberlyst® A26-OH, potassium carbonate (≥ 99 %), chloroform-*d* (99.8 atom%D) and benzene-*d*₆ (99 atom%D) were purchased

from Sigma-Aldrich. Irganox 1330 was available from Ciba Specialty Chemicals. Magnesium sulfate (99 %) was purchased from Acros Organics. Acetic acid (glacial, 99-100 %), pyridine (99.5 %) and D₂O (99.8 atom%D) were purchased from Merck. Trifluoroacetic acid-*d* (99.5 atom%D) was purchased from Cambridge Isotope Laboratories, Inc. Activated carbon was purchased from Norit. 1,1,1,3,3,3-Hexafluoro-2-propanol (HFIP), diethyl ether, methanol, ethanol and dry chloroform were purchased from Biosolve. All the chemicals were used as received, unless denoted otherwise.

The synthetic strategies and the synthesis of the monomers and polymers were developed and performed by Dr. Lidia Jasinska from the Polymer Chemistry group of Eindhoven University of Technology. More details are available in the publication cited in the references.⁵⁰

3.2.2 Polymerization of Salt Monomers. This example is representative for all conducted co(polymerizations). A mixture of diaminoisoidide-sebacic acid salt (0.66 g) and 1,4-diaminobutane-sebacic acid salt (2.0 g), 1,4-diaminobutane (0.2 g, 2.3 mmol), and diaminoisoidide (0.066 g, 0.45 mmol) was stirred in a three-necked round bottom flask equipped with a mechanical stirrer, vigreux column and a Dean-Stark type condenser. The reaction mixture was heated to 160 °C and then the temperature was raised to 190 °C. The polycondensation process was conducted in the presence of Irganox 1330 (0.026 g) as an antioxidant. The reaction was carried out for 2 h under argon atmosphere. The low molecular weight polyamide was ground into powder, washed with demineralized water at 80 °C for 12 h, filtered, and dried under reduced pressure at 80 °C. In order to increase the molecular weight of the polyamide prepolymer Solid State Polymerization (SSP) was applied. SSP of the polyamide powder was carried out in a glass tube reactor (2.5 cm diameter) equipped with a sintered glass plate at the bottom on which the polyamide prepolymer powder was deposited. Below this glass plate the SSP reactor contained an inert gas inlet through which the heated gas was introduced. During the reaction course

the temperature was raised gradually from 200-205 °C for 27 h and maintained 10-15 °C below the melting point of the polyamide. The reactor was heated using a salt mixture of KNO₃ (53 wt%), NaNO₂ (40 wt%), NaNO₃ (7 wt%).³⁷ SSP was carried out in Ar atmosphere at a gas flow rate of 2.5 L/min.

3.2.3 Interfacial Polycondensation. To a solution of diaminoisoidide (0.72 g, 0.005 mol) and potassium carbonate (1.38 g, 0.01 mol) in water (35 mL) a solution of sebacyl chloride (1.19 g, 0.005 mol) in dry chloroform (5 mL) was added dropwise. The heterogeneous mixture was stirred at room temperature for 2 h under Ar atmosphere. The obtained polyamide was filtered, washed with water, ethanol, and dried under reduced pressure at 80 °C (1.42 g, 92 %).

3.2.4 Measurements. Size exclusion chromatography analyses (SEC) in 1,1,1,3,3,3-hexafluoro-2-propanol were performed using a set-up equipped with a Shimadzu LC-10AD pump and a waters 2414 differential refractive index detector. PSS (2×PFG-lin-XL, 7 μm, 8×300 mm) columns were used. The eluent flow rate was 1.0 mL/min. Calibration of the measurements was carried out with PMMA standards. The data acquisitions were performed using Viscotek OmniSec 4.0 and Waters Empower 2.0 software.

2D NMR spectra were recorded on a Varian Unity 500 plus spectrometer at room temperature. Chemical shifts were referenced to residual solvent signals (C₆D₆ or TFA-*d*). *Correlation Spectra* (COSY) were acquired using standard programs provided by a Varian spectrometer library. *Heteronuclear Multiple-Bond Correlation Spectra* (HMBC) were recorded with pulse field gradients. The spectral windows for ¹H and ¹³C axes were 3399.6 Hz and 12574.7 Hz, respectively. The data were collected in a 1024×200 matrix and processed in a 1K×1K matrix. ¹H NMR and ¹³C NMR spectra were recorded using a Varian Mercury V_x spectrometer with the frequency of 400 MHz.

Thermogravimetric analyses (TGA) were performed on a TA Instruments Q500 TGA in a nitrogen atmosphere. Samples were heated from 50 to 600 °C with a heating rate of 10 °C/min.

DSC measurements were performed using a DSC Q100 from TA Instruments. The measurements were carried out in a nitrogen atmosphere with a heating rate of 10 °C/min. The transitions were deduced from the second heating and cooling curve.

Fourier Transform Infrared spectra (FT-IR) were obtained using a Varian 610-IR spectrometer equipped with an FT-IR microscope. The spectra were recorded at 30 °C in transmission mode with a resolution of 2 cm⁻¹. PA films obtained from HFIP were analyzed on a zinc selenium disk and heated using a Linkam TMS94 hotstage and controller. Varian Resolution Pro software version 4.0.5.009 was used for the analysis of the spectra.

X-ray diffraction patterns were obtained employing a Bruker AXS HI-STAR area detector installed on a P4 diffractometer, using graphite-monochromated Cu K α radiation ($\lambda = 1.5418 \text{ \AA}$) and a 0.5 mm collimator. The data were collected at room temperature on SSP-synthesized powder contained in glass capillaries. The 2D data were subsequently background-corrected and transformed into 1D profiles via integration.

3.3 Results and Discussion

3.3.1 Synthesis and Molecular Characterization of Polyamides.

Copolyamides (co-PAs) were prepared via melt and solid state bulk polycondensation of the salts obtained from sebacic acid, diaminoisoidide and 1,4-diaminobutane, as described in the experimental section. This method was also used for the synthesis of the homopolyamide PA1 based on sebacic acid and 1,4-diaminobutane. The purity of the salts was checked by ¹H NMR spectroscopy while their thermal properties were measured using DSC and TGA. These parameters are highly important in view of the time/temperature conditions of the polycondensation. The melting points of the sebacic acid/DAII and sebacic acid/DAB salts were 133 °C and 130 °C, respectively. Despite the

relatively low melting points of both salts and high thermal stability of sebacic acid/DAB salt (maximal rate of decomposition at $T_{\max} = 468$ °C) the low thermal stability of the synthesized sebacic acid/DAII salt (maximal rate of decomposition at $T_{\max} = 266$ °C) limited the temperature conditions of the polycondensation reaction of the salt mixtures in the melt. Therefore, an extensive duration of the polymerization above 200 °C should be avoided and so a two-step method for the synthesis of co-PAs leading to white products with M_n above 18,000 g/mol was applied. In a first step (bulk melt-polycondensation at 190 °C) low molecular weight prepolymers with variable molar ratios DAB/DAI were obtained, which were subsequently subjected to Solid State Polymerization (see Table 1).

As expected, the presence of diaminoisoidide in the polymer backbone of the synthesized copolymers significantly affected their properties, including molecular weight and polydispersity index. The first step of the polycondensation yielded products with M_n ranging between 2500-9600 g/mol (Table 1). The homopolymer PA1 based on 1,4-DAB and sebacic acid exhibits an M_n value around 9600 g/mol, decreasing to approximately 2500 g/mol with increasing DAII monomer residue concentration. These results clearly indicate the lower reactivity of the secondary amine - diaminoisoidide in comparison to 1,4-diaminobutane. It is well known, that mechanical and thermal properties of polyamides are directly related to their molecular weight, where a high molecular weight promotes good properties.¹⁸

Table 1. Characteristics of co- and homopolyamides from sebacic acid, 1,4-diaminobutane and diaminoisoidide.

| Symbol | Monomer feed, mol ratio (DAB/DAII) ^a | Built-in composition (DAB/DAII) ^b | M _n ^c (g/mol) | PDI ^c | M _n ^d (g/mol) | PDI ^d |
|------------------|---|--|-------------------------------------|------------------|-------------------------------------|------------------|
| PA1 | 1.0/0 | 1.0/0 | 9,600 | 2.3 | 21,900 | 3.0 |
| coPA2 | 0.91/0.09 | 0.89/0.11 | 6,500 | 2.0 | 21,300 | 2.7 |
| coPA3 | 0.83/0.17 | 0.86/0.14 | 5,000 | 1.8 | 18,700 | 2.7 |
| coPA4 | 0.78/0.22 | 0.80/0.20 | 5,500 | 1.8 | 20,400 | 2.9 |
| coPA5 | 0.55/0.45 | 0.57/0.43 | 2,500 | 1.7 | 3,900 | 1.9 |
| PA6 ^e | 0/1.0 | 0/1.0 | 4,200 | 2.3 | - | - |

DAB = 1,4-diaminobutane, DAII = diaminoisoidide, ^aDetermined by weighed-in monomers, ^bDetermined by NMR, ^cDetermined for polyamides before Solid State Polymerization using SEC method with PMMA standards in HFIP solvent, ^dDetermined for polyamides after Solid State Polymerization using SEC method with PMMA standards in HFIP solvent, ^ePA obtained via interfacial polymerization, PA1 = PA 4.10, PA2 = PA 4.10/DAII.10-2, PA3 = PA 4.10/DAII.10-3, PA4 = PA 4.10/DAII.10-4, PA5 = PA 4.10/DAII.10-5, PA6 = PA DAII.10

Therefore, taking into account the low thermal resistance of both DAII and the sebacic acid/DAII salt, the use of SSP for obtaining the targeted polymers with molecular weights above 15,000 g/mol turned out to be the most advantageous method (Table 1). Besides, due to the low melting temperature of coPA 5 (see further) and hence the need for carrying out the SSP of this specific prepolymer at 150°C, which is not sufficient for proper polycondensation, coPA5 having only slightly enhanced molecular weight was obtained.

2D NMR spectra of the synthesized copolyamides provided detailed information regarding the chemical structure, purity and possible conformational changes of DAII, which could occur during the synthesis of PA. The analysis of *Correlation Spectra COSY* (Figure 1) and *Heteronuclear Multiple-Bond Correlation Spectra (HMBC)* (Figure 2) proved the absence of detectable amounts of unreacted diacid or diamine residuals, since correlation signals of monomers having both functional groups and not involved in the

formation of amide groups were not found. Due to the absence of separated signals related to the amine end-groups of PA, the calculation of their molecular weights from NMR spectra was impossible. However, given the structure of polyamides and the possible sequence of the different monomer residues (Scheme 2), 2D NMR spectra should clearly display the signals related to diaminoisoidide, 1,4-diaminobutane and sebacic acid as double-side bonded units.

The analysis of the signals originating from DAII residues was successfully accomplished by the study of ^1H - ^1H *COSY* ^1H - ^{13}C *HMBC* spectra. The cross-peaks H^7/H^4 , H^4/H^6 , H^4/H^6 , H^6/H^6 and H^5/H^4 found in the *COSY* spectrum at 7.78 ppm, 4.46 ppm, 4.02 ppm, 3.96 ppm, and 4.80 ppm proved the presence of protons H^7 , H^4 , H^6 , H^6 , and H^5 , respectively. Besides, two- and three-bond correlations between these protons and adequate carbons were verified by *HMBC* spectra. The signals at 4.80/57.8, 4.80/71.5 and 4.46/86.2 were assigned to the correlations H^5/C^4 , $\text{H}^5/\text{C}^{6,6}$ and H^4/C^5 , while H^6/C^4 , H^6/C^4 , H^6/C^5 , H^6/C^5 signals were found at 4.02/57.8 ppm, 3.96/57.8 ppm, 4.02/86.2 ppm, and 3.96/86.2 ppm. Further assignments of the signals at 4.46/180.5 ppm, 7.78/180.5 ppm, 7.78/57.8 ppm, 7.78/71.5 ppm for H^4/C^{14} , H^7/C^{14} , H^7/C^4 and $\text{H}^7/\text{C}^{6,6}$ correspond to the linkage between diaminoisoidide and sebacic acid units. Based on these results it should be noted that due to the absence of additional peaks any changes of L-ido into D-manno conformation of the diamine after synthesis were not observed.

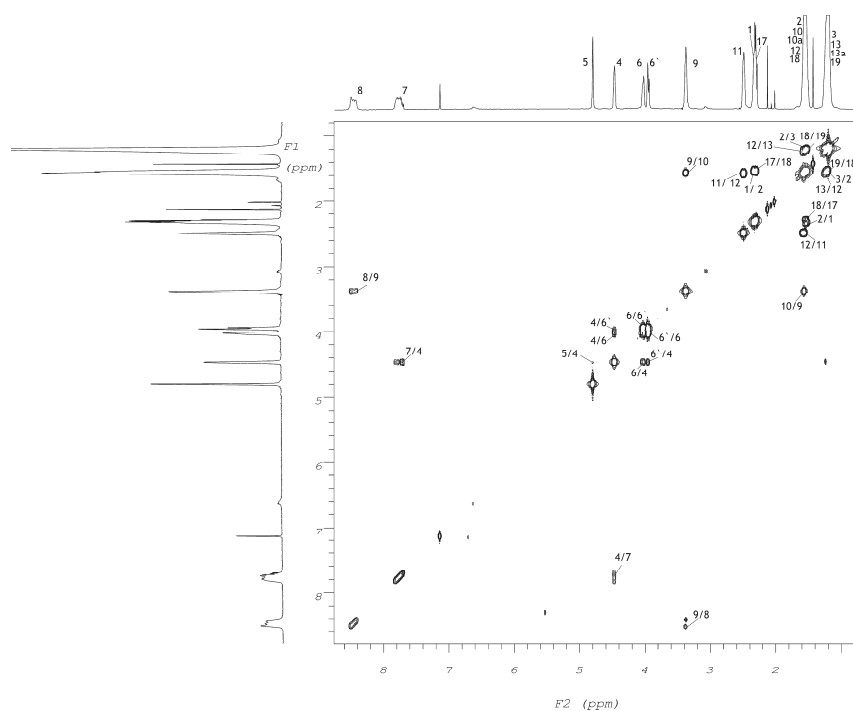


Figure 1. 500 MHz correlation spectrum (COSY) of copolyamide coPA5.

The sequence of 1,4-diaminobutane bonded with sebacic acid units (Scheme 2) was confirmed by the presence of the cross-peaks H^9/H^{10} and H^9/H^8 at 3.38 ppm in the corresponding *COSY* spectrum (see Figure 1). Additional evidence for the presence of this structural fragment in the copolyamids were the signals at 3.38/25.0 ppm, 3.38/180.5 ppm, 1.57/42.0 ppm and 8.43/180.5 ppm assigned to H^9/C^{10} , H^9/C^{15} , H^{10}/C^9 and H^8/C^{15} in the *HMBC* spectrum, as shown in Figure 2.

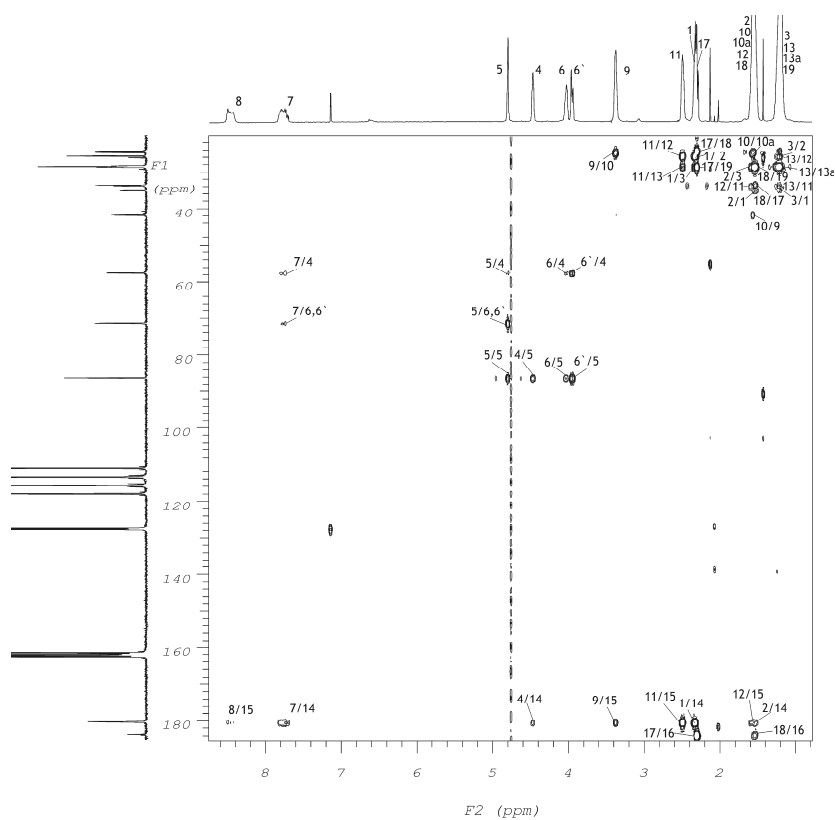
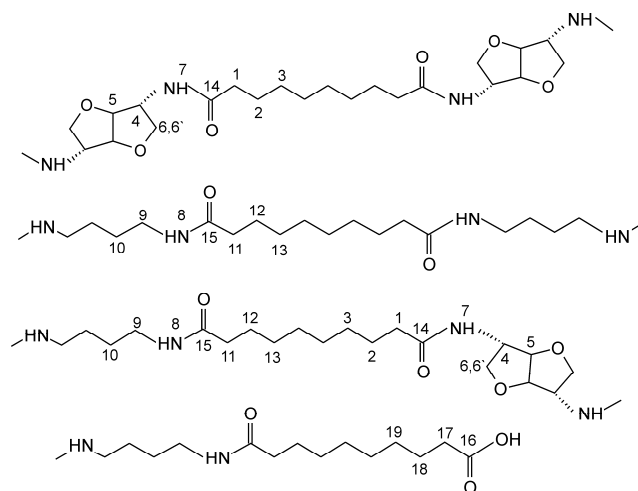


Figure 2. 500 MHz Heteronuclear Multiple-Bond Correlation spectrum (HMBC) of copolyamide coPA5.

To fully accomplish proton and carbon peak assignment the analysis of sebacic acid units in PA was performed. In the *COSY* spectrum the cross-peaks at 2.32 ppm, 1.52 ppm, 1.21 ppm have been described as H^1/H^2 , H^2/H^3 and H^3/H^2 signals and are related to sebacic acid residues bonded with diaminoisoidide. This unit sequence was also confirmed by the *HMBC* spectrum by the presence of the signals at 2.32/26.0 ppm, 2.32/28.5 ppm, 1.52/35.2 ppm, 1.52/28.5 ppm, 1.21/26.0 ppm, 1.21/35.2 ppm from H^1/C^2 , H^1/C^3 , H^2/C^1 , H^2/C^3 , H^3/C^2 , and H^3/C^1 correlations. Two- and three-bond correlations between H^1/C^{14} and H^2/C^{14} were found at 2.32/180.5 ppm and 1.52/180.5 ppm (Figure 2). Similarly, the presence of sebacic acid units bonded with 1,4-diaminobutane were analyzed

based on the cross-peaks at 1.21 ppm, 1.58 ppm and 2.50 ppm, depicted as H¹³, H¹², H¹¹ (Scheme 2 and Figure 1). A careful examination of the *HMBC* spectrum allowed to indentify these signals as H/C correlations at 1.21/36.0 ppm, 1.21/34.0 ppm, 1.58/34.0 ppm, 2.50/26.0 ppm, 2.50/28.5 ppm. Additional evidence of sebaccic acid units bonded with 1,4-diaminobutane were the signals at 2.50/180.5 ppm and 1.58/180.5 ppm from H¹¹/C¹⁵ and H¹²/C¹⁵, respectively. Finally, due to the presence of the signals at 2.30/184.0 ppm and 1.52/184.0 ppm and originating from two- and three-bond correlations of H¹⁷/C¹⁶ and H¹⁸/C¹⁶, it was possible to prove the existence of sebaccic acid units as end groups of PA (Figure 2).



Scheme 2. The possible sequences of monomer residues of sebaccic acid, diaminoisoidide and 1,4-diaminobutane in the co- and homopolyamides.

Polyamide based exclusively on sebaccic acid and diaminoisoidide (entry 6 in Tables 1, 2, 3) was obtained via interfacial polycondensation of diaminoisoidide and sebaccyl chloride in water/chloroform emulsion. The reaction was carried out in the presence of potassium carbonate. As reported by Thiem and Bachmann²⁸ the formation of polyamides during interfacial polycondensation takes place in the organic solvent near the aqueous phase. Simultaneously, the

results presented by these authors clearly indicate that the molecular weight of polyamides based on DAI is dependent on many factors such as: temperature, type of organic solvent or molar ratio of the used monomers. SEC data show that the molecular weight of the polyamide based on diaminoisoidide and sebacic acid is slightly above 4000 g/mol (Table 1). This low molecular weight might be reasonably explained as caused by the high solubility of diaminoisoidide in water, reducing the tendency to accumulate around the interface, and possible hydrolysis of diacid chloride resulting in a change of the molar ratio of the used compounds.¹⁸ The ¹H NMR spectrum presented in Figure 3 provided information regarding the chemical structure of PA based on sebacic acid and diaminoisoidide (entry 6 in Table 1, see also Scheme 2 for the labeling of the protons). The signals at 8.05 ppm were recognized as related to H⁷ protons from the amide group. The peaks at $\delta = 4.33, 4.07, 3.80,$ and 3.58 ppm were assigned to DAI protons H⁵, H⁴, H⁶ and H⁶. They do not suggest any change of the DAI structure. As expected, the signals related to sebacic acid units, H¹, H² and H³ were observed at 2.05, 1.44 and 1.20 ppm, respectively.

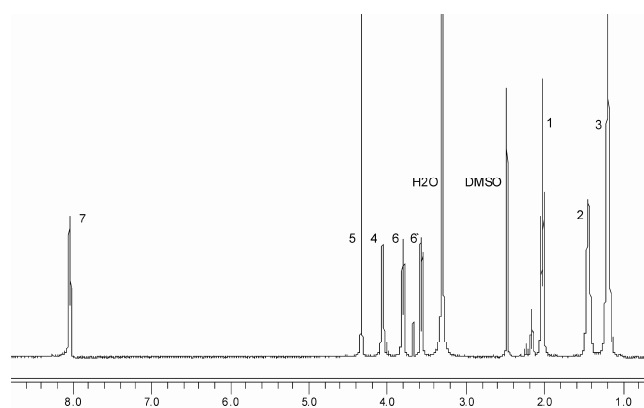


Figure 3. 400MHz ¹H NMR spectrum of the homopolyamide based on diaminoisoidide and sebacic acid.

Figures 4a and 4b show FT-IR spectra for the synthesized polyamides and copolyamides recorded at 30 °C. The spectra were normalized according to the

area under the symmetric and asymmetric methylene bands in the interval 2800-3000 cm^{-1} . In Figure 4a the spectral range from 2800 to 3500 cm^{-1} is presented. It shows several significant differences between the synthesized materials with different DAII contents. The signals at 3301-3315 cm^{-1} , 3201 cm^{-1} and 3060-3072 cm^{-1} are assigned to the NH stretch, NH stretch and Amide (I+II overtone), and NH stretch with Amide II overtone vibrations, respectively.³⁸⁻⁴¹ It is interesting, however, that for the polyamides with increasing content of DAII (coPA2-PA6) these bands appear broader and weaker, which suggests decrease of crystalline order and reduction in hydrogen bond density. This phenomenon is consistent with the appearance and growth of the intensity of the bands around 1720 cm^{-1} associated with “free” non hydrogen-bonded carbonyl groups (Figure 4b).⁴² The infrared spectra in the region 1800-800 cm^{-1} show signals related to Amide I (CO stretch, 1636-1642 cm^{-1}), Amide II (in-plane NH deformation with CO and CN stretches, 1542-1543 cm^{-1}), Amide III coupled with hydrocarbon skeleton (1358 cm^{-1} , 1291 cm^{-1} , 1189-1190 cm^{-1}) and the Amide IV “crystallinity band” (C-CO stretch, 946 cm^{-1}).^{40, 41, 43} Interesting information is also provided by the presence of bands at 1476 cm^{-1} , 1466 cm^{-1} and 1418 cm^{-1} , which are assigned to CH_2 scissoring next to NH groups with trans conformation and visible exclusively for PA 4.10 and copolymers having 1,4-diaminobutane residues, CH_2 scissoring not adjacent to the amide group and CH_2 scissoring next to the CO group with trans conformation, respectively.^{39, 41} Furthermore, the weak bands at 1135-1142 cm^{-1} were identified and are assigned to skeletal C-C stretch, gauche conformation.⁴⁴ In the analyzed spectral region also bands related to C-O stretching vibrations at 1080-1100 cm^{-1} , CH_2 wagging/twist at 1392 cm^{-1} and 1314 cm^{-1} , skeletal C-C stretch at 1255 cm^{-1} and 1231 cm^{-1} , CH_2 rocking vibrations at 971 cm^{-1} and amide stretching vibrations in the “crystalline phase” at 903 cm^{-1} were found.⁴⁴⁻⁴⁶ The signals at 903 cm^{-1} are visible for the polymers having DAII units and give strong evidence for the presence of DAII in the crystalline phase of these polyamides.

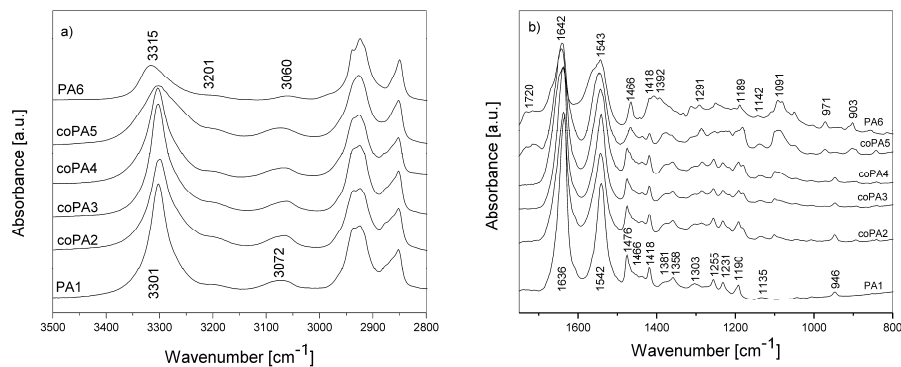


Figure 4. FT-IR spectra of homopolymers PA1, PA6 and copolymers coPA2, coPA3, coPA4, coPA5, recorded at 30 °C. The spectra show frequency ranges from 3500-2800 (a) and 1800-800 cm^{-1} (b).

3.3.2 Thermal Properties of Polyamides. From the thermogravimetric and DSC analysis data, presented in Table 2, it is clear that the thermal stability of the novel renewable polyamides is directly related to the content of diaminoisoidide units in the polymers. With increasing DAII content in the polyamides a reduction in their thermal stability was observed. Upon heating of PA1 (commercially known as PA 4.10) a 5 wt% weight loss was observed at around 420 °C, decreasing to 300 °C (Entry 6 in Table 2) with increasing DAII content. However, for the compositions with a DAB/DAII mol ratio of 0.80/0.20 the differences in thermal stability, compared to PA 4.10, were less pronounced (5% of weight loss $T_{5\%} = 377$ °C). The explanation of this phenomenon might be oxidation at the carbon atom in the α -position of the ether oxygens in the diaminoisoidide residues, resulting in a lower thermal stability of the materials containing DAII units.

Table 2. Thermal stability, melting and crystallization temperatures and enthalpy of the transitions analyzed from the second DSC heating and cooling runs.

| Symbol | T _{5%} (°C) | T _{max} (°C) | T _m (°C) | ΔH _m (J/g) | T _c (°C) | ΔH _c (J/g) |
|--------|-------------------------|--------------------------|------------------------|--------------------------|------------------------|--------------------------|
| PA1 | 424 | 483 | 246 | 67.3 | 221 | 75.4 |
| coPA2 | 388 | 457 | 242 | 57.3 | 209 | 56.0 |
| coPA3 | 379 | 460 | 236 | 50.6 | 201 | 47.8 |
| coPA4 | 377 | 456 | 232 | 40.9 | 198 | 45.3 |
| coPA5 | 321 | 455 | 179, 198 | 32.8 | 156 | 39.3 |
| PA6 | 300 | 437 | 152 | 15.1 | 96 | 11.4 |

T_{5%} = temperature of 5% mass loss, T_{max} = temperature of maximal rate of decomposition, T_m = melting point, T_c = crystallization temperature, ΔH = enthalpy of the transition

To investigate the melting and crystallization of the polyamides DSC analyses were performed. From the data presented in Table 2, taken from the second heating and cooling scans, it follows that a partial replacement of DAB units by diaminoisoidide in the structure of polyamide 4.10 influences the melting point. The copolyamides containing diaminoisoidide have lower melting and crystallization temperatures in comparison to the homopolymer based on sebacic acid and 1,4-diaminobutane. The synthesized, fully renewable copolyamides exhibit tunable polarities and melting points. Lower melting points, and therewith lower processing temperatures of the obtained DAII-containing copolyamides, can facilitate processing of these materials. The presence of DAII in the structure of the PAs influences ΔH of the observed transitions. With increasing DAII content in the polymers the enthalpy of the transitions is strongly reduced compared to entry PA1 in Table 2. These changes can be understood in terms of a reduction of the hydrogen bond density in the copolyamides, as was found by FT-IR spectroscopy discussed above, less perfect chain packing of DAII-containing polymers and reported by many researchers a reduction of lamellar crystal thickness.⁴³ Moreover, the widely

reported effect related to structural rearrangement and the resulting two-peak melting,⁴⁷ was especially visible for the copolymer containing around 43 mol% of DAII (see Figure 5). This phenomenon can be explained by melting of imperfect crystals (low temperature peak), recrystallization upon heating and re-melting of the more perfectly formed crystals (high temperature peak) or as presented in the next chapter, due to the coexistence of two crystalline forms.

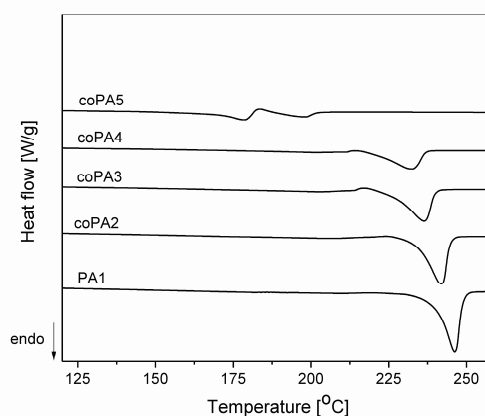


Figure 5. DSC traces of the second heating cycle of the co- and homopolyamides with different contents of diaminoisoidide.

3.3.3 Wide-Angle X-ray Diffraction. The synthesized polyamides are semi-crystalline in the whole studied range of copolymer compositions (see Figure 6). The X-ray diffraction profiles of all copolymers present strong analogies with the X-ray diffraction patterns of the corresponding homopolymers. In particular the profiles of samples with a DAII content lower than 43 mol% are similar to that of the sebacic acid/DAB homopolymer, displaying the typical four polyamide reflections in the 2θ ranges $3-7^\circ$, $10-12^\circ$ and $18-25^\circ$, indexed as 001 , 002 , 100 and $010/110$ (Table 3). Therefore it can be concluded that coPAs with DAII contents lower than 43 mol% have a crystal structure similar to that of the polyamide 4.10 homopolymer. This structure consists of stacked hydrogen-bonded sheets, in which the polymer chains are arranged side-by-side.^{24, 48} The 100 peak corresponds to the interchain distance and the $010/110$ peak to the

intersheet distance. With increasing DAI content the $010/110$ reflection decreases in intensity, but it doesn't show any shift in position. This suggests that the intersheet distance is not affected by increasing the DAI content for coPAs with a DAI content lower than 43 mol%.

The XRD pattern of the copolyamide with a DAI content of 43 mol% shows close resemblance to that of the sebacic acid/DAI homopolymer, i.e. it gives only two strong reflections in the 2θ range $3-7^\circ$ and $15-25^\circ$ (see Figure 6). The latter single peak in the 2θ range of $15-25^\circ$ indicates that the material has crystallized into a close to hexagonal packing of polymer chains.

In the XRD patterns of the coPA 5 and SA/DAI-based homopolyamide the reflection indexed as 001 shifts to lower 2θ values compared to the same reflection of the other polyamides. This shift reveals an increase of the c-axis dimension of coPA 5 due to cocrystallization of the two comonomers in the same crystal lattice.⁴⁹

Further and more detailed information will be described in the following chapters concerning crystallographic studies of the new biobased copolyamides. It will be also shown that for the copolymers having up to 20 mol% of DAI, the comonomer units will be included in the crystalline PA 4.10 phase even though visible changes of the unit cell dimensions do not occur.

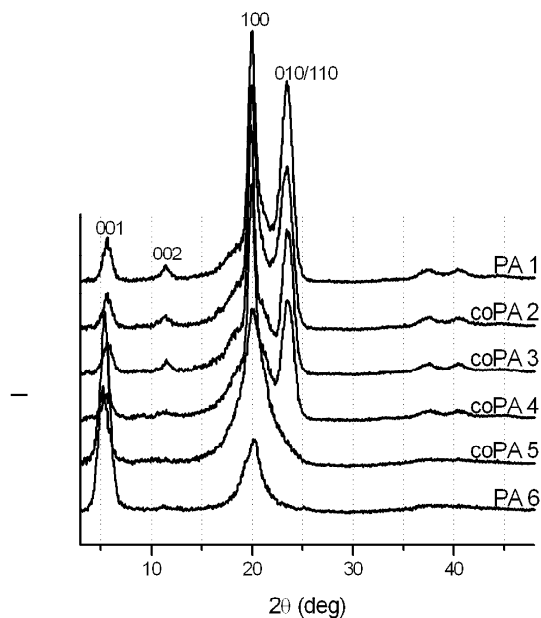


Figure 6. X-ray powder diffraction patterns of as-prepared co- and homopolyamides with different contents of diaminoisoidide measured at room temperature. The indices correspond to the packing mode of the α -phase and the β -phase of common polyamides.

3.4 Conclusions

Fully biobased polyamides from sebacic acid, 1,4-diaminobutane and diaminoisoidide (prepared from isomannide) were successfully synthesized by either bulk melt polycondensation followed by solid state polymerization (SSP) or by interfacial polycondensation. The molecular weight and chemical structure of the polymers were characterized by SEC, FT-IR and 2D NMR, *viz.* by recording correlation spectra COSY and Heteronuclear Multiple-Bond Correlation spectra (HMBC). Using bulk polycondensation and SSP white products with number average molecular weights above 18,000g/mol and polydispersity indexes below 3.0 were obtained. However, the interfacial polymerization route led to polymers with significantly lower molecular weight, which may have been caused by hydrolysis of diacid chloride during the course

of the reaction. The analysis of 2D NMR spectra proved the presence of diaminoisoidide, 1,4-diaminobutane and sebacic acid units as chain fragments, while sebacic acid residues were also found as end-groups of the macromolecules. More details were provided by FT-IR spectroscopy which showed that the presence of DAII influenced the hydrogen bond density in the copolyamides. Moreover, FT-IR analysis also allowed to distinguish bands at around 903 cm^{-1} related to DAII residues incorporated into the crystal structure. XRD analysis showed that the new biobased copolyamides are semi-crystalline. The XRD data indicate that with increasing DAII content the typical polyamide structure with different interchain and intersheet distances is preserved for samples with DAII content lower than 43 mol%. At higher DAII contents the structure changes into a structure with a close to hexagonal packing of polymer chains. As expected, with the introduction of DAII into the main chain of the polyamides the melting temperature decreased. Significant differences between the melting points of the homopolymers based on sebacic acid/1,4-diaminobutane ($T_m = 246\text{ }^\circ\text{C}$) and sebacic acid/diaminoisoidide ($T_m = 152\text{ }^\circ\text{C}$) provide many opportunities for the synthesis of copolyamides with tunable melting temperatures. For example for fiber applications lower melting points are required than for engineering plastics applications. The lower melting enthalpies together with the lower melting points imply lower energy consumption during processing. In view of the expected higher moisture absorption, due to the presence of the hydrophilic DAII residues, fibers based on the copolyamides are expected to result in a higher wearing comfort of clothes based thereon.

References

1. Aharoni, S. M., *n-Nylons: Their Synthesis, Structure and Properties* John Wiley&Sons: New York, **1997**.
2. Kohan, M. I., *Nylon Plastics Handbook*. Hanser Publishers: Munich Vienna New York, **1995**.
3. Vanhaecht, B.; Rimez, B.; Willem, R.; Biesemans, M.; Koning, C., *E. J. Polym. Sci. Part A: Polym. Chem.* **2002**, *40*, 1962-1971.
4. Koning, C., E; Teuwen, L.; De Jong, R.; Janssen, G.; Coussens, B., *High Perf. Polym.* **1999**, *11*, 387-394.
5. Gaymans, R. J.; van Utteren, T. E. C.; van Berg, J. W. A.; Schuyter, J. J. *Polym. Sci. Part B: Polym. Chem.* **1977**, *15*, 537-545.
6. Steeman, P.; Nijenhuis, A., *Polymer* **2010**, *51*, 2700-2707.
7. Hasan, M. M.; Zhou, Y.; Mahfuz, H.; Jeelani, S. *Mater. Sci. Eng.* **2006**, *429*, 181-188.
8. Cooper, S., J.; Atkins, E., D., T.; Hill, M., J. *J. Polym. Sci. Part A: Polym. Chem.* **1998**, *36*, 2849-2863.
9. Angelo, R. J.; Miura, H.; Gardner, K. H. D.; Chase, B.; English, A. D. *Macromolecules* **1989**, *22*, 117-121.
10. Jouffret, F.; Madec, P. J. *J. Polym. Sci. Part A: Polym. Chem.* **1996**, *34*, 2363-2370.
11. Botelho, E., C; Scherbakoff, N.; Rezende, M., C. *Polym. Inter.* **2002**, *51*, 1261-1267.
12. Kim, K. S.; Yu, A., J. *J. Appl. Polym. Sci.* **1979**, *23*, 439-444.
13. Wang, L. H.; Porter, R., S. *J. Polym. Sci. Part B: Polym. Phys.* **1995**, *33*, 785-790.
14. Johnson, G., C; Mathias, L., J. *Polymer* **1993**, *34*, 4978-4980.
15. Prieto, A.; Iribarren, I.; Munoz-Guerra, S. *J. Mater. Sci.* **1993**, *28*, 4059-4062.

16. Wang, L., H.; Calleja, F., J.; Kanamoto, T.; Porter, R., S. *Polymer* **1993**, *34*, 4688-4691.
17. Kricheldorf, H. R.; Bornhorst, K.; Schellenberg, J.; Schwarz, G. J. *Macromol. Sci. Part A: Pure Appl. Chem.* **2007**, *44*, 119 - 124.
18. Arai, Y.; Watanabe, M.; Sanui, K.; Ogata, N. *J. Polym. Sci. Part A: Polym. Chem.* **1985**, *23*, 3081-3093.
19. Ballistreri, A.; Garozzo, D.; Giuffrida, M.; Impallomeni, G.; Montaudo, G. *Polym. Degrad. Stab.* **1989**, *23*, 25-41.
20. Ramesh, C. *Macromolecules* **1999**, *32*, 3721-3726.
21. De Koning, G., J.; Koning, C., E.; Teuwen, L., M., J. WO 2000009586, **2000**.
22. Atkins, E. D. T.; Hill, M.; Hang, S. K.; Keller, A.; Organ, S. *Macromolecules* **1992**, *25*, 917-924.
23. Jones, N. A.; Atkins, E. D. T.; Hill, M. J. *Macromolecules* **2000**, *33*, 2642-2650.
24. Jones, N. A.; Atkins, E. D. T.; Hill, M. J.; Cooper, S. J.; Franco, L. *Polymer* **1997**, *38*, 2689-2699.
25. Jones, N. A.; Atkins, E. D. T.; Hill, M. J.; Cooper, S. J.; Franco, L. *Macromolecules* **1996**, *29*, 6011-6018.
26. Li, Y.; Yan, D. *Polymer* **2001**, *42*, 5055-5058.
27. Stoss, P.; Hemmer, R.; Derek, H. *Adv. Carbohydr. Chem. Biochem.* **1991**, *49*, 93-173.
28. Thiem, J.; Bachmann, F. *Makromol. Chem.* **1991**, *192*, 2163-2182.
29. Thiyagarajan, S.; Gootjes, L.; Vogelzang, W.; Wu, J.; Haveren, J.; van Es, D. *Tetrahedron* **2010**, *67*, 383-389.
30. Fenouillot, F.; Rousseau, A.; Colomines, G.; Saint-Loup, R.; Pascault, J. P. *Progr. Polym. Sci.* **2010**, *35*, 578-622.
31. Caouthar, A. A.; Loupy, A.; Bortolussi, M.; Blais, J.; Dubreucq, L.; Meddour, A. *J. Polym. Sci. Part A: Polym. Chem.* **2005**, *43*, 2480-2491.

32. Caouthar, A.; Roger, P.; Tessier, M.; Chatti, S.; Blais, J. C.; Bortolussi, M. *Europ. Polym. J.* **2007**, *43*, 220-230.
33. Okada, M.; Yamada, M.; Yokoe, M.; Aoi, K. *J. Appl. Polym. Sci.* **2001**, *81*, 2721-2734.
34. Gomurashvili, Z.; Kricheldorf, H. R.; Katsarava, R. *J. Macromol. Sci. Pure Appl. Chem.* **2000**, *A37*, 215-227.
35. Katsarava, R.; Beridze, V.; Arabuli, N.; Kharadze, D.; Chu, C. C.; Won, C. Y. *J. Polym. Sci. Part A: Polym. Chem.* **1999**, *37*, 391-407.
36. Philip, B.; Sreekumar, K. *Polym. Internat.* **2001**, *50*, 1318-1323.
37. Kirk, R., E.; Othmer, D., F. *Kirk-Othmer Encyclopedia of Chemical Technology*. Wiley-Interscience: New York, **1997**, *22*, 400.
38. Yoshioka, Y.; Tashiro, K.; Ramesh, C. *J. Polym. Sci. Part B: Polym. Phys.* **2003**, *41*, 1294-1307.
39. Yoshioka, Y.; Tashiro, K. *J. Phys. Chem.* **2003**, *107*, 11835-11842.
40. Nair, S. S.; Ramesh, C.; Tashiro, K. *Macromolecules* **2006**, *39*, 2841-2848.
41. Cooper, S. J.; Coogan, M.; Everall, N.; Priestnall, I. *Polymer* **2001**, *42*, 10119-10132.
42. Coleman, M. M.; Lee, K. H.; Skrovanek, D. J.; Painter, P. C. *Macromolecules* **1986**, *19*, 2149-2157.
43. Vinken, E.; Terry, A. E.; Hoffmann, S.; Vanhaecht, B.; Koning, C. E.; Rastogi, S. *Macromolecules* **2006**, *39*, 2546-2552.
44. Vasanthan, N.; Salem, D. R. *J. Polym. Sci. Part B: Polym. Phys.* **2000**, *38*, 516-524.
45. Vasanthan, N.; Murthy, N. S.; Bray, R. G. *Macromolecules* **1998**, *31*, 8433-8435.
46. Li, W.; Huang, Y.; Zhang, G.; Yan, D. *Polym. Intern.* **2003**, *52*, 1905-1908.
47. Roberts, R. C., *J. Polym. Sci. Part B: Polym. Lett.* **1970**, *8*, 381-394.
48. Bunn, C. W.; Garner, E. V. *R. Soc. Lond. Ser. A, Math. Phys. Sci.* **1947**, *189*, 39-68.

49. Hoffmann, S.; Vanhaecht, B.; Devroede, J.; Bras, W.; Koning, C. E.; Rastogi, S. *Macromolecules* **2005**, *38*, 1797-1803.
50. Jasinska, L., Villani, M., Wu, J., van Es, D., Klop, E., Rastogi, S. and Koning, C. E. *Macromolecules*, **2011**, *44* (9), pp 3458–3466.

Chapter 4

Local Conformation and Cocrystallization Phenomena in Renewable Diaminoisoidide-Based Polyamides Studied by FT-IR, Solid State NMR and WAXD*

Biobased polyamides synthesized from diaminoisoidide (DAII), 1,4-diaminobutane and sebacic acid are investigated by FT-IR, $^{13}\text{C}\{^1\text{H}\}$ magic-angle spinning/cross-polarization (CP/MAS) NMR spectroscopy and WAXD. Their molecular conformation and mobility undergo distinct changes as a function of temperature and diaminoisoidide content in the compositions. The presence of randomly distributed diaminoisoidide (DAII) in the polyamides reduces their hydrogen bond density and affects the *trans/gauche* conformer population. FT-IR and $^{13}\text{C}\{^1\text{H}\}$ CP/MAS NMR were successfully employed to prove the incorporation of DAII both in the crystalline and amorphous phase of these materials. Changes in the position and intensities of the diaminoisoidide-assigned FT-IR and NMR signals prove that the DAII monomer causes a conformational disorder of the polyamides and thus influences the crystal structure of these materials, as also shown by WAXD experiments. Extensive *ab initio* calculations using a combination of DFT and MP2 methods reveal a number of stable conformers of DAII and thus an unexpectedly high flexibility of the isohexide unit.

*reproduced from Lidia Jasinska-Walc, Maurizio Villani, Dmytro Dudenko, Otto van Asselen, Enno Klop, Sanjay Rastogi, Michael Ryan Hansen, and Cor E. Koning, *Macromolecules*, **2012**, 45 (6), 2796–2808.

4.1 Introduction

Isohexides have been recently regarded as one of the most promising alternatives for petrochemical monomers. The possible use of starch-based 1,4;3,6-dianhydrohexitols (isosorbide, isomannide and isoidide) or their diamino derivatives with D-manno or L-ido conformation in the synthesis of poly(ester-amides) (PEAs) or polyamides (PAs) provides partially or entirely biobased materials and consequently demonstrates their multiple applications.¹⁻⁸ These bicyclic compounds are of natural origin and their degradation products are nontoxic and Kricheldorf et al.⁴ and Okada et al.⁷ proved that isohexitol-based polymers can be successfully used as bioanalogous or biodegradable materials. Furthermore, a new approach towards poly(ester-amides) from isosorbide was proposed by Philip and Sreekumar.⁸ These authors obtained optically active materials with high T_g 's, which can be applied as electro-optic devices. Hitherto, isohexides are usually used as T_g -enhancing agents. However, our recent investigations revealed that diaminoisoidide (DAII), the *exo-exo* diamine derivative of dianhydrohexitols, incorporated into the PA 4.10 backbone reduces the hydrogen bond density and thus the melting point of the polyamides.⁹ This aspect in turn is especially important in view of their practical applications, since this allows tailoring hydrogen bonding which is required for some applications where melting temperature is not of critical importance.

Regardless of the chemical composition, polyamides exhibit a characteristic semi-crystalline structure consisting of chain-folded, hydrogen-bonded sheets held together by van der Waals forces.^{10, 11} As reported previously, depending on the distance between recurring amide groups, the sheets can stack together either with a progressive shear, yielding the so-called α -phase, or with an alternating shear, yielding the so-called β -phase.¹²⁻²⁰ The X-ray diffraction profiles of such polyamides display a typical diffraction peak indexed as *100*

related to the interchain distance, as well as a *010/110* diffraction peak, related to the intersheet distance. Generally, for the known and commercially available PAs the formation of a pseudo-hexagonal phase is observed upon a solid state crystal to crystal transition upon heating (Brill transition).^{13, 21, 22} The transformation of the triclinic structure with different interchain/intersheet distances into the pseudo-hexagonal form can be associated to the formation of hydrogen bonds between chains lying in adjacent sheets of the polyamides.²³ However, more recently it was proposed that no intersheet H-bonding occurs at the Brill transition temperature and that the intersheet and interchain distances become equal by a kind of cylindrical rotation of the methylene units between the H-bonded amide groups.²⁴ As it is well known, the Brill transition observed using temperature-dependent WAXD experiments occurs as the merging of two X-ray diffraction peaks corresponding to the interchain and intersheet distances into a single diffraction peak. These changes, depending on the chemical structure and length of the repeat unit of the polyamides, can usually be observed either somewhat below or at the melting point of the polymers. Nonetheless, the XRD study carried out at room temperature for the copolyamides based on diaminoisoidide, 1,4-diaminobutane (DAB) and sebacic acid,⁹ reported in the previous chapter, showed that with increasing diaminoisoidide content in the copolyamides the typical structure with different interchain and intersheet distance was preserved for the products with DAII contents lower than around 40 mol%, while for the materials with higher DAII contents the structure changed into a close to hexagonal packing of polymer chains.

To follow the conformational changes of nylons several spectroscopic techniques have been employed successfully. One of the commonly used methods for the analysis of polyamide chain motions is FT-IR spectroscopy. As reported earlier a detailed insight into the position and intensity of FT-IR signals allowed to establish that during the Brill transition marked conformational changes occur in the methylene sequences of the polyamides, which reveal an

enhanced mobility upon heating.^{25, 26, 27, 28} The conformational reorganization together with the weakening of the hydrogen bonding of the polymers can also be observed by $^{13}\text{C}\{^1\text{H}\}$ cross-polarization NMR spectroscopy (CP/MAS NMR).²⁹⁻³² More interesting, however, is that $^{13}\text{C}\{^1\text{H}\}$ CP/MAS NMR analysis can provide information regarding the co-existence of various crystalline polymorphs in the polymers and the differences in the conformational freedom of polymer chains within crystalline and noncrystalline regions.^{33, 34}

In chapter 3, we reported the synthetic route and the structural and thermal characterization of novel, fully renewable homo- and copolyamides from diaminoisoidide (synthesized from isomannide), 1,4-diaminobutane (in nature known as putrescine) and sebacic acid (derived from castor oil) (see Figure 1).⁹ The X-ray analysis of the polyamides revealed that the presence of the DAII units in the polyamides affects their crystal structure. The present chapter focuses on the conformational changes and local chain dynamics of diaminoisoidide-based polyamides upon heating. $^{13}\text{C}\{^1\text{H}\}$ CP/MAS NMR and FT-IR spectroscopy were used as powerful techniques for the analysis of the structural behavior and mobility of the polyamides as function of the temperature. Particular attention was given to phase separation and the presence of diaminoisoidide in the crystal structure of the biobased materials. These techniques in combination with WAXD analysis were used to investigate cocrystallization of the comonomers.

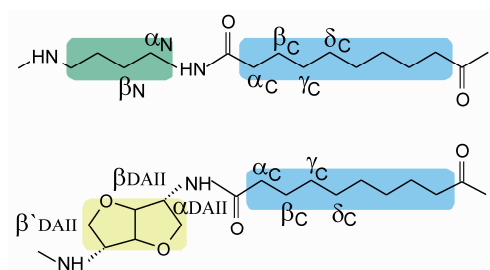


Figure 1. Sebacic acid(SA)/1,4-diaminobutane(DAB) and sebacic acid(SA)/diaminoisoidide(DAII) repeat units in the polyamides. Blue, green and yellow areas depict PA chain fragments between the amide groups. Carbon labels, presented also in Table 2, were used for solid state NMR analysis.

4.2 Experimental Section

4.2.1 Materials. The homopolyamides and copolyamides based on diaminoisoidide (DAII), 1,4-diaminobutane (DAB) and sebacic acid (SA) (Figure 1) were synthesized via bulk polycondensation followed by Solid State Polymerization (SSP) or by interfacial polycondensation, as described in the previous chapter.⁹ Here we report the characterization of the polyamides including solution state NMR experiments, SEC, FT-IR, TGA, DSC, and room temperature WAXD analysis was presented. Temperature dependent FT-IR, solid state NMR and WAXD studies were carried out on the homopolymers based on 1,4-diaminobutane and sebacic acid (PA1) or diaminoisoidide and sebacic acid (PA2) as well as on the copolymers containing 20 mol% and 43 mol% of diaminoisoidide (coPA3, coPA4), respectively. For an overview of the molecular characterization and thermal properties of these polyamides see Table 1.

Table 1. Built-in composition, molecular weight, melting and crystallization temperatures, and enthalpy of the transitions analyzed from the second DSC heating and cooling runs of the homo- and copolyamides.

| Symbol | Built-in composition (DAB/DAII) ^a | M _n (g/mol) | T _m (°C) | ΔH _m (J/g) | T _c (°C) | ΔH _c (J/g) |
|--------|--|------------------------|---------------------|-----------------------|---------------------|-----------------------|
| PA1 | 1.0/0 | 21,900 | 246 | 67.3 | 221 | 75.4 |
| PA2 | 0/1.0 | 4,200 | 152 | 15.1 | 96 | 11.4 |
| coPA3 | 0.80/0.20 | 20,400 | 232 | 40.9 | 198 | 45.3 |
| coPA4 | 0.57/0.43 | 3,900 | 179, 198 | 32.8 | 156 | 39.3 |

^a = molar ratio determined by NMR, T_m = melting point, T_c = crystallization temperature, ΔH = enthalpy of the transition during melting (m) or crystallization (c).

4.2.2 FT-IR. Fourier Transform Infrared spectra (FT-IR) were obtained using a Varian 610-IR spectrometer equipped with an FT-IR microscope. The spectra were recorded in a transmission mode with a resolution of 2 cm^{-1} . PA films obtained from 1,1,1,3,3,3-hexafluoroisopropanol were analyzed on a zinc selenium disk and heated from $30\text{ }^{\circ}\text{C}$ to slightly above melting points of the polyamides. For the purpose a Linkam TMS94 hotstage and controller were used. The samples were cooled in $10\text{ }^{\circ}\text{C}$ steps and reheated with the same heating steps. For the study the spectra from the second heating run were collected. Varian Resolution Pro software version 4.0.5.009 was used for the analysis of the spectra.

4.2.3 DSC. DSC measurements were carried out using DSC Q100 from TA Instruments. The analyses were performed in a nitrogen atmosphere with a heating rate of $10\text{ }^{\circ}\text{C}/\text{min}$. The events were analyzed from the second heating and cooling curve.

4.2.4 Solid State NMR. Variable-temperature (VT) $^{13}\text{C}\{^1\text{H}\}$ magic-angle spinning/cross-polarization (CP/MAS) NMR experiments were carried out on a Bruker ASX-500 spectrometer employing a double-resonance probe for rotors with 4.0 mm outside diameter. These experiments used 10.0 kHz MAS and a $4\text{ }\mu\text{s}$ $\pi/2$ pulse for ^1H . All VT $^{13}\text{C}\{^1\text{H}\}$ CP/MAS NMR spectra were recorded using a CP contact time of 3.0 ms and TPPM decoupling³⁵ during acquisition. The temperature was controlled using a Bruker temperature control unit in the range from $30\text{ }^{\circ}\text{C}$ to $210\text{ }^{\circ}\text{C}$. The VT $^{13}\text{C}\{^1\text{H}\}$ CP/MAS NMR spectra were recorded under isothermal conditions at intervals of $10\text{ }^{\circ}\text{C}$, employing a heating rate of $2\text{ }^{\circ}\text{C}/\text{min}$ between temperatures. Reported temperatures are corrected for friction induced heating due to spinning using ^{207}Pb MAS NMR of $\text{Pb}(\text{NO}_3)_2$ as a NMR thermometer.³⁶ The 2D ^1H - ^1H Double-Quantum Single-Quantum (DQ-SQ) correlation and $^{13}\text{C}\{^1\text{H}\}$ Frequency-Switched Lee-Goldburg HETERO-nuclear CORrelation (FSLG-HETCOR) experiments^{37, 38} were performed on a Bruker AVANCE-III 850 spectrometer using a double-resonance probe for rotors with 2.5 mm outside diameter. These experiments used spinning

frequencies of 25.0 kHz and 15.0 kHz, respectively. DQ excitation was performed using the BaBa sequence and the FSLG-HETCOR experiment used a CP time of 3.0 ms. Chemical shifts for ^1H and ^{13}C MAS NMR are reported relative to TMS using solid adamantane as an external reference.³⁹ CP conditions were optimized using L-alanine. All samples were annealed just below their melting temperature for 5 min under a flow of nitrogen gas before NMR analysis to remove precipitation induced structural conformations.

4.2.5 Geometry Optimization and NMR Chemical Shift Calculations. All calculations were performed with a Gaussian03 program package (see Ref.6 in Supporting Information). The geometries of 21 possible conformations obtained from the 1D potential energy surface (1D-PES) scanning procedure (Fig. S1) were further fully optimized at the MP2/6-31G*, MP2/6-311G** and the computationally less demanding B97-1/6-311G** level of theory. Harmonic vibrational frequencies and the Gibbs free energy differences were evaluated at the MP2/6-31G* and B97-1/6-311G** levels of theory. The most favorable conformers by energy (for both DFT and MP2 methods) have been proceeded for further NMR chemical shifts calculations at the B97-1/6-311G** level of theory. Further details about the 1D-PES procedure and the NMR chemical shift calculations are given in the Supporting Information.

4.2.6 WAXD. X-ray diffraction patterns were obtained employing a Bruker AXS HI-STAR area detector installed on a P4 diffractometer, using graphite-monochromated $\text{CuK}\alpha$ radiation ($\lambda = 1.5418 \text{ \AA}$) and a 0.5 mm collimator. The data were collected on SSP-synthesized powder contained in glass capillaries during heating at 10 °C/min from around 40 °C to melt and cooling from the melt to 40 °C with acquisition times of 5 minutes, using a Linkam TMS94 hotstage. Successively, the values of the temperatures reported here for heating/cooling cycles have been obtained by correcting the displayed temperature observed using the modified Linkam hotstage (see Supporting Information). This correction was made using a calibration curve with well known melting temperature standards. The 2D data were corrected for detector

non-uniformity and spatial distortion, subsequently background-corrected and transformed into 1D profiles via integration.

4.3 Results and Discussion

Spectroscopic techniques are very valuable to elucidate the conformational changes and chain motions of polymers. For the analysis of polymer chain organization, the combination of Fourier Transformed Infrared (FT-IR) and solid state NMR spectroscopy is particularly suitable for obtaining complementary results. We employed FT-IR and $^{13}\text{C}\{^1\text{H}\}$ CP/MAS NMR spectroscopy for probing local conformations and co-crystallization of the comonomers in the crystal lattice of diaminoisoidide-based copolyamides. WAXD analysis was used to confirm the influence of local conformation on the chain packing of diaminoisoidide-based copolyamides.

4.3.1 Infrared Analysis of the Polyamides.

FT-IR spectra of the homopolyamides PA1, PA2 and copolyamides coPA3, coPA4 (see Table 1) recorded at 30 °C are presented in Figures 2a, b. The Figures show spectra normalized according to the area under the symmetric and asymmetric methylene bands ($2800\text{-}3000\text{ cm}^{-1}$) in two spectral ranges *viz.* $2700\text{-}3600\text{ cm}^{-1}$ and $800\text{-}1750\text{ cm}^{-1}$. By comparison of the bands at $3301\text{-}3320\text{ cm}^{-1}$ and $3060\text{-}3070\text{ cm}^{-1}$, which are assigned to the NH stretch and NH stretch with Amide II overtone vibrations, significant changes in intensity can be observed. As reported by Schroeder et al.⁴⁰ and Skrovanek et al.^{41, 42} the broadness and decrease in the intensity of the N-H stretching mode at $3300\text{-}3320\text{ cm}^{-1}$ upon heating of the linear polyamides is caused by a decrease in the absorptivity coefficient reflecting hydrogen bond diminishes and transformation of the hydrogen-bonded N-H groups into “free” and non-hydrogen bonded N-H groups. Furthermore, the FT-IR studies employed by authors of even- and odd-type nylons revealed that the frequency of such bands reflects the average

strength of the hydrogen-bonded N-H groups.⁴² Following these observations and comparing the N-H stretching mode of the DAII-based polyamides one can conclude that the decrease and broadening of these signals, observed with increasing DAII content in the polyamides, is attributed to the change of their crystalline order and different strength of the hydrogen bonds in these materials. In the spectra recorded at 30 °C non-hydrogen bonded N-H bands, usually observed at 3440-3450 cm⁻¹, were not detected as a result of their relatively low intensity and/or broadening of the hydrogen-bonded N-H mode. However, the FT-IR analysis supported by the 2D ¹³C{¹H} FSLG-HETCOR results discussed below indicate that the incorporation of DAII units affects the hydrogen bond density and formation of non-hydrogen bonded N-H groups in the synthesized polyamides. On this basis, the band visible at 1720 cm⁻¹ and more pronounced for DAII-rich compositions can be assigned to non-hydrogen bonded carbonyl groups. These signals for linear polyamides are usually visible around 1670-1690 cm⁻¹ however, the presence of isohexide units in the backbone of the polyamides might affect the shift in frequency of non-hydrogen bonded Amide I bands. Moreover, C-O-C groups of isohexide can contribute in the formation of the hydrogen bonds influencing the amount of carbonyl groups that do not participate in hydrogen bonding. Simultaneously, in the region 800-1750 cm⁻¹ (Fig. 2b) several differences between the recorded spectra can be observed. For the copolymers and the homopolymer PA2 based on diaminoisoidide new signals at 1333 cm⁻¹ were found which are attributed to the Amide III vibrations.^{25, 28} The presence of diaminoisoidide in the structure of the polymers was also proven by the development of the bands in the vicinity of 1080-1100 cm⁻¹. These signals are characteristic for the asymmetric COC stretching mode in ethers⁴³ and the bands increase in intensity with increasing diaminoisoidide content of the PAs. An increased absorbance is also observed at 971 cm⁻¹, 911-915 cm⁻¹ and at 903 cm⁻¹. These bands are assigned to CH₂ rocking vibrations and to the C-CO stretching vibration in the crystalline phase.⁴⁴ Interesting information is also provided by bands at 1563 cm⁻¹ and 1411 cm⁻¹, found for

PA2 synthesized via interfacial polycondensation and assigned to asymmetric and symmetric COO^- stretch vibrations, respectively.⁴³ These bands are characteristic for carboxylic acid ammonium salt and imply the presence of polyamide salt residuals formed as a by-product during the synthesis.

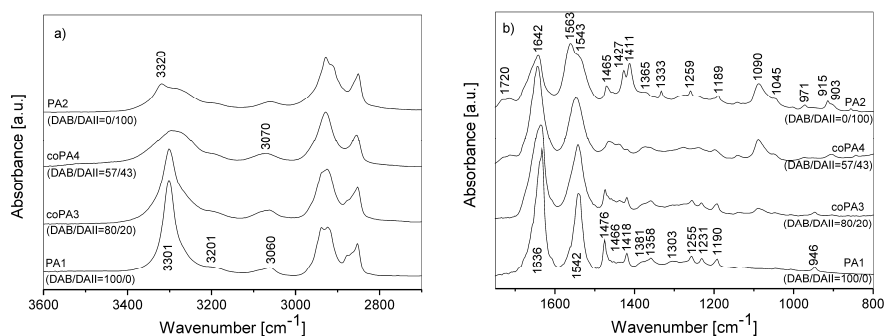


Figure 2. FT-IR spectra of homopolyamides PA1, PA2 and copolyamides coPA3, coPA4 recorded at 30 °C. The spectra show frequency ranges from 3600-2700 (a) and 1750-800 cm^{-1} (b), respectively.

In Figure 3, FT-IR spectra recorded upon heating of the homopolymers PA1, PA2 and the copolymers containing 20 mol% and 43 mol% of DAII (coPA3, coPA4) are presented. The spectra of PA1 and coPA3 show broadening and weakening of the bands at 1476 cm^{-1} and 1418 cm^{-1} , which are considered as CH_2 scissoring next to NH moieties with *trans* conformation and CH_2 scissoring next to CO moieties with *trans* conformation, respectively.^{27, 28} As reported by Yoshioka et al.²⁷ the conformational changes of methylene segments attached to NH and CO moieties are related to the Brill transition of polyamides. Due to the lower energy barrier of the torsion around $\text{CH}_2\text{-NH}$ the thermal motion of these chain fragments is more pronounced as compared to the $\text{CH}_2\text{-CO}$ fragments. These results are in agreement with our observations, since along with the decrease of hydrogen bond density the vibrations of the bands assigned to $\text{CH}_2\text{-NH}$ at around 190 °C show a significantly reduced intensity, consistent with the hexagonal packing of PA1 chains above the Brill temperature. Simultaneously, when the *trans* conformation is lost upon heating, the signals around 1450 cm^{-1}

and 1440 cm^{-1} assigned to the CH scissor vibrations of *gauche* conformers, become more visible. On the other hand the signals at 1381 cm^{-1} , 1303 cm^{-1} , 1255 cm^{-1} , 1231 cm^{-1} and 1044 cm^{-1} originating from CH_2 wagging or twisting and skeletal C-C stretch vibrations show broadening and weakening with increasing temperature.^{25, 26, 28, 45} Since the bands at 1381 cm^{-1} , 1303 cm^{-1} and 1044 cm^{-1} almost disappear above 190°C , they can be considered as Brill bands. The Amide II and Amide III coupled with hydrocarbon skeleton bands at 1542 cm^{-1} , 1358 cm^{-1} and 1190 cm^{-1} also become broader and weaker, however their presence is visible up to the melting point of the polyamide.²⁸ The copolymer containing 20 mol% of DAII (coPA3) undergoes similar conformational changes as PA1. However, as demonstrated previously,⁹ diaminoisoidide-rich coPA4 and PA2 show a different behavior and crystallize into a close to hexagonal packing of the polymer chains. In agreement with this, the characteristic Brill bands visible for PA1 and coPA3 and the band at 1476 cm^{-1} , related to CH_2 scissoring next to NH moieties with *trans* conformation, are not observed for these polyamides (Figure 3). On the other hand several new peaks assigned to the amorphous or crystalline phase of the polyamides were recognized. The bands observed above the melting point at $1080\text{-}1090\text{ cm}^{-1}$, 1333 cm^{-1} , 1259 cm^{-1} and 915 cm^{-1} in the spectra of the PA2 are related to the amorphous phase. Simultaneously, as discussed above, the presence of amide stretching vibration bands at $902\text{-}903\text{ cm}^{-1}$ in the spectra of PA2 and coPA4 and the vanishing of these bands at around $150\text{-}180^\circ\text{C}$ can be considered as further proof that DAII is present in the crystal phase of the PAs. This is in agreement with DSC measurements ($T_{m,\text{PA}2} = 152^\circ\text{C}$, $T_{m,\text{coPA}4} = 179^\circ\text{C}$, see Table 1) and ^{13}C MAS NMR analysis of these polyamides (see below). Similar behavior, depicted by broadening and finally disappearance, show the bands assigned to the C-CO stretch “crystalline band” at 946 cm^{-1} in the spectra of PA1 and coPA3, *i.e.* they become broader and weaker until disappearing when the melting temperature has been reached.²⁸

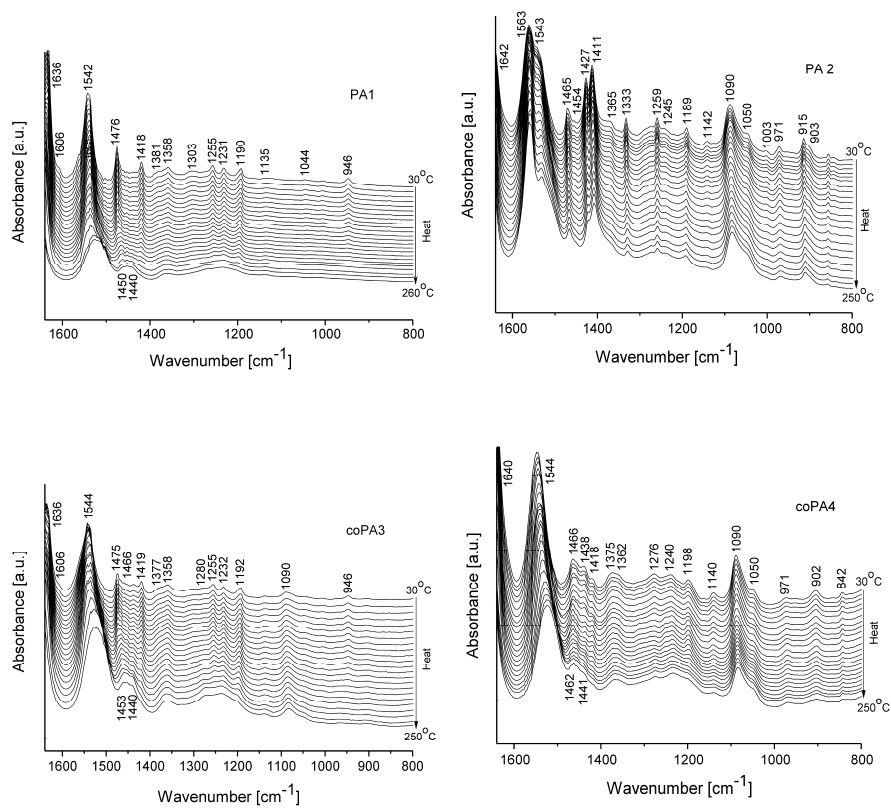


Figure 3. FT-IR spectra recorded on heating from 30°C to above the melting point of the homopolyamides PA1, PA2 and copolyamides coPA3, coPA4 containing 23 wt% and 48 wt% of diaminoisoidide, respectively.

4.3.2 Variable-Temperature Solid State NMR Study.

In Chapter 3 we applied 2D solution-state NMR experiments (^1H - ^1H COSY and ^1H - ^{13}C gHMBC) to investigate the partial substitution of the linear 1,4-diaminobutane (DAB) in polyamide 4.10 by diaminoisoidide (DAII).⁹ The examination revealed the presence of both DAB and DAII residues bonded to sebacic acid with almost expected compositions. In the solid state of these polymers, however, the packing will be governed by the hydrogen bonding efficiency of the amide groups between the neighboring polymer chains as well as the flexibility of the DAII unit. Such complex packing behavior may lead to the presence of DAB and DAII residues in both crystalline and amorphous regions in the polymer samples. To reveal this kind of information we used $^{13}\text{C}\{^1\text{H}\}$ CP/MAS NMR spectroscopy as a powerful technique for the analysis of the structural behavior of chain parts of the polyamides and their mobility upon heating. Furthermore, the experiments were performed as a function of temperature to characterize the different chain conformations and their populations in the samples. Particular attention was given to investigate phase separation and the presence of DAII in the crystal structure of the biobased materials. For the overall picture of the sample compositions with respect to crystalline and non-crystalline domains, the temperature dependent $^{13}\text{C}\{^1\text{H}\}$ CP/MAS NMR experiments will give comparable results to those that can be obtained using T_1 - or $T_{1\rho}$ -filtering of ^{13}C .^{34, 46} This is due to interference effects that occur during the CP transfer step leading to a signal loss if the rate of molecular dynamics is on the time scale of the applied MAS or radio-frequency spin-lock fields. A recent example where this strategy has been utilized to determine phase compositions includes the characterization of block copolymers based on polypeptides.⁴⁷ For $^{13}\text{C}\{^1\text{H}\}$ CP/MAS NMR experiments the homopolyamides from DAB/DAII and SA (PA1 and PA2) were chosen as well as the co-polyamide coPA4 with a DAB/DAII mol ratio of 0.57/0.43. The results presented in Figures 4-7, using the labeling scheme shown in Figure 1

and Table 2, summarize the isotropic ^{13}C chemical shifts for the α -, β -, γ -, and δ -methylene signals of the synthesized polyamides.

Table 2. ^{13}C chemical shifts for the homopolyamides PA1, PA2 and copolyamide coPA4 at 41.0°C and close to the melting point (211.5°C or 164.1°C).

| | ^{13}C Chemical shift (ppm) | | | | | | | | | |
|----------|--------------------------------------|---------------------|---------------------|---------------------|---------------------|--------------------|--------------------|------------------------|-----------------------|------------------------|
| | C=O | α_{N} | α_{C} | γ_{C} | δ_{C} | β_{N} | β_{C} | α_{DAII} | β_{DAII} | β'_{DAII} |
| PA1 | | | | | | | | | | |
| 41.0 °C | 173.9 | 43.1 | 36.1 | 34.2 | 32.2 | 28.1 | 27.3 | - | - | - |
| 211.5 °C | 174.2 | 41.3 | 37.6 | 33.0 | 32.7 | 28.7 | 27.2 | - | - | - |
| PA2 | | | | | | | | | | |
| 41.0 °C | 173.9 179.8 | - | 39.4 37.4 | 33.5±29.9 | 33.5±29.9 | - | 26.7 | 57.5 55.0 | 87.2 | 70.2 |
| 164.1 °C | 179.3 | - | 39.9 37.0 | 33.2±29.5 | 33.2±29.5 | - | 26.3 | 57.8 | 88.1 | 73.0 |
| coPA4 | | | | | | | | | | |
| 41.0 °C | 174.0 | 43.2 | 40.8 | 36.5 | 34.0±21.0 | 34.0±21.0 | 34.0±21.0 | 57.5 | 89.0 | 70.2 |
| 164.1 °C | 174.5 | 42.4 | 40.3 | 37.3 | 34.0±25.0 | 34.0±25.0 | 34.0±25.0 | 58.2 | 88.4 | 73.3 |

For PA1 several signals in the aliphatic region 25-45 ppm can be observed at 41.0 °C (Figure 4). These signals, together with the single carbonyl at 173.9 ppm, appear relatively broad as a result of sample heterogeneity, conformational distributions, and local susceptibility present in the solid state of the polymer.^{31, 48} A careful examination of the ^{13}C aliphatic region allows the assignment of both sets of α - and β -methylene carbons related to the SA and DAB parts (see Figure 1 and Table 2). Moreover, the resonances originating from the γ_{C} - and δ_{C} -methylene groups can also be assigned. Upon heating additional signals for PA1 are observed. Changes in their chemical shift position and intensity indicate a dynamic balance in statistics and populations of *trans* and *gauche*

conformers.⁴⁹⁻⁵¹ The two different conformers are related to crystalline and non-crystalline parts of the sample, respectively, where the latter is a result of increased local chain mobility. For example, the *gauche* conformers for the α_N signal of PA1 are visible at a relatively low temperature of ~ 110 °C, whereas these conformers for α_C become clearly visible at ~ 190 °C only. Similar trends can be observed for the β_C and β_N resonances where the *gauche* conformers for both signals are visible at ~ 115 °C. These observations suggest that the increased local molecular dynamics of the methylene units between hydrogen-bonded amide motifs, holding the polymer chains together in a sheet-like structure, first induces *gauche* conformations in the DAB part, while the SA part is affected at higher temperatures. Moreover, the ^{13}C chemical shift position of the α_C signal closely follows that of the carbonyl, supporting the idea that the increase in dynamics of the methylene motif is first propagated towards the DAB part. For the inner methylene groups of the SA part, γ_C and δ_C , the increase in mobility and appearance of *gauche* conformers is already visible at ~ 120 °C. These observations show that the increase in dynamics of the amide motifs by out-of-plane wagging lead to a gradual reduction in hydrogen-bonding strength, causing displacement of the carbonyl and α_C to low field (higher ppm values). In addition to this dynamic process, the γ_C and δ_C methylene groups of the SA part also display increased mobility even at lower temperatures. For all resonances the gradual appearance of more *gauche* conformers causes a visible reduction in the fraction of *trans* conformers, although the performed $^{13}\text{C}\{^1\text{H}\}$ CP/MAS experiments are not quantitative, *i.e.* the CP transfer step mediated through the dipole-dipole coupling between ^{13}C and ^1H is reduced by mobility. Nevertheless, this observation is in line with the FT-IR analysis of PA1 (Figure 3, PA1), where above 190 °C the signals related to CH_2 scissoring vibration next to NH moieties with *trans* conformation and CH_2 scissoring vibration next to CO moieties with *trans* conformation at 1476 cm^{-1} and 1418 cm^{-1} , respectively, become broader and then almost vanish. This finally leads to the Brill transition for PA1 (see WAXD analysis below).

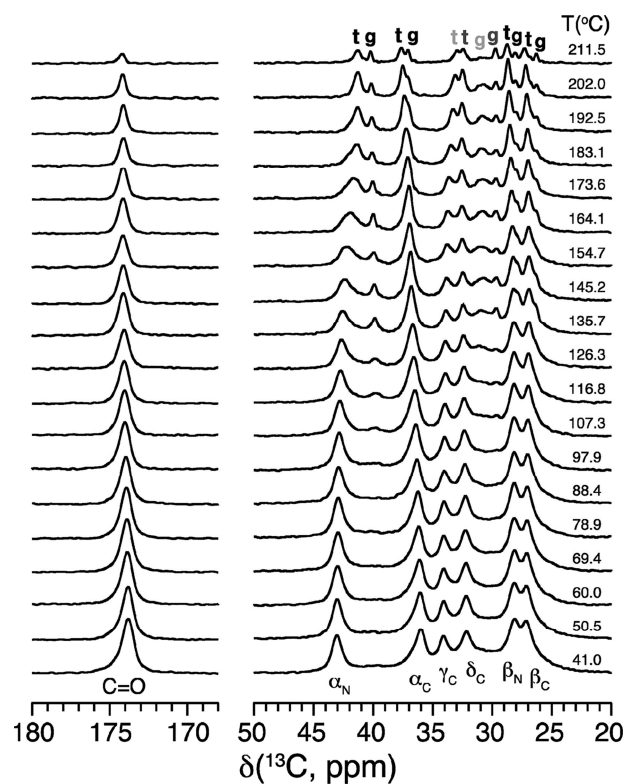


Figure 4. Variable-temperature solid-state $^{13}\text{C}\{^1\text{H}\}$ CP/MAS NMR spectra of the homopolyamide PA1 (commercially known as PA 4.10) recorded at 11.75 T (500 MHz for ^1H). Letters above the spectra indicate the positions of trans(t) and gauche(g) conformers while the assignment below employs the scheme shown in Figure 1.

For the homopolymer PA2 based on SA and DAII (Figure 1), the temperature-induced structural changes by increased molecular dynamics of the amide and methylene groups are less pronounced due to a broad overlap of the resonances in the region 20-45 ppm (Figure 5a). However, the PA 2 sample includes two different carbonyl signals at 179.8 and 173.9 ppm, indicating two different chemical environments for PA2. Considering the low molecular weight of PA2 (see Table 1) and the difference in ^{13}C chemical shifts, it is possible to assign the signal at 173.9 ppm to SA bonded to DAII in the polymer chains, forming

amide groups, and the signal at 179.8 ppm to non-polymerized SA end groups, *i.e.* carboxylic acid groups. The presence of two different carbonyl environments also influences the DAII units found in the region 50–90 ppm. Here, the α_{DAII} resonances at ~55 ppm are split into two distinct signals, while the resonance for β_{DAII} and β'_{DAII} at ~85 ppm and ~70 ppm, respectively display broad multiple overlapping signals. These spectral features show that the DAII groups are quite flexible and can adopt a range of conformations (see below). Interestingly, the carbonyl signal at 173.9 ppm decreases on increasing temperature whereas the signal at 179.8 ppm does not. Likewise, the decrease in signal intensity on going to higher temperatures can also be seen for the DAII units where only one of the signals from the α_{DAII} and β_{DAII} resonances, right and left most, respectively, follow this trend. Thus the carbonyl signal at 173.9 ppm and the signals following its decrease arise from amide groups in the polymer chains, which suggests that these signals originate from the crystalline part of the sample. The disappearance of the amide carbonyl signal at 173.9 ppm above 145 °C illustrate that the hydrogen bonds formed between the polymer chains in PA2 are somewhat weaker than those formed in PA1, resulting in the lower melting point for PA2. In contrast, the resonances associated with the carboxyl groups at 179.8 ppm represent the amorphous regions, which were further supported by the chemical shift position of these signals in the molten state of PA2 (top spectrum in Figure 5a). Surprisingly, the amorphous regions give a stronger CP signal than the corresponding signals from the crystalline domains. This could be related to dimer formation of the carboxyl end groups or trapping caused by entanglement.⁵² To further characterize the hydrogen bonding and molecular packing of PA2 the 2D $^{13}\text{C}\{^1\text{H}\}$ FSLG-HETCOR and $^1\text{H}\text{-}^1\text{H}$ DQ-SQ correlation spectra shown in Figures 5b and 5c have been recorded. From these spectra it is apparent that the amide groups give rise to two distinct ^1H signals centered at 5.0 ppm and 7.3 ppm with quite different intensities (Figure 5b). The signals are not in close spatial proximity since no clear auto-correlation or off-diagonal cross peaks

between them is observed in the 2D ^1H - ^1H DQ-SQ correlation spectrum (Figure 5c). Based on the ^1H chemical shifts, their intensities and the values expected for hydrogen bonding of polyamides around 8 ppm,⁵³ the signals at 5.0 ppm and 7.3 ppm can be assigned to DAII residues for which no hydrogen bonding occurs, and to DAII groups with weak hydrogen bonding to the SA part, respectively. Combining the above results for PA2 suggests that the DAII units can be incorporated in both crystalline and non-crystalline regions of the sample. The crystalline regions are characterized by a pseudo-hexagonal structure where weak hydrogen bonds between the polymer chains are formed. The amorphous regions are on the other hand less structured and appear to be more stable with respect to temperature than the crystalline part, which most likely is caused by trapping of the carboxyl groups due to entanglement formation of polymer chains and/or dimer formation between them.

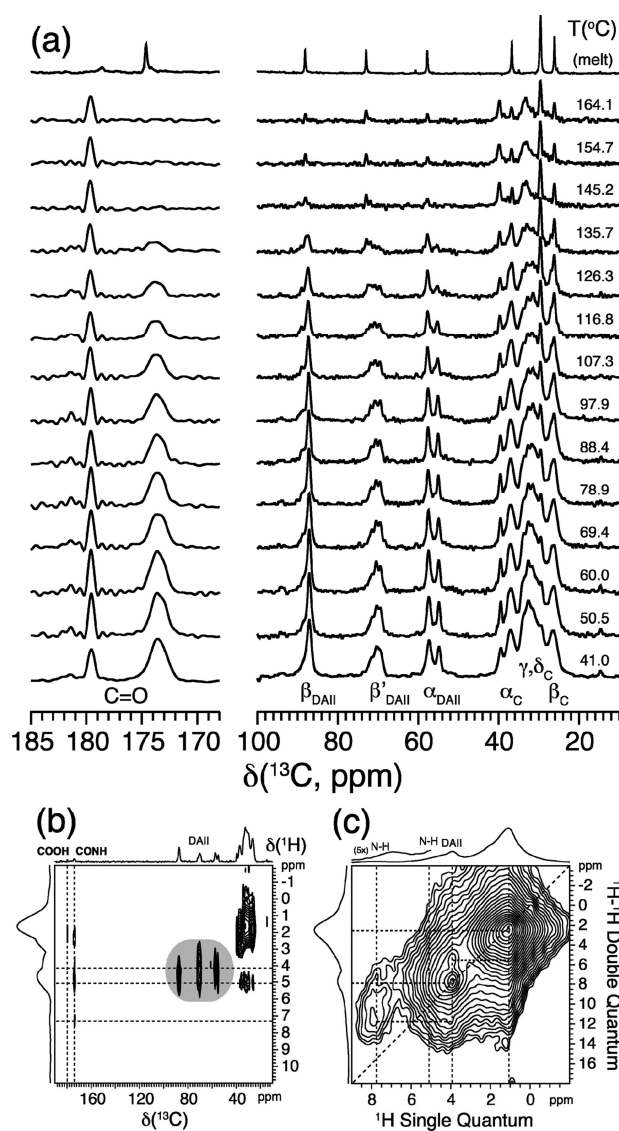


Figure 5. (a) Variable-temperature solid-state $^{13}\text{C}\{^1\text{H}\}$ CP/MAS NMR spectra of the homopolyamide PA2 recorded at 11.75 T (500 MHz for ^1H). (b) 2D $^{13}\text{C}\{^1\text{H}\}$ FSLG-HETCOR spectrum acquired using a 3.0 ms CP step and five FLSG blocks per t_1 increment to improve the ^1H resolution. (c) 2D ^1H - ^1H Double-Quantum Single-Quantum (DQ-SQ) spectrum recorded using 80.0 μs of BaBa recoupling time. Both 2D spectra were recorded at 20.0 T corresponding to 850.27 MHz for ^1H . The dashed lines in (b) and (c) identify selected cross and auto correlation peaks.

Figure 6 displays the VT $^{13}\text{C}\{^1\text{H}\}$ CP/MAS NMR results for the copolymer coPA4 with a DAB/DAII molar ratio of 0.57/0.43. From these spectra it is clear that all DAII-based fragments are fully incorporated into the copolymer since only a single, albeit broad amide carbonyl resonance with a shoulder to high frequency is observed (cf. Figure 6a). At 41 °C the main signal is located at 174.0 ppm and the shoulder at 175.0 ppm. Upon increasing the temperature the shoulder gradually disappears, while the main signal shifts to higher frequency as a result of the increased mobility of the amide groups and weakening of the hydrogen bonds between the polymer chains (cf. Figure 4). Moreover, the presence of two different carbonyl resonances suggests that coPA4 includes two or more hydrogen bond environments. The larger number of methylene groups present in both the SA and DAB residues, with very similar ^{13}C chemical shifts, makes the region from 20 ppm to 45 ppm crowded and difficult to interpret. However, some hints of the increased molecular dynamics as a function of temperature are visible on the high frequency side, where the signals from the α_{N} and α_{C} groups related to the DAB and SA residues, respectively, are located. The α_{N} DAB signal at 43.2 ppm displays a slow decrease on increasing temperature accompanied with a shift to lower frequency, leading to a broadening of the α_{C} resonances. A similar dependence on temperature for this resonance was observed in PA1 (Figure 4), which led to the introduction of *gauche* conformers (see above). The temperature at which these conformers start to appear is similar for both PA2 and coPA4, suggesting that the SA and DAB-based domains of the copolymer behave like in PA1, and that the lower melting point is mainly caused by the presence of DAII residues in the copolymer. The structural changes as a result of increased temperature are also visible for the DAII residues in the region 50–90 ppm. At 41 °C all resonances, α_{DAII} , β_{DAII} , and β'_{DAII} , appear quite broad where the resonances from α_{DAII} and β'_{DAII} have shoulders at the low and high frequency side, respectively. Compared to PA2, where distinct resonances from α_{DAII} are observed, the larger spread of these resonances indicates that the DAII fragments built into the

polymer chains in coPA4 are quite flexible and can adopt a number of different conformations. The DAI_{II} resonances show even more pronounced conformational changes as compared to those in PA2 upon increasing the temperature. For α_{DAI} a gradual change of the low frequency shoulder into a single resonance at higher frequency occurs, as also observed for PA2 (Figure 5a). Interestingly, the resonances for both β_{DAI} and β'_{DAI} show coexisting sharp signals of their high and low frequency parts in the temperature range 110-150 °C. Information about the local organization of polymer chains in coPA4 can be achieved from the 2D correlation spectra shown in Figures 6b and 6c. From the 2D $^{13}\text{C}\{^1\text{H}\}$ FSLG-HETCOR spectrum the presence of two different hydrogen bond environments can clearly be identified since the carbonyl signal is split into two signals with different intensities centered at 173.8 ppm and 174.9 ppm. These signals show intense and broad correlations to the amide proton at 8.4 ppm and the aliphatic moieties, indicating stronger hydrogen bonding between the polymer chains in coPA4 as compared to PA2. The presence of two carbonyl signals also demonstrates that hydrogen bonds are formed between PA 4.10-PA 4.10, PA DAI_{II}.10-PA DAI_{II}.10, and PA 4.10- PA DAI_{II}.10 fragments, which, based on the experiments performed for PA1 and PA2 above, allow the assignment of the two former hydrogen bonds to the carbonyl at 173.8 ppm and the new DAI_{II}-based PAs hydrogen bond to the carbonyl at 174.9 ppm. As for PA2, the DAI_{II} units in coPA4 also include a signal at 5.0 ppm in the 2D $^{13}\text{C}\{^1\text{H}\}$ FSLG-HETCOR spectrum originating from DAI_{II} residues that do not participate in the hydrogen bonding. Further, the amide protons involved in hydrogen bonding are not in close spatial proximity, since no clear auto-correlation or off-diagonal cross peaks are observed in the 2D ^1H - ^1H DQ-SQ correlation spectrum (Figure 6c). The above analysis shows that introduction of flexible DAI_{II} segments into the structure of PA 4.10 gives rise to an additional type of hydrogen bond, which appears to be compatible with a chain-folded structure as found in other PAs. Due to the unexpected flexible nature of the

DAII units a fraction of these does not participate in hydrogen bonding, which can lead to less ordered domains.

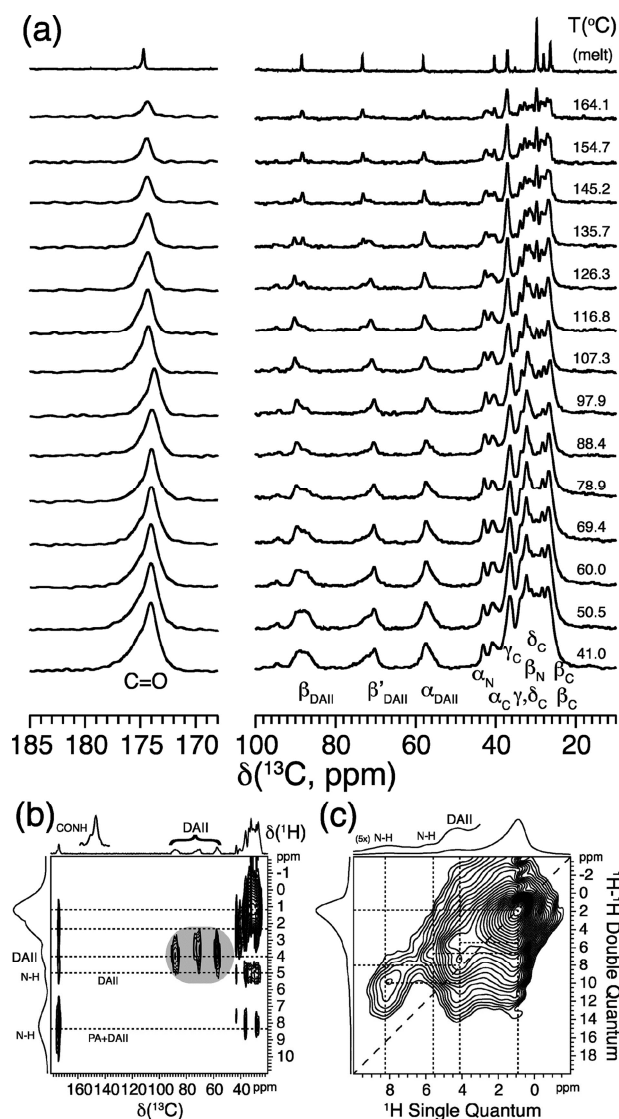


Figure 6. (a) Variable-temperature solid-state $^{13}\text{C}\{^1\text{H}\}$ CP/MAS NMR spectra of the copolymer coPA4 recorded at 11.75 T (500 MHz for ^1H). (b) 2D $^{13}\text{C}\{^1\text{H}\}$ FSLG-HETCOR spectrum acquired using a 3.0 ms CP step and five FLSG blocks per t_1 increment to improve the ^1H resolution. (c) 2D ^1H - ^1H Double-Quantum Single-Quantum (DQ-SQ) spectrum recorded using 80.0 μs of BaBa recoupling time. Both 2D spectra were recorded at 20.0 T corresponding to 850.27 MHz for ^1H . The dashed lines in (b) and (c) identify selected cross and auto correlation peaks.

4.3.3 DAII Conformers from *ab initio* Calculations

To characterize the flexibility and possible conformers for the DAII fragment and relate these to the experimentally observed ^{13}C chemical shifts found above for PA2 and coPA4 we have employed *ab initio* calculations using a combination of DFT and MP2 methods. Since such calculations are quite expensive and we do not know the specific polymer chain organization in either of the investigated samples, the calculations were performed for the gas phase on a simplified DAII fragment with propanoic acid side chains attached to both of its sides. Further details about the computations and the strategy for obtaining the conformational profiles are given in the Appendix B.

The DAII fragments in both PA2 and coPA4 display broad ^{13}C resonances with hints of multiple signals from all of its three different carbon moieties. This fact might be attributed either to a coexistence of several conformers as reported by W. Liu et al.⁵⁴ and J. Wu et al.,⁵⁵ who carried out X-ray and *ab initio* studies on different isohexide derivatives, or to the coexistence of several, slightly different DAII domains with the same conformer. From the 1D potential energy surface-scanning procedure (see Figure S1) 21 possible conformations were obtained. These were further optimized at different levels of theory, revealing that a number of the 21 possible conformations are not stable and consequently interconvert as summarized in Table S1. This leaves 9 conformers where the three most abundant ones according to their Boltzmann probabilities are labeled (i), (ii) and (iii), and shown in Figure 7a. We note that all nine conformers are within an energy difference of about 1-4 kcal illustrating that the DAII fragment is indeed quite flexible (see Table S1). The NMR calculations performed for all nine conformers are graphically summarized in Figure 7b as an isotropic ^{13}C NMR spectrum, assuming a narrow linewidth of 0.25 ppm for each resonance. From this theoretical spectrum it is clear that all nine conformers give rise to quite large spreads of isotropic ^{13}C chemical shifts with averages centered at 92, 76 and 63 ppm for β_{DAII} , β'_{DAII} , and α_{DAII} , respectively. The average ^{13}C chemical shifts for β_{DAII} and β'_{DAII} are in reasonable agreement with the

isotropic ^{13}C chemical shifts observed in this work (Figures 5 and 6), whereas the shift for α_{DAII} shows a larger discrepancy. This discrepancy is most likely reflecting our simplified model with two short propanoic acid fragments attached at the α_{DAII} -position of the DAII unit as compared to two long polymer chains. Furthermore, the ^{13}C chemical shifts calculated for the most abundant conformer (i) are in a very good agreement with our previous liquid-state NMR measurements using HMBC (see Figure S2). The populations of the DAII conformers calculated in the gas phase can obviously change when going to a solid packing of the polymer chains, *i.e.* spatial and/or steric effects may favor other conformers than (i), taking into account the low energy barrier between them. Conformers with less effective volume, and thus less entropy demands, can in this way be favored, while in the gas phase they may not be the most abundant. The compatibility of the DAII fragments with the crystalline and the non-crystalline domains will obviously depend on their hydrogen bond formation possibilities and thereby on the orientation of the amide groups attached at the α_{DAII} position. Assuming that all DAII conformers determined for the gas phase are equally possible in the solid, the superimposed spectrum of all found conformers in Figure 7 illustrate a continuous spread of ^{13}C signals in the range from 50 ppm to 90 ppm. The largest spread observed for β'_{DAII} is in agreement with the experimental solid-state $^{13}\text{C}\{^1\text{H}\}$ CP/MAS NMR spectra recorded for PA2 and coPA4 (Figures 5 and 6). A clear trend between DAII conformations (Figure S3) and the ^{13}C chemical shift for the α_{DAII} position (Table S2) is difficult to derive. However, the two distinct ^{13}C resonances for α_{DAII} in PA2 compared to the spread of ^{13}C chemical shifts in Figure 7b suggest that these signals are related to two different domains. The ^{13}C chemical shift difference of ~ 2 ppm for the two signals, which is in the order of what we estimate for hydrogen bond formation between DAII fragments, could indicate that the two conformers are the same, with and without hydrogen bonding. This assumption is supported by the smooth decrease of the signal related to the crystalline domains on increasing temperature, which happens independently,

whereas the signal from the amorphous phase displays almost no decrease. Comparison of PA2 and coPA4 (Figures 5 and 6) shows that the DAII fragments in coPA4 give rise to a much larger spread of ^{13}C chemical shifts, however, comparable to the spread observed for all 9 conformers in Figure 7b. This suggests that the DAII fragments have more conformational freedom in coPA4 than in PA2. The conformers related to the α_{DAII} position in coPA4 start to show traces of the two conformers present in PA2 on increasing temperature. Based on this observation we conclude that the DAII units in coPA4 are capable of linking polymer strands via hydrogen bonds to both PA4.10 and DAII-based fragments, leading to a range of DAII conformations at low temperatures. At higher temperatures, the hydrogen-bonded networks of DAII conformers in both PA2 and coPA4 undergo significant molecular dynamics. This results in complete averaging of the ^{13}C chemical shifts for the DAII units with almost identical ^{13}C chemical shifts in the melt for both polymers.

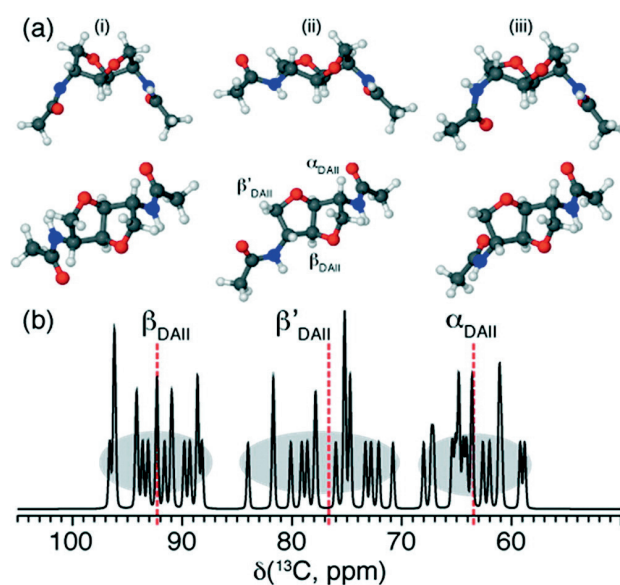


Figure 7. (a) Top and side view of the three most stable conformers found via gas phase MP2/6-31G* level of theory (see SI for details). For clarity only methyl groups are shown while calculations were performed on propyl substituted DAII fragments. (b) Graphical representation of the calculated ^{13}C chemical shifts for all found conformers (see Table S2). Vertical red dashed lines indicate the mean ^{13}C chemical shifts corresponding to 92.3 ± 2.8 ppm, 76.7 ± 3.6 ppm, and 63.5 ± 2.7 ppm for β_{DAII} , β'_{DAII} , and α_{DAII} , respectively.

4.3.4 WAXD

In Chapter 3 reporting XRD analysis of DAII-, DAB- and SA-based copolyamides we showed that these bio-based materials are semi-crystalline over the whole range of compositions. It was also shown that the typical polyamide structure with different interchain and intersheet distances is preserved for samples with DAII contents lower than 50 mol%.⁹ Samples having a higher DAII content crystallize into a close to hexagonal packing of polymer chains. In order to investigate how the DAII-based polyamide units are built into the crystal structure of PA 4.10 and which conformational modifications this entails, temperature dependent X-ray diffraction measurements were performed on materials with a comparable and well defined thermal history.

All samples were subjected to a first heating-cooling cycle at 10 °C/min, starting from about 40 °C and reaching a temperature well above their respective melting temperatures. During this cycle 2D X-ray diffraction patterns were collected at increasing temperature. After the first cycle, 2D X-ray diffraction patterns were collected for all the samples during a second heating/cooling cycle with the same rate and using the same temperature step. In Figure 8a X-ray diffraction profiles of the PA1 are shown. The profiles are reported as a function of temperature and represent the first heating cycle applied on the as-synthesized sample PA1. The PA1 crystallizes into the typical α and/or β form of the polyamide, displaying the four diffraction peaks in the range of 3-7° (2 θ), 10-12° (2 θ) and 18-25° (2 θ), indexed as *001*, *002*, *100* and *010/110* (Table 4). The *100* diffraction peak corresponds to the interchain distance which represents the distance between two chains lying within the same hydrogen bonded sheet, while the *010* peak corresponds to the intersheet distance, i.e. the distance between two adjacent hydrogen bonded sheets. The *001* and *002* diffraction peaks give information on the length of the chemical repeat unit. The *001* and *002* diffraction peaks shown in Figure 8a remain constant up to melting (~ 225 °C), while the interchain *100* and intersheet *010/110* diffraction peaks tend to merge with increasing temperature. The latter behavior is typically called the Brill transition in polyamides and the temperature at which it occurs is the Brill transition temperature. The Brill transition for sample PA1, crystallized under the conditions described above, occurs at 196 °C. To follow the merging phenomena associated with the Brill transition, the *d*-spacing values of all the samples are reported in Figures 9a and 9b as function of temperature for the first and the second heating runs, respectively. The *d*-spacing values have been calculated via Bragg's law. The analysis of WAXD profiles of PA1 shows that melting of this polyamide starts around 225-230 °C (Figure 8a) where an amorphous halo tends to strengthen in intensity. The observed temperature is consistent with the melting temperature of PA1 measured by DSC (reported in Table 1). Similar phenomena are

observed for PA1 during the second heating run (Figure 8a'). The Brill transition occurs at 196 °C and the polymer melts completely around 225 °C. On cooling from the melt reverse behavior is observed, and further relevant data are available in the Appendix B.

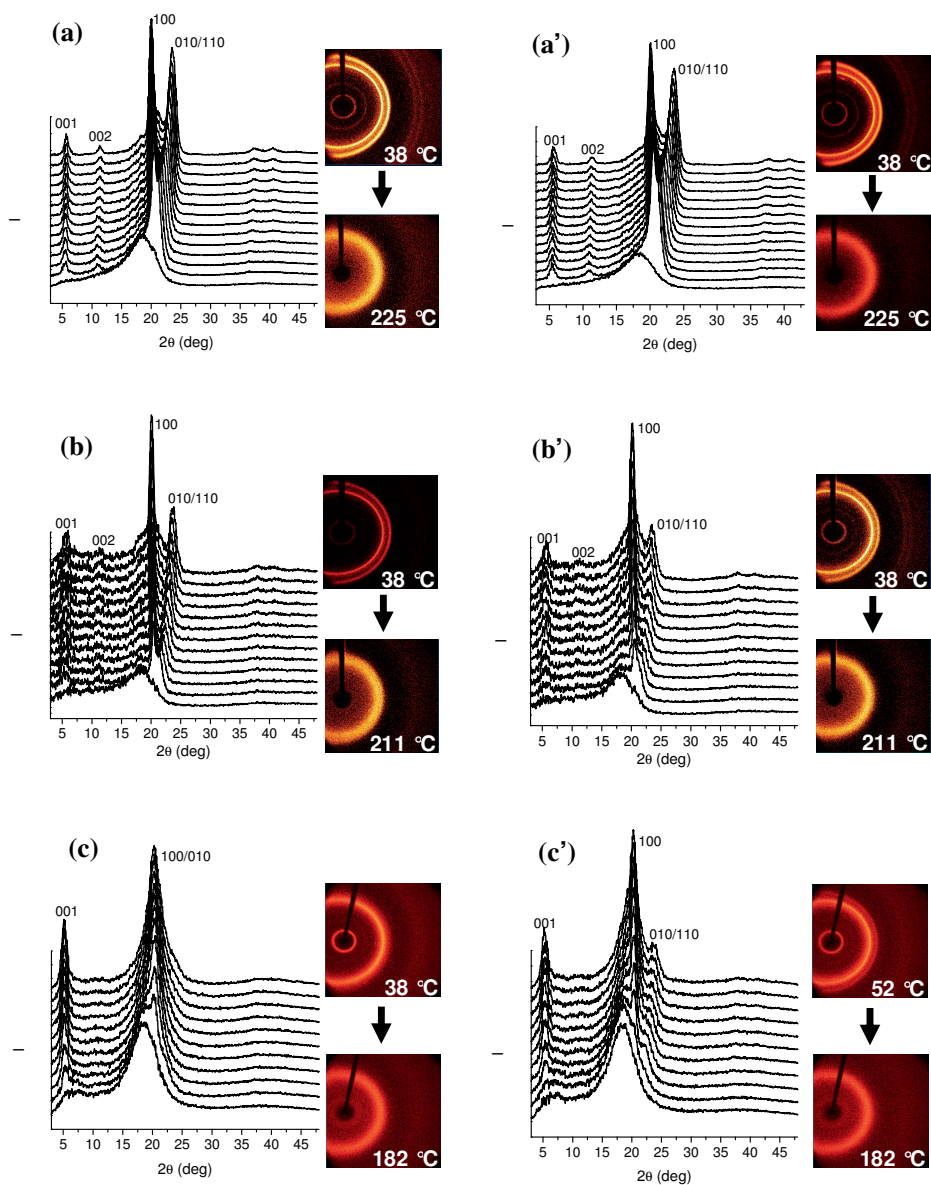


Figure 8. X-ray powder diffraction profiles of as-prepared homopolyamide PA1 ((a), (a')) and copolyamides coPA3 ((b),(b')) and coPA4 ((c),(c')) collected from around 40 °C till the melting temperature. The 1D integrated profiles are reported as function of the temperature and correspond to the two heating runs applied for each sample (I heating run (a), (b), (c)); II heating run (a'),(b'),(c')). The indices correspond to the packing mode of the α -phase and the β -phase of common polyamides. The temperatures of the recorded profiles are reported in the supporting information and they are listed in Table 3.

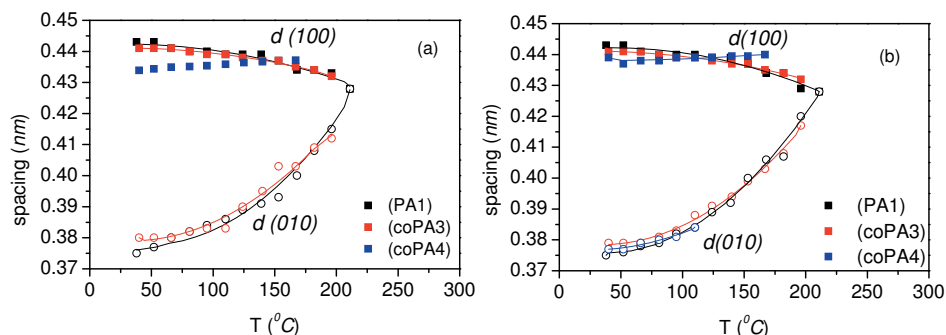


Figure 9. Temperature dependent variations of 100, 010/110 spacing values calculated via Bragg's Law considering the collected profiles (Figure 8) during the first heating run (a) and the second heating run (b).

In Table 3 crystallinity indexes calculated using the formula shown below are reported for each profile:

$$X_c = \frac{A_c}{A_c + A_a} \cdot 100$$

where A_c and A_a are the integrated intensities from the crystalline and amorphous phases, respectively. The integrated intensities were extracted from the experimental XRD patterns by a fitting procedure using the XRD profile of the material after melting, as explained in the Appendix A. From the calculated X_c values one can conclude that the degree of crystallinity decreases as a function of temperature.

The coPA3 with DAB/DAII mol ratio 0.80/0.20 crystallizes into a crystal structure similar to that of PA1. The same four diffraction peaks typical for polyamides are displayed in the range of 3-7° (2 θ), 10-12° (2 θ) and 18-25° (2 θ), indexed as 001, 002, 100 and 010/110 (Figure 8b). Their corresponding d -spacing values obtained from the pattern collected at room temperature are reported in Table 4. On comparing the d -spacing values of the four diffraction peaks for the two mentioned samples PA1 and coPA3, no significant differences were observed. However, a decrease of the 002 diffraction peak intensity is observed upon increasing the DAII content in the synthesized materials. In fact

the *002* diffraction peak decreases in intensity for coPA3 and totally disappears for coPA4 as a consequence of the crystal disorder caused by the increased DAII content in the copolymers. Simultaneously, the degree of crystallinity is lower than that of PA1, as presented in Table 3. Upon heating of the coPA3 sample, the *001* and *002* diffraction peaks remain constant up to melting (around 211 °C), while similar merging phenomena are observed for the interchain *100* and intersheet *010/110* diffraction peaks as compared to PA1. The Brill transition, however, is not observed for this sample. Clearly, this is due to the lower value of the melting temperature observed from WAXD measurements which decreases from 221 °C for PA1 to 211 °C for coPA3. Moreover, the crystallinity values for coPA3 presented as a function of temperature are lower than the respective values for PA1. Similar trends of the degree of crystallinity are also observed for these two samples during the second heating/cooling cycle.

The coPA4 crystallizes into a close to hexagonal cell similar to that of PA2.⁹ The XRD pattern displays two strong diffraction peaks in the range of 3-7° (2θ) and 15-25° (2θ), indexed as *001* and *100*. The *001* diffraction peak shifts to lower values of 2θ compared to the same diffraction peak of the other polyamides (Figure 8c, Table 4).⁹ This indicates that the projection on the *c*-axis of the DAII monomer residue is somewhat longer than that of the DAB monomer residue and it shows that the comonomers co-crystallize in the same crystal lattice. The different electronic density of the DAII fragments compared to the DAB fragments influences the intensity of the *001* diffraction peak, which is more intense for diaminoisoidide-rich coPA4 than the same diffraction peak observed for the other polyamides. Clearly the as-synthesized coPA4 does not show a Brill transition. Only a decrease of the crystallinity index as a function of temperature is observed. CoPA4 presents a different diffraction profile after the first heating/cooling cycle (Figure 8c'). Considering that the crystallization occurs approximately with a rate of 10 °C/min, it could be concluded that the different crystallization conditions give rise to the

coexistence of the two observed crystal structures. However, α and/or β phase can be considered to be less abundant compared to pseudo-hexagonal phase. In fact the diffraction peak $010/110$ is less intense compared to the corresponding diffraction peak of PA1 at low temperature. Upon increasing the temperature only a decrease of the degree of crystallinity is observed. Moreover no meaningful differences have been observed on comparing the temperature dependent FTIR spectra collected for coPA4 during the two heating runs. Melting also occurs for the sample subjected to a second heating run around 182 °C. Similar behavior is observed on cooling from the melt but the diffraction peak $010/110$ is now only present as a shoulder with a low intensity (see Appendix B). This seems to confirm our conclusion on the influence of crystallization conditions for the coPA4.

Table 3. Crystallinity indexes (X_c) calculated for each profile reported in Figure 8.

| T (°C) | X_c (%) | | | | | |
|--------|-----------|------------|-----------|------------|-----------|------------|
| | PA1 | | coPA3 | | coPA4 | |
| | I heating | II heating | I heating | II heating | I heating | II heating |
| 38 | 50 | 43 | 36 | 32 | 25 | 29 |
| 52 | 49 | 39 | 33 | 27 | 23 | 27 |
| 66 | 47 | 36 | 30 | 26 | 21 | 26 |
| 81 | 44 | 32 | 26 | 25 | 18 | 22 |
| 95 | 41 | 31 | 24 | 24 | 17 | 19 |
| 110 | 39 | 30 | 22 | 23 | 13 | 17 |
| 124 | 37 | 28 | 20 | 22 | 12 | 15 |
| 139 | 35 | 27 | 19 | 21 | 10 | 10 |
| 153 | 33 | 26 | 18 | 19 | 5 | 8 |
| 168 | 31 | 25 | 16 | 15 | 2 | 5 |
| 182 | 30 | 24 | 16 | 14 | - | - |
| 196 | 29 | 23 | 15 | 13 | - | - |
| 211 | 28 | 23 | - | - | - | - |
| 225 | - | - | - | - | - | - |

Table 4. X-ray diffraction spacings of as-prepared co- and homopolyamides with different contents of diaminoisoidide measured at room temperature.

| Symbol | X-ray diffraction (nm) | | | | 2 θ (deg) | | | |
|--------|------------------------|-------|-------|---------|------------------|-------|-------|---------|
| | 001 | 002 | 100 | 010/110 | 001 | 002 | 100 | 010/110 |
| PA1 | 1.561 | 0.776 | 0.442 | 0.379 | 5.66 | 11.38 | 20.00 | 23.46 |
| coPA3 | 1.555 | 0.775 | 0.442 | 0.380 | 5.68 | 11.40 | 20.00 | 23.44 |
| coPA4 | 1.686 | - | 0.442 | - | 5.24 | - | 20.00 | - |
| PA2 | 1.624 | - | 0.442 | - | 5.44 | - | 20.00 | - |

4.4 Conclusions

The conformation and flexibility of diaminoisoidide-, 1,4-diaminobutane-, and sebacic acid-based polyamide fragments and their influence on the chain organization in the crystalline and amorphous phases were investigated by FT-IR, solid-state NMR, and WAXD. This combined approach provided detailed information concerning nanophase separation and allowed identification of the specific differences between rigid and more flexible motifs in these semicrystalline polyamides. The spectroscopic analysis of the diaminoisoidide-based polyamides is particularly important for the investigation of their crystal structure stability. Simultaneously, the combination of the experimental techniques with *ab initio* calculations provides more insight into the flexibility of isohexide unit which in this case affects the hydrogen bonding and chain conformation of the polyamides. FT-IR measurements revealed that the incorporation of diaminoisoidide into the structure of PA1 (commercially known as PA 4.10) affects the hydrogen-bond density, causing conformational disorder of the chain fragments of the polymer. Upon heating of polyamide 4.10

and copolyamide coPA3, containing 20 mol% of diaminoisoidide, the FT-IR signals at 1475-1476 cm^{-1} and 1418-1419 cm^{-1} , assigned to CH_2 scissoring with *trans* conformation, become less visible. This comes as a result of an increased number of *gauche* conformers, which leads to a hexagonal packing of the polymer chains. The dynamic balance between *trans* and *gauche* conformers of the polyamides was demonstrated by VT $^{13}\text{C}\{^1\text{H}\}$ CP/MAS NMR experiments. Besides, on combining spectroscopic techniques with *ab initio* calculations *viz.* DFT and MP2 methods the most abundant conformers of DAII were defined. The calculations showed a number of possible DAII conformers with a low energy barrier between them and therefore relatively high flexibility of the isohexide unit.

Wide-angle X-ray scattering revealed that PA1 and coPA3 having DAII content of 20% mol crystallize into α and/or β forms with different interchain and intersheet distances. Upon heating PA1 undergoes a Brill transition, while the more diaminoisoidide-rich compositions greatly facilitate the formation of a pseudo-hexagonal phase, which is even observed at room temperature (Figure 10).

Of particular interest was the analysis of the diaminoisoidide distribution in the crystalline and non-crystalline phases of the polyamides. The crystalline regions, containing hydrogen-bonded DAII residues, were identified by FT-IR C-CO stretching vibrations at 903 cm^{-1} together with ^{13}C resonances in the vicinity of 50-90 ppm. The decrease of the FT-IR signal intensities close to the melting point of the polyamides suggests that DAII comonomer is indeed incorporated into the crystalline phase of these materials. Moreover, relatively broad ^{13}C resonances of isohexide fragments suggested the coexistence of different DAII conformers in the crystalline and non-crystalline/amorphous domains, which was especially pronounced for the copolymer coPA4 based on SA, DAB and DAII (DAII content of 43% mol). The cocrystallization of DAB and DAII fragments followed by WAXD measurements revealed a shift of the 001 diffraction peak for the DAII-rich polyamides to lower 2θ values in

comparison to PA 4.10. Further analysis of the X-ray data showed that the projection onto the *c*-axis of the DAII residue is longer than the DAB residue, in agreement with the fact that DAII residues are longer than the DAB residues, and that the comonomers cocrystallize. With an increasing content of DAII in the PAs, the crystal disorder increased and thus, the degree of crystallinity was lower than that of the SA/DAB-based polyamide 4.10.

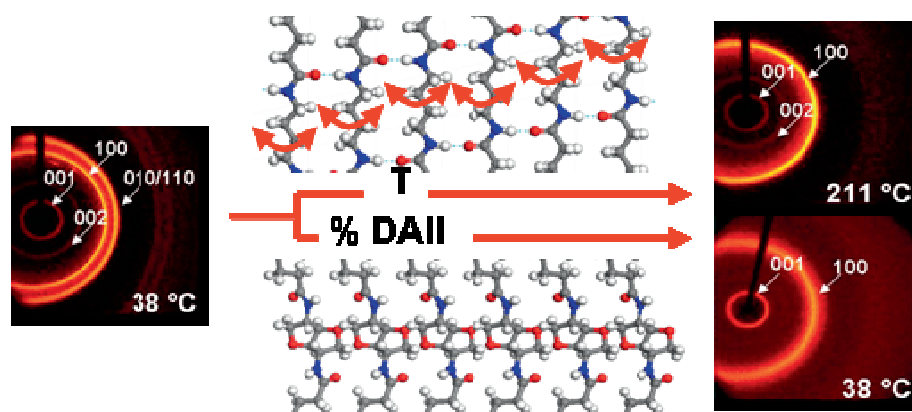


Figure10. Polymorphism of polyamide 4,10. The transition from α/β to γ form is influenced from the temperature and from the DAII content co-crystallized.

References

1. Fenouillot, F.; Rousseau, A.; Colomines, G.; Saint-Loup, R.; Pascault, J. P. *Prog. Polym. Sci.* **2010**, *35*, 578.
2. Thiem, J.; Bachmann, F. *Makromol. Chem.* **1991**, *192*, 2163.
3. Stoss, P.; Hemmer, R.; Derek, H. *Adv. Carbohydr. Chem. Biochem.* **1991**, *49*, 93.
4. Gomurashvili, Z.; Kricheldorf, H. R.; Katsarava, R. *J. Macromol. Sci., Pure Appl. Chem.* **2000**, *A37*, 215.
5. Caouthar, A. A.; Loupy, A.; Bortolussi, M.; Blais, J.; Dubreucq, L.; Meddour, A. *J. Polym. Sci., Part A: Polym. Chem.* **2005**, *43*, 2480.
6. Caouthar, A.; Roger, P.; Tessier, M.; Chatti, S.; Blais, J. C.; Bortolussi, M. *Europ. Polym. J.* **2007**, *43*, 220.
7. Okada, M.; Yamada, M.; Yokoe, M.; Aoi, K. *J. Appl. Polym. Sci.* **2001**, *81*, 2721.
8. Philip, B.; Sreekumar, K. *Polym. Int.* **2001**, *50*, 1318.
9. Jasinska, L.; Villani, M.; Wu, J.; van Es, D.; Klop, E.; Rastogi, S.; Koning, C. E. *Macromolecules* **2011**, *44*, 3458.
10. Dreyfuss, P.; Keller, A. *J. Macromol. Sci., Part B Phys.* **1970**, *B4*, 812.
11. Atkins, E. D. T.; Hill, M. J.; Hong, S. K.; Keller, A.; Organ, S. *Macromolecules* **1992**, *25*, 917.
12. Bunn, C.; Garner, E. V., *R. Soc. London Ser. A, Math. Phys. Sci.* **1947**, *189*, 39.
13. Jones, N. A.; Atkins, E. D. T.; Hill, M. J.; Cooper, S. J.; Franco, L. *Polymer* **1997**, *38*, 2689.
14. Franco, L.; Cooper, S. J.; Atkins, E. D. T.; Hill, M. J.; Jones, N. A. *J. Polym. Sci. Part B: Polym. Phys.* **1998**, *36*, 1153.
15. Cooper, S. J.; Atkins, E. D. T.; Hill, M. J. *Polymer* **2002**, *43*, 891.
16. Hill, M. J.; Atkins, E. D. T. *Macromolecules* **1995**, *28*, 604.

17. Jones, N. A.; Atkins, E. D. T.; Hill, M. J.; Cooper, S. J.; Franco, L. *Macromolecules* **1996**, *29*, 6011.
18. Atkins, E. D. T.; Hill, M. J.; Jones, N. A.; Cooper, S. J. *J. Polym. Sci., Part B: Polym. Phys.* **1998**, *36*, 2401.
19. Bermúdez, M.; León, S.; Alemán, C.; Muñoz-Guerra, S. *J. Polym. Sci. Part B: Polym. Phys.* **2000**, *38*, 41.
20. Bermúdez, M.; León, S.; Alemán, C.; Muñoz-Guerra, S. *Polymer* **2000**, *41*, 8961.
21. Brill, R., *J. Prakt. Chem.* **1942**, *161*, 49.
22. Brill, R., *Macromol. Chem.* **1956**, *18/19*, 294.
23. Colclough, M. L.; Baker, R. J. *J. Mater. Sci.* **1978**, *13*, 2531.
24. Wendoloski, J. J.; Gardner, K. H.; Hirschinger, J.; Miura, H.; English, A. D. *Science* **1990**, *247*, 431.
25. Vinken, E.; Terry, A. E.; Hoffmann, S.; Vanhaecht, B.; Koning, C. E.; Rastogi, S. *Macromolecules* **2006**, *39*, 2546.
26. Vasanthan, N.; Murthy, N. S.; Bray, R. G. *Macromolecules* **1998**, *31*, 8433.
27. Yoshioka, Y.; Tashiro, K. *Polymer* **2003**, *44*, 7007.
28. Cooper, S. J.; Coogan, M.; Everall, N.; Priestnall, I. *Polymer* **2001**, *42*, 10119.
29. Ando, I.; Asakura, T., *Solid State NMR of Polymers, Studies in Physical and Theoretical Chemistry* **1998**, *84*.
30. Hirschinger, J.; Miura, H.; Gardner, K. H.; English, A. D. *Macromolecules* **1990**, *23*, 2153.
31. Harings, J. A. W.; Yao, Y.; Graf, R.; van Asselen, O.; Broos, R.; Rastogi, S. *Langmuir* **2009**, *25*, 7652.
32. Yao, Y. F.; Graf, R.; Spiess, H. W.; Rastogi, S. *Macromolecules* **2008**, *41*, 2514.
33. Holstein, P.; Spevacek, J.; Geschke, D.; Thiele, V. *Progr. Coll. Polym. Sci.* **1991**, *85*, 60.

34. Schreiber, R.; Veeman, W. S.; Gabrielse, W.; Arnauts, J. *Macromolecules* **1999**, *32*, 4647.
35. Bennett, A. E.; Rienstra, C. M.; Auger, C. M.; Lakshmi, K. V.; Griffin, R. G. *J. Chem. Phys.* **1995**, *103*, 6951.
36. Bielecki, A.; Burum, D. P. *J. Magn. Reson., Ser. A* **1995**, *116*, 215.
37. van Rossum, B.; Forster, H.; de Groot, H. *J. Magn. Reson.* **1997**, *124*, 516.
38. Feike, M.; Demco, D.; Graf, R.; Gottwald, J.; Hafner, S.; Spiess, H. W. *J. Magn. Reson., Ser. A* **1996**, *122*, 214.
39. Marcombe, C.; Zilm, K. *J. Magn. Reson.* **2003**, *162*, 479.
40. Schroeder, L. R.; Cooper, S. L. *J. Appl. Phys.* **1976**, *47*, 4310.
41. Skrovanek, D. J.; Stephen, E. H.; Painter, P. C.; Coleman, M. M. *Macromolecules* **1985**, *18*, 1676.
42. Skrovanek, D. J.; Painter, P. C.; Coleman, M. M. *Macromolecules* **1986**, *19*, 699.
43. Silverstein, R. M.; Webster, F. X. *Spectrometric Identification of Organic Compounds*. John Wiley & Sons, Inc.: **1998**.
44. Vasanthan, N.; Salem, D. R. *J. Polym. Sci., Part B: Polym. Phys.* **2000**, *38*, 516.
45. Li, W.; Huang, Y.; Zhang, G.; Yan, D. *Polym. Int.* **2003**, *52*, 1905.
46. Vanderhart, D. L.; Earl, W.; Garroway, A., *J. Magn. Reson.* **1981**, *44*, 361.
47. Gitsas, A.; Floudas, G.; Mondeshki, M.; Lieberwirth, I.; Spiess, H. W.; Iatrou, H.; Hadjichristidis, N.; Hirao, A. *Macromolecules* **2010**, *43*, 1874.
48. Vasanthan, N.; Willem, R.; Biesemans, M.; Goderis, B.; Basiura, M.; Magusin, P. C. M. M.; Bolbnya, I.; Koning, C. E. *Macromolecules* **2004**, *37*, 421.
49. Vanderhart, D. L., *J. Magn. Reson.* **1981**, *44*, 117.
50. Earl, W.; Vanderhart, D. L. *J. Magn. Reson.* **1982**, *48*, 35.
51. Ando, I.; Asakura, T. *Solid state NMR of Polymers*, Elsevier, Amsterdam **1998**, 84.

52. Bohle, A.; Brunklaus, G.; Hansen, M. R.; Schleuss, T. W.; Kilbinger, A. F. M.; Seltmann, J.; Spiess, H. W. *Macromolecules* **2010**, *43*, 4978.
53. Vinken, E.; Terry, A. E.; van Asselen, O.; Spoelstra, A. B.; Graf, R.; Rastogi, S. *Langmuir* **2008**, *24*, 6313.
54. Liu, F. W.; Yan, L.; Zhang, J. Y.; Liu, H. M. *Carboh. Res.* **2006**, *341*, 332.
55. Wu, J.; Eduard, P.; Thiyagarajan, S.; van Haveren, J.; van Es, D.; Koning, C. E.; Lutz, M.; Fonseca Guerra, C. *Chem. Sus. Chem.* **2011**, *4*, 599.

Appendix B

Computational Details

The importance of using a large basis set including the electronic correlation correction for conformational energy calculation by *ab initio* methods has been reported frequently.¹⁻³ The reason is that, the energy difference between flexible conformers calculated at the level of DFT often do not agree with the experimental energy difference. On the other hand, calculated conformational energies at the MP2 level employing a reasonably large basis set (6-311G**) have a high accuracy and agree quite well with the experimentally determined values. Furthermore, as pointed out by Ke et al.,⁴ DFT is in many cases unable to locate all stationary points predicted by MP2. Therefore, both levels of theory (DFT and MP2) were applied in parallel to test the effects of different treatments of electron correlation and the effect of the basis set. Admittedly, the frequency analysis and the Gibbs free energy calculations become quite expensive and for this reason we decided to constrain the vibrational and thermal analyses to the MP2/6-31G* and B97-1/6-311G** levels of theory. Vibrational frequencies were calculated to ensure that all described geometries are local minima (not saddle points).

Conformational Analysis

Since the methylene part of the homopolymer PA2 and copolymer coPA4 is of minor importance for the interpretation of the experimental ¹H and ¹³C chemical shifts for the isohexide fragment, the NMR calculations were carried out for a simplified model with terminal propyl groups attached to both sides of the isohexide unit. In addition, we have replaced the propyl groups by methyl groups in the conformational search.

The conformations of the isohexide moiety itself are quite similar to the chair/boat conformations of cyclohexane. We have defined UU and DD as the dominant conformations of a boat when both CH₂ groups are pointing either up

or down, respectively, while both $\beta_{\text{N,DAII}}$ protons are pointing down. Consequently, UD and DU conformations are the mirrored chair-conformations. Fixing the possible conformations of the isohexide unit to one of the conformations UU, DU, UD, and DD, by varying the torsional angle φ (see Figure S1), one obtains the energy profiles summarized in Figure S1. The variation of the torsion angle φ was performed in clockwise steps of 15° where, during energy minimizations, the conformation of DAII core was fixed, while the rest of the fragment was allowed to relax. The sampled points were then used to plot 1D-PES curves (Figure S1, right), i.e. for each geometry and angle φ the lowest energy conformation was selected. The abundance of the conformers was estimated by first computing Boltzmann probabilities for each conformer at 25°C . All identified conformers were proceeded for further NMR calculations. An extensive quantum-chemical conformational analysis (via DFT and MP2) revealed the three most abundant conformers as depicted in Figure 7 in the chapter and elucidated corresponding torsional angle profiles, which are in Table S1 labeled as (1), (4), and (6), respectively. Both methods confirm the conformer (i) (Figure 7) to be significantly more populated than two other conformers (ii) and (iii). According to a single point energy calculation at the B97-1/6-311G** level for MP2/6-31G* geometries, the conformer (i) is found to be more stable by 1.13 kcal/mol and 0.58 kcal/mol than conformers (ii) and (iii), respectively. The MP2/6-31G* analysis slightly changes the relative stability of the conformers (ii) and (iii) with energy differences of 2.95 kcal/mol and 1.91 kcal/mol, respectively. Despite of these differences, we have chosen to label the second most abundant conformer as (iii) in order to link it logically to the torsional angle φ , which is 90° , 195° and 300° for the initial conformations (1), (4), and (6) in Table S1, respectively. The angles presented in Table S1 are taken from 1D-PES scans (Figure S1) and do not entirely represent the final torsional angles φ of the further optimized conformers (i), (ii) and (iii). It is worth to mention that in the frame of the DAII conformational analysis, the DFT method fails, since it reveals two extra conformations to be minima, while

the MP2 method, accounting properly for van der Waals interactions, rules these conformations out. Additionally, as is apparent from Table S1, many other possible conformations do interconvert into 9 real conformers.

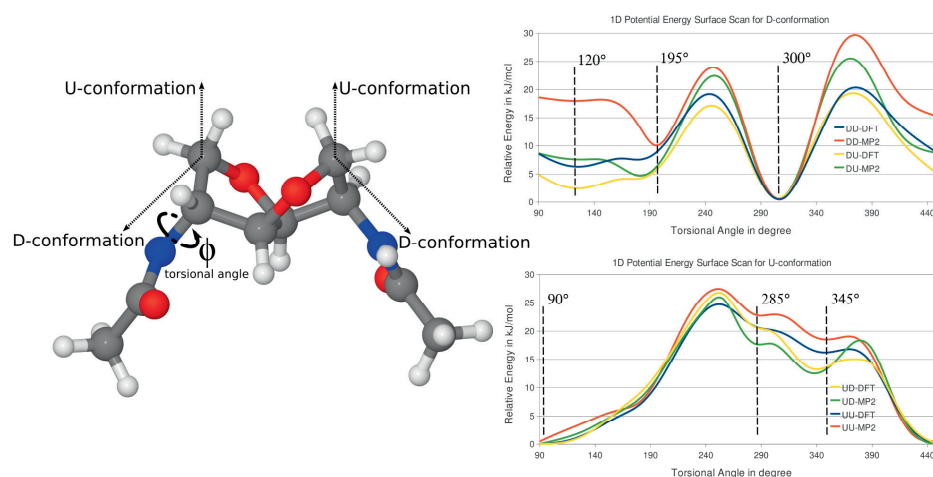


Figure S1. Conformational search scheme for the different boat and chair conformations (UU, UD, DU, and DD) of the isohexide unit (left) and corresponding 1D potential energy plots (right). For clarity only methyl groups have been attached. Full calculations were performed using propyl side chains.

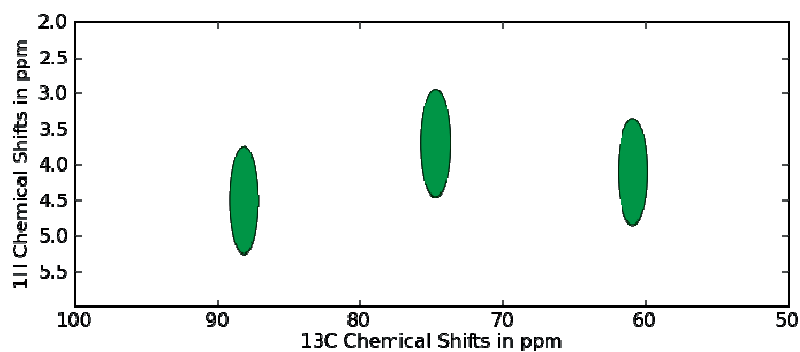


Figure S2. Calculated 2D $^{13}\text{C}\{^1\text{H}\}$ HETCOR spectrum of the isohexide unit. The green ellipses illustrate computed ^1H - ^{13}C correlations of $\text{C}(\alpha_{\text{N,DAII}})$, $\text{C}(\beta_{\text{N,DAII}})$, and $\text{C}(\beta'_{\text{N,DAII}})$ with $\text{H}(\alpha_{\text{N,DAII}})$, $\text{H}(\beta_{\text{N,DAII}})$, and $\text{H}(\beta'_{\text{N,DAII}})$, respectively. The blue translucent ellipses show the same correlations based on the HBMC experiment determined in our previous work.⁵

Table S1. Summary of all optimized conformations obtained from the 1D-PES scanning procedure (Figure S1). Stable conformers are indicated in blue (DFT) and green (MP2).

| UU | 90° | 285° | 345° | DU | 90° | 285° | 345° | DD | 120° | 195° | 300° |
|-----------|-----|------|------|-----------|-----|------|------|-----------|------|------|------|
| 90°(DFT) | 1 | 6 | 2 | 120°(DFT) | 3 | 10 | 5 | 120°(DFT) | 1 | 9 | 8 |
| 90°(MP2) | 1 | 6 | 2 | 120°(MP2) | 4 | 5 | 5 | 120°(MP2) | 1 | 4 | 10 |
| 285°(DFT) | | 11 | 7 | 195°(DFT) | 4 | 5 | 5 | 195°(DFT) | | 9 | 10 |
| 285°(MP2) | | 11 | 7 | 195°(MP2) | 4 | 5 | 5 | 195°(MP2) | | 9 | 10 |
| 345°(DFT) | | | 11 | 300°(DFT) | 6 | 11 | 7 | 300°(DFT) | | | 11 |
| 345°(MP2) | | | 7 | 300°(MP2) | 6 | 11 | 7 | 300°(MP2) | | | 11 |

Table S2. Initial and MP2/6-31G* optimized geometries for the DAII fragments (see Figure S1 for definition of angles and conformations U(up) and D(down)), calculated ¹³C chemical shift, Boltzmann distribution and total energies relative to the most stable conformer at different levels of theory. The most stable conformers 1, 4, and 6 (grey) correspond to those shown in Figure 7.

| # | Start Geometry | Optimized Geometry | β_{DAII} (ppm) | | β'_{DAII} (ppm) | | α_{DAII} (ppm) | | MP2/6-31G* E(kcal) BDist.(%) | | CPMD/DFT-D E(kcal) BDist.(%) | |
|----------|-----------------|--------------------|----------------------|-------------|-----------------------|-------------|-----------------------|-------------|-----------------------------------|-------------|-----------------------------------|-------------|
| | | | | | | | | | | | | |
| 1 | U90,U90 | U78,U78 | 88.6 | 88.6 | 75.2 | 75.2 | 61.1 | 61.1 | 0.0 | 95.4 | 0.0 | 80.2 |
| 2 | U90,U345 | U80,U344 | 93.1 | 88.2 | 76.0 | 80.1 | 60.9 | 67.3 | 4.6 | 0.0 | 4.1 | 0.1 |
| 4 | D195,U90 | D183,U81 | 94.1 | 89.8 | 79.1 | 72.8 | 64.4 | 59.2 | 2.9 | 0.7 | 1.8 | 4.0 |
| 5 | D195,U345 | D179,U327 | 96.6 | 89.3 | 78.6 | 77.8 | 62.6 | 65.1 | 5.0 | 0.0 | 4.0 | 0.1 |
| 6 | D300,U90 | D306,U83 | 91.6 | 91.0 | 72.1 | 73.3 | 68.0 | 58.8 | 1.9 | 3.8 | 1.0 | 14.1 |
| 7 | D300,U345 | D306,D327 | 94.2 | 90.9 | 70.8 | 77.9 | 67.1 | 65.4 | 6.2 | 0.0 | 5.1 | 0.0 |
| 9 | D195,D195 | D182,D182 | 92.3 | 92.3 | 81.7 | 81.7 | 63.6 | 63.6 | 6.8 | 0.0 | 4.2 | 0.1 |
| 10 | D195,D300 | D182,D308 | 96.1 | 93.6 | 84.0 | 75.2 | 62.0 | 64.1 | 5.0 | 0.0 | 2.7 | 0.8 |
| 11 | D300,D300 | D307,D307 | 96.2 | 96.2 | 74.7 | 74.7 | 64.8 | 64.8 | 4.9 | 0.0 | 2.9 | 0.6 |

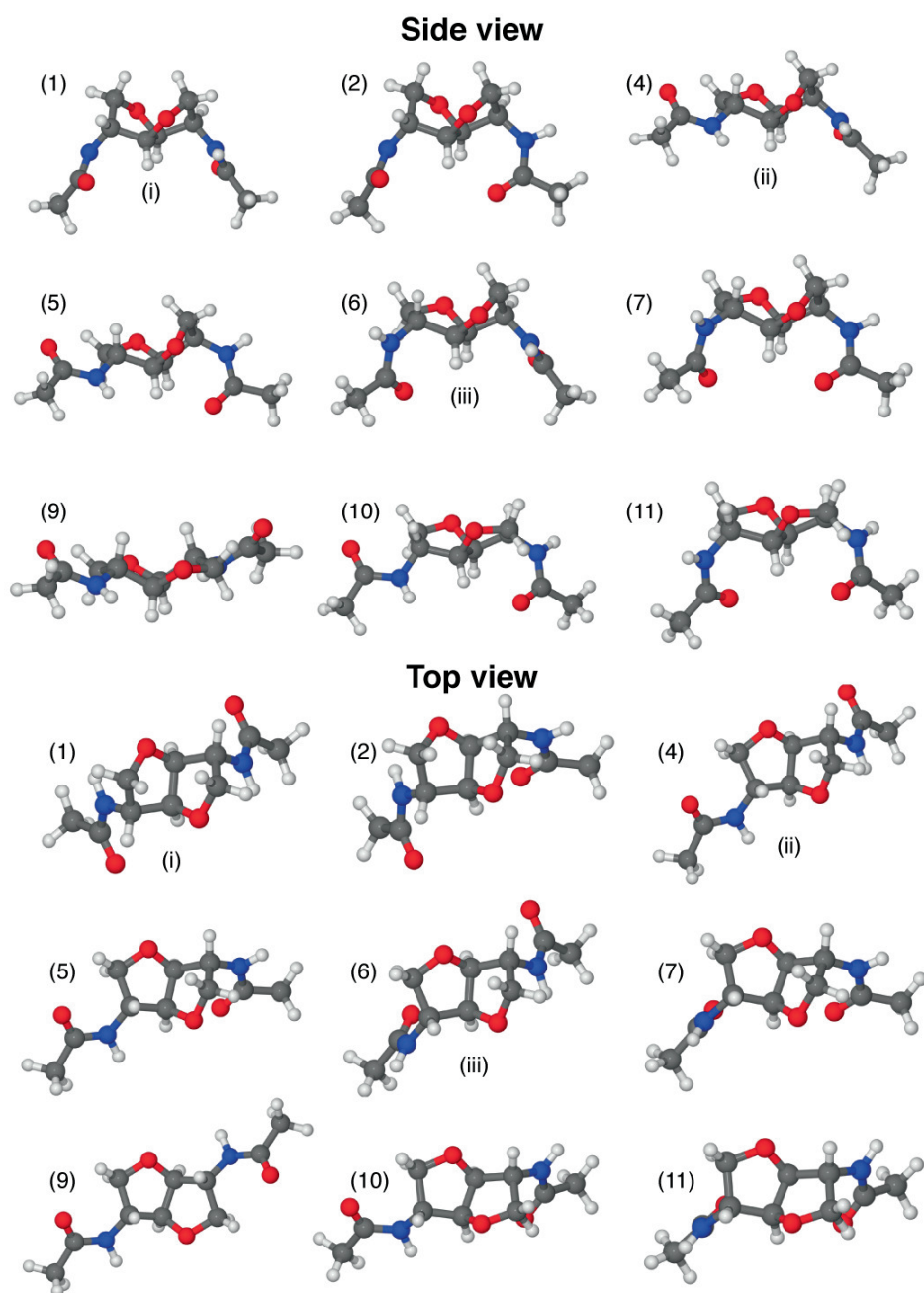


Figure S3. Top and side view of the found DAII conformers listed in Table S1 and S2. Roman numbers correspond to the three most abundant conformers in the gas phase calculations (also shown in Figure 7). For clarity only methyl groups are shown at each side of the DAII fragments.

X-Rays Analysis of the Polyamides

The homopolyamides and copolyamides based on diaminoisoidide (DAII), 1,4-diaminobutane (DAB) and sebacic acid (SA) were characterized collecting X-ray diffraction patterns employing a Bruker AXS HI-STAR area detector installed on a P4 diffractometer, using graphite-monochromated Cu K α radiation ($\lambda = 1.5418 \text{ \AA}$) and 0.5 mm collimator.

The data were collected during heating at 10 °C/min from around 40 °C to the melt and cooling from the melt to 40 °C using a modified Linkam TMS94 hot stage on SSP-synthesized powder contained in glass capillaries. The external shield of the Linkam was substituted with a new designed external shield with reduced dimensions (Figure S4). The resized shield has been designed in order to make the hot stage installable in the diffractometer. The 2D data were subsequently background-corrected and transformed into 1D profiles via integration.

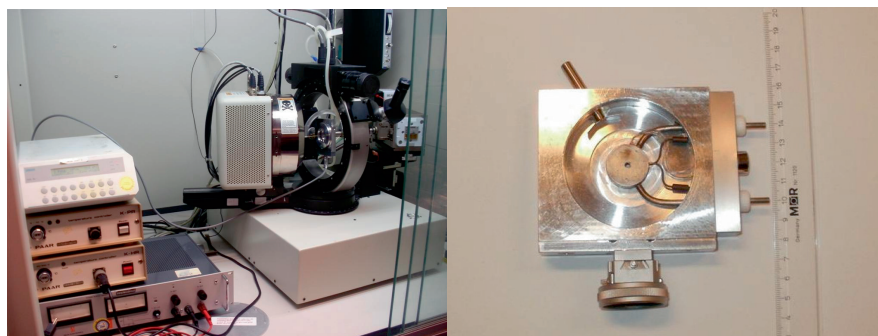


Figure S4. WAXS experimental setup and modified external shield of the Linkam hotstage.

Experimental Method

Using the designed set up of the Linkam hot stage it was possible to acquire temperature dependent WAXD pattern according with the scheme presented in Figure S5. Starting from the as-synthesized PA1, coPA3 and coPA4 we collected WAXD patterns performing two heating–cooling cycles for each sample. The melting temperatures observed from WAXD and DSC measurements can be considered as consistent. The differences observed for some samples can be attributed to the different experimental setup of the two considered techniques.

To measure the eventual difference between the displayed temperature values during the experiments and the real temperature, well known temperature calibration standards have been used and similar experiments were performed at the melting points of the standards. Considering the difference between the known melting temperature and the displayed temperature collected from the Linkam controller it was possible to make a temperature calibration curve (Figure S6). In Figure S6 is also presented a table with displayed temperature and the real temperature of the measurements. Successively the values of the temperature for each collected pattern have been corrected and used for the data analysis in the present chapter.

The used temperature standards are as follows:

Azobenzene ($T_m=68\text{ }^\circ\text{C}$)

Phenacetin ($T_m=134.5\text{ }^\circ\text{C}$)

Salophen ($T_m=191\text{ }^\circ\text{C}$)

Saccharin ($T_m=228\text{ }^\circ\text{C}$)

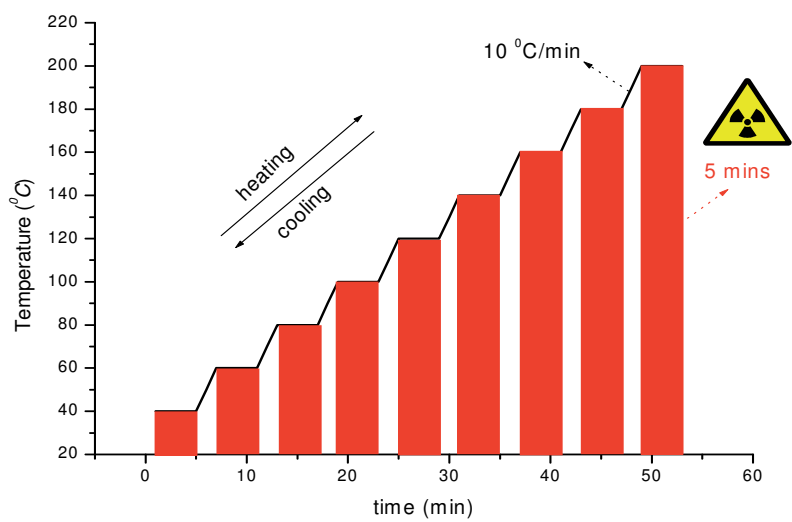


Figure S5. General scheme of WAXD temperature dependent experiments.

| T displayed (°C) | T real (°C) |
|------------------|-------------|
| 0 | 8.8 |
| 20 | 23.2 |
| 40 | 37.7 |
| 60 | 52.1 |
| 80 | 66.5 |
| 100 | 81.0 |
| 120 | 95.4 |
| 140 | 109.9 |
| 160 | 124.3 |
| 180 | 138.8 |
| 200 | 153.2 |
| 220 | 167.7 |
| 240 | 182.1 |
| 260 | 196.5 |
| 280 | 211.0 |
| 300 | 225.4 |
| 320 | 239.9 |
| 340 | 254.3 |
| 360 | 268.8 |

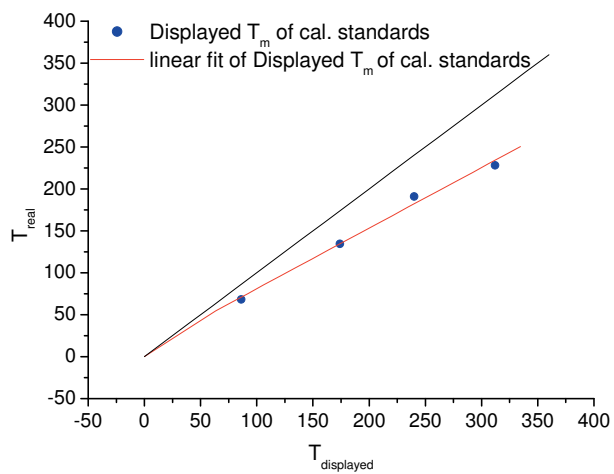


Figure S6. Temperature calibration curve calculated performing heating/cooling experiments on well known temperature calibration standards. In the table displayed temperatures and real temperatures of the measurements are compared.

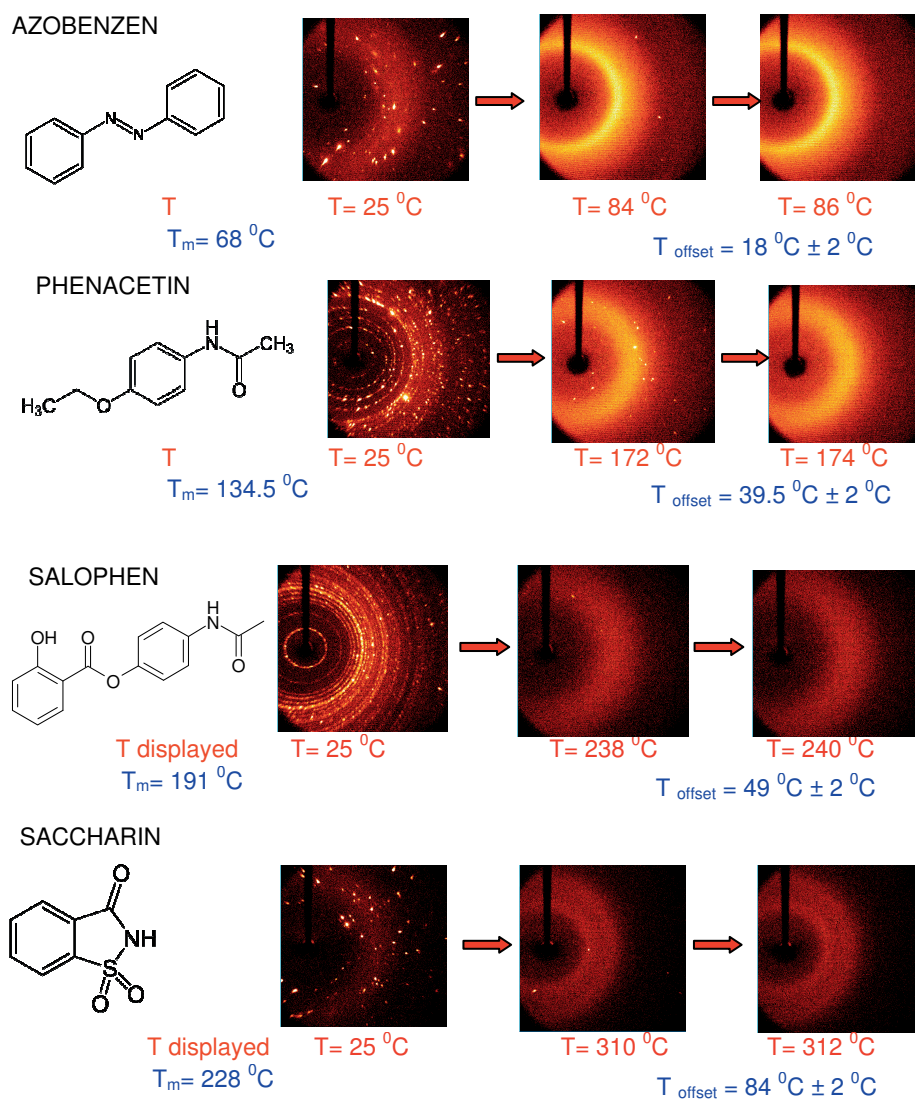


Figure S7. Temperature dependent WAXS performed on well known temperature calibration standards.

WAXD Experiments

In Figure S8 are shown the X-rays patterns collected for the as synthesized PA1. The patterns have been collected during the first heating run applied to the material starting from 38 °C to 225 °C. PA1, as already mentioned in the chapter 3, crystallizes into the typical α and/or β form of the polyamide. The interchain 100 and intersheet 010/110 diffraction peaks tend to merge with increasing temperature. The pattern at 225 °C shows that PA1 is amorphous and confirms that the material melts upon reaching this temperature.

In Figure S9 are presented the X-ray patterns collected for the PA1 during the first cooling run. A reversible behavior can be observed. Similar behavior is observed also for the PA1 during the second heating-cooling cycle (Figures S10, S11). The Brill transition temperature occurs at 196 °C and the melting of PA 1 starts at 225 °C.

Similar behavior is observed for the coPA3 during the two heating cycles (Fig. S12-15). The difference between this copolymer and PA 4.10 is the lack of a Brill transition below the melting point of the sample.

The XRD patterns of the coPA4 (Figures S16-19) show only two strong diffraction peaks indexed as 001 and 100. As reported in our previous paper⁵ the 001 diffraction peak shifts to lower values of 2θ compared to the same diffraction peak of the other polyamides. After the first heating/cooling cycle the presence of a 010/110 diffraction peak with very low intensity is observed. During the second cooling run this diffraction peak appears as a low intense shoulder. Detailed explanations of this phenomenon are reported previously in the chapter.

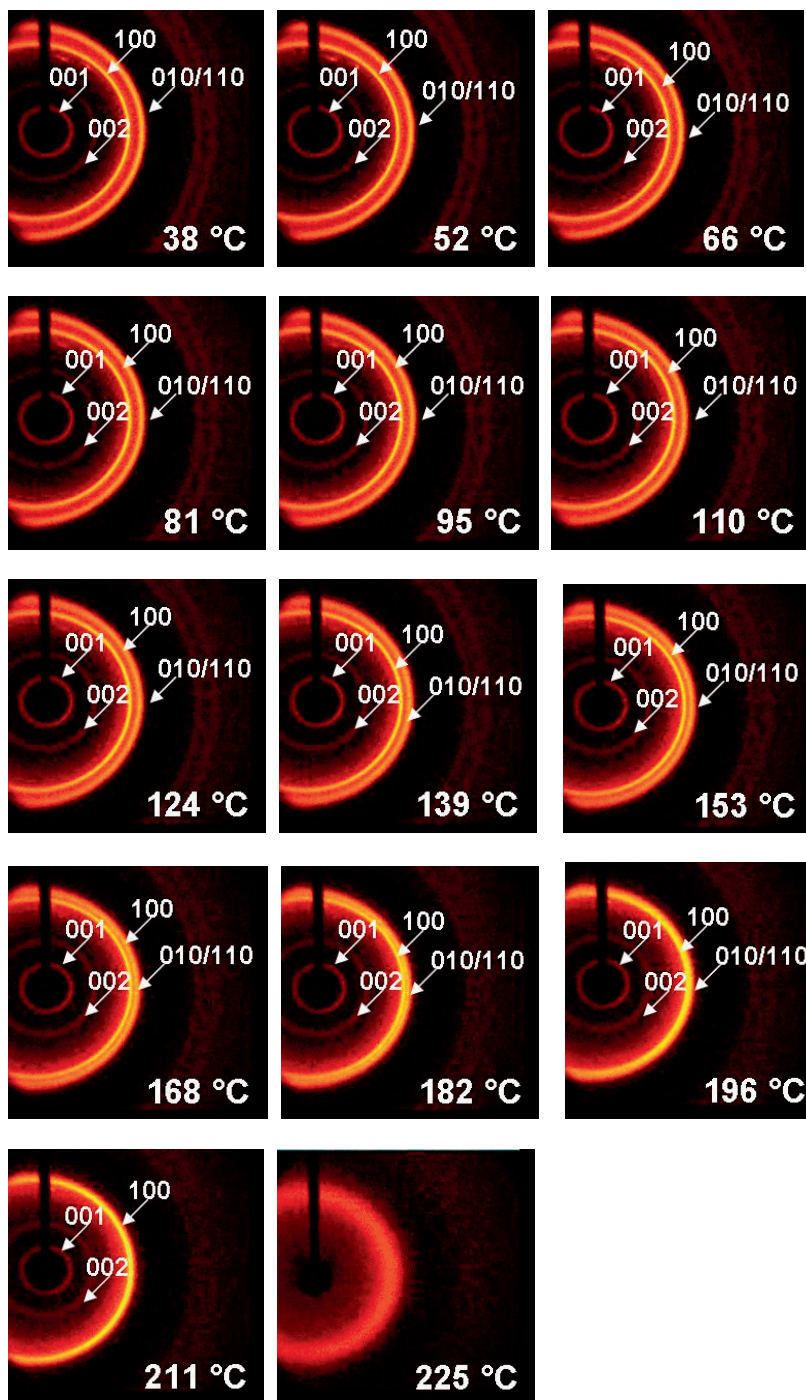


Figure S8. X-ray patterns collected for the PA1 during the first heating run applied to the material starting from 38 °C to 225 °C.

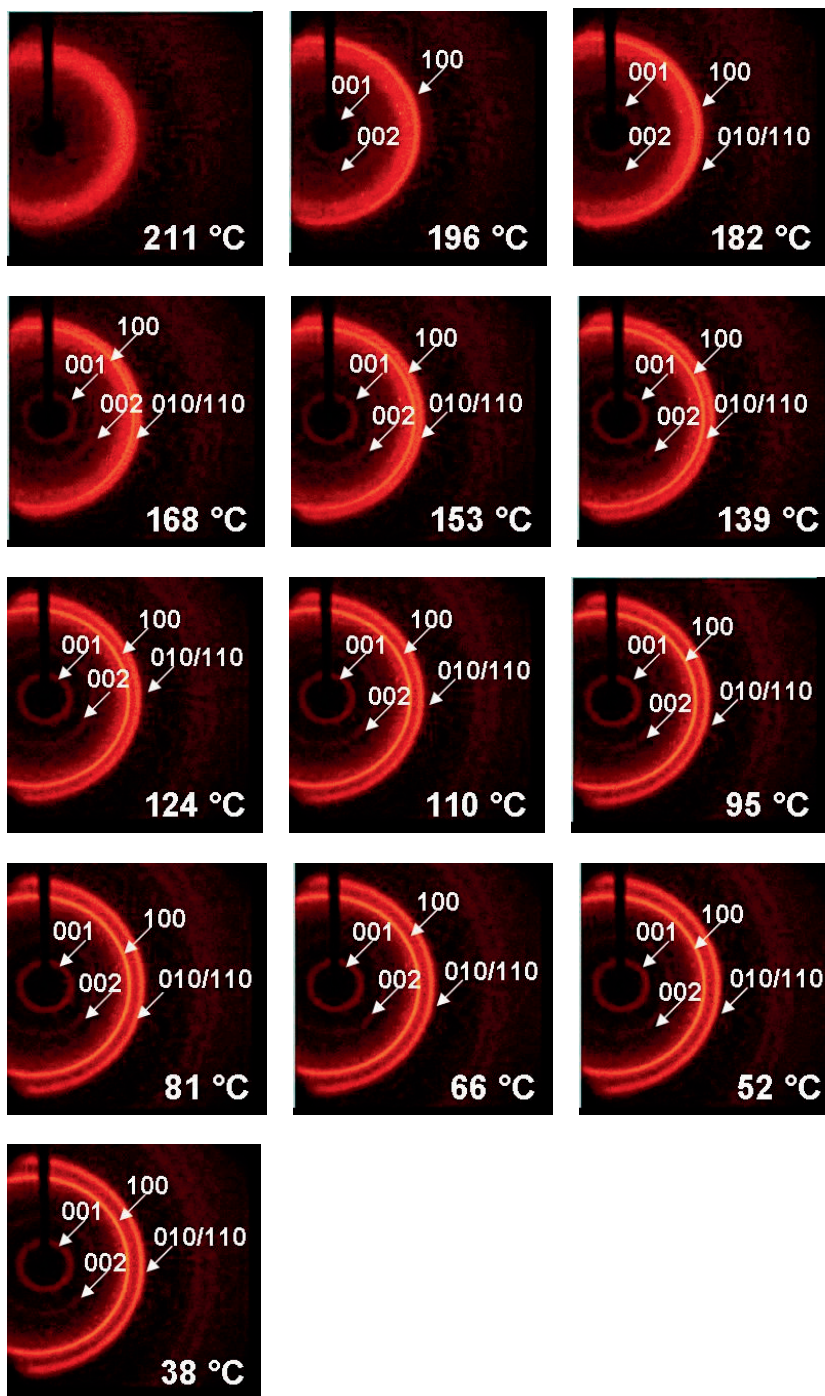


Figure S9. X-ray patterns collected for the PA1 during the first cooling run applied to the material starting from 225 °C to 38 °C.

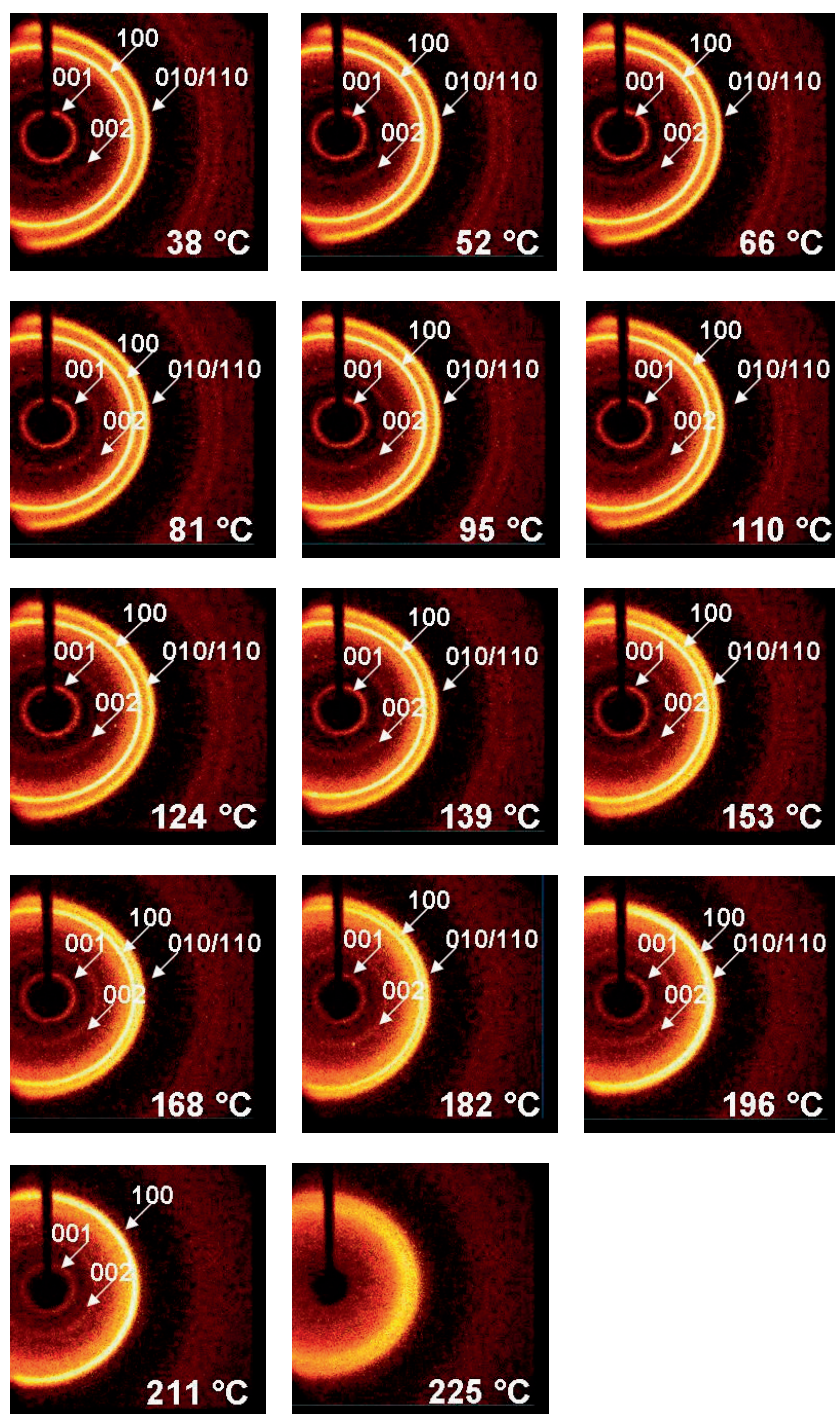


Figure S10. X-ray patterns collected for the PA1 during the second heating run applied to the material starting from 38 °C to 225 °C.

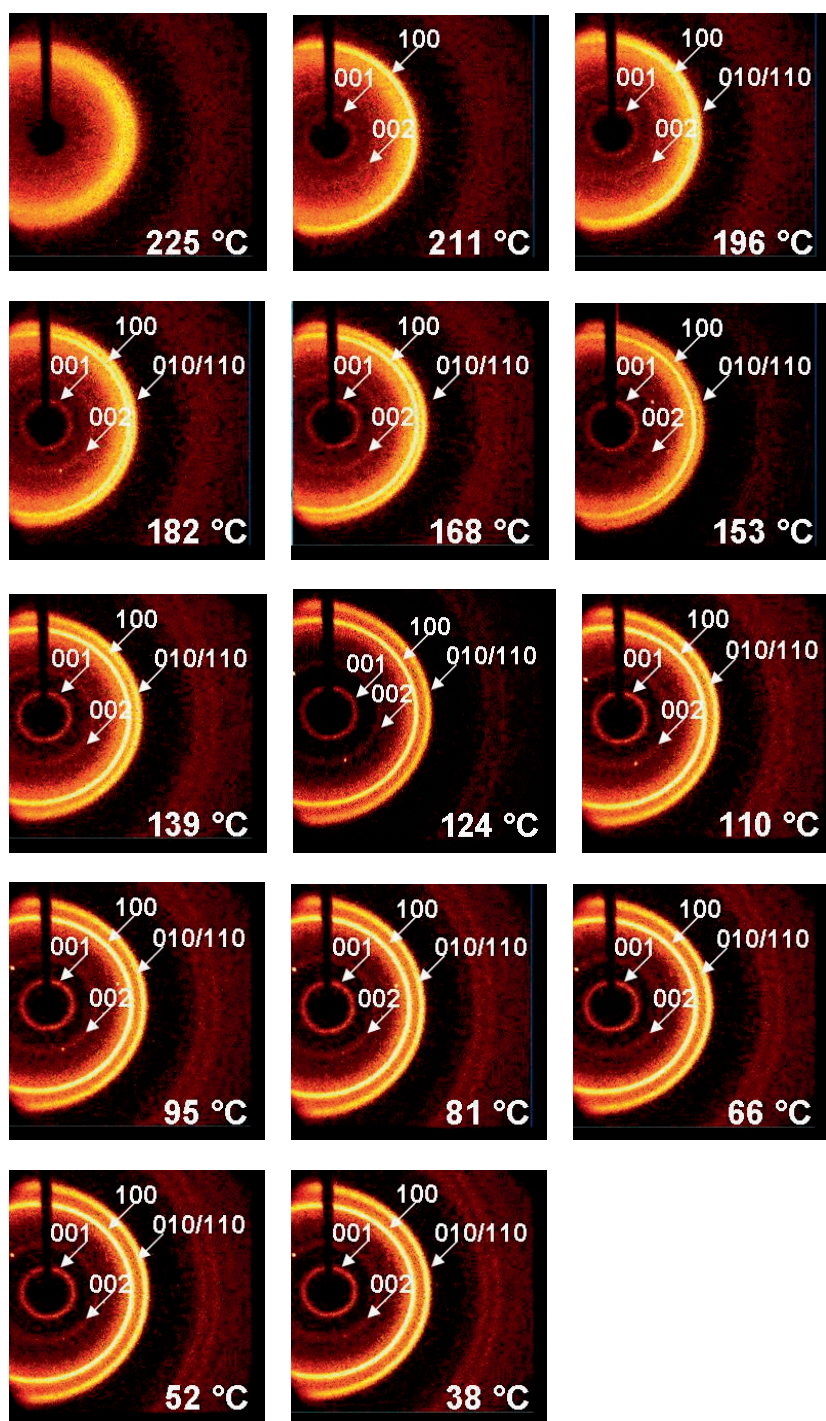


Figure S11. X-ray patterns collected for the PA1 during the second cooling run applied to the material starting from 225 °C to 38 °C.

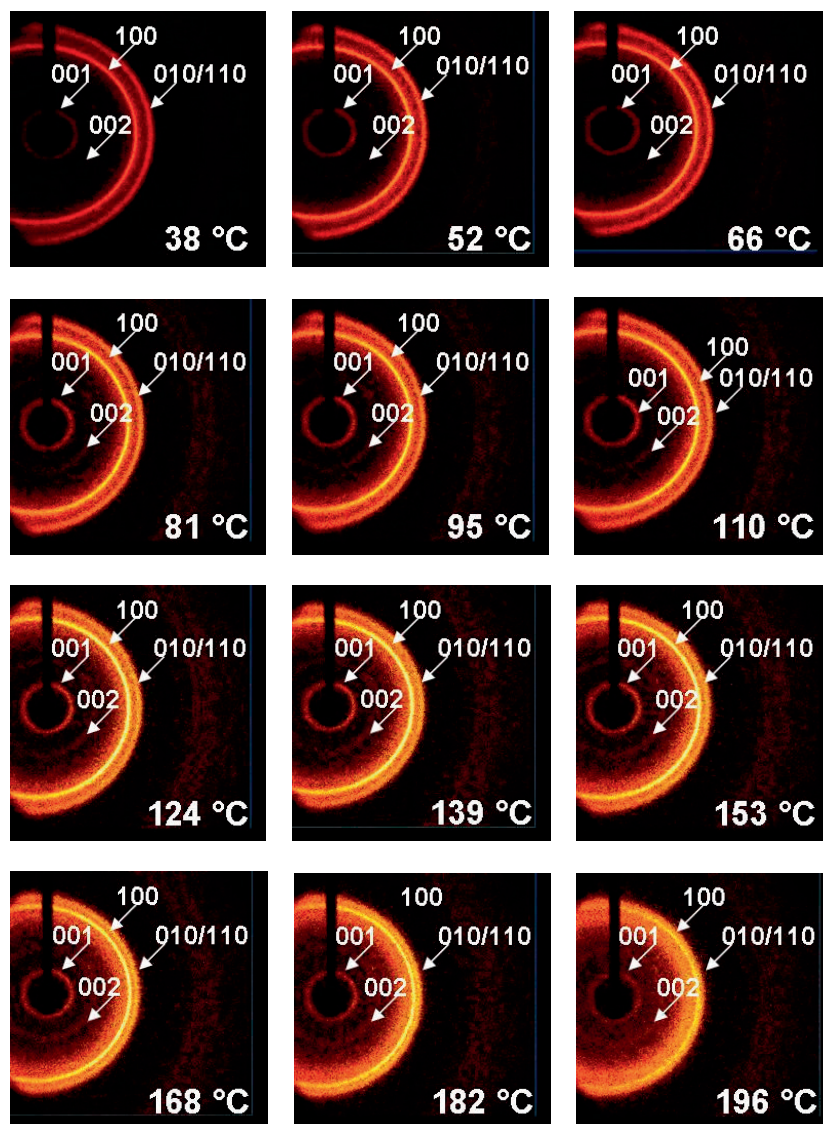


Figure S12. X-ray patterns collected for the coPA3 during the first heating run applied to the material starting from 38 °C to 196 °C.

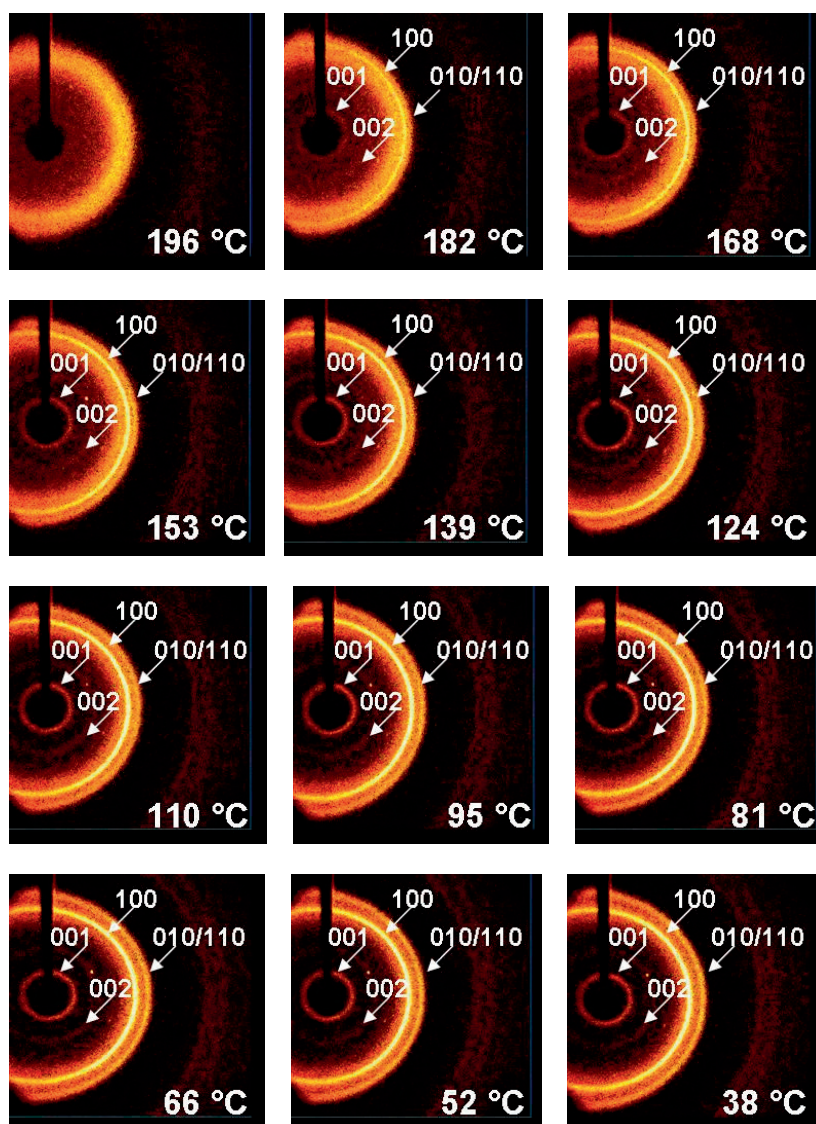


Figure S13. X-ray patterns collected for the coPA3 during the first cooling run applied to the material starting from 196 °C to 38 °C.

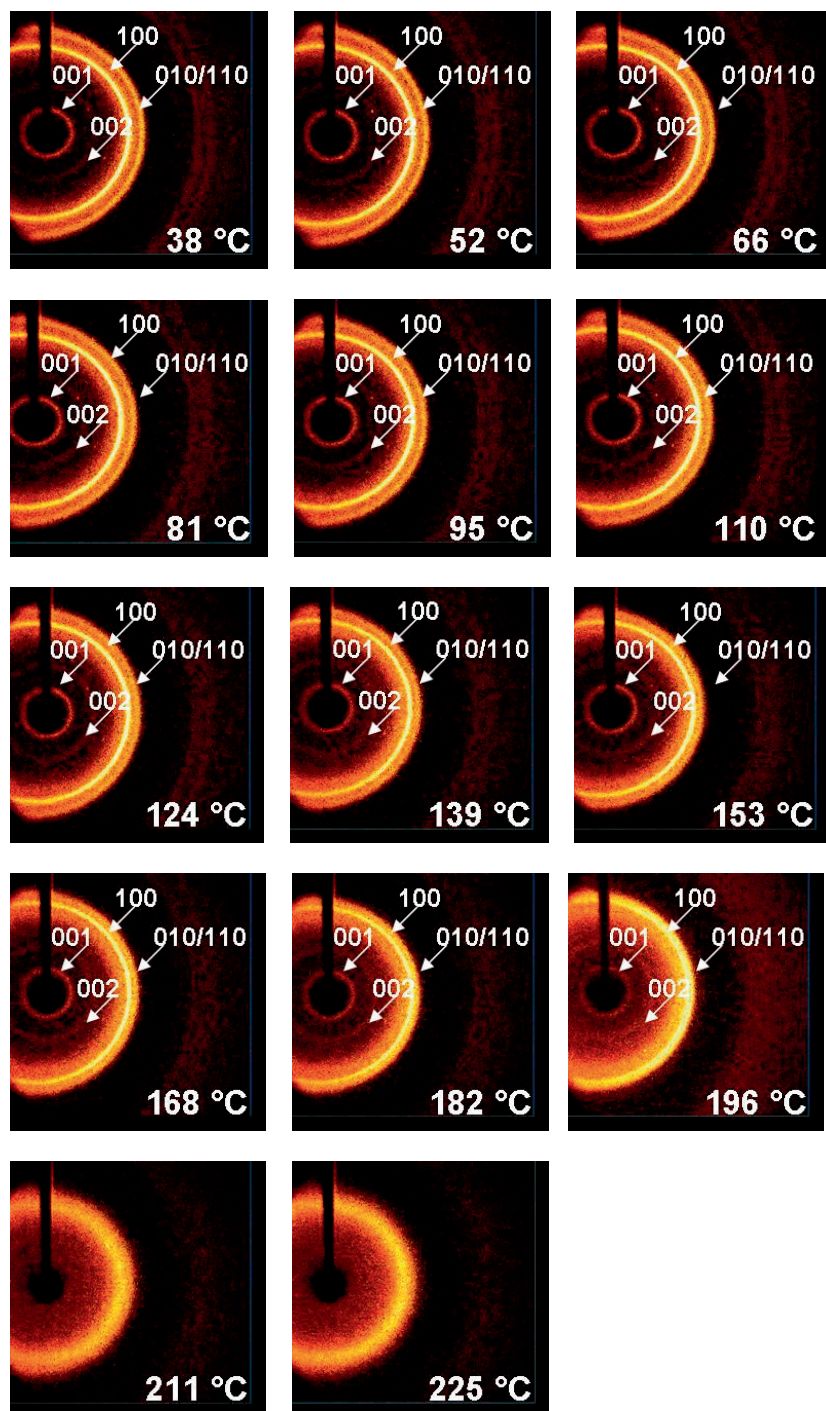


Figure S14. X-ray patterns collected for the coPA3 during the second heating run applied to the material starting from 38 °C to 225 °C.

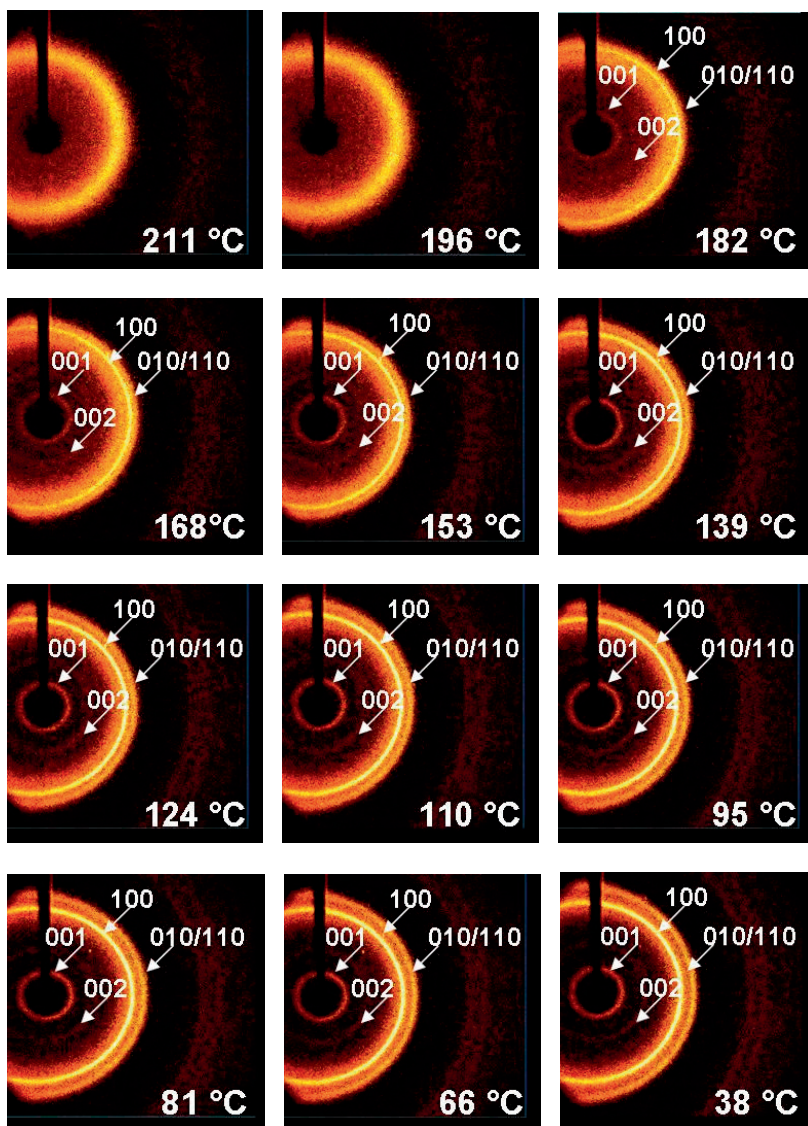


Figure S15. X-ray patterns collected for the coPA3 during the second cooling run applied to the material starting from 211 °C to 38 °C.

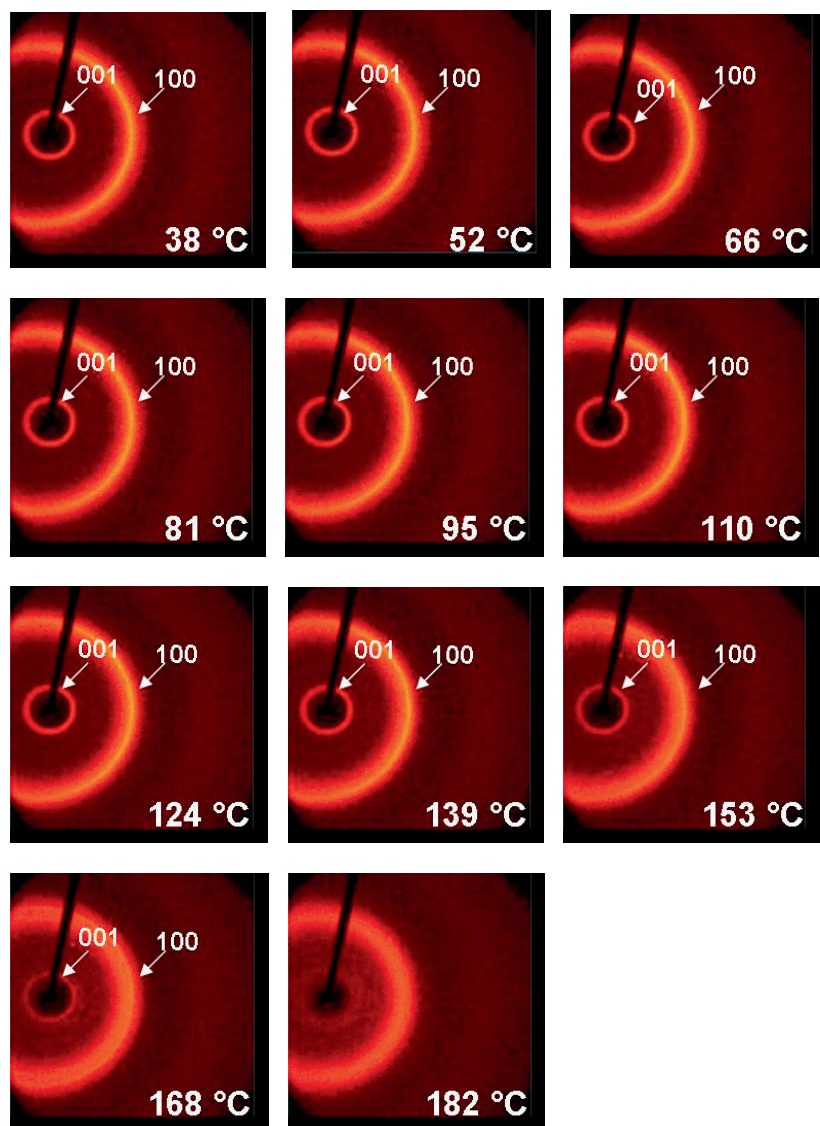


Figure S16. X-ray patterns collected for the coPA4 during the first heating run applied to the material starting from 38 °C to 182 °C.

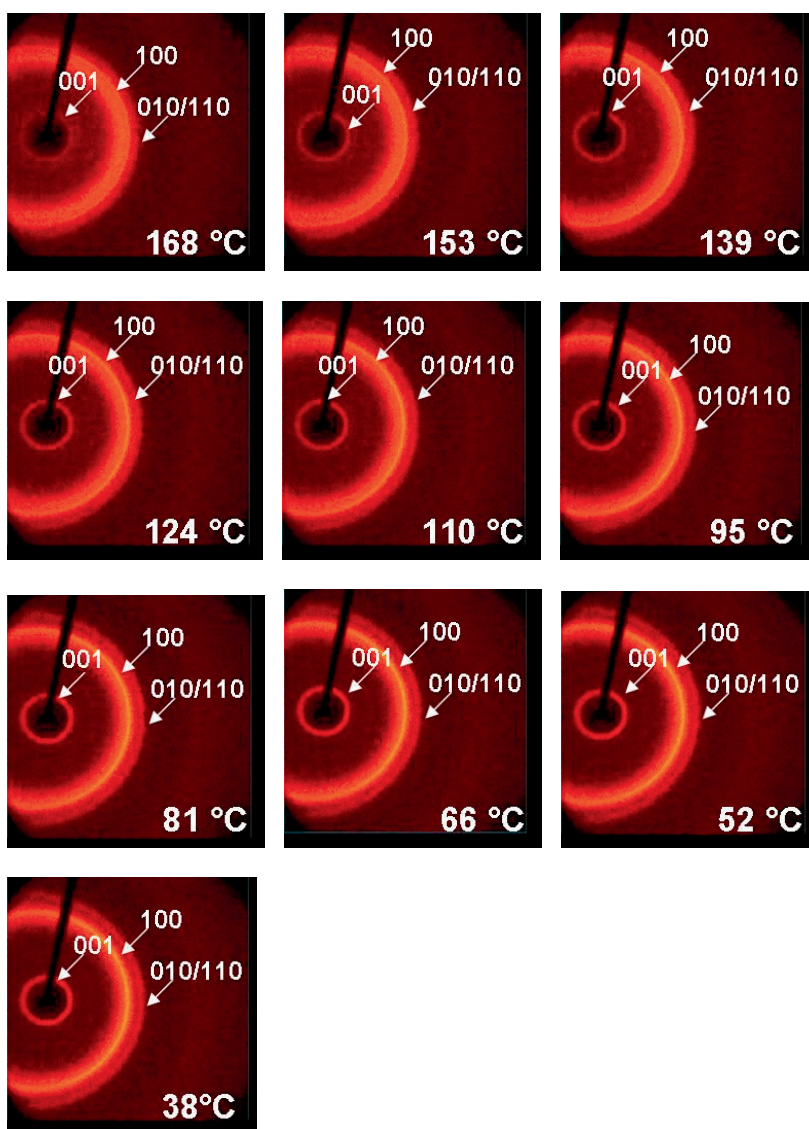


Figure S17. X-ray patterns collected for the coPA4 during the first cooling run applied to the material starting from 168 °C to 38 °C.

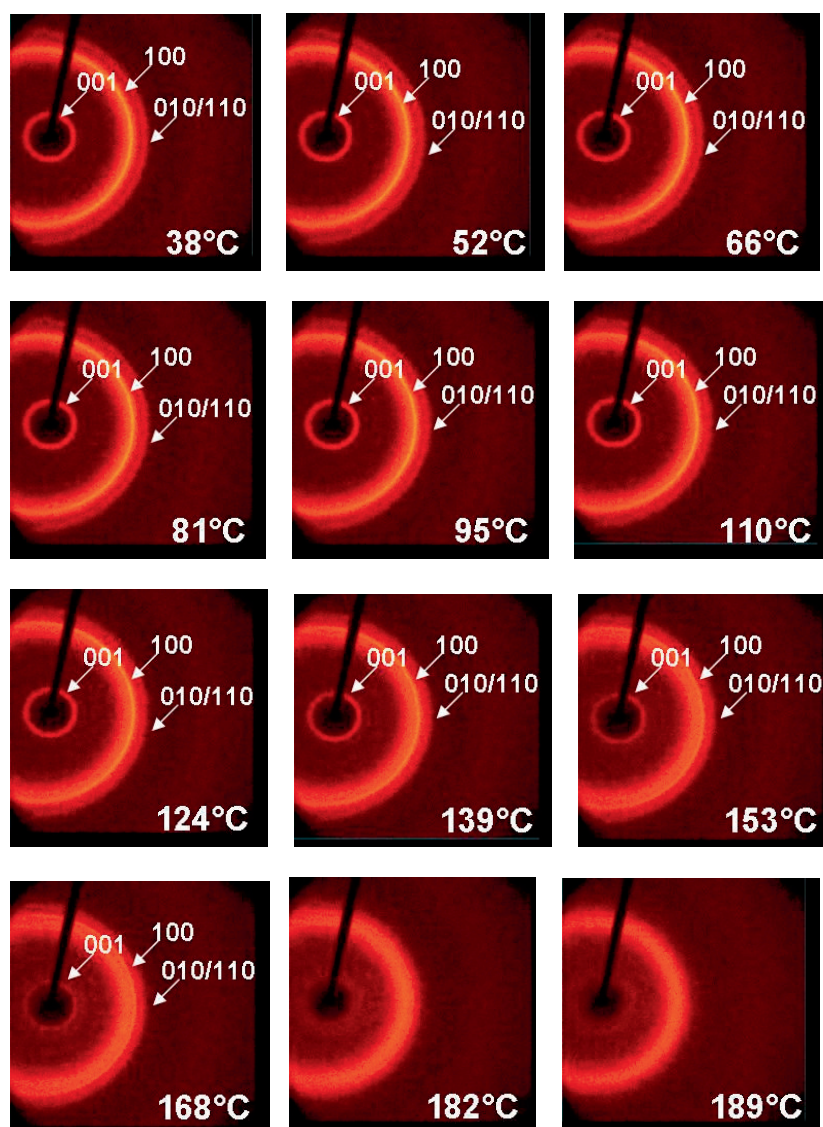


Figure S18. X-ray patterns collected for the coPA4 during the second heating run applied to the material starting from 38 °C to 189 °C.

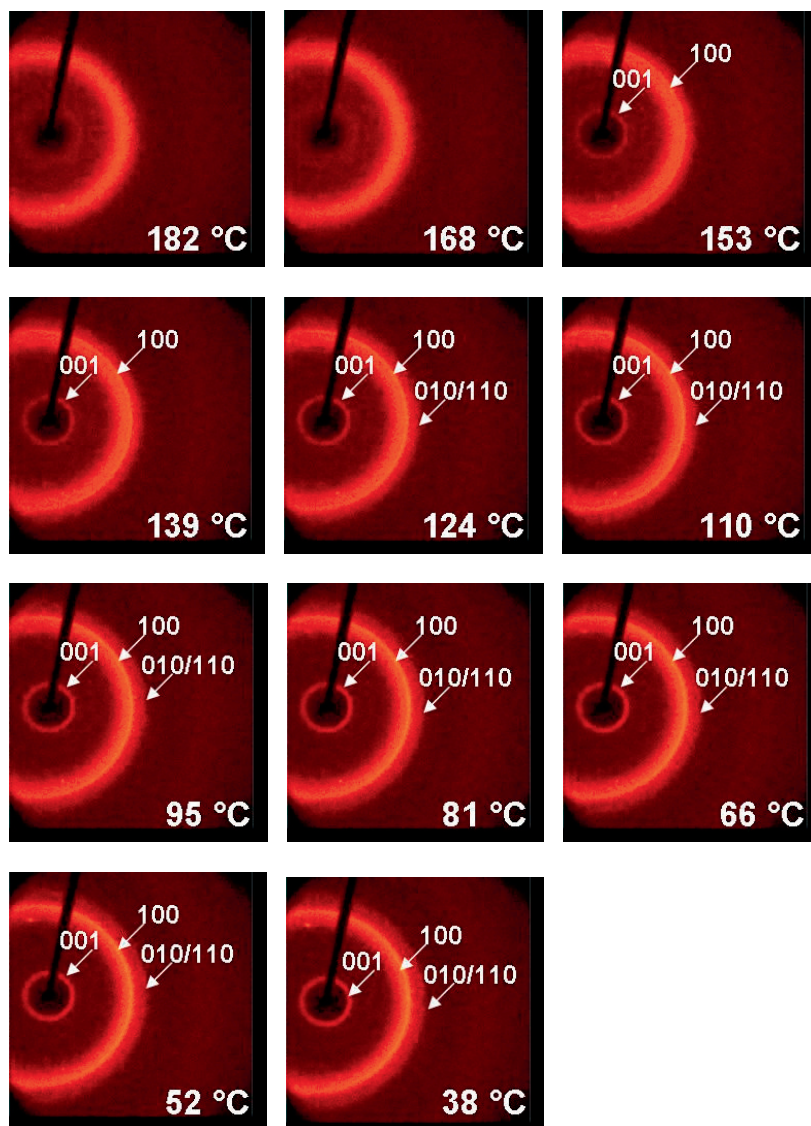


Figure S19. X-ray patterns collected for the coPA4 during the second cooling run applied to the material starting from 182 °C to 38 °C.

The crystallinity indexes have been calculated using the Hermans and Weidinger method.⁷ In particular this means that each sample profile has been baseline corrected by subtracting the background scattering. The amorphous halo was obtained collecting the XRD pattern for each sample once the melting temperature was reached. In order to avoid possible errors due to the shifting of the amorphous peak as function of the different temperatures, four diffraction profiles at different temperature have been considered (Figure S20). Considering the observed amorphous peak shifting a calibration curve was calculated to extrapolate the 2θ value of the amorphous peak to the experimentally used temperature. The applied formula for the calculation of the degree of crystallinity is the following:

$$X_c = \frac{A_c}{A_c + A_a} \cdot 100$$

where A_c and A_a are the integrated intensities from the crystalline and amorphous phases, respectively. The integrated intensity A_a is obtained by fitting the profile of the material after melting to the scattering pattern of the sample at the required temperature, as demonstrated in Figure S21. This fitting process amounts to multiplying the latter profile by a factor K . In order to calculate K , the amorphous halo was subtracted considering 3 different contact points (**A**, **B**, **C**) between each sample profile and amorphous profile as shown in Figure S21. Keeping the contact points fixed, the intensity of the amorphous halo was varied with respect to the sample intensity, in order to obtain a close fit.

As an example, the calculations of the degree of crystallinity for the PA1 sample at 3 different temperatures are reported in Figure S21. In this case the K constant ranges from a value of around 0.5 for Fig 2a to 0.83 for Figure S21c. This gives the possibility of keeping the same 3 contact points between the amorphous halo and each profile, ensuring the consistency of the method.

Considering the presence of very intense peaks in the region of $2\theta = 5^\circ$, especially in the sample coPA 4, we have integrated the areas of amorphous and crystalline domains in the range of $3-48^\circ$ (2θ).

In the employed crystallinity determination the amorphous contribution is probably somewhat overestimated. Trends in the variation of crystallinity, however, will not be influenced.

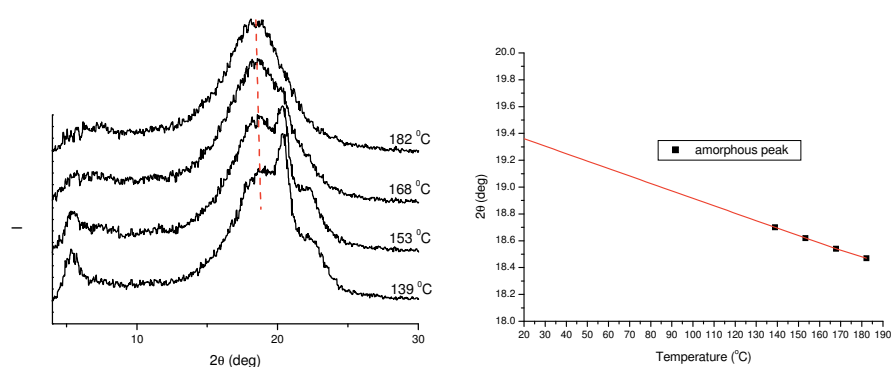


Figure S20. X-ray powder diffraction profiles of coPA4 measured at four different temperatures. The reported profiles show the amorphous peak shifting as function of the temperature.

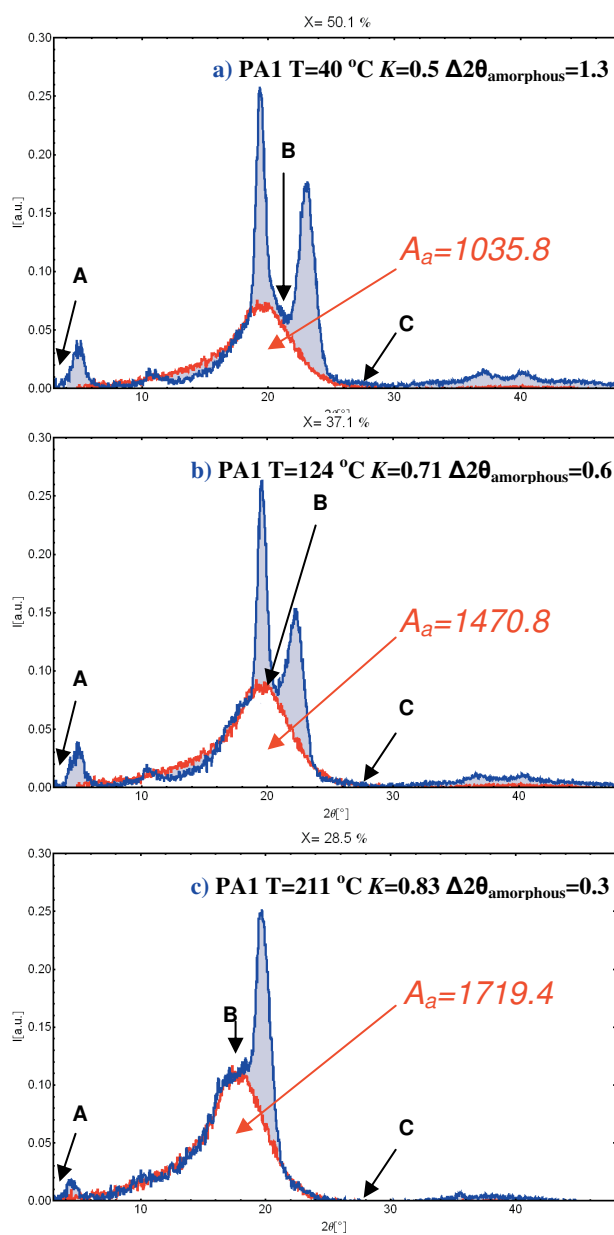


Figure S21. X-ray powder diffraction profiles of PA1 collected at 3 different temperatures. The profiles show the crystalline and amorphous contribution in each measurement. In the figure the contact points considered for the subtraction of the amorphous area (A, B, C), the K values considered and the amorphous peak shifting values are also reported ($\Delta 2\theta$).

References Appendix B

1. Allinger, N. L.; Grev, R. S.; Yates, B. Y.; Schaefer, H. F. *J. Am. Chem. Soc.* **1990**, 112, 114-118.
2. Wiberg, K. B.; Murcko, M. A. *J. Comp. Chem.* **1988**, 9, 488-494.
3. Tsuzuki, S.; Uchimarui, T.; Tanabe, K.; Hirano, T. *J. Phys. Chem.* **1993**, 97, 1346-1350.
4. Ke, H. W.; Rao, L.; Xu, X.; Yan, Y. J. *J. Theoret. Comp. Chem.* **2008**, 4, 889-909.
5. Jasinska, L.; Villani, M.; Wu, J.; van Es, D.; Klop, E.; Rastogi, S.; Koning, C. E. *Macromolecules* **2011**, 44, 3458-3466.
6. Frisch, M. J. et al. Gaussian 03 Revision D. 02; Gaussian, Inc., Wallingford, CT, **2004**.
7. Hermans, P.,H., Weidinger, A. *Makromol. Chem.* **1961**, 44, 24.

Chapter 5

Structure-Property Relationships of Diaminoisoidide-based Copolyamides*

Biobased polyamides synthesized from diaminoisoidide, 1,4-diaminobutane and sebacic acid are investigated by FT-IR, WAXD and electron diffraction of sedimented crystal mats and single crystals. The presence of diaminoisoidide (DAII) in the copolyamides reduces the hydrogen bonding efficiency and thus the melting point of the copolyamides. DAII copolymers are semi-crystalline over the whole range of compositions. The typical polyamide structure with different interchain and intersheet distances has changed into a pseudo hexagonal structure at a DAII content of 43%. Diffraction modeling suggests that the basic structural scheme found in polyamides, consisting of hydrogen-bonded sheets packed in a triclinic structure with the *ab*-plane tilted with respect to the *c*-axis, still applies for these copolymers. We propose that the structure is a perturbed form of the α -phase of polyamide 4.10 resulting from the conformational rearrangement of the polymer chains due to the introduction of bulky DAII monomer fragments.

**reproduced from Maurizio Villani, Lidia Jasinska-Walc, Anne Spoelstra, Cor E. Koning, Enno Klop and Sanjay Rastogi, Macromolecules, to be submitted.*

5.1 Introduction

Several detailed crystal structure studies of polyamides have been reported in the last 50 years. To recall, the crystal structure of the α -phase as proposed by Bunn and Garner² consists of hydrogen-bonded sheets that show progressive shear. Moreover different authors have reported on the pseudo-hexagonal or γ -phase.^{3, 4} The hydrogen bonding scheme in the α -phase is confined to one direction (the *ac* plane). The formation of the pseudo-hexagonal phase has been related to the presence of hydrogen bonds in two separate directions,³⁻⁶ or in three separate directions.⁷ In many of these studies the γ -phase is obtained at elevated temperatures, above the Brill transition temperature, where the resultant structure is a consequence of the mobility of methylene units.⁸ Considering that the high mobility of the methylene units leads to conformational disorder that influences the chain packing, as demonstrated in chapter 4, the conformational disorder responsible for the pseudo-hexagonal packing can also be obtained by introducing bulky chain fragments that affect the crystallization of polyamides. Insight into the nature of hydrogen bonding is considered of interest because hydrogen bonding influences the mechanical properties.

The use of renewable dicarboxylic acids with the diamino derivatives of starch-based 1,4;3,6-dianhydrohexitols (isosorbide, isomannide and isoidide) or their diamino derivatives with D-manno or L-ido conformation in the synthesis of polyamides (PAs) gives access to entirely bio-based materials and may demonstrate their possible applications.⁹⁻¹⁶ The incorporation of diaminoisoidide residues into the PA 4.10 backbone reduces the hydrogen bond density and thus the melting point of the polyamides.¹⁷ We propose a structure for DAII based copolyamides, based on X-ray data and electron diffraction data, that together with Dynamic Mechanical Thermal Analysis shed light on the structure-property relationships of this class of copolyamides.

5.2 Experimental Section

5.2.1 Synthesis and characterization. Homopolyamides and copolyamides based on diaminoisoidide (DAII), 1,4-diaminobutane (DAB) and sebacic acid (SA) were synthesized via bulk polycondensation followed by Solid State Polymerization (SSP) or by interfacial polycondensation, as described in chapter 3.¹⁷ In that chapter characterization of the polyamides was presented using 2D NMR spectroscopy, SEC, FT-IR, TGA, DSC and WAXD. Temperature dependent FT-IR, solid state NMR and WAXD studies were reported in chapter 4.¹ An overview of the molecular characterization and thermal properties of the polyamides is presented in Table 1.

Fourier Transform Infrared spectra (FT-IR) were obtained using a Varian 610-IR spectrometer equipped with an FT-IR microscope. The spectra were recorded in transmission mode with a resolution of 2 cm^{-1} . Solvent casted PA films obtained from 1,1,1,3,3,3-hexafluoroisopropanol were analyzed on a zinc selenium disk and heated from 30°C to slightly above the melting point of the respective polyamides. For controlled heating a Linkam TMS94 hotstage was used. The samples were cooled in 10°C steps and reheated with the same heating rate. For this study the spectra from the second heating run were collected. Varian Resolution Pro software version 4.0.5.009 was used for the analysis of the spectra.

DSC measurements were carried out using a DSC Q1000 from TA Instruments. The analyses were carried out in a nitrogen atmosphere with a heating rate of $10^{\circ}\text{C}/\text{min}$. The events analyzed from the second heating and cooling curve are reported in Figure 3 of chapter 4. Figure 3 presents an overview of the analyses performed on the samples PA1 and coPA5 that are used for the crystal structure analysis.

5.2.2 Structural characterization. Polymer crystals were obtained from very dilute solutions [0.01-0.05% (w/v)] in 1,4 butanediol. The polymers were dissolved at high temperature 170-140 °C and then transferred into an oil bath maintained at a constant temperature between 80-120 °C, depending on the dissolution temperature of the individual polymer. The polymer was left to anneal isothermally in the oil bath between 12-24 hours until a sufficient amount of crystals is grown. The crystals were collected by ultra-centrifugation and repeatedly washed with n-butanol according to the procedure described by Aceituno et al.¹⁸

For electron microscopy, the crystals were deposited on carbon-coated Cu TEM grids, coated with gold as an internal diffraction reference. Low dose diffraction images were collected on a Fei Technai 20 transmission electron microscope operated at 200 kV. The source to sample distance was calibrated using standard grating replicas.

The X-ray diffraction patterns of CoPAs reported in Figure 1 were obtained employing the data presented in chapter 4, and as previously described the diffraction patterns were collected during heating at 10 °C/min from 40 °C to the melt and subsequent cooling from the melt to 40°C. The data acquisition time was 5 minutes. For the heating a Linkam TMS94 hot stage was applied with the sample in powder form encapsulated in Lindemann glass capillaries. The obtained 2D diffraction patterns were subsequently corrected for spatial distortion and background scattering (air and glass). Using azimuthal integration the patterns were transformed into 1D profiles.

Crystal structure analysis was performed using the Cerius2 software package employing the Compass force field.¹⁹

5.2.3 Mechanical properties. Dynamic mechanical thermal analysis (DMTA) was performed on the PA1 and coPA3 samples, using a DMAQ800 (TA) in tensile film mode. The dimensions of the specimen were 15 x 5.1 x 1 mm. The compression-molded samples were measured from -140 to 200 °C at a heating rate of 3 °C/min and at a frequency of 1Hz with a constant amplitude of 10 µm.

5.3 Results and Discussion

The homopolyamide PA1 based on sebacic acid and 1,4 diaminobutane and the copolyamide coPA5 obtained from sebacic acid, diaminoisodide and 1,4 diaminobutane were prepared via melt and solid state polycondensation as described in chapter 3. The physical properties of the homopolymer (PA1) and the copolymer (coPA5), summarized in Table 1 are reproduced from chapters 3 and 4. These parameters are of relevance for the structural investigations reported in the present chapter.

After the first polycondensation step the homopolymer PA1 has a molecular weight M_n of 9,600 g/mol. Higher molecular weight was obtained after subsequent solid state polymerization (SSP) of the low molecular weight polymer. However, even after SSP the coPA5 copolymer (DAB/DAII 0.57/0.43) maintained low molar mass, with an M_n of 3,900 g/mol. The low molar mass of coPA5 is attributed to the low melting temperature of the copolymer that influences the polycondensation reaction. The thermal stability is strongly affected with increasing DAII content, as was shown in chapter 3. The poor thermal stability is attributed to the presence of the ether oxygens of the diaminoisodide residues that strongly promote oxidation of the materials with the inclusion of DAII along the main chain. The increased amount of DAII residues in coPA5 influences the melting point of the copolymer and the heat of fusion ΔH during transition. The progressive reduction of the melting temperatures of the copolymers with increasing DAII content reported in Table 1 and Figure 5 of chapter 3 can be attributed to a less perfect chain packing of DAII-containing polymers and to a reduction in lamellar thickness.²⁰ Moreover coPA5 shows two melting peaks close to each other (see Table 1 and Figure 3a'). The two melting temperatures may be associated with the coexistence of two different crystalline phases; the pseudo-hexagonal phase and the α and/or β

phases resulting from different crystallization conditions, or phase segregation resulting from an inhomogeneous distribution of DAII along the chain.

Table 1. Built-in composition, molecular weight, melting and crystallization temperatures, enthalpy of the transitions analyzed from the second DSC heating and cooling runs of the homo- and copolyamides and the crystallinity indexes calculated from each XRD profile reported in chapter 4.

| Symbol | Built-in composition (DAB/DAII) ^a | M _n (g/mol) | T _m (°C) | ΔH _m (J/g) | T _c (°C) | ΔH _c (J/g) | X _c (%) (I heating) | X _c (%) (II heating) |
|--------|--|------------------------|---------------------|-----------------------|---------------------|-----------------------|--------------------------------|---------------------------------|
| PA1 | 1.0/0 | 21,900 | 246 | 67.3 | 221 | 75.4 | 50 | 43 |
| coPA5 | 0.57/0.43 | 3,900 | 179, 198 | 32.8 | 156 | 39.3 | 25 | 29 |

^a = molar ratio determined by NMR, T_m = melting point, T_c = crystallization temperature, ΔH = enthalpy of the transition during melting (m) or crystallization (c), X_c = crystallinity indexes.

The XRD patterns reported in Figure 1 show differences between the crystal structure of the homopolymer PA1 and that of the copolymer coPA5. In chapter 3 it was described that copolymers with DAII content lower than 43% mol have a crystal structure similar to polyamide 4.10, while the copolyamide having DAII content of 43% mol crystallizes into a pseudo-hexagonal structure. In accordance with the results described in chapter 3, the pseudo-hexagonal form observed for coPA5 is a direct consequence of the incorporation of the diaminoisoidide fragments into the structure of polyamide 4.10. This causes a conformational disorder of the polymer chain affecting the chain packing, while for PA1 the pseudo-hexagonal form is only observed above its Brill transition temperature (Figure 1b). The *d*-spacing values measured at room temperature for PA1 and coPA5 are reported in Table 2, whereas Figures 3b and 3b' depict changes in the *d*-spacing as a function of temperature during the first and second heating runs of the two samples.

| | | X-ray diffraction (nm) | | | | | |
|-------|---|------------------------|-----------|-----------|---------|-------|--|
| Symbo | l | 001 | 002 | 100 | 010/110 | 0 | |
| PA1 | | 1.56 1 | 0.77 6 | 0.442 | 0.379 | PA1 | |
| coPA5 | | 1.68 6 | - | 0.442 | - | coPA5 | |
| | | 2θ (deg) | | | | | |
| Symbo | l | 001 | 002 | 100 | 010/110 | 0 | |
| PA1 | | 5.66 | 11.3 8 | 20.0 0 | 23.46 | | |
| coPA5 | | 5.24 | - | 20.0 | - | | |

Table 2. Lattice spacings and X-ray diffraction angles of PA1 and coPA5 with different contents of diaminoisoidide measured at room temperature.

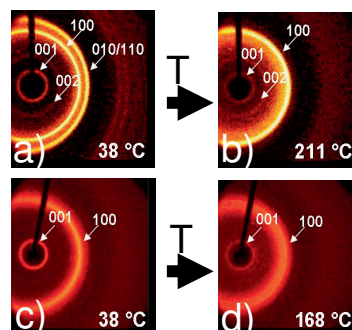


Figure 1. X-ray patterns collected for PA1 and coPA5 during the first heating run applied to the material starting from 38 °C to just below their melting temperature.

To correlate the changes in crystal structure with conformational changes, FT-IR data from chapter 4 are reproduced in Figure 2. This Figure shows temperature dependent infrared spectra in the frequency range 3500–3100 cm^{-1} and in the range 1750-650 cm^{-1} for PA1 and coPA5, respectively. The spectra in Figure 2a and Figure 2b are plotted on an absolute intensity scale to quantify differences in intensities and the associated conformations. At room temperature the infrared data of PA1 show the polyamide NH-stretching vibration at 3301 cm^{-1} (Figure 2a).²¹⁻²⁴ Figure 3c shows the temperature dependence of changes in the peak position of the NH-stretching band, together with changes in its half-height width, whereas Figure 3d depicts its normalized absorbance. By normalizing the NH stretching band at different temperatures by

the peak area of the 3301 cm^{-1} band at room temperature, changes in the NH stretching band are monitored. The wave number of the stretching band is directly related to the strength of the intermolecular hydrogen bonds. In the case of PA1, the band shifts to higher frequency with increasing temperature (Figure 3c). Around 200°C , close to the melting point, an upswing in the frequency with temperature is observed. This corresponds to the onset of the broad endothermic region as observed with DSC (Figure 3a).

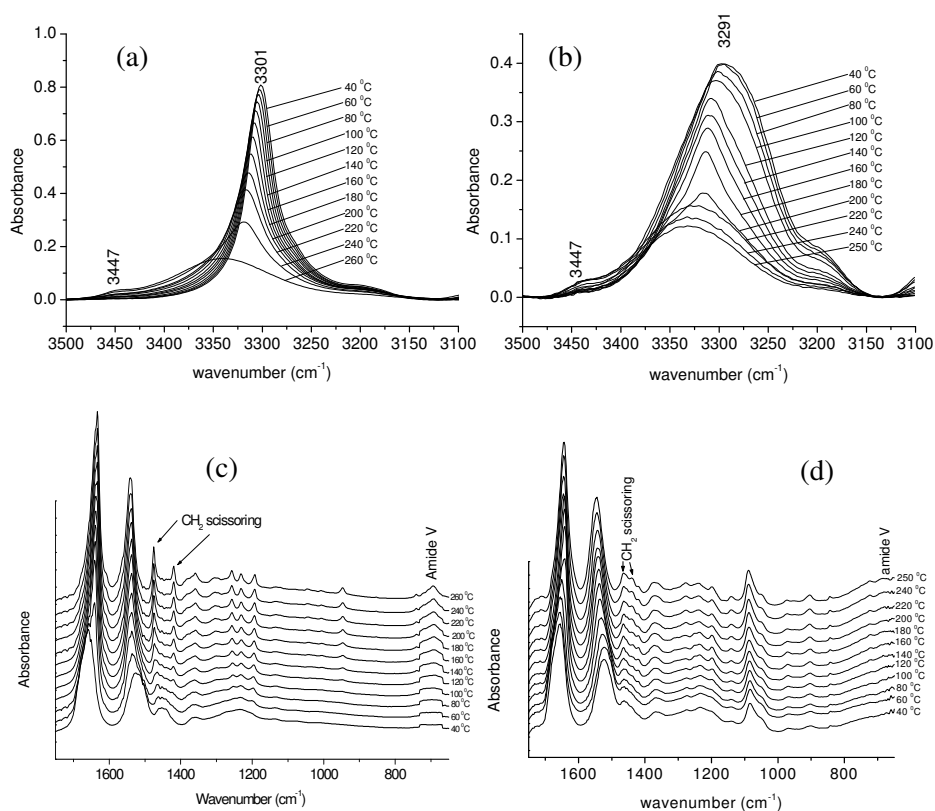


Figure 2. FT-IR spectra of PA1 recorded from 40°C to 260°C in the range of $3100\text{--}3500\text{ cm}^{-1}$ (a) and in the range of $670\text{--}1750\text{ cm}^{-1}$ (c). FT-IR spectra of coPA5 recorded from 40°C to 250°C in the range of $3100\text{--}3500\text{ cm}^{-1}$ (b), and in the range of $670\text{--}1750\text{ cm}^{-1}$ (d).

From the combined FT-IR and WAXD data it can be concluded that with increasing temperature, in the vicinity of the Brill transition, the hydrogen bonding weakens gradually (Regime II in Figures 3a-3e). Figure 3d shows changes in normalized absorbance of the Amide V band [NH out of plane (690 cm^{-1})] with temperature, where the normalization is performed with the NH out of plane (690 cm^{-1}) band at room temperature. The observed changes are similar to those observed for the NH stretching band, in agreement with weakening of the hydrogen bonding with temperature. In contrast to the NH stretching band, with increasing temperature the Amide V band shows a small frequency shift or remains unchanged (Figure 2c).

As was already mentioned, changes in the position and half-height width of the NH stretching band are shown in Figure 3c as function of temperature. Above $200\text{ }^{\circ}\text{C}$, at the onset of melting of PA1, a sudden increase in the band width is observed. As reported by Skrovanek et al.,²³ changes in the bandwidth point to a distribution of hydrogen bonded groups over different geometries. The presence of a very broad band centered at high frequency in the amorphous PA1 is consistent with a decrease in the average strength of the hydrogen bonds. Therefore the NH stretching vibration can be considered as a suitable monitor of the distribution of hydrogen bonding strength, although it appears to be insensitive to conformational changes. Further information on the conformational changes can be obtained from the bands at 1476 cm^{-1} and 1418 cm^{-1} , related to CH_2 scissoring next to NH and CO moieties respectively, (Figures 2c and 2d). In Figure 3e, a plot of normalized area of these two bands as a function of temperature is presented. Once again the normalization of the bands is performed with the peak intensity at room temperature. From the figure it is apparent that the CH_2 scissoring close to the NH side shows a faster decrease in intensity compared to the CH_2 next to the CO group. In literature conformational changes of methylene segments next to NH and CO moieties are associated with the Brill transition in polyamides.²⁵ Our findings are in

agreement with the studies by Yoshioka et al.²⁵ The induced disordering in the methylene units influences hydrogen bonding efficiency of the amide motifs and promotes gauche conformers in the methylene units between the hydrogen bonding groups. The faster decrease of the CH₂-NH (1476 cm⁻¹) scissoring band suggests that weakening of hydrogen bonding is initiated by methylene units next to the NH group compared to CO. Introduction of these defects causes a gradual decrease in the interchain distance within the hydrogen bonding sheets with temperature, as quantified by the *d*(100) spacing (Figure 3b). Ultimately this results in a structural transformation from the triclinic phase to the pseudo-hexagonal phase at the Brill transition temperature.

In Figure 2b FT-IR spectra of the NH stretching region of coPA5 from 40 °C to 250 °C are presented. Conformational changes similar to those of the homopolymer PA1 are observed as a function of temperature. The area of the NH stretching band for coPA5 also decreases with temperature (Figures 2b and 3d'). But in the copolymer, the half-height width value of the band is larger compared to the homopolymer, even at room temperature (Figure 3c'). The difference in the band width can be attributed to the DAII content in coPA5 which influences the polyamide chain conformation, and therefore the crystal lattice. This is due to an increased number of *gauche* conformers which in turn leads to hexagonal packing as demonstrated by VT ¹³C{¹H} CP/MAS NMR experiments, see chapter 4. The peak position of the NH stretching band for coPA5 shifts more gradually and does not show any sudden upswing prior to melting (Figure 3c'). This is expected for this material as it does not show any structural transformation like a Brill transition. The width of the NH stretching band for coPA5 shows a marked decrease in the temperature range 120-180 °C. This decrease suggests some enhancement in hydrogen bonding efficiency due to annealing of the sample during data collection (which takes nearly 10 minutes at a fixed temperature). This interpretation is confirmed because on

cooling the annealed sample the peak sharpening is retained. The normalized absorbance of the NH stretching band of coPA5, recorded during heating, decreases more gradually compared to PA1 (Figure 3d').

It has not been possible to follow the trend of the Amide V band [NH out of plane (690 cm^{-1})] for coPA5 as a function of temperature. This is due to the fact that in the coPA5 spectra (Figure 2d) this band is not well defined. However, an increase in the conformational disorder with increasing temperature becomes apparent with the reduction in intensity of methylene scissoring bands next to NH and CO groups (Figure 3e'). No conclusion from crossing over of the two intensities at higher temperatures can be made due to poorly defined conformational nature of the starting material.

Apart from the reduction in the area of the NH stretching band, a new NH stretching band at higher frequency (3447 cm^{-1}) is observed in the two polymers (Figures 2a and 2b) with increasing temperature. The new band may be attributed to free or non-hydrogen bonded NH groups.

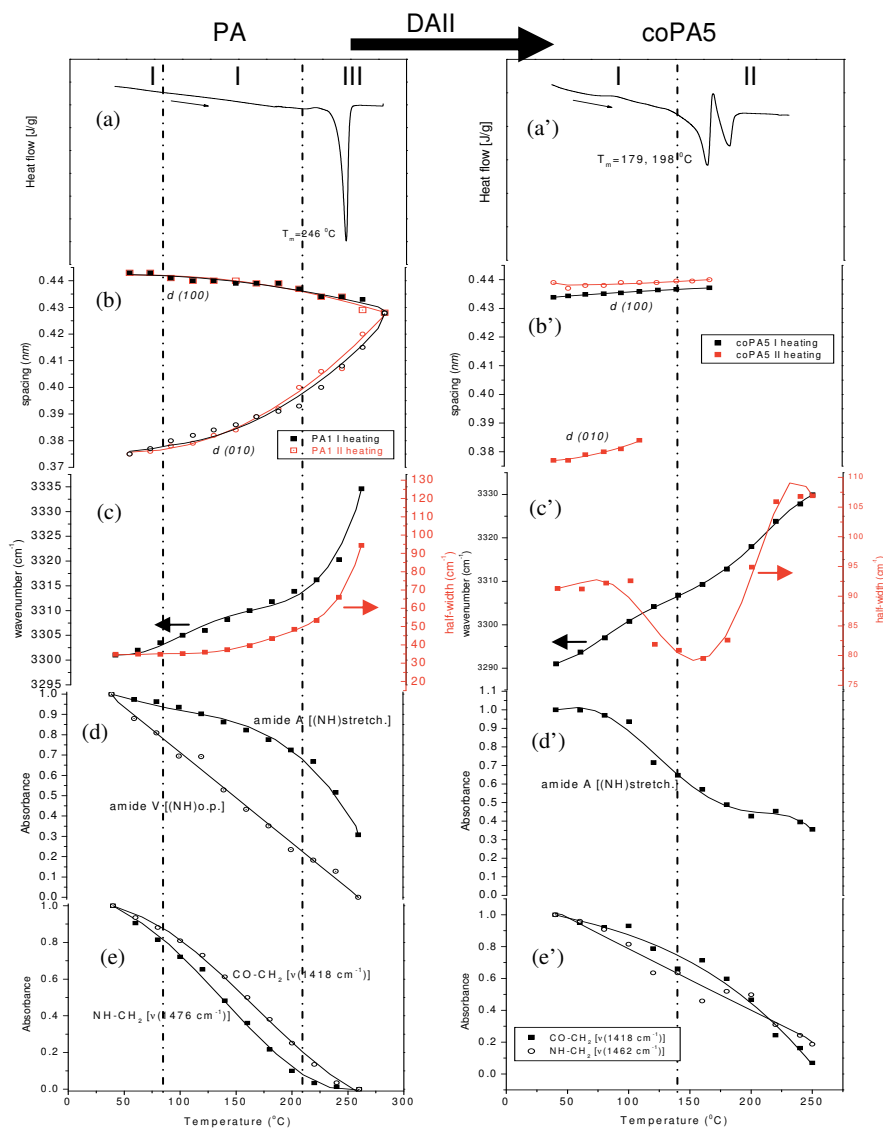


Figure 3. Temperature dependence of infrared data evaluated for (c), (d), (e) PA1 and (c'), (d'), (e') coPA5 in comparison with the DSC thermograms (a), (a') and with X-ray diffraction spacings of PA1 and coPA5.

To examine the crystal structure of DAII copolymers molecular modeling has been used and a comparison between the homopolymer and the copolymer has been made.

Figure 4 shows different views of the XRD patterns obtained by azimuthal integration of the 2D XRD patterns of the homopolymers PA1 (polyamide 4.10) and PA6 and the DAII copolymers. As discussed before the PA1 XRD pattern shows *001* and *002* reflections giving information on the projection of the polymer repeat unit on the *c*-axis of the crystal unit cell. The strong *100* and *010/110* reflections give information on the intrasheet distance and the intersheet distance respectively. The triclinic crystal structure of polyamide 4.10 was described by Jones et al.²⁶ In the latter report the values of the *a* and β unit cell parameters were set at 4.9 Å and 77° respectively, assuming linear hydrogen bonds within the hydrogen bonded sheets. The value of the *c* dimension of the unit cell was calculated from the number of backbone bonds, assuming an all-trans conformation for the polyamide chains.

The crystal structure of PA1 was built using the Cerius² modeling software, employing unit cell parameters taken from Jones et al.²⁶ The structure was energy minimized using the Compass force field and is shown in Figure 5. The cell parameters after minimization were *a* = 4.95 Å, *b* = 5.40 Å, *c* = 19.98 Å, α = 49.0°, β = 76.5°, γ = 63.5°, which are very close to the unit cell parameters of Jones et al. (*a* = 4.90 Å, *b* = 5.32 Å, *c* = 19.8 Å, α = 49°, β = 77°, γ = 63°). Simulation of the powder XRD pattern using Cerius² produces the XRD pattern shown in Figure 6. Clearly the simulated XRD pattern matches the experimental pattern very well, thus confirming the PA1 crystal structure model. The hydrogen bond length in the model is 2.9 Å.

As Figure 4 shows, the XRD patterns of the PA copolymers with a DAII content below 43% turn out to be very similar to the XRD pattern of the PA1 homopolymer. This suggests that the basic structural scheme, consisting of hydrogen bonded sheets packed in a triclinic structure with the *ab*-plane tilted with respect to the *c* axis, still applies for these copolymers. Nevertheless the XRD data in Figure 4 show that the intensity of the *010/110* reflection decreases with increasing DAII content, until it has almost completely vanished at a DAII

content of 43% (although a shoulder at the right hand side of the reflection at 20° (2θ) is visible). Clearly this gradual change in intensities as a function of DAII content indicates that at least part of the DAII comonomer residues are incorporated into the crystal structure of the copolymer.

The observation that the $010/110$ reflection in the XRD pattern of coPA5 is lost indicates that the copolymer chains are packed in a closely hexagonal lattice. In order to set up a structural model for coPA5 we will use the PA1 structure as a starting point. Using the Cerius² software the DAII monomer was built and incorporated into a four-chain unit cell as shown in Figure 7. In the previous chapter the various conformations of the DAII monomer were discussed. The *exo-exo* conformation (i) of the DAII monomer as shown in Figure 7 of chapter 4 turned out to be significantly more populated than the other *exo-exo* conformations, based on gas phase *ab initio* calculations. Although in the present analysis we are not dealing with the gas phase but with the solid phase this conformation was built into the structural model of coPA5. Clearly this choice is a simplification since other DAII conformations may be present as well. Note that the unit cell contains 4 DAII monomers and 4 DAB monomers positioned such that the model pertains to a 50/50 perfectly alternating copolymer. Again this is a simplification since the actual copolymer is a random copolymer: in the actual crystal structure the substitution of DAB monomers for DAII monomers will be a random substitution instead of the regular substitution in our model. Site occupation factors could have been introduced to model the substitutional disorder and to take into account the statistical character of the substitution. However, although both the substitutional disorder and the conformational disorder are not incorporated into our model, the simplified diffraction calculations are still useful to interpret the observed XRD pattern, in view of the low level of crystalline perfection of the structure, as observed in the XRD pattern.

Using the model set up as described above the unit cell dimensions were adapted by diffraction modeling using the Compass force field. In this procedure a combination of energy minimization and diffraction pattern matching is used until the simulated XRD pattern matches the observed XRD pattern. Note that the approach by Jones et al. of setting the values of the a and β unit cell parameters at 4.9 Å and 77° respectively, in order to have linear hydrogen bonds, cannot be used here, since the incorporation of DAII units may lead to a different hydrogen bond geometry. Although the TEM image of the coPA5 single crystal (Figure 10b) confirms the hexagonal nature of the lattice it provides no solution to the problem of determining the unit cell parameters, since it provides only information on the projection unit cell and not on the full three-dimensional unit cell.

With the unit cell parameters determined using the diffraction modeling procedure the final unit cell parameters are: $a = 10.0$ Å, $b = 11.21$ Å, $c = 41.6$ Å, $\alpha = 73^\circ$, $\beta = 81^\circ$, $\gamma = 120^\circ$. The final model is shown in Figure 7. The observed XRD pattern of coPA5 is shown in Figure 8, together with the XRD pattern calculated on the basis of the final model. Note that the agreement between observed and simulated XRD patterns is satisfactory. The hydrogen bond length in the model ranges from 2.9 to 3.2 Å, within the assumptions implicit in the model as discussed above. Clearly, if the conformational and substitutional disorder would have been incorporated into the model the range of hydrogen bond lengths is expected to be larger, and in particular the upper bound of hydrogen bond lengths will be higher. Hence based on the XRD results we conclude that the average hydrogen bond length in the crystalline domains of the coPA5 copolymer has increased by the introduction of DAII comonomer units, as compared to the hydrogen bond length in the PA1 homopolymer. The longer average hydrogen bond length translates into a reduced hydrogen bonding efficiency, in agreement with the FT-IR results.

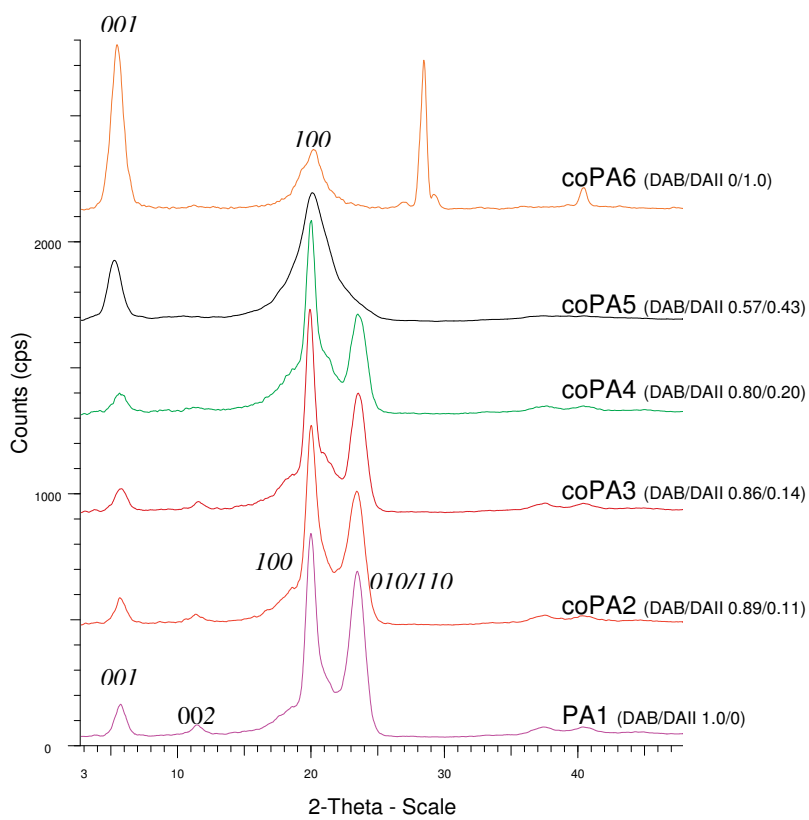
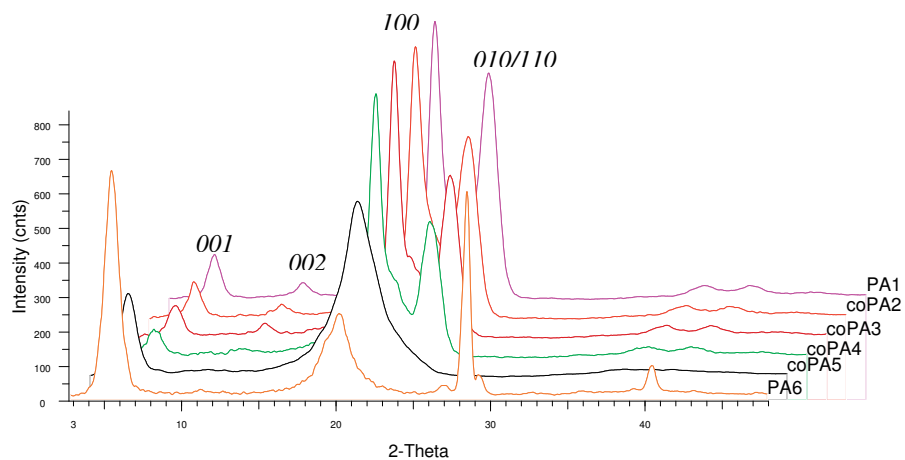


Figure 4. Different views of the XRD patterns of the homopolymers PA1 (nylon 4,10) and PA2 and the DAII copolymers obtained by azimuthal integration of the 2D XRD patterns.

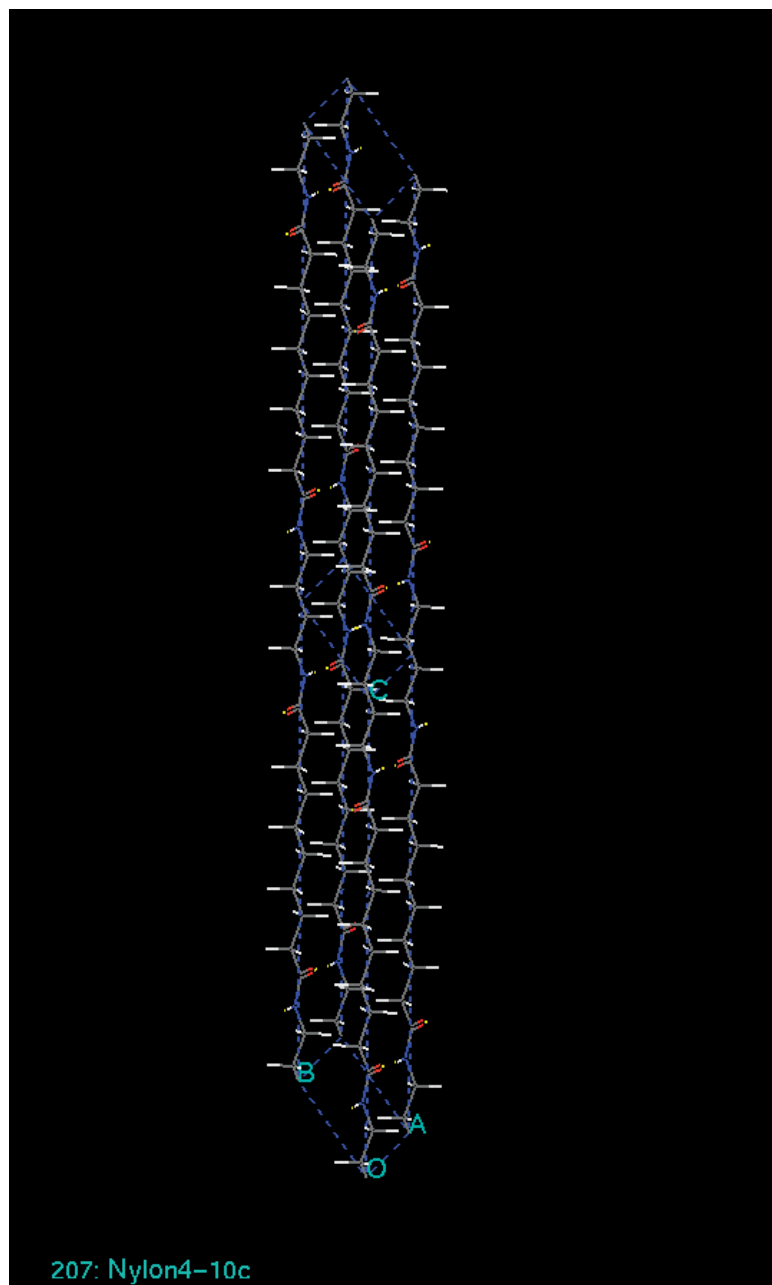


Figure 5. Crystal structure of PA1 built using the Cerius² modeling software.

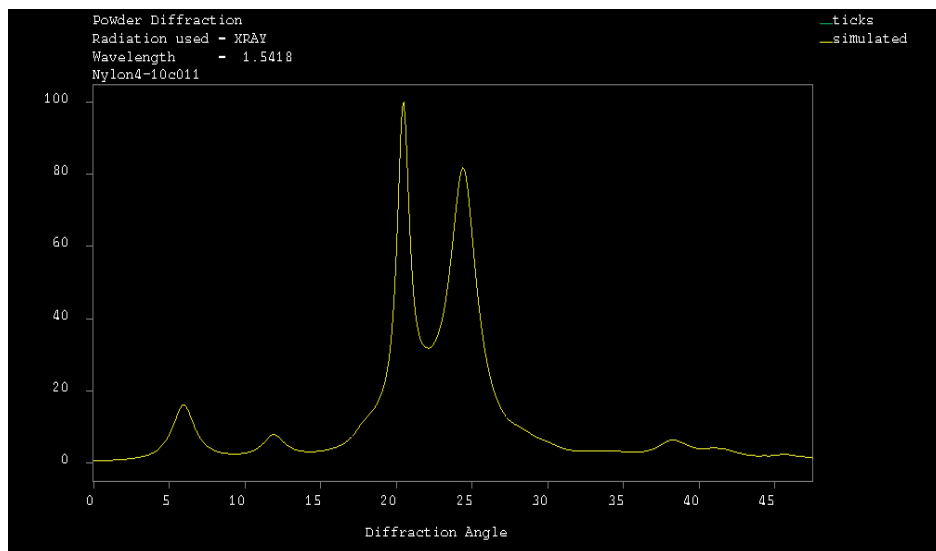


Figure 6. Powder XRD pattern simulated using Cerius² on the basis of the PA1 structure shown in Figure 5.

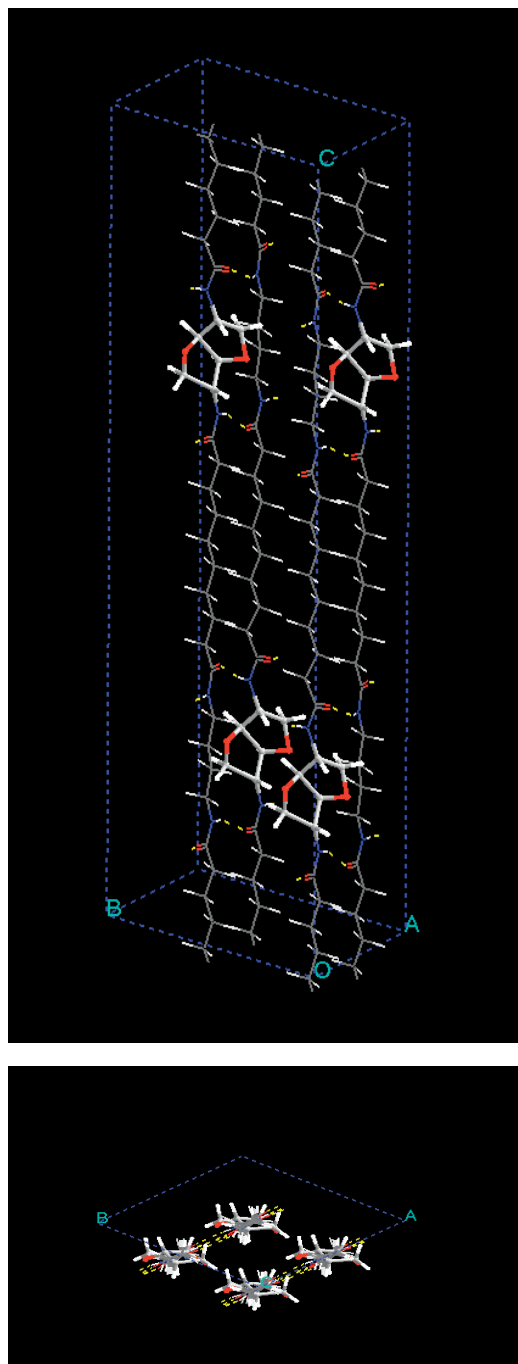


Figure 7. Crystal structure model of the coPA5 copolymer.

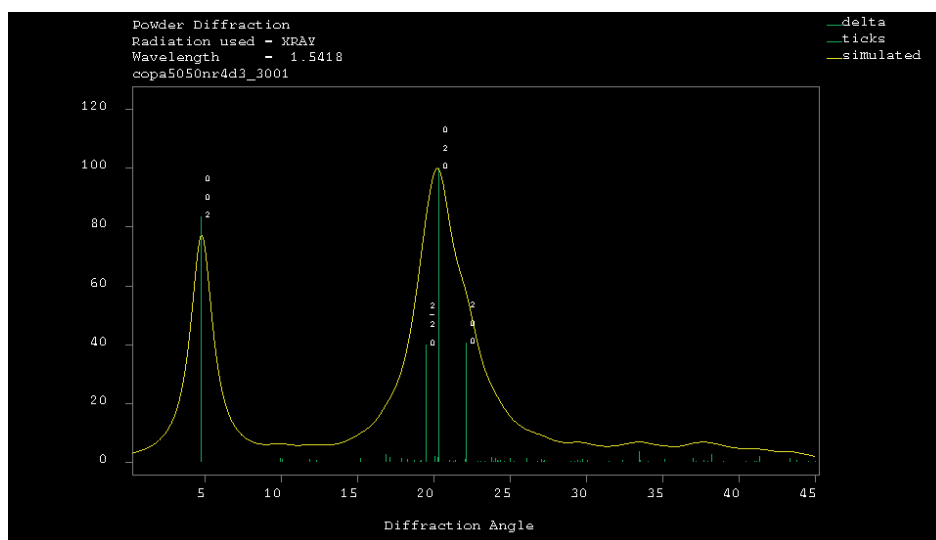
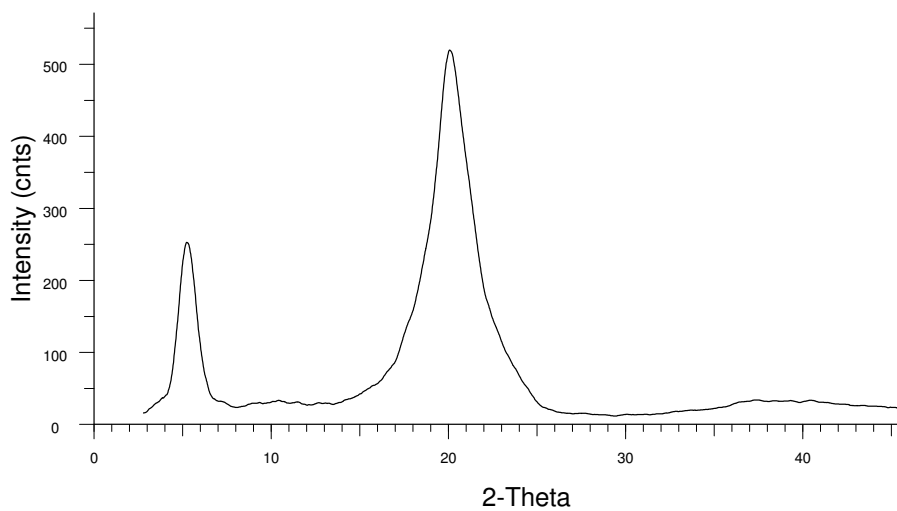


Figure 8. Observed XRD pattern of the coPA5 (upper part) and simulated powder XRD pattern calculated on the basis of the coPA5 structure shown in Figure 7.

To continue our structural investigation of the effects of the incorporation of DAII residues, electron diffraction patterns are collected on single crystals of PA1 and coPA5. The crystals of PA1 and coPA5 for electron microscopy were obtained from very dilute solutions [0.01-0.05% (w/v)] in 1,4 butanediol following the procedure described in the experimental section. The crystals are shown in Figures 9b and 10b. The electron micrograph shown in Figure 9a, reveals lath-like lamellae morphology for the PA1 sample.²⁷ From the micrograph it is evident that the crystals of PA1 are elongated and multilayered. The corresponding electron diffraction pattern, Figure 9b, supports the multilayered nature of crystals. The pattern shows diffraction signals with Bragg spacings of 0.45 nm indexed as 100 , and 0.37 nm indexed as $010/110$, common to both α and β phases. In addition, these diffraction signals appear as rings confirming sedimentation of crystals. The ring with a spacing of 0.45 nm is much stronger in intensity than the ring with a spacing of 0.37 nm. The fact that the 100 diffraction signal is strong suggests that the 100 planes are tilted 13° relative to the primary electron beam, whereas the 010 and 110 planes are likely to be tilted at larger angles, in agreement with the Bunn and Garner triclinic crystal structure.^{2, 28, 29} Similar results were reported for nylon 6.6 single crystals.²⁹

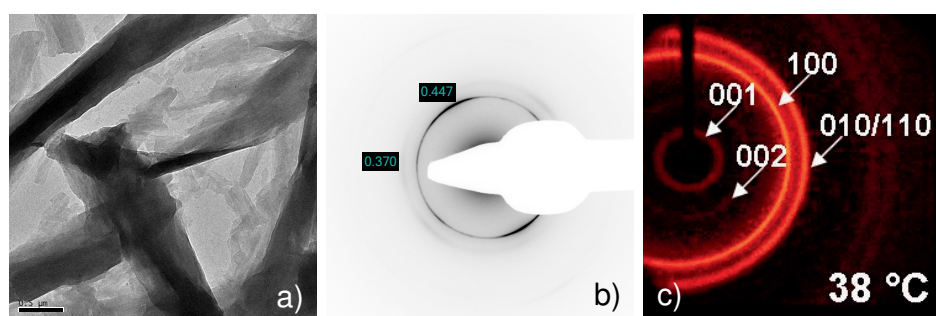


Figure 9. (a) Transmission electron micrograph of PA1 lath like crystals, and (b) its selected area electron diffraction pattern and, (c) comparison with the XRD pattern of PA1. A scale bar 0.5 μm is shown for the electron micrograph.

Figure 10a shows the transmission electron micrograph of a coPA5 single crystal grown from the 1,4 butanediol solution. Clearly the DAII copolymer can produce single crystals having lozenge shapes. The corresponding selected area electron diffraction pattern is reported in Figure 10b. The pattern shows 6 equidistant diffraction spots at 0.44 nm, typical of a pseudo-hexagonal crystal structure. Although the diffraction pattern is clearly hexagonal in terms of spacings, it is not hexagonal in terms of intensities. The two diffuse rings at spacings 0.23 and 0.20 nm correspond to gold, used as an internal reference. The lower molecular weight of the coPA5 copolymer, compared to the PA1 homopolymer, is likely to enhance the formation of single crystals.

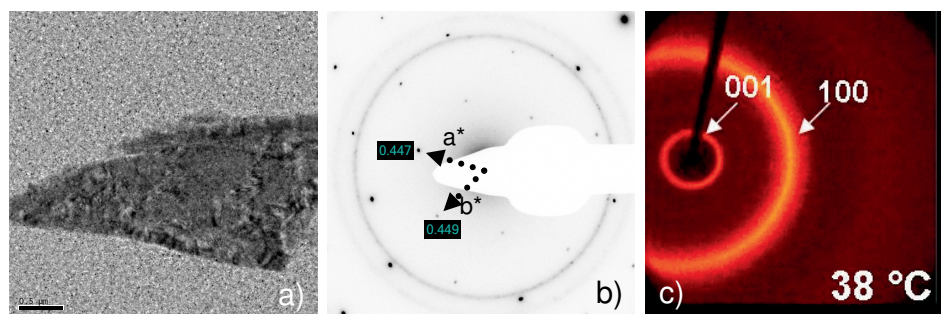


Figure 10. (a) Transmission electron micrographs of coPA5, (b) the respective electron diffraction pattern showing hexagonal packing of chains, (c) WAXD of coPA5. The electron micrograph shows a scale bar of 0.5 μm .

5.3.1 Mechanical properties. To investigate the effects of structural changes on the mechanical properties some preliminary experiments were performed to study changes in stiffness resulting from the presence of comonomer residues. Due to the low molecular weight of coPA5 samples (Table 1), it was not possible to compression-mold homogeneous films for the investigation of the

mechanical properties of this sample. Therefore films of the PA1 sample are compared with film of the coPA3 sample that present the characteristics reported in Table 3.

Table 3. Characteristics of co-polyamide coPA3 from sebacic acid, 1,4-diaminobutane and diaminoisoidide.

| Symbol | Monomer feed, mol ratio (DAB/DAII) ^a | Built-in composition (DAB/DAII) ^b | M_n^c (g/mol) | PDI ^c | M_n^d (g/mol) | PDI ^d |
|--------|--|--|--------------------|------------------|--------------------|------------------|
| coPA3 | 0.78/0.22 | 0.80/0.20 | 5,530 | 1.8 | 20,400 | 2.9 |

DAB = 1,4-diaminobutane, DAII = diaminoisoidide, ^aDetermined by weighed-in monomers, ^bDetermined by NMR, ^cDetermined for polyamides before Solid State Polymerization using SEC method with PMMA standards in HFIP solvent, ^dDetermined for polyamides after Solid State Polymerization using SEC method with PMMA standards in HFIP solvent, ^ePA obtained via interfacial polymerization, coPA3 = PA 4.10/DAII 10-4.

Figure 11 shows the storage and loss moduli (G' and G'' , respectively) of PA1 and coPA3 as function of temperature. The difference in the glass transition temperature (T_g) of the two samples is apparent. PA1 shows a T_g at approximately 76.3°C whereas the T_g of the coPA3 copolymer is observed at 84.6°C (Table 4). The increase in T_g with increasing amount of DAII is in agreement with the enhanced rigidity of the main chain. The hydrophobic nature of polyamides, due to the presence of unsaturated hydrogen bonding motifs, is also likely to influence the glass transition temperature. To prevent the influence of water the samples were annealed for 5 days at 120°C under a nitrogen atmosphere prior to the experiments. The influence of DAII on the mechanical properties is evident from Figure 11. The difference in storage modulus, G' , above T_g of the two samples may be attributed to crystal structure, crystallinity and conformational disorder. Some sub- T_g transitions were also observed in the glassy state of the two polymers. Usually these sub- T_g transitions are associated with conformational dynamics occurring in the glassy state and they can provide some additional information. For example, Nylon 6,6

shows decrease in toughness, measured as impact resistance, with decreasing area under the T_{β} peak in the $\tan \delta$ curve.³⁰

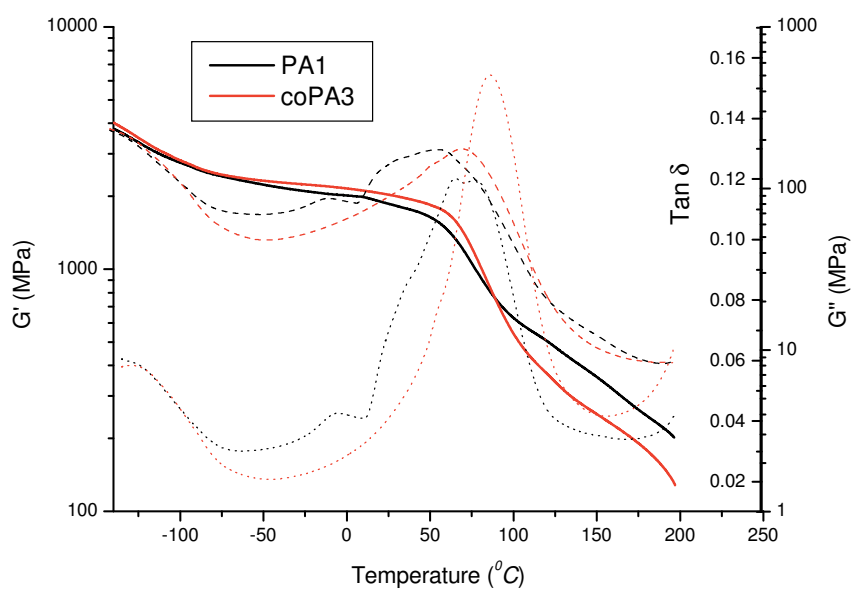


Figure 11. DMTA curves of PA1 and coPA3 (DAB/DAII 75/25).

Table 4. Glass transition temperature (T_g) and storage moduli (G') of PA1 and coPA3 (DAB/DAII 75/25).

| | T_g ($^{\circ}\text{C}$) | G' (MPa) 25°C | G' (MPa) 125°C |
|-------|------------------------------|------------------------------------|-------------------------------------|
| PA1 | 76.3 | 1858 | 477 |
| CoPA3 | 84.6 | 2028 | 340 |

5.4 Conclusions

The following conclusions can be drawn from the results presented in this chapter:

1. The incorporation of DAII residues in polyamide 4,10 reduces the hydrogen bond efficiency and thus the melting point of the polyamides. Biobased polyamides are semi-crystalline over the whole range of compositions and the typical polyamide structure with different interchain and intersheet distances is preserved for samples with DAII contents lower than 43 mol%.
2. A gradual change in the intensity of the $010/110$ reflection with increasing DAII content indicates that at least part of the DAII comonomer residues are incorporated into the crystal structure of the copolymer. The observation that the $010/110$ reflection in the XRD pattern of coPA5 is lost indicates that the copolymer chains are packed in a closely hexagonal lattice. This is confirmed by selected area electron diffraction results.
3. Diffraction modeling suggests that the basic structural scheme consisting of hydrogen bonded sheets packed in a triclinic structure with the ab -plane tilted with respect to the c axis, still applies for the DAII copolymers.
4. The introduction of DAII monomers into the polymer structure influences the mechanical properties of the copolyamides. The difference in storage modulus, G' , above T_g of the samples PA1 and coPA3 having different DAII content, may be attributed to differences in crystal structure, crystallinity and conformational disorder.

References

1. Jasinska-Walc, L., Villani, M., Dudenko, D., van Asselen, O., Klop, E., Rastogi, S., Hansen, M. R., Koning, C. E., *Macromolecules*, **2012**, *45* (6), 2796–2808.
2. Bunn, C.W. and Garner, E. V. , *Proc. R.Soc. London*, **1947**, A189, 139.
3. Xenopoulos, A. and Clark, E. S., *Nylon plastic handbook*, ch.5, ed. M.I.Kohan. Hanser Publishers, Munich, **1995**.
4. Kinoshita, Y., *Makromol. Chem.*, **1959**, *33*, 1.
5. Navarro, E., Franco, L., Navarro, E., Subirana, J.A. and Puiggali, J., *Macromolecules*, **1995**, *28*, 8742.
6. Auriemma, F., Petraccone, V., Parravicini, L., Corradini, P., *Macromolecules*, **1997**, *30*, 7554-7559.
7. Franco, L., Navarro, E., Subirana, J.A. and Puiggali, J., *Polymer*, **1998**, *39*, 22, 5553.
8. Franco, L., Subirana, J.A., Puiggali, J., *Polymer*, **1999**, *40*, 2429.
9. Fenouillot, F.; Rousseau, A.; Colomines, G.; Saint-Loup, R.; Pascault, J. P. *Prog. Polym. Sci.* **2010**, *35*, 578.
10. Thiem, J.; Bachmann, F. *Makromol. Chem.* **1991**, *192*, 2163.
11. Stoss, P.; Hemmer, R.; Derek, H. *Adv. Carbohydr. Chem. Biochem.* **1991**, *49*, 93.
12. Gomurashvili, Z.; Kricheldorf, H. R.; Katsarava, R. *J. Macromol. Sci., Pure Appl. Chem.* **2000**, *A37*, 215.
13. Caouthar, A. A.; Loupy, A.; Bortolussi, M.; Blais, J.; Dubreucq, L.; Meddour, A. *J. Polym. Sci., Part A: Polym. Chem.* **2005**, *43*, 2480.
14. Caouthar, A.; Roger, P.; Tessier, M.; Chatti, S.; Blais, J. C.; Bortolussi, M. *Europ. Polym. J.* **2007**, *43*, 220.

15. Okada, M.; Yamada, M.; Yokoe, M.; Aoi, K. *J. Appl. Polym. Sci.* **2001**, *81*, 2721.
16. Philip, B.; Sreekumar, K. *Polym. Int.* **2001**, *50*, 1318.
17. Jasinska, L.; Villani, M.; Wu, J.; van Es, D.; Klop, E.; Rastogi, S.; Koning, C. E. *Macromolecules*, **2011**, *44*, 3458.
18. Aceituno, J. E., Tereshko, V., Lotz, B. and Subirana, J.A., *Macromolecules*, **1996**, *29*, 1886.
19. *Cerius²*, Version 4.2, Accelrys Software Inc., San Diego.
20. Vinken, E.; Terry, A. E.; Hoffmann, S.; Vanhaecht, B.; Koning, C. E.; Rastogi, S. *Macromolecules* **2006**, *39*, 2546-2552.
21. Jakes J, Krimm S. *Spectrochimica Acta*, **1971**, *27A*, 35.
22. Komatsu T, Makino D, Kobayashi M, Tadokoro H. *Rep. Prog. Polym. Phys. Jpn.* **1970**, *13*, 1051.
23. Skrovanek, D.J, Painter, P.C, Coleman, M.M., *Macromolecules* **1986**, *19*, 699.
24. Schmidt P, Hendra PJ. *Spectrochimica Acta*, **1994**, *50A*, 1999.
25. Yoshioka, Y., Tashiro, K., Ramesh, C. *Polymer*, **2003**, *44*, 6407.
26. Jones, N. A., Atkins, E. D. T., Hill, M. J., Cooper, S. J., Franco, L., *Polymer*, **1997**, *38*, 2689.
27. Li, W., Yan, D., *Cryst. growth des.*, **2003**, *3*, 4, 531.
28. Atkins, E. D. T., Keller, A., Sadler, D.M., *J. Polym. Sci.* **1972**, *A2*, 863.
29. Holland, M.J., *Makromol. Chem.* **1964**, *71*, 204.
30. Menard, K.P., *Encyclopedia of Analytical Chemistry*, Online © **2006–2008** John Wiley & Sons, Ltd.

Chapter 6

Technological Assessment and outlook

The possibility of understanding the influence of molecular microstructure on the properties of materials has furnished high scientific and industrial relevance in polymer science.

For example, the advent of a new class of catalysts, metallocene based catalysts, has led to a class of polyolefins with a higher control of the distribution of stereo- and regio-defects, giving the possibility to correlate the crystalline structure to the amount and nature of chain defects. In this approach, the role of secondary interactions and the effect of imposed perturbation on the crystal structures become extremely interesting for systems where the interplay between hydrogen bonding interactions, van der Waals interactions and conformational flexibility are crucial for the final properties of the materials. For this reason, in this dissertation we have explored the role of secondary interactions such as hydrogen bonds on the crystallization of new bio-based polyamides and the role of bio-based monomers in influencing the secondary interactions. Moreover we have also explored a new approach to extract oligopeptides, from insoluble proteins such as keratin obtained from sustainable sources such as feathers and hair, affecting the secondary interactions responsible for the high insolubility of these materials. The extraction process has been carried out using water under well specified pressure-temperature conditions, with the original idea of simply dissolving these fibrous proteins using an approach developed in our group that has given good response on materials such as polyamides.

However unlike synthetic aliphatic polyamides, the constitutional complexity of keratin and the presence of disulphide bonds in this material, has only led to the hydrolysis of the protein, showing that the dissolution is not achievable. Natural systems are often characterized by a complex chemical structure and any thermal treatment designed for their processing usually results into thermal degradation and thus reduces the possibility of processing. On the contrary, we have proven that in the “superheated state”, water molecules could easily permeate into the polymer chains and weaken the hydrogen bonds and disulphide bonds so that feather keratins could be hydrolyzed into oligopeptides, confirming that proteins can be extracted or purified from waste products or other natural resources in a similar way. Moreover, the method described could be used for natural proteins like silk, where the lower constitutional and structural complexity should enhance the dissolution and not the hydrolysis under “superheated water” conditions, giving the possibility of partially mimicking the spider silk spinning using the proper conditions in order to shield and mediate the hydrogen bonding motifs. A separate study along the same lines have been carried out at the DWTI center of the Aachen University, where the group of Prof Crisan Popescu and Prof Martin Moeller, have successfully shown the electrospinning of keratin fibers from feather solutions. The work has been further extended to human hair. These spun fibers have been used as scaffolds for anchoring bio-based block copolymers that have the potential to be used as bio-degradable scaffolds or coatings on textile fabrics or in cosmetics.

In the chapters 3, 4 and 5 of this dissertation we have proven that a perturbation of the hydrogen bonding network in very well known materials can be achieved following a different strategy, namely by affecting the microstructure of the polyamides by varying the constitution of the polymer chains. A new class of fully biobased copolyamides with tailored properties, depending on their diaminoisoidide (DAII) content is identified which hold promises in

applications that may benefit from the presence of a hydrophilic group along the PA chain such as a DAII residue.

The two fused tetrahydrofuranic rings of DAII units have a high mobility and it has been observed that with increasing DAII content the typical polyamide structure with different interchain and intersheet distances is preserved for samples with DAII contents lower than 43 mol%. At higher DAII contents the structure changes into a structure with a close to hexagonal packing of polymer chains, providing new opportunities for the synthesis of copolyamides with tunable melting temperatures. It has also been observed that the mechanical properties are affected by the different microstructure and that in particular the different crystal structure and/or crystallinity of the CoPAs with a different DAII content influence the modulus of the material.

On the contrary the costs associated with the synthesis of DAII residues and the impossibility of bio-composting biobased polyamides could limit the interest for these new based materials. Also the thermal stability of these copolyamides remains an issue.

Acknowledgements

It is my pleasure to express my sincere gratitude to a great number of people who have contributed to this thesis and have contributed to make my last three years in Eindhoven a good time.

First of all, I would like to acknowledge Prof. Sanjay Rastogi who offered me the possibility of doing a PhD. Thank you Sanjay for all the impressive ideas and discussions, this work could not have been done without your guidance. Working with you I learned a lot and I had great opportunities to collaborate with valid and interesting people. I am grateful to Prof. Lemstra for the opportunity to perform PhD in SKT and for his valuable teachings and comments. Part of this work was carried out in collaboration with SPC and I want to thank Prof. Cor Koning for this great opportunity. Thank you Cor, for the interesting meetings, for your valuable comments and moreover for the possibility you gave to me of being involved in several interesting projects.

I would like to extend my sincere gratitude to Dr. Enno Klop. Dear Enno, it has been a great pleasure for me to collaborate with you. Thank you very much for your immense support, the interesting suggestions and for the possibility of working in “your” fantastic XRD Lab.

I also wish to thank Prof. Claudio De Rosa for participation in reading committee and for all his teachings. Dear Prof. De Rosa, you and Prof. Finizia Auriemma taught me a lot and introduced me to this interesting world of polymer physics. I could not have had better guidance for that!!! Grazie mille di cuore!!!

I also want to thank Prof. Jan van Hest for providing the opportunity to perform a part of the work performed in chapter 2 of this thesis in his lab and for the interesting and fruitful collaboration and Prof. Thijs Michels for his suggestions and participation in the committee.

Many people within and outside the university contributed to this thesis. First of all, I would like to thank Dr. Lidia Jasinska from SPC for the synthesis of some of the materials object of this thesis and for her collaboration in some characterization experiments. Special thanks to Dr. Michael Ryan Hans and Dr. Dimitro Dudenko from Max Planck Institute of Mainz for their valuable help in solid state NMR experiments and DFT and MP2 calculations. Many thanks to Dr. Dennis Lowick from Radboud University of Nijmegen for his help and support in the solid state peptide synthesis experiments. I want to acknowledge Dr. Giuseppe Portale and Dr. Daniel Hermida Merino for the nice discussions and the support at the BM26.

At TU/e, I was benefited from the support by number of people. I would like to thank Dr. Han Goossens for his support and nice discussions especially on IR and XRD experiments. I am thankful to Anne Spoelstra and Pauline Schmit for TEM analysis and Optical Microscopy, Maria and Yogesh for TGA and DSC experiments and Dr. Joost van Dongen for chromatography experiments. I would like to thank all the present and past SKT/PTG colleagues for the nice time during my stay: Maria T., Maria E., Yogesh, Altug, Denka, Peter, Erik, Piming, Elena, Tamara, Pim, Benny, Karel, Sai, Jules, Chunxia, Artur, Rafiq, Weizhen, Yuliya, Marloes, Cees, Martijn, Bijorn, Bob, Gizela, Thierry, Timo and all the students of STO 0.45. The list includes also my officemates at STO 0.43 Altug, Sai, Artur and especially Maria E. (grazie di tutto mia amica svedese!). Guys thank you very much for your support, help and good time!!! I wish you all the best for your future!!! My sincere gratitude goes to Elly, Ineke and Mariolijn for their sympathy, availability and secretarial support.

At Loughborough I spent my first year of PhD and I am very thankful to Maria, Carmine, Nilesh, Sara, Giuseppe, Anurag, Yohan, Mario and Gianfranco. Thank you for the nice and friendly atmosphere, some of you more than colleagues have been friends.

My life in Eindhoven would have been less funny without the company of my Italian gang! Per questo con affetto ringrazio: Daniele, con la sua ben fornita

rubrica telefonica che al confronto Gianni Minà sembra un principiante (Guagliooo fa fridddd!!!), Dario col quale si può tranquillamente parlare di cristallizzazione anche dopo la decima birra e perdersi insieme nell'universo oscuro della forma gamma, Alberto il vero sindaco di Eindhoven, Stefano l'ambasciatore italiano in Polonia e Ucraina, Vincenzo l'unico siciliano che conosca a non sentir freddo ad Eindhoven, Luigi 'o` paesan bell', Chiara e Maria che è stata una splendida compagna di viaggio in tutta quest' avventura e al quale vanno tutti i miei ringraziamenti per la pazienza avuta e per tutte le belle cose vissute insieme!

Other people have contributed to my great time in Eindhoven. Many thanks to Ece, Bruno, Camille, Ivelina, Isabelle, Arash, Mindaugas, Mattias, Natalia, My, Paul, Gozde, Bahar, Seda and many others. My Sundays spent here in Eindhoven have been dedicated to football. Special thanks to my football mates Alberto, Stefano, Nico, George, Evert, Anthony, Ezequiel, Alex and to the SSCN per avermi regalato momenti fantastici quest'anno!!!

Per chiudere ringrazio tutta la mia famiglia. Questa tesi è dedicata a tutti loro per il continuo sostegno e incoraggiamento.

Curriculum Vitae

Maurizio Villani was born on March 30th 1978 in Napoli, Italy. After finishing secondary school (Liceo Scientifico 'E. Torricelli', Somma Vesuviana, Napoli, Italy) he studied Industrial Chemistry at the University 'Federico II' of Napoli (Italy). In 2007 he graduated within the Polymer Physics group on "Structure and mechanical properties of isotactic Poly(1-butene) samples synthesized via metallocene catalysts" under the supervision of Prof. Claudio De Rosa.

At the beginning of 2008, he started his PhD in the group of Prof. Sanjay Rastogi at Loughborough University, Leicestershire (UK). From May 2009 he moved to Eindhoven where he continued his PhD project in the Polymer Technology group (SKT) at Eindhoven University of Technology of which the results are presented in this dissertation.

List of publications

- Jasinska-Walc, Lidia; Villani, Maurizio; Dudenko, Dmytro; van Asselen, Otto; Klop, Enno; Rastogi, Sanjay; Hansen, Michael Ryan and Koning, Cor “Local conformation and cocrystallization phenomena in diaminoisoidide-based copolyamides studied by FT-IR, solid state NMR and WAXD”, *Macromolecules*, 2012, 45 (6), pp 2796–2808.
- Jasinska, Lidia; Villani, Maurizio; Wu, Jing; van Es, Daan; Klop, Enno; Rastogi, Sanjay; Koning, Cor “Novel, fully biobased semicrystalline polyamides”, *Macromolecules*, 2011, 44 (9), pp 3458–3466.
- Villani, Maurizio; Lowik, Dennis; van Hest, Jan; Rastogi, Sanjay “Morphogenesis in the self-assembling process of oligopeptides obtained from keratins”, to be submitted.
- Villani, Maurizio; Jasinska-Walc, Lidia; Spoelstra, Anne; Koning, Cor; Klop, Enno and Rastogi, Sanjay “Structure-property relationships of diaminoisoidide-based copolyamides”, to be submitted.
- Cakir, Seda; Jasinska-Walc, Lidia; Villani, Maurizio; Hansen, Michael and Koning, Cor “Investigation of local chain conformation and morphology of polyamide 6 based copolymers”, in preparation.
- Vitagliano, Vincenzo; Castagnolo, Dario; De Chiara, Giuseppe; Vitagliano, Pier Luigi; De Luca, Dario; Pannico, Marianna; Tommasone, Maria; Villani, Maurizio; Zampino, Paolo “Diffusion boundaries behavior during a parabolic flight”, *Microgravity sci. technol.* XIV/4 (2003).
- Villani, Maurizio; Lowik, Dennis; van Hest, Jan; Rastogi, Sanjay “Morphogenesis in self-assembling process of oligopeptides obtained from keratins”, ACS 241st National meeting and exposition - PMSE 2011.
- Jasinska, Lidia; Villani, Maurizio; Wu, Jing; van Es, Daan; Rastogi, Sanjay; Koning, Cor “Synthesis and characterization of novel renewable, diaminoisoidide-based polyamides”, ACS 241st National meeting and exposition 2011.

